ALFRED-WEGENER-INSTITUT
HELMHOLTZ-ZENTRUM FÜR POLAR- UND MEERESFORSCHUNG

719
2018

Berichte
zur Polar- und Meeresforschung

Reports on Polar and Marine Research

The Expeditions PS106/1 and 2 of the Research Vessel POLARSTERN to the Arctic Ocean in 2017

Edited by
Andreas Macke and Hauke Flores
with contributions of the participants

HELMHOLTZ GEMEINSCHAFT

Die Berichte zur Polar- und Meeresforschung werden vom Alfred-Wegener-Institut, Helmholtz-Zentrum für Polar- und Meeresforschung (AWI) in Bremerhaven, Deutschland, in Fortsetzung der vormaligen Berichte zur Polarforschung herausgegeben. Sie erscheinen in unregelmäßiger Abfolge.

Die Berichte zur Polar- und Meeresforschung enthalten Darstellungen und Ergebnisse der vom AWI selbst oder mit seiner Unterstützung durchgeführten Forschungsarbeiten in den Polargebieten und in den Meeren.

Die Publikationen umfassen Expeditionsberichte der vom AWI betriebenen Schiffe, Flugzeuge und Stationen, Forschungsergebnisse (inkl. Dissertationen) des Instituts und des Archivs für deutsche Polarforschung, sowie Abstracts und Proceedings von nationalen und internationalen Tagungen und Workshops des AWI.

Die Beiträge geben nicht notwendigerweise die Auffassung des AWI wider.

Herausgeber
Dr. Horst Bornemann

Redaktionelle Bearbeitung und Layout
Birgit Reimann

Alfred-Wegener-Institut
Helmholtz-Zentrum für Polar- und Meeresforschung
Am Handelshafen 12
27570 Bremerhaven
Germany

www.awi.de
www.reports.awi.de

The Reports on Polar and Marine Research are issued by the Alfred Wegener Institute, Helmholtz Centre for Polar and Marine Research (AWI) in Bremerhaven, Germany, succeeding the former Reports on Polar Research. They are published at irregular intervals.

The Reports on Polar and Marine Research contain presentations and results of research activities in polar regions and in the seas either carried out by the AWI or with its support.

Publications comprise expedition reports of the ships, aircrafts, and stations operated by the AWI, research results (incl. dissertations) of the Institute and the Archiv für deutsche Polarforschung, as well as abstracts and proceedings of national and international conferences and workshops of the AWI.

The papers contained in the Reports do not necessarily reflect the opinion of the AWI.

Editor
Dr. Horst Bornemann

Editorial editing and layout
Birgit Reimann

Alfred-Wegener-Institut
Helmholtz-Zentrum für Polar- und Meeresforschung
Am Handelshafen 12
27570 Bremerhaven
Germany

www.awi.de
www.reports.awi.de

Titel: Eine Eisbärenmutter und ihr Junges inspizieren die Versuchsaufbauten auf der Scholle während der Driftexpedition PS106/1 (PASCAL) (Foto: Hauke Flores, AWI)

Cover: A polar bear mother and her cub are investigating experimental installations on the ice floe of drift expedition PS106/1 (PASCAL) (photo: Hauke Flores, AWI)

The Expeditions PS106/1 and 2 of the Research Vessel POLARSTERN to the Arctic Ocean in 2017

Edited by
Andreas Macke and Hauke Flores
with contributions of the participants

Please cite or link this publication using the identifiers
http://hdl.handle.net/10013/epic.4ff2b0cd-1b2f-4444-a97f-0cd9f1d917ab and
https://doi.org/10.2312/BzPM_0719_2018

ISSN 1866-3192

PS106

PS106/1
23 May 2017 - 21 June 2017
Bremerhaven - Longyearbyen

Chief scientist
Andreas Macke

PS106/2
23 June 2017 - 20 July 2017
Longyearbyen - Tromsø

Chief scientist
Hauke Flores

Coordinator
Rainer Knust

Contents

1. ÜBERBLICK UND FAHRTVERLAUF

Hauke Flores[1], Andreas Macke[2]

[1]AWI
[2]TROPOS

Überblick

Die Polargebiete sind wichtige Bestandteile des globalen Klimasystems. Die großflächige Schnee- und Eisbedeckung beeinflusst maßgeblich die Bodenenergiebilanz, welche wiederum stark an die atmosphärische und ozeanische Zirkulation gekoppelt ist. Das Wechselspiel verschiedener arktischer Rückkopplungsmechanismen ist dabei noch nicht vollständig verstanden. So ist z.B die Kopplung zwischen Meereis, Wolken und Aerosol in der Übergangszone zwischen offenem Ozean und Meereis bislang noch nicht gut verstanden. Daher wurde im Projekt **PASCAL** (Physical feedbacks of Arctic PBL, Seaice, Cloud And Aerosol) dieser Aspekt untersucht, um letztlich unser Verständnis der aktuellen dramatischen Abnahme des arktischen Meereises im nordhemisphärischen Sommer zu verbessern. Zu diesem Zwecke lieferte die TROPOS-OCEANET- und -Aerosol-Instrumentierung an Bord von *Polarstern* sowie weitere spektrale Strahlungsmessungen die Oberflächenenergiebilanz und eine detaillierte Charakterisierung der Oberfläche, der Wolken und des Aerosols. Während des Transits und der Meereisarbeiten von *Polarstern* wurden identische Messungen auf der deutsch – französischen *AWIPEV* Forschungsbasis in Ny-Ålesund nahe des offenen Ozeans vorgenommen. Die Messungen auf *Polarstern* und der AWIPEV Basis wurden durch koordinierte Flüge der AWI Messflugzeuge *Polar 5* und *Polar 6* zwischen den Stationen und entlang des Gradienten der arktischen Meereiskonzentration begleitet. Diese luftgetragenen Messungen wurden durch weitere Messungen der Grenzschichtstruktur (mittlere und turbulente Größen) auf der Eisstation mittels Fesselballons und mehrerer kleiner « Unmanned Airborne Vehicles“ (UAV’s) unterstützt. Parallel wurden auf der Eisscholle ozeanographische, meereisphysikalische und biologische Arbeiten durchgeführt.

In arktischen Ökosystemen kommt dem weit verbreiteten Polardorsch *Boreogadus saida* eine Schlüsselrolle zu, da er eine Hauptnahrungsquelle für Robben und Seevögel ist. Junge Polardorsche nutzen häufig den Lebensraum an der Unterseite des Meereises, der ihnen als Jagdrevier und Unterschlupf vor Räubern dient. Bedingt durch den Klimawandel vermindert sich die räumliche Ausdehnung des Untereis-Lebensraumes zusehends. **SiPCA** (Survival of Polar Cod in a Changing Arctic Ocean; PS106/2) hat die Bedeutung des Meereises für den Polardorsch in der Barents-See und dem angrenzenden Arktischen Ozean genauer untersucht (Abb. 1.1). Die räumliche Verteilung des Polardorsches, seiner Nahrungsgrundlagen, seiner Fressfeinde und anderer Umweltparameter wurden simultan beprobt. Auf fünf Meereisstationen wurden die physikalischen und biogeochemischen Eigenschaften sowie die Biodiversität von Meereis und Schmelztümpeln untersucht. Am Ende der Expedition wurde die Eisscholle von PS106/1 angefahren, um erneut Messungen durchzuführen und Proben zu nehmen sowie zurückgelassene Instrumente zu bergen. Die auf dieser Expedition gewonnenen Daten tragen bei zu einem verbesserten quantitativen Verständnis der Bedeutung des Meereises für den Polardorsch, sowie für physikalische und biogeochemische Prozesse in Meereis, Schmelztümpeln, Ozean und Atmosphäre.

Fahrtverlauf

Die Expedition PS106/1 unter Leitung von Andreas Macke begann am 24. Mai 2017 um 14:00 von Bremerhaven und erreichte auf direktem Kurs am 3.6. morgens bei (82°57.7‘ N, 10°14.6‘ E) eine geeignete, nahezu kreisrunde Eisscholle mit einem Durchmesser von etwa 2.5 nautischen Meilen (nm). Auf der Hinfahrt wurde täglich etwa um die Mittagszeit aufgestoppt, um per Schlauchboot Wasserproben zu sammeln und Strahlungsmessungen durchzuführen. Weiterhin wurden auf dem Weg fünf SVP-Drifter und vier ARGO-Floats ausgelegt. Ab Höhe Longyearbyen bis zum Ende von PS106/1 wurde ein tägliches CTD-Programm gefahren. Auf der Eisstation wurden im Rahmen des PASCAL-Projektes vom 4. 6. bis zum 15. 6. nahezu kontinuierlichen Messungen der Energiebilanz am Boden und des Zustands der bewölkten Atmosphäre vorgenommen. Parallel wurden meereisphysikalische, biologische und biogeochemische Messungen im Meereisbereich durchgeführt. Tabelle 1.1 gibt einen Überblick der Tage, an denen *Polarstern* an der Eisscholle fest lag. Wegen schlechter Sichtbedingungen mussten die Messungen auf der Eisscholle am 6.6. und 9.6. teilweise sowie am 12.6. ganztägig abgebrochen werden. Schiffseitig wurden zweimal täglich regelmäßig CTD-Messungen bis zum Meeresboden sowie mehrere Sedimentbeprobungen und Multinetzeinsätze ausgeführt. Hubschraubereinsätze wurden für Auf- und Abbau und hauptsächlich für Fernerkundung und Probennahmen durchgeführt (siehe Tabelle 1.2). Am 16.6. fuhr *Polarstern* nach Longyearbyen mit Ankunft am 21.6. Bis zum Ende von PS106 am 20.7.2017 in Tromsø wurden die bordseitigen atmosphärischen Messungen kontinuierlich weitergeführt. Die atmosphärischen Messungen fanden größtenteils im Rahmen des Sonderforschungsbereiches TR 172 „Arctic Amplification“ statt. Die gesamte Fahrtroute ist in Abbildung 1.1 dargestellt; Abbildung 1.2 zeigt die Übersicht über die Expeditionsgebiete beider Fahrtabschnitte, 1.3 die Driftroute während der zweiwöchigen Eisstation während der Expedition PS106/1.

Der Fahrtabschnitt PS106/2 unter Leitung von Hauke Flores startete plangemäß mit dem Auslaufen in Longyearbyen am 23.06.2017. *Polarstern* umrundete die Südspitze Spitzbergens, um erste Stationen auf dem Barentssee-Shelf östlich des Archipels anzulaufen. Auf dem Weg in dieses Gebiet wurden nach Verlassen der 12-Meilen-Zone das auf PS106/1 begonnene Programm kontinuierlicher Messungen von Parametern der Wassersäule und der Atmosphäre wieder aufgenommen. Neu hinzugekommen war die Quantifizierung von Vögeln und Meeressäugern durch ein Beobachtungsteam von Wageningen Marine Research (WMR). Ab dem 25.06.2017 wurde die Oberflächenschicht täglich vom Schlauchboot aus beprobt, und ein regelmäßiges Programm von CTD-Stationen begonnen. Von nun an wurden bei geeigneten Wetterbedingungen spektraloptische Messungen, Wildtierzählungen und Eisdickensurveys mit dem Helikopter durchgeführt. Am 26.06.2017 wurde die erste von insgesamt fünf Eisstationen auf PS106/2 durchgeführt. Im Anschluss wurde die Grundschleppnetz-Beprobung in der Eisrandzone südlich der Insel Kvitoya begonnen. Die zweite Eisstation wurde nördlich von Kvitoya am 29.06.2017 durchgeführt. Danach wurde die regelmäßige Beprobung von Zooplankton und Untereis-Lebensgemeinschaften und biologischen und physikalischen Wassersäulenparametern mit SUIT, RMT, Multinetz, LOKI und CTD begonnen. Bei der Überquerung des Schelfhanges wurde ein hydrographischer Transekt mit CTD-Stationen im Abstand von 2-3 Seemeilen durchgeführt. Danach setzten wir unser Beprobungsprogramm entlang 33°0 in Richtung Norden fort. Am 3. Juli erreichten wir die dritte Eisstation bei 81°39’N 32°27‘0. Von dort aus wurde das Beprobungsprogramm fortgesetzt, bis *Polarstern* die nördlichste Position dieser Reise mit einer Eisstation am 07.07.2017 bei 83°43’N 32°18’0 erreichte. Von dort aus verlief der Kurs in südwestlicher Richtung auf die Eisscholle von PS106/1 zu. Die PASCAL-Scholle wurde am 11.07.2017 erreicht. Hier wurden nach dem üblichen physikalischen, biologischen und atmosphärenkundlichen Beprobungsprogramm autonome Messgeräte geborgen, die seit Verlassen der Scholle einen Monat zuvor Daten aufgezeichnet hatten. Im Anschluss an diese letzte Eisstation wurde ein weiterer hydrographische Transekt über den Schelfhang Spitzbergens absolviert. Im Anschluss umfuhr *Polarstern* die Inseln

Spitzbergen und Nordaustlandet nordseitig, um in der Eisrandzone östlich dieser Inseln die Grundschleppnetzfischerei wiederaufzunehmen. Nach der erfolgreichen Durchführung von sieben Fischereistationen mit begleitender CTD- und Zooplanktonbeprobung wurde die Stationsarbeit am 17.07.2017 beendet. *Polarstern* erreichte den Hafen von Tromsø plangemäß am 20.07.2017 morgens.

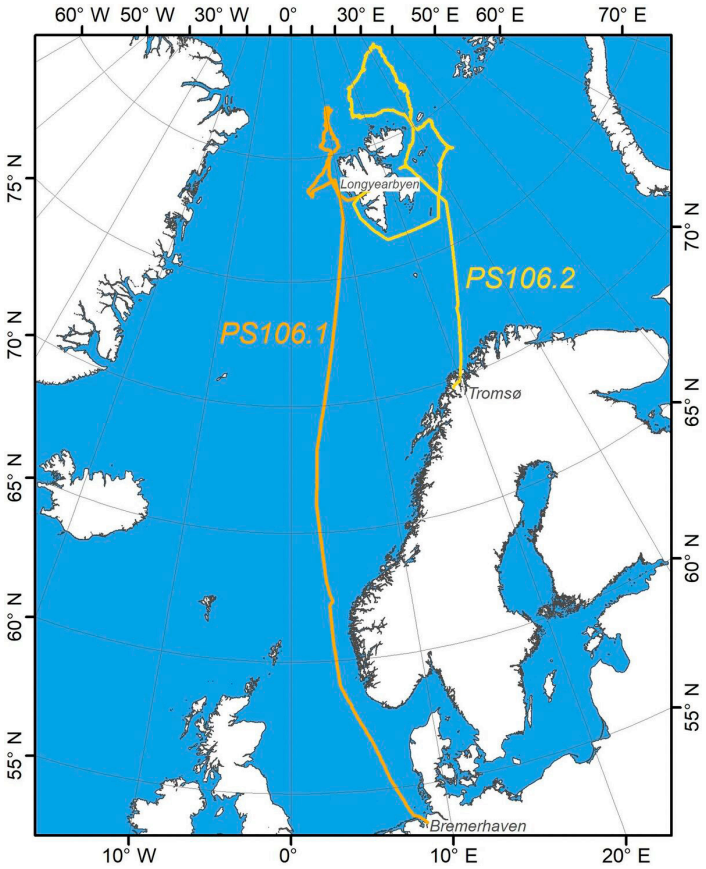

Abb. 1.1: Verlauf der Polarstern-Expeditionen PS106/1 and 2

Siehe https://doi.pangaea.de/10.1594/PANGAEA.881579 und https://doi.pangaea.de/10.1594/PANGAEA.881580 für eine Darstellung des master tracks inVerbindung mit der Stationsliste für PS106/1.

Fig 1.1: Cruise track of Polarstern expeditions PS106/1 and 2.

See https://doi.pangaea.de/10.1594/PANGAEA.881579 and https://doi.pangaea.de/10.1594/PANGAEA.881580 to display the master track in conjunction with the list of stations for PS106/2.

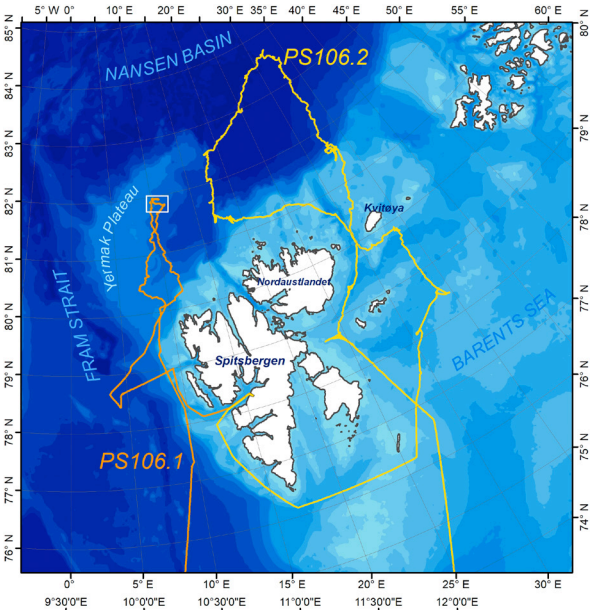

Abb. 1.2: Übersicht des Expeditionsgebietes
Fig. 1.2: Overview of the expedition area

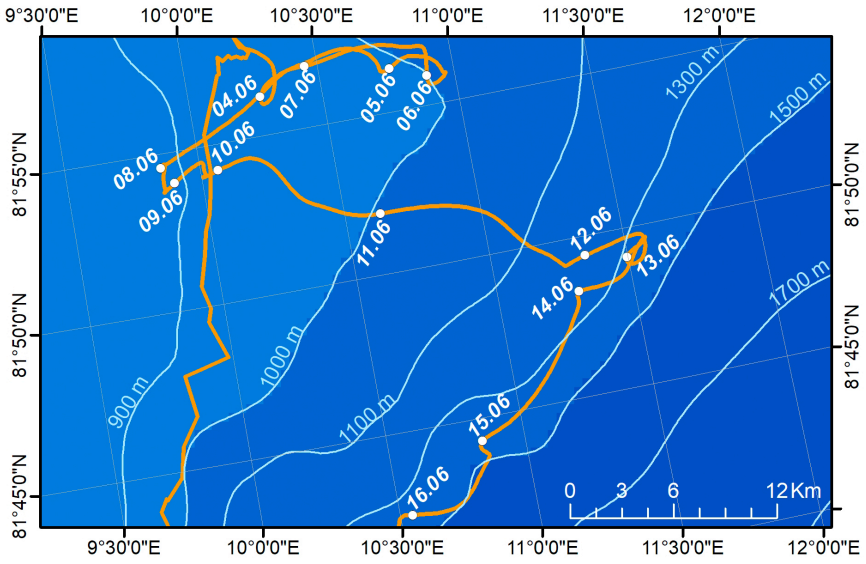

Abb. 1.3: Driftroute während der zweiwöchigen Eisstation während PS106

Fig. 1.3: Drift pattern during the 2 week ice station of PS106

SUMMARY AND ITINERARY

Summary

The Polar Regions are important components in the global climate system. The widespread surface snow and ice cover in Polar Regions strongly impacts the surface energy budget, which is tightly coupled to global atmospheric and oceanic circulations. Here, the interaction of different Arctic feedback mechanisms is not yet completely understood. For example, the coupling of sea ice, clouds and aerosol in the transition zone between open ocean and sea ice is not fully understood so far. Therefore, this issue has been addressed in the **PASCAL** (Physical feedbacks of Arctic PBL, Seaice, Cloud And Aerosol; PS106/1) project to improve our understanding of the recent dramatic reduction in Arctic sea-ice in the boreal summer. For this purpose the TROPOS-OCEANET and aerosol instrumentation on board of *Polarstern* provide standard and additional spectral radiation measurements to determine the surface energy budget and a detailed characterization of surface, cloud and aerosol properties. Identical measurements have been carried out from the German – French *AWIPEV* Research Base in Ny-Ålesund close to the open ocean while *Polarstern* remained in the sea ice. The observations of both surface stations had been closely coordinated with collocated airborne activities of the *Polar 5* and *Polar 6* AWI aircraft operating between both stations along the gradient of sea ice

concentration as well as close to *Polarstern*. These airborne observations were supplemented by observations of the boundary layer structure (mean and turbulent quantities) from tethered balloon and several small Unmanned Airborne Vehicles UAV's, which were operated during the ice station nearby *Polarstern*. In parallel oceanographic, physical and biological research were conducted on the drifting ice floe.

Polar cod *Boreogadus saida* takes a key role in Arctic ecosystems, because it constitutes the staple food of seals and seabirds. Young polar cod live often associated with the underside of sea ice for foraging and protection from higher predators. Due to climate change, the extent of the under-ice habitat is decreasing. On PS106/2, **SiPCA** (Survival of Polar Cod in a Changing Arctic Ocean; PS106/2) aimed to investigate the importance of sea ice for polar cod in the Barents Sea and the adjacent Arctic Ocean. We simultaneously sampled the spatial distribution of polar cod, its prey, its predators and other environmental parameters using fishing nets and ocean sensors. In parallel, we continued large parts of the continuous atmospheric sampling programme begun on PS106/1, and investigated the physical and biogeochemical properties of sea ice and melt ponds during five sea ice stations. At the end of the expedition, we revisited the ice floe of PS106/1 to collect more samples, conduct measurements, and to retrieve instruments left for continuous measurements during PS106/2. The data obtained from this expedition will contribute to a more quantitative understanding of the sea ice-associated ecosystem, its importance for polar cod, physical and biogeochemical processes of sea ice and meltponts, as well as atmospheric dynamics in the Arctic.

Itinerary

On May 24 2017 *Polarstern* set sails in Bremerhaven and reached a suitable nearly circular ice floe with a diameter of roughly 2.5 nautical miles (nm) at (82° 57.7' N, 10° 14.6' E) in the morning of June 3. On the way to the floe daily stops around noon were performed to sample water probes operating from a rubber boat and to perform radiation measurements. Furthermore, five SVP drifter and four ARGO floats were released on the way. After passing Longyearbyen daily CTD programme was running until the end of PS106/1. On the ice floe camp continuous measurements of the energy budget at the surface and the state of the cloudy atmosphere were performed from June 4 to June 15. In parallel, sea ice physical, biological and biogeochemical measurements were carried out. Table 1.1 provides an overview on those days where *Polarstern* was fixed to the ice floe. Due to bad visibility conditions the measurements on the ice floe were cancelled for parts of June 6 and June 9 as well as completely for June 12. On the sea side regular CTD measurements down to the ocean floor on a daily basis as well as several sediment samples and multi-net operations were carried out. Helicopter operations were performed for mounting and dismounting and mainly for remote sensing and probing of samples (see Table 1.2). On June 16 *Polarstern* continued to Longyearbyen with arrival on June 21. The continuous ship-based atmospheric measurements were running until the end of PS106 in Tromsø on July 20 2017. The atmospheric measurements were mainly performed in the framework of the Collaborative Research Cluster TR 172. Fig 1.1 shows the cruise track of *Polarstern* expedition PS106, Fig. 1.2 provides an overview of the expedition area, and Fig. 1.3 the drift pattern during the 2 week ice station of the expedition PS106.

Polarstern left Longyearbyen according to schedule on June 23, 14:00 local time. We sailed around Svalbard, first on its southern, then eastern side. Continuous measurements of the water column and the atmosphere were started after leaving the 12 nm-zone, as noted in the research application. On June 24 we started a series of daily sampling stations focussing on the chemical composition of the sea surface microlayer. An ice station was completed on June 26. Here, we took samples of sea ice and the underlying water and deployed our ROV. We then

performed 3 stations south of the island Kwitoya, where we used bottom trawls, CTDs, plankton nets and collected water samples. On June 27, we continued our way northwards. North of the island Kwitoya, we performed another ice station on June 29. Proceeding northwards from there, we sampled with various plankton nets and CTDs. After arriving on the shelf slope, we started a hydrographical transect into the deep sea, performing CTD casts at high spatial resolution. On July 1, we concluded our hydrographical transect across the Barents Sea shelf slope between 32 and 33°E. We then proceeded northwards conducting continuous measurements of atmospheric properties and biological water column parameters. Surface microlayer samples were taken, CTDs, zooplankton nets and our under-ice trawl were deployed at regular intervals together with optical and acoustical zooplankton detectors. On the night from June 2 to June 3 we conducted the third ice station of this expedition. We then resumed our sampling of atmospheric, environmental and biological parameters as we continued north until reaching our northernmost position at 83°43'N 32°18'E on July 6. At this location we performed the fourth ice station of PS106/2. From there we proceeded south, towards the PASCAL ice floe of PS106/1. Here, we completed the fifth ice station of this expedition on the night from July 11 to July 12. Leaving the PASCAL floe, we conducted a hydrographical transect up the Svalbard shelf slope in the night from July 12 to July 13. From July 15 to July 17 we conducted a bottom trawl survey to the east of the islands Nordaustlandet and Spitsbergen, between the ice edge and the 12-miles zone. This survey also comprised daily casts with the CTD and various plankton samplers. The scientific station work was completed on July 17. According to schedule we arrived at our final destination Tromsø in the morning of July 20.

Tab. 1.1: List of Ice stations at the ice floe during PS106/1. All data correspond to the start of the ice station.

Ice station number & cast	Start date time [UTC]	Latitude	Longitude	Depth [m]	Speed [kn]	Course	Wind Dir [°]	Wind speed [m/s]
PS106_20-1	03.06.17 09:30	81° 57.827‘ N	010° 14.607‘ E	979,3	0,3	115,5	265,0	6,5
PS106_21-2	04.06.17 06:07	81° 56.954‘ N	010° 24.533‘ E	1002,4	0,2	78,3	194,0	5,3
PS106_22-1	05.06.17 07:25	81° 56.381‘ N	010° 55.797‘ E	1076,5	0,2	131,7	305,0	2,7
PS106_23-2	06.06.17 06:14	81° 56.869‘ N	010° 53.947‘ E	1070,6	0,0	90,0	98,0	5,4
PS106_24-2	07.06.17 06:40	81° 56.535‘ N	010° 18.455‘ E	987,5	0,3	232,6	50,0	6,9
PS106_25-1	08.06.17 06:10	81° 54.591‘ N	009° 52.256‘ E	930,8	0,1	212,3	108,0	2,3
PS106_26-2	09.06.17 06:37	81° 54.526‘ N	010° 00.361‘ E	946,8	0,1	118,0	173,0	5,7
PS106_27-1	10.06.17 06:45	81° 54.249‘ N	010° 13.820‘ E	983,4	0,3	125,5	240,0	5,1
PS106_28-2	11.06.17 06:15	81° 51.438‘ N	010° 59.766‘ E	1150,6	0,3	120,5	257,0	8,9
PS106_29-2	12.06.17 06:31	81° 49.749‘ N	011° 32.560‘ E	1534,4	0,1	91,1	252,0	4,5
PS106_31-2	14.06.17 06:14	81° 47.884‘ N	011° 17.088‘ E	1485,9	0,1	201,4	7,0	6,1
PS106_32-2	15.06.17 06:41	81° 43.860‘ N	010° 51.458‘ E	1608,1	0,0	140,0	4,0	2,9
PS106_33-2	16.06.17 06:37	81° 42.400‘ N	010° 30.094‘ E	1405,6	0,0	239,4	38,0	4,0

Tab. 1.2: Scientific use of *Polarstern* helicopters during PS106/1. Pilots: Vaupel=VAL; Kendzia=KEJ / PS=*Polarstern* / ZZZZ=undefined landing site (e.g. ice flow = Eisscholle)

No	Date	Start	Landing	Pilot	Start-time	Landing time	Flight time	Scientific purpose
1	31.05.17	PS	ZZZZ	VAL	07:56	08:25	0:29	Abbergen Boje Nikolaus
2	31.05.17	ZZZZ	PS	VAL	09:22	10:02	0:40	Abbergen Boje Nikolaus
3	04.06.17	PS	PS	VAL	07:53	08:08	0:15	Außenlast ROV
4	04.06.17	PS	PS	VAL	08:44	08:58	0:14	Außenlast Tomate
5	04.06.17	PS	PS	VAL	10:46	11:07	0:21	Außenlast ROV
6	05.06.17	PS	PS	KEJ	08:46	09:24	0:38	Erkundung Oppelt
7	05.06.17	PS	PS	KEJ	11:55	12:26	0:31	Birnbaum Kamera
8	07.06.17	PS	PS	KEJ	11:18	12:18	1:00	Birnbaum Kamera
9	08.06.17	PS	ZZZZ	VAL	08:15	08:19	00:04	Erkundung Oppelt
10	08.06.17	ZZZZ	PS	VAL	09:19	09:35	00:16	Erkundung Oppelt
11	08.06.17	PS	PS	VAL	13:25	14:20	00:55	Birnbaum Kamera
12	09.06.17	PS	PS	VAL	07:04	07:13	00:09	Erkundung Macke
13	09.06.17	PS	PS	KEJ	13:24	13:34	00:10	Erkundung Macke
14	10.06.17	PS	PS	KEJ	07:16	09:07	01:51	Birnbaum Kamera
15	10.06.17	PS	PS	VAL	10:02	10:15	00:13	Fotos ROV
16	10.06.17	PS	PS	KEJ	11:42	13:12	01:30	Birnbaum Kamera
17	14.06.17	PS	PS	KEJ	11:38	12:52	01:14	Birnbaum Kamera
18	15.06.17	PS	PS	VAL	11:39	13:12	01:33	Birnbaum Kamera
19	16.06.17	PS	PS	VAL	07:44	08:02	00:18	Außenlast ROV
20	16.06.17	PS	PS	VAL	11:37	11:48	00:11	Außenlast Tomate
21	17.06.17	PS	PS	KEJ	11:41	13:34	01:53	Birnbaum Kamera
22	18.06.17	PS	PS	KEJ	07:53	09:52	01:59	Birnbaum Kamera
1	6/25/2017	PS	PS	VAL	16:45	18:19	1:34	Bram Tierzählung
2	6/25/2017	PS	PS	KEJ	19:07	21:01	1:54	Gerit Fotoflüge
3	6/26/2017	PS	PS	VAL	11:25	13:14	1:49	Gerit Fotoflüge
4	6/26/2017	PS	PS	KEJ	14:04	16:10	2:06	Bram Tierzählung
5	6/27/2017	PS	PS	VAL	10:14	11:50	1:36	Ben EMBird
6	6/27/2017	PS	PS	KEJ	13:58	14:23	0:25	Gerit Fotoflüge
7	6/27/2017	PS	PS	KEJ	15:07	16:43	1:36	Gerit Fotoflüge
8	6/30/2017	PS	PS	KEJ	13:40	14:57	1:17	Gerit Fotoflüge
9	7/1/2017	PS	PS	KEJ	9:26	10:54	1:28	Ben EMBird
10	7/1/2017	PS	PS	VAL	13:37	15:23	1:46	Gerit Fotoflüge
11	7/1/2017	PS	PS	VAL	16:20	16:29	0:09	Bram Tierzählung
12	7/2/2017	PS	PS	KEJ	10:02	12:06	2:04	Ben EMBird

No	Date	Start	Landing	Pilot	Start-time	Landing time	Flight time	Scientific purpose
13	7/2/2017	PS	PS	VAL	13:02	15:02	2:00	Bram Tierzählung
14	7/2/2017	PS	PS	VAL	16:41	18:42	2:01	Gerit Fotoflüge
15	7/3/2017	PS	PS	KEJ	9:44	11:41	1:57	Gerit Fotoflüge
16	7/3/2017	PS	PS	VAL	13:10	15:12	2:02	Bram Tierzählung
17	7/3/2017	PS	PS	KEJ	16:00	17:26	1:16	Gerit Fotoflüge
18	7/5/2017	PS	PS	VAL	10:17	11:52	1:35	Gerit Fotoflüge
19	7/9/2017	PS	PS	KEJ	13:31	15:14	1:43	Gerit Fotoflüge
20	7/11/2017	PS	PS	VAL	10:38	12:34	1:56	Gerit Fotoflüge
21	7/11/2017	PS	PS	KEJ	17:00	19:08	2:08	Ben EMBird
22	7/12/2017	PS	PS	VAL	6:51	7:14	0:23	Außenlast Marcel
23	7/12/2017	PS	PS	KEJ	8:28	10:23	1:55	Gerit Fotoflüge
24	7/12/2017	PS	PS	VAL	10:51	13:00	2:09	Bram Tierzählung
25	7/12/2017	PS	PS	KEJ	14:57	15:13	0:16	Außenlast Marcel
26	7/14/2017	PS	PS	KEJ	10:57	12:25	1:28	Bram Tierzählung
27	7/14/2017	PS	PS	VAL	13:19	14:15	0:56	Gerit Fotoflüge
28	7/15/2017	PS	PS	VAL	9:14	11:22	2:08	Ben EMBird
29	7/15/2017	PS	PS	KEJ	12:36	14:36	2:00	Gerit Fotoflüge
30	7/15/2017	PS	PS	VAL	15:15	16:17	1:02	Bram Tierzählung

2. WEATHER CONDITIONS DURING PS106/1 AND PS106/2

Max Miller[1], Hartmut Sonnabend[1] [1]DWD

At noon on Wednesday, May 24, 2017, *Polarstern* left Bremerhaven for the campaign PS106/1. Moderate to fresh north-westerly winds, 14°C and cloudy skies were observed.

A high over the English Channel spread slowly towards North Sea and north-westerly winds continued at 4 to 5 Bft on Ascension Day (May 25). Afterwards the high built a ridge towards another high over Greenland. Therefore winds veered south and freshened up to Bft 6 on Friday. The warmer air masses caused temporary fog over the colder water off Norway.

Meanwhile a low had reached Iceland and headed towards Norway. It crossed *Polarstern* during the night to Sunday (May 28). Winds veered west at first and then suddenly east while increasing up to Bft 7 and causing a sea state of 3.5 m. Another low had moved from Russia to Novaya Zemlya heading towards Barents Sea. On Monday (May 29) we got at its west side and northerly winds peaked at Bft 8 during the night to Tuesday. The low moved on to North Cape and therefore north-easterly winds caused a Föhn situation off the west coast of Svalbard with sunny skies. But on Wednesday (May 31st) easterly winds increased rapidly up to Bft 7 at the north-western edge of the island forced by the parallel north coast. At the same time we reached the ice and first fog patches were present.

On Thursday (June 01st) a high spread from Severnaya Zemlya towards Greenland Sea via Svalbard and got the dominant feature for some days. *Polarstern* (now at an ice floe for 2 weeks) operated at its northwest side. South-westerly winds peaked at Bft 6 on Saturday (June 03) and abated to Bft 4 afterwards. Low stratus clouds were prevailing.

On Whit Monday the high weakened. On Tuesday (June 06) a low moved from the Lofoten Islands towards Jan Mayen. Winds veered east and freshened up to Bft 5 for short times. But the low level clouds with poor contrast continued.

A high over Beaufort Sea built a ridge towards Barents Sea and on Friday (June 09) a separate high centre formed over Svalbard. Winds veered southwest and increased up to Bft 6 for short times. On Saturday the subsidence temperature inversion reached the ground and caused a sunny day at +2° C. But already during the night to Sunday (Jun 11) the moist ground layer was renewed connected with low stratus and fog patches.

On Tuesday (June 13) a low over Kara Sea spread northwest and therefore the light to moderate winds veered north. The low moved slowly towards Severnaya Zemlya and *Polarstern* stayed at its outer edge during the rest of the week. Northerly winds didn't exceed Bft 4 and light snowfall was temporarily observed.

On Sunday (June 18) a ridge built from Greenland towards Svalbard. At first light winds were prevailing, but on Tuesday (June 20) northerly winds were accelerated up to 5 to 6 Bft by a jet like effect along the west coast of Svalbard.

On Wednesday morning, June 21, 2017, *Polarstern* anchored off Longyearbyen at light to moderate winds from northwest.

On early Friday afternoon, June 23, 2017, *Polarstern* left Longyearbyen again for PS106/2 at light to moderate north-westerly winds, 5°C and cloudy skies.

The high over Greenland still built a ridge east across Svalbard. Leaving the fjord winds from northwest freshened up to Bft 5. But already during the night to Saturday (June 24) winds abated while we rounded-up the south-western end of Svalbard and remained light and variable until Sunday.

A low near North Pole was on its way to Ellesmere Island and built a trough to Fram Strait. Inside the trough a secondary low formed and moved northeast crossing Svalbard. Only on Tuesday (June 27) southerly winds increased up to 6 Bft for short times. The low passed *Polarstern* on Thursday (June 29), moderate winds veered north and it was snowing.

On Saturday (July 01) a small high formed south of Svalbard and moved slowly east. On Sunday and Monday it caused mostly clear skies and good flight conditions at moderate south-westerly winds. Again a low (now near the New Siberian Islands) built a trough to Fram Strait, which followed the high to east. On Tuesday (July 04) low stratus and fog patches became dominant again at south to southwest 4 to 5 Bft. Later on winds abated.

On Friday (July 07) a low developed north of the Kola Peninsula, which moved north across Franz-Josef-Land. On Saturday northerly winds freshened up to Bft 5 at its west side and veered southwest until Monday (July 10). Low ceiling and fog patches hampered flight operations. A high near Novaya Zemlya built a ridge to Svalbard. Moderate to fresh winds veered south drying the moist ground layer from Tuesday (July 11) on.

On Wednesday (July 12) a low formed over the Gulf of Bothnia, moved north and crossed *Polarstern* during the night to Friday (July 14) while still operating north of Svalbard. At first winds veered east, increased up to 6 Bft and jumped west to southwest on Friday with peaks at Bft 7. On Saturday a ridge followed causing light winds from south and good flight conditions.

A new low over Denmark Strait moved to Jan Mayen and from Sunday (July 16) on *Polarstern* (now east of Svalbard) got at its northeast side. Southeast to easterly winds didn't exceed Bft 6. Another low formed near St. Petersburg and reached North Cape on Tuesday (July 18). On Wednesday we observed west to north-westerly winds 6 and for short times 7 Bft while we were heading to Tromsø. At the same time a high near Trondheim was already on its way north.

On Thursday morning, July 20, 2017, *Polarstern* reached Tromsø at light to moderate northerly winds.

For further statistics see Fig. 2.1 – Fig. 2.5.

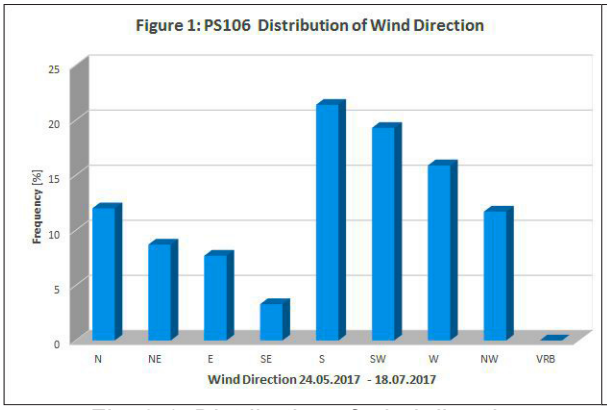

Fig. 2.1: Distribution of wind direction

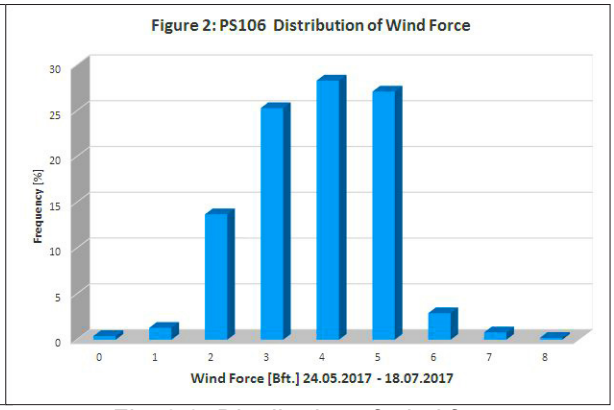

Fig. 2.2: Distribution of wind force

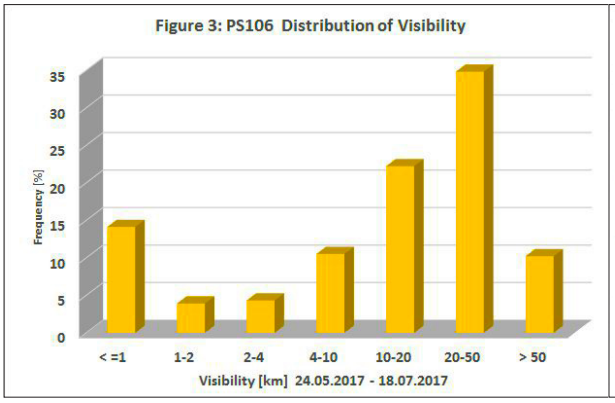

Fig. 2.3: Distribution of visibility

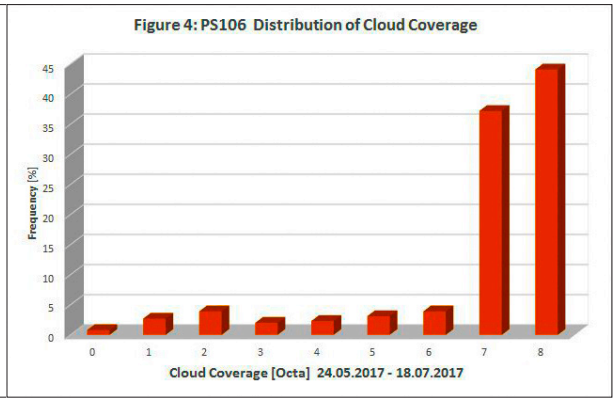

Fig. 2.4: Distribution of cloud coverage

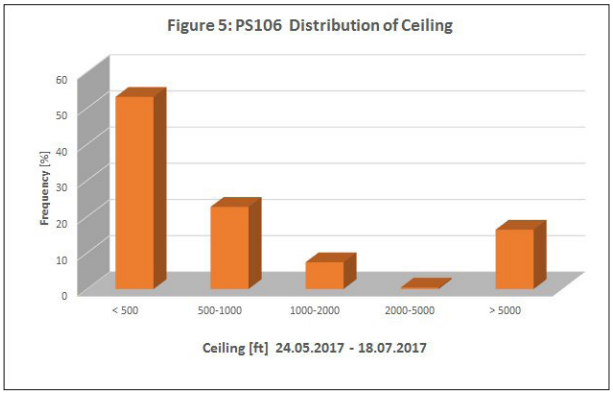

Fig. 2.5: Distribution of ceiling

3. PHYSICAL FEEDBACKS OF ARCTIC PBL, SEAICE, CLOUD AND AEROSOL (PASCAL)

Andreas Macke[1], Carola Barrientos[1], Marlen Brückner[2], Thomas Conrath[1], Ulrike Egerer[1], Ronny Engelmann[1], Susanne Fuchs[1], Xianda Gong[1], Matthias Gottschalk[2], Hannes Griesche[1], Markus Hartmann[1], Simonas Kecorius[1], Henry Kleta[3], Ulrich Küster[4], Felix Lauermann[2], Manuela van Pinxteren[1], Martin Radenz[1], Thomas Ruhtz[4], Stephan Schön[5], Hannes Schulz[6], Kai Szodry[1], Teresa Vogl[1], André Welti[1], Jonas Witthuhn[1], Marco Zanatta[6], Sebastian Zeppenfeld[1]
not on board : Hartmut Herrmann[1], Maik Merkel[1], Frank Stratmann[1], Alfred Wiedensohler[1]

[1]TROPOS
[2]LIM
[3]DWD
[4]FU-Berlin
[5]SZ via TROPOS
[6]AWI

Grant-No. AWI_PS106/1_2-00

Objectives

a) Radiation budget & atmosphere remote sensing

The net energy budget at the surface is the driving force for most physical processes in the climate system. It is mainly determined by the complex spatial distribution of humidity, temperature and condensates in the atmosphere. The project aims at observing both the radiation budget and the state of the cloudy atmosphere as accurate as possible to provide realistic atmosphere-radiation relationships for use in climate models and in remote sensing. While similar experiments have been performed from land (Macke et al.,, 2017)) and open ocean stations (Kalisch and Macke, 2012), only few data from measurements exist over polar areas.

A multichannel microwave radiometer is applied to continuously retrieve temperature and humidity profiles as well as cloud liquid water path over the ocean. Time series of these profiles will resolve small-scale atmospheric structures as well as the effects of the mean state of the atmosphere and its variability on the co-located measurements of the downwelling shortwave and longwave radiation with different types of pyranometers (thermal and optical, fixed and gimbal-mounted) to allow intercomparison with model and satellite data (Hanschmann et al., 2012). Most instruments are integrated in the container-based atmosphere observatory. A network of autonomous pyranometer stations enables to retrieve the spatiotemporal variability of the downwelling solar irradiance (Madhavan et al., 2017) that may have an influence on the melting processes of the Arctic sea ice and melt pond mix.

Since more than 20 years TROPOS develops and operates advanced lidar systems in order to study optical and microphysical aerosol and cloud properties in the troposphere. The system PollyXT, a semi-autonomous multiwavelength polarization Raman lidar was operated inside a container, together with the radiation and microwave sensing equipment. The lidar is able to measure independently profiles of particle backscatter at three wavelengths and extinction at two wavelengths, which allows identifying particle type, size, and concentration

(Kanitz et al., 2013). Additionally particle depolarisation is measured in order to discriminate between spherical and non-spherical particles, e.g. water clouds vs. ice clouds. The lidar is equipped with a measurement channel for atmospheric water-vapour, too. The data are used to characterize long-range transport of aerosol and to identify pollution. The determined height-resolved aerosol extinction completes the radiation measurements.

A 35 GHz cloud radar is utilized to obtain continuous time series of vertical profiles of cloud and ice water as well as vertical velocity throughout the entire troposphere. These are the key data to resolve two dimensional cloud processes for comparison with high-resolution dynamical models and with remote sensing from space as for radiation closure studies. The algorithms to convert radar reflectivity measurements into cloud physical properties have been developed over the years within the framework of the European ACTRIS project (Bühl et al., 2016).

The aim of up and down-welling spectral radiance measurements and auxiliary data analysis from FU-Berlin is the retrieval of aerosol parameter and the measurement of the upwelling and downwelling polarized light coming from the Sun, scattered by the atmosphere and reflected by the surface. For this cruise reflectance measurements of ice, snow and water during different atmospheric conditions were performed. Together with the standard radio soundings, the vertical profiles of temperature and pressure a sufficient set of input parameters will drive radiative transfer models to characterize the status of the atmosphere. The results of the radiative transfer model and the measurements can be compared to find differences between model and measurements of the light field to improve the existing retrieval methods and to develop new methods with the additional information of the polarized state of light.

b) Aerosol in-situ measurements

The portfolio of the Aerosol Group at TROPOS includes the *in-situ* characterization of atmospheric aerosols in urban as well as remote background atmospheres, the characterization of regional and urban air quality, the examination of hygroscopic particle properties, the measurement and simulation of *in-situ* aerosol optical properties, the investigation of atmospheric transport processes, and the development of new and improved instruments for physical aerosol characterization.

Furthermore, AWI performed black carbon measurements both on the ship and on the ice floe. The scientific goal is to understand atmospheric feedbacks of black carbon on snow and sea ice. This will be done by quantifying atmospheric black carbon presence and its properties close to the surface of sea ice. Black carbon concentration, properties and absorption have been determined in the snow layer overlaying the sea ice. Snow properties have been monitored with an IceCube. The campaign is also the test bench for the freshly developed single particle soot photometer with extended range.

Ice Nucleating Particles (INP) and Cloud Condensation Nuclei (CCN) may significantly influence the microphysical and radiative properties of Arctic clouds. Information concerning the concentrations of Arctic INP, their chemical nature (mineral and/or organic), and their origin (local sources or long range transport) is sparse, therefore the Cloud Group at TROPOS plans to investigate and quantify the Arctic aerosol in respect to its ability to form ice and liquid cloud droplets. In collaboration with the chemical analysis performed by *d) Sea surface microlayer (SML) measurements* we may able to identify potential sources of INP and CCN.

c) Tethered balloon-borne measurements of energy budget of the cloudy atmospheric boundary layer in the central Arctic

The quantification of the energy fluxes (turbulent fluxes of sensible and latent heat, momentum and radiative fluxes) within the Atmospheric Boundary Layer (ABL) in the central Arctic

represents a key issue for an improved understanding of the Arctic response to Global Warming ("Arctic Amplification"), see Jeffries et al. (2012, 2013), Overland et al. (2012), Wendisch et al., (2017). The melting of Arctic sea ice is decisively linked with the surface energy fluxes. Surface sensible and latent turbulent heat fluxes are comparably low over sea ice and in this case the energy budget is dominated by the solar and terrestrial radiative fluxes, which are mostly influenced by the local cloud situation (e.g., Curry, 1986). If sea-ice is noticeably reduced, as observed within the past 20 years, the mean surface temperature increases and the typical low-level temperature inversion is weakened (lower stability). This would increase the turbulent energy fluxes in the Arctic ABL including the moisture flux, which would promote cloud formation.

Arctic low-level clouds exhibit several typical features compared to mid-latitude clouds, which cause important and specific effects (e.g., in terms of radiative transfer) and challenge the numerical modeling of Arctic low-level clouds. In particular, the often mixed-phase character of Arctic low-level clouds and the more complicated vertical structure of the ABL in the Arctic cause major issues compared to mid-latitudes. Arctic low-level clouds mostly warm the ABL. They are frequently organized in several distinct layers and the turbulent energy fluxes can be de-coupled from the surface fluxes (e.g. Shupe et al., 2013). Occasionally, moisture inversions coincide with the temperature inversion and the cloud layers penetrate the inversions, that is, the temperature inversion is not necessarily capping the cloud layer.

For an improved understanding of the cloudy ABL in the Arctic tethered balloon–borne measurements of turbulent and radiative energy fluxes are performed under different cloudy conditions and thermal stratification during the ice camp of this *Polarstern* cruise.

d) Sea surface microlayer (SML) measurements

The oceans are suggested to be a significant source for aerosol particles in the marine boundary layer. In this context not only the bulk water but especially the uppermost layer of the ocean, the sea surface microlayer (SML), might play an important role in the transport of matter to the atmosphere as it is the interface for all gaseous, liquid and particulate mass transfer between sea and air (e.g. Cunliffe et al., 2013). The role of the SML is poorly understood to date. However, especially in the Arctic region the SML is supposed to be the origin of organic biopolymers, among them acidic polysaccharides, which are suggested to be transported into the atmosphere via bubble bursting processes (Orellana et al., 2011; Wilson et al., 2015). These compounds might be important in aerosol and cloud processes, e.g. acting as ice nuclei (IN). We aim for a detailed chemical investigation of the SML and the bulk water with emphasis on studying the broad spectrum of carbohydrate composition and transparent exopolymer particles (TEP). Simultaneously, we will study the ice nucleating abilities of the SML and the bulk water to combine the chemical information with their potential physical effects. We will also collect data of possible biogeochemical drivers for the marine biopolymers.

Work at sea

Upon departure from Bremerhaven both container-based atmosphere observatories will be installed at the deck of *Polarstern*. Most measurements will be performed continuously underway and at the ice station. The following individual instruments are combined:

1. Multichannel microwave radiometer HATRPO. The instrument requires a calibration with liquid nitrogen at the port of Bremerhaven
2. Whole sky imager for cloud structure measurements
3. Multiwavelength polarization Raman lidar PollyXT

4. 35 GHz cloud radar
5. Handheld sun photometer (Microtops) for aerosol and cloud optical thickness
6. Standard meteorological data logging with extended radiation measurement equipment
7. Multispectral shadow-band radiometer
8. *In-situ* aerosol measurements
9. Measurement of cloud- and ice-nuclei concentration
10. Tethered ballon
11. Deployment of meteorological and oceanographic drifters and floats (SVP and ARGO).
12. Regular calibration of SP2xr (black carbon measurements)
13. Spectral solar radiation measurements of irradiance and radiance
14. Digitel filter sampler (PM1 & PM10 on quartz fibre filter; PM1 on polycarbonate)
15. Cloud water sampler
16. 5 stage Berner impactor for size segregated aerosol sampling
17. Glass plate SML sampler

During the passage towards the ice five meteorological drifting buoys and four ARGO floats were deployed in international waters.

Within the OCEANET container the automatic weather station SCAWS had been operated during the entire cruise. The measured parameters included atmospheric pressure, air temperature, rel. humidity and downwelling shortwave and longwave radiation.

Additionally, further pyranometers were installed on the aerosol container and operated during the entire cruise to allow intercomparison between different mounting methods.

a) Radiation budget & atmosphere remote sensing

The OCEANET remote sensing and surface energy budget components were up and running soon after departure from Bremerhaven and measured continuously for the entire cruise except for short shutdowns for maintenance and for safety reasons during helicopter starts and landings. On the ice flow, a network of 15 autonomous pyranometer had been installed to obtain the spatiotemporal variability of the global radiation (Tab. 3.1). The pyranometer are positioned around a high precision shadowband radiometer that serve**d** as a validation point.

The OCEANET container was set up at the aft of the vessel during PS106. The container was stored in the second level at the working deck for the first time. Therefore a scaffolding stair was installed for safe and easy access. During the setup in Bremerhaven, the instruments were put into operation. The microwave radiometer was calibrated with liquid nitrogen before leaving the port, as the ships motions doesn't allow the calibration at sea. The laser was installed in the Raman lidar and measurements were started. The All-Sky camera, the standard meteorological measurements as well as the Pyrgeometer and two fast shortwave radiation sensors were installed at the container roof. Work at sea included continuous observation of the instruments, data backup, quicklook generation, and cleaning of the lidar windows and radiation domes.

During PS106 a web-application was installed which allowed the helicopter pilots to turn of

Fig. 3.1: 35 GHz cloud radar on RV Polarstern during PS106

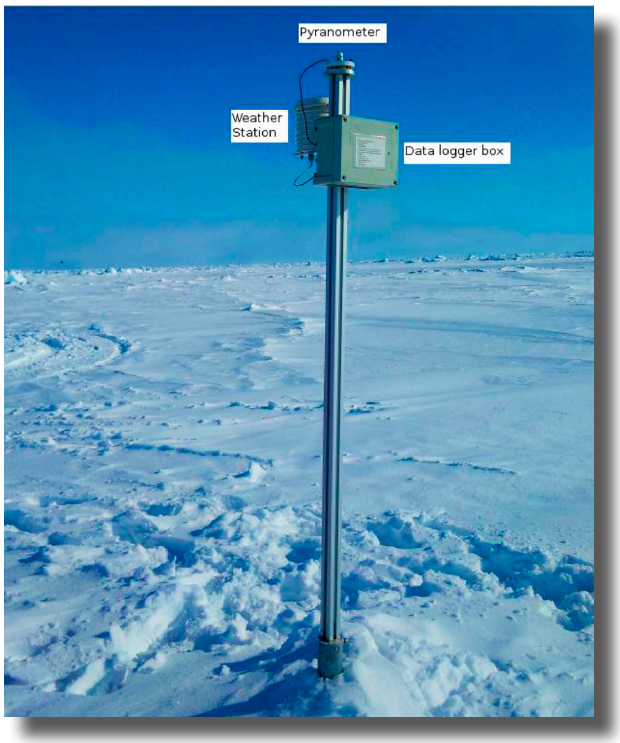

Fig. 3.2: Picture of a pyranometer station in the Arctic ice

the laser beam easily during critical flight manoeuvres above the lidar.

A MICROTOPS sun photometer was operated for the Maritime Aerosol Network (MAN). Unfortunately, not many clear-sky observations were possible because of low clouds.

Additionally to the atmospheric remote sensing devices in the OCEANET container a 35 GHz cloud radar measured continuous profiles of cloud and ice water as well as vertical velocity throughout the entire troposphere since the 25 of May. Only short interruptions due to maintenance of the cloud radar were necessary. The cloud radar was mounted on a stabilization platform to be corrected for the pitch and roll movement of the RV, see Fig. 3.1. To be able to correct the vertical motion of the ship heave data provided by the Hydrins System of *Polarstern* was stored with a frequency of 20 Hz during the whole cruise.

During PS106/1 ice-float (June 5, 2017 – June 16, 2017) 15 pyranometer (see Fig. 3.2) were installed in a relatively large section of the ice-float covering an area of approximately 1,2 km^2 with the aim to capture the small-scale variability of cloud induced radiation fields at the surface. The cleanliness of the dome of the pyranometer and the leveling were checked daily to assure the quality of the data. This process consisted in assigning values to the cleanliness of the dome and the leveling of the pyranometer.

Spectral radiations measurements of down-ward irradiance and radiance were obtained from the Sky RAdiation And Polarization Package (SRAPP). The optical inlets were installed at the top of the aerosol container (see Fig. 3.3). The measured radiation is transported to a spectrometer box in the container by optical fibers. The spectrometer splits up the radiation according to the wavelengths. The spectral range from these measurements is 350-2,200 nm. Under good weather conditions, SRAPP was calibrated as often as possible with a small Ulbricht-integrating sphere. It creates diffuse radiation from a directionally orientated radiation. To obtain the background noise in the data also a dark calibration was performed. During

PASCAL, we already observed different Arctic cloud types like low-level boundary layer clouds, Stratocumulus and mixed-phase clouds as well as high ice clouds. From those measurements after radiometric calibration in the lab, cloud optical and microphysical properties of Arctic clouds will be retrieved using radiative transfer calculations (Brückner et al., 2014). Furthermore, results from these retrievals will be compared to aircraft measurements form *Polar 5* overpasses where identical measurements have been performed. With those collocated observations we will compare the retrievals from two different perspectives, from the ship locking upward and from the aircraft looking downward at the same cloud.

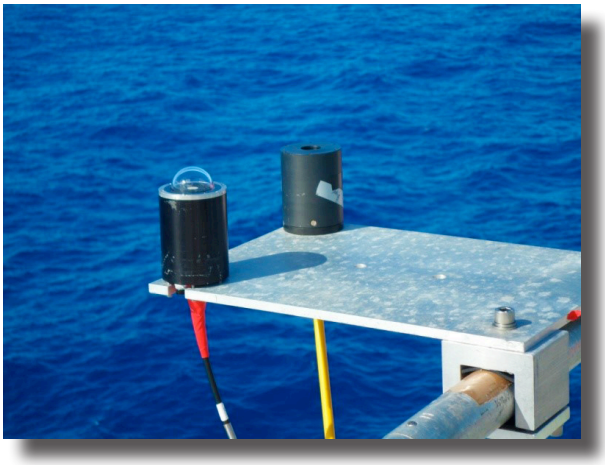

Fig. 3.3: Optical inlets from SRAPP for spectral radiance (right) and irradiance (left) during PASCAL

Spectral irradiance measurements on the ice floe were obtained with the COmpact RAdiation measurement System (CORAS, see Fig. 3.4) with two optical inlets for spectral irradiance. One sensor is measuring the downward radiation from above and one sensor is looking downward to measure the upward spectral radiation. CORAS was calibrated with a small Ulbricht sphere as often as possible. From those observations the spectral surface albedo can be retrieved in a spectral range from 350 to 2200 nm. Using a retrieval algorithm it is possible to retrieve snow grain sizes and also black carbon in snow. Furthermore, two pyrgeometers are measuring broadband terrestrial radiation. To measure the heat fluxes in different snow depth we are using two identical heat flux sensors, which are distributed in different snow depths.

Fig. 3.4: Tripod from CORAS with broadband pyrgeometers (left) and spectral irradiance inlets (right) on the ice floe during PASCAL

Furthermore, during the entire cruise, two upward looking pyranometer have been installed at starboard and portside with the quarter sphere facing the ship shaded, so that both instruments together measure the upwellling broadband solar radiation. Together with the measured incoming solar irradiance this allows to obtain the surface albedo.

Up- and downwelling radiance were measured with two optical systems. A scanning DOAS instrument (Pandora-2s) was mounted at the Peildeck and a scanning hyperspectral polarimeter (URMS/AMSSP) at the Crow's Nest. The Pandora-2s performed scans in the upper hemisphere with 2 high-resolution spectrometer in the UV, VIS and NIR spectral range from 320 to 1,000 nm. Profiles and horizontal distribution of the trace gases NO_2, O_3 and H_2O can be retrieved with the analysed data. The second instrument was scanning the left hemisphere in the spectral range of 400-785 nm and 256 spectral channels. URMS/AMSSP was proposed within the framework of the German priority programme (PP 1294, Atmosphären- und Erdsystemforschung mit dem Forschungsflugzeug HALO (High Altitude and Long Range Research Aircraft)).

b) Aerosol in-situ measurements

Onboard *Polarstern* all measurements were conducted inside a temperature-controlled container laboratory (see Fig. 3.5a) with focus on the particle characterization using high-end scientific instruments (see Fig. 3.5b) in order to study:

- physical aerosol properties using an Aerodynamic Sizer (APS) and Scanning Mobility Particle Sizer (SMPS) for particle number size distributions from 10 nm to 10 µm, and a Volatility and Humidifying Tandem Differential Mobility Particle Sizer (VH-TDMPS) for the hygroscopic growth of the particles;
- Optical properties using a nephelometer and an absorption photometer to measure the particle light scattering and absorption coefficients, respectively; and
- Particle chemical composition using a High Resolution Time of Flight Aerosol Mass Spectrometer (HR-ToF-AMS) for the non-refractory PM1.
- Cloud Condensation Nuclei (CCN) number size distribution and particle number size distribution to determine the particle hygroscopicity using a DMT CCN counter-100 and a Scanning Mobility Particle Sizer (SMPS)
- Ice Nucleating Particle (INP) number concentration using a DMT Spectrometer for Ice Nuclei (SPIN)

In addition to the on-line instrumentations, a Digitel high volume filter sampler (PM10; quartz fibre filters; 3 day sampling) and a Digitel low volume filter sampler (PM1; polycarbonate filters; 8 hour sampling) are installed on the roof of the aerosol container. A cloud water sampler in front of the container collects fog droplets. All these offline samples will be analyzed at TROPOS for their ice nucleating behavior and in close collaboration with the Atmospheric Chemistry Department these will be also characterized chemically. SML, bulk seawater, snow and ice core samples collected around the ship and on the ice floe are also shared between the cloud group (measurement of ice nucleating behavior) and the ACD (chemical characterization).

Most of the instruments measured continuously for the entire cruise except for short shutdowns for maintenance. Exceptions are SPIN, which experienced some problems and only measured irregularly in the first week, and the VH-TDMPS, which also has irregular measurement gaps.

Furthermore, snow sampling and snow properties determination were carried out in the context of black carbon measurements.

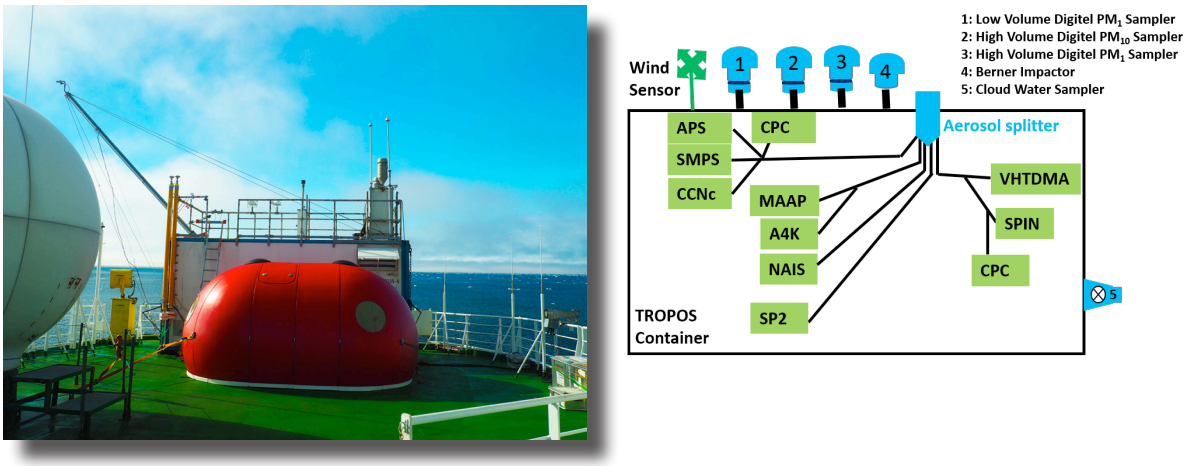

Fig. 3.5: a) Aerosol container on the Peildeck. Main inlets points towards the front of Polarstern (left) (b) schematic of the instruments associated with the container (schematic is courtesy of Xianda Gong)

c) Tethered balloon-borne measurements of energy budget of the cloudy atmospheric boundary layer in the central Arctic

Tethered balloon observations were performed within the two-week ice floe camp during the cruise (see Fig. 3.6). A 90 m^3-helium-filled balloon with a maximum payload of 9 kg was deployed on the ice floe to profile the ABL from the ground up to 1,500 m altitude. Several measurement units were fixed at the tether below the balloon to study vertical profiles of turbulent and radiative energy fluxes.

The balloon site was situated about 200 m away from the ship on the ice floe. Balloon flights were performed on nine days during the ice floe camp in different weather conditions, which included clear sky, a low level jet (up to 14 m/s), low clouds of different thickness and multiple cloud layers (see Tab. 3.2). In general, the balloon handling worked well. The balloon could carry payloads up to 10 kg and was operated at wind speeds of up to 14 m/s. Icing was observed at the tether and at the instruments and which influenced the measurements during the short time period.

Fig. 3.6: Preparation for balloon operations on June 8, 2017. View towards Polarstern with the meteorological measurement site in front

Turbulence parameters were measured alternatively with a lightweight hot-wire anemometer package and a three-dimensional ultrasonic anemometer. The balloon-borne turbulent energy flux measurements were complemented by measurements of humidity, temperature and virtual temperature at high frequencies. Radiative fluxes were measured with two broadband packages to complete the energy budget profiles. Radiance was measured within the solar spectral range by two spectrometers to retrieve cloud optical thickness and the effective radius of the clouds,

Since the maximum payload of the balloon has to be respected, different payloads were combined during different ascents according to the specific scientific question (see Tab. 3.2).

In addition, a filter aerosol sampler of the TROPOS chemistry department was attached to the tether on June 10, which measured over a period of 3 hours above the inversion layer.

The 10 m meteorological mast was installed about 30 m apart from the balloon site and completes the balloon measurements. Its main sensors are an Ultrasonic anemometer wind speeds and a Licor for humidity at 20 Hz. Unfortunately, the Licor did not work properly on most days.

Together with the COmpact RAdiation measurement System (CORAS) equipped with two pyrgeometer and heat flux sensors, the ground-based measurements provide the full surface energy budget, which can be compared to the balloon-borne vertical profiles of the energy budget.

The balloon flights and mast data are summarized in Table 3.2 and Table 3.3, respectively.

During the time of the ice floe, the polar aircraft *Polar 5* and *6* operated in the same area. As instrumentations are similar to the balloon, a comparison of both platforms is planned. Due to fog conditions in Longyearbyen, collocated measurements are sparse.

d) Sea surface microlayer (SML) measurements

The sampling of the SML was performed with an established glass plate technique (e.g. van Pinxteren et al., 2012), while bulk seawater was sampled in glass bottles from a depth of ca. 1 m. We sampled the SML and the bulk water on a daily basis on the way from Bremerhaven to the Arctic - to detect possible changes in the chemical and physical characteristics. At the ice station, we performed SML sampling at suitable sampling spots once per day. We sampled the open water with the Zodiac, from the ice edge and we also probed melt ponds, which are suggested to be an important source for sugar-like compounds (Fig. 3.7). All in all, we performed 53 SML sampling events during PS106/1 and PS106/2 (details in Table 3.4) at the end of this chapter.

Fig. 3.7: SML sampling at the ice edge

In addition, we sampled bulk aerosol particles with a High volume Digitel sampler (PM_1) and size segregated aerosol particles with two Berner impactors in five stages between 50 nm and 10 µm. All sampling information concerning aerosol sampling are listed in Table 3.5 which is attached to the end of this chapter.

Preliminary results

a) Radiation budget & atmosphere remote sensing

The time series of integrated water vapor (IWV) and liquid-water path (LWP) from measurements with the microwave radiometer HATPRO within the OCEANET container are shown in Fig. 3.8. IWV values were found to be around 20-30 kg/m² during departure from Bremerhaven. Upon arrival in the Arctic, the IWV decreased occasionally even below 5 kg/m². Most observed values were about 10 kg/m². LWP values were mostly found between 0 and 200 g/m².

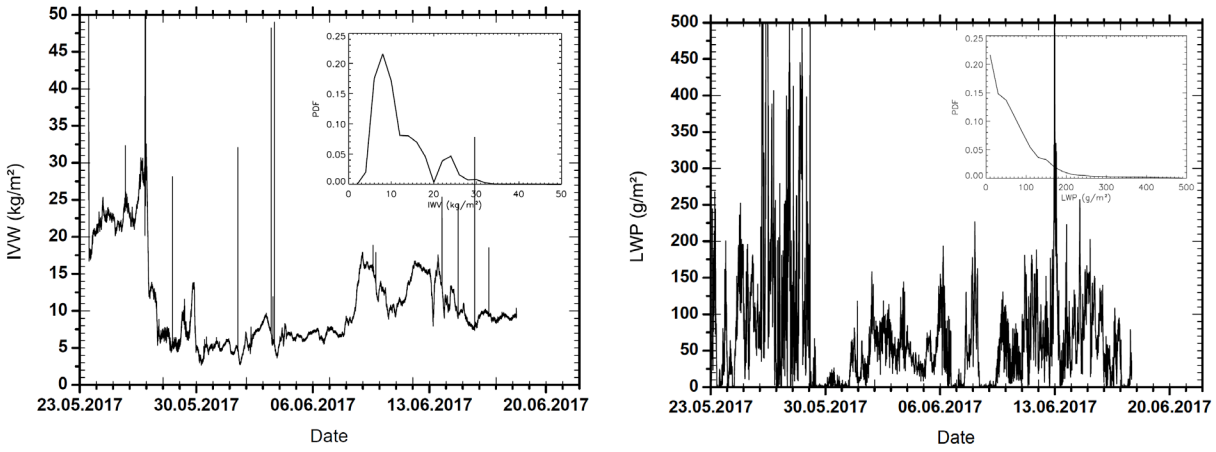

Fig. 3.8: Integrated water vapor and liquid-water path measured with the microwave radiometer during PS106/1. The inset shows the histogram of the time series. Distinctive spikes in the IWV time series were caused by obstructions to the sky during maintenance operations.

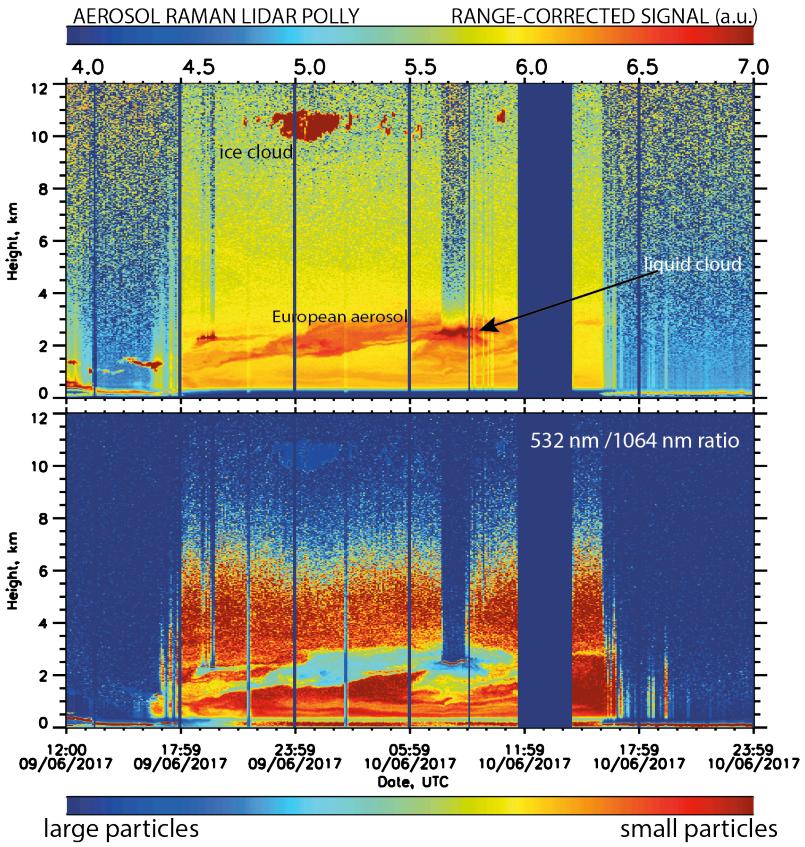

Fig. 3.9: Quicklook of a clear-sky measurement with the Raman lidar Polly. On top, the range-corrected signal at 1064 nm is shown. In the bottom plot, the ratio of the 532 and 1064 nm signals is shown and gives an indication about the particle size.

Measurements with the Raman lidar PollyXT were generally very difficult, as the sky over *Polarstern* was mostly cloudy. In low clouds, the laser beam is attenuated after a few tens of meters. Therefore, only the rare clear-sky situations allowed an aerosol profiling. Fig. 3.9 shows a measurement between 9 and 10 June 2017 at the ice floe. A lofted aerosol layer between 1 and 3 km was observed. First analysis of DWD trajectories showed that the air masses were transported to the Arctic from Central Europe. The color ratio between different laser wavelengths gives also an indication about particle size. During later analysis the Angström exponent can be derived, which will lead to better particle characterization. At around 8 UTC on June 10 a liquid altocumulus cloud was formed within the aerosol layer. Below the tropopause at 11 km height, a cirrus was observed in addition.

The cloud radar measured continuously with only short shutdowns due to maintenance during the whole cruise of PS106/1. In 10 and 11, quicklooks of the measured reflectivity (left), the linear depolarization ratio (LDR, middle) and the Doppler velocity (V_D, right) for two days are shown. Fig. 3.10 shows the time series for 31 May 2017. During this day cirrus cloud between 9 and 10 km height occurred until 6 am which were too thin to be detected in the LDR. Few lofted stratus cloud patches had been present during the whole day and intensified during the afternoon. In Fig. 3.11 the cloud radar for June 8, 2017 is presented. Especially in the early morning low stratus clouds are visible. Until 09:00 stratus cumulus clouds had been present between 6 and 8 km height with some thin cirrus above. At 19:00 lower clouds occurred up to 2 km height occurred. Note that V_D still has to be corrected for the vertical motion of the RV.

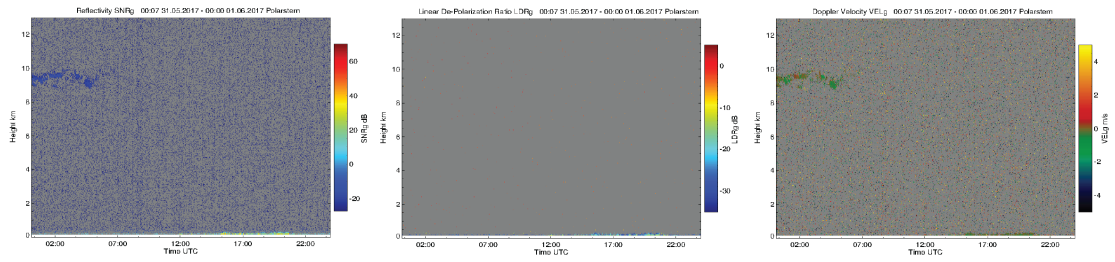

Fig. 3.10: Profile of reflectivity (left), linear depolarization ratio (middle) and Doppler velocity (right) for May 31,2017

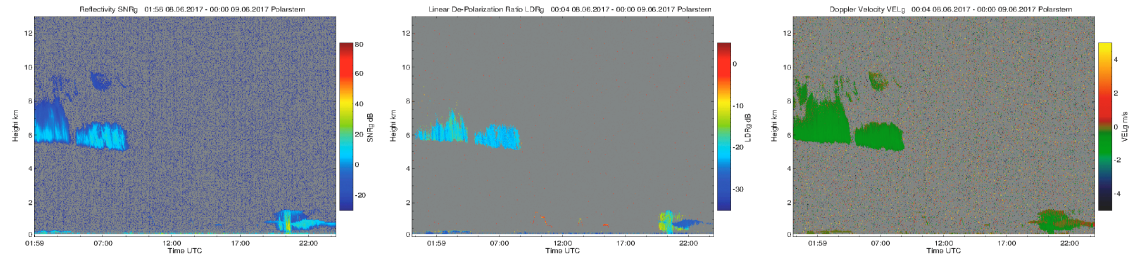

Fig. 3.11: Same as Fig. 3.11 but for June 8, 2017

During the ice station we recognized three important days, which are described with the meteorological data in Fig. 3.12. On June 8 the lowest temperatures were reached with values below -7.5 °C, whereas the warmest temperature occurred on June 10 with values up to 3 °C (Fig. 3.12). Around 09:00 on the 8 June a surface temperature and relative humidity increase can be seen in Fig. 3.13. The fluctuations of the direct radiation during the day are due to lower clouds, which can be seen in the all sky camera (not shown). After 19:00 when lower thick clouds occurred the measured direct radiation went down.

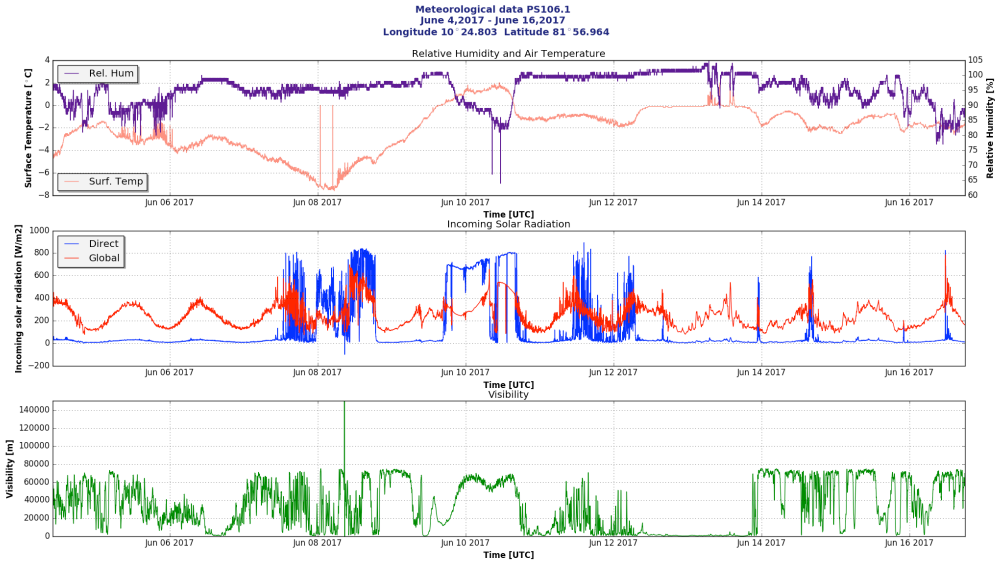

Fig. 3.12: Meteorological data during ice station of PS106/1. The upper row shows the relative humidity (purple) and surface temperature (pink). In the middle the direct (blue) and global radiation (red) is presented. The bottom row represents the visibility.

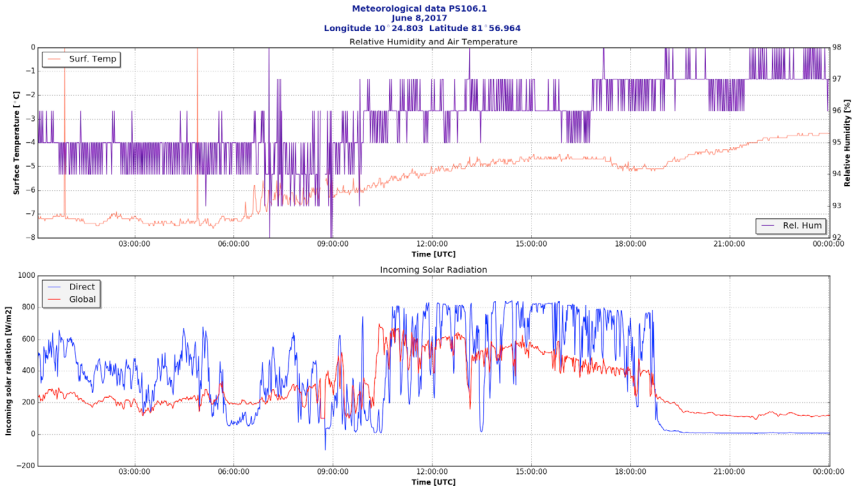

Fig. 3.13: Meteorological data for the 8 June 2017. The upper row shows the relative humidity (purple) and the surface temperature (pink). The bottom row represents the direct (blue) and global (red) radiation.

An important fog event occurred from June 12 to June 13 due to a persistent thermic inversion, which interrupted the standard work on the ice.

These characteristics had direct effects on the pyranometers' network (Fig. 3.14). On June 8 icing over the pyranometers' dome were identified and due to the relative warm temperature on June 10 and the decrease of the relative humidity of 65 % most of the pyranometers had leveling problems (*cf*. Fig. 3.14).

Table 3.1 provides a list of all pyranometer stations together with location and duration of measurements.

Fig. 3.14: Quality control of pyranometer. The upper plot shows the level quality and the bottom plot the cleanliness quality.

Tab. 3.1: Station list of the pyranometer network. The x- and y-positions are given as marked on the station map with the ROV-station as coordinate centre.

IceStationID PS106_	x[m]	y[m]	Lat	Lon	start [UTC]	end [UTC]
21_PYRNET_01	-811	983	81.883	10.680	04.06.2017T12:34:24	16.06.2017T13:20:58
21_PYRNET_02	-555	1048	81.885	10.666	04.06.2017T12:21:57	16.06.2017T13:12:12
21_PYRNET_03	120	690	81.891	10.662	04.06.2017T11:39:04	16.06.2017T12:43:25
21_PYRNET_04	-418	1062	81.886	10.660	04.06.2017T12:07:36	16.06.2017T13:00:58
21_PYRNET_05	-276	961	81.889	10.657	04.06.2017T11:53:29	16.06.2017T12:53:42
21_PYRNET_06	164	530	81.894	10.657	04.06.2017T10:54:35	16.06.2017T12:05:58
21_PYRNET_07	3	110	81.895	10.682	04.06.2017T09:49:58	16.06.2017T11:39:03
21_PYRNET_08	16	710	81.892	10.655	04.06.2017T11:13:29	16.06.2017T12:16:01
21_PYRNET_09	143	114	81.896	10.677	04.06.2017T10:06:34	16.06.2017T11:45:21
21_PYRNET_10	279	251	81.896	10.664	04.06.2017T10:29:35	16.06.2017T11:58:17
21_PYRNET_11	-137	13	81.895	10.692	04.06.2017T09:17:04	16.06.2017T11:20:58
21_PYRNET_12	-112	115	81.894	10.687	04.06.2017T09:31:04	16.06.2017T11:31:31

IceStationID PS106_	x[m]	y[m]	Lat	Lon	start [UTC]	end [UTC]
21_PYRNET_13	-274	2	81.894	10.697	04.06.2017T09:01:59	16.06.2017T11:10:58
21_PYRNET_14	-480	60	81.893	10.705	04.06.2017T08:08:04	16.06.2017T07:30:35
21_PYRNET_15	-516	105	81.892	10.704	04.06.2017T08:34:28	16.06.2017T07:40:06

b) Aerosol in-situ measurements

During the transect from Bremerhaven to the ice floe, number concentrations of a few hundred particles per cm³ were usually observed while being still on open water. During the ice floe drift, the concentrations occasionally dropped to typically some 10 particles cm^{-3}. Periods of very clean conditions (< 10 particles cm^{-3}) occurred occasionally during the ice floe stay. Exceptions were the periods with new particle formation (NPF) (see section New Particle Formation). When the exhaust plume of the ship was blown directly towards the container, particle concentrations easily went up to 10,000s particles cm^{-3}. Fig. 3.15 shows the transition from a low particle concentration period to a period with higher concentrations. The influence of the exhaust plume is visible (spikes at ca. 1 PM) as well.

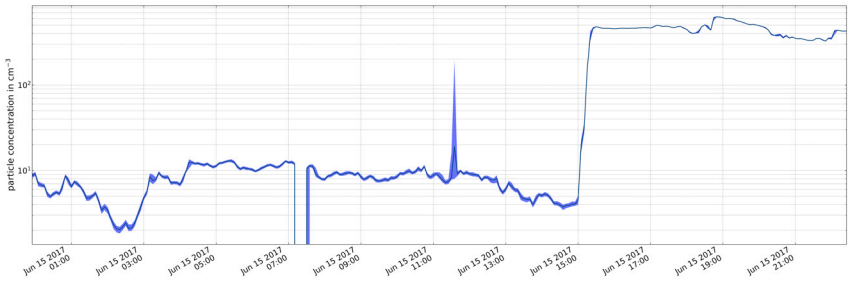

Fig. 3.15: Total number concentration on June 15. The gap between 7 AM and 8 AM is due to the calibration routine

New particle formation (NPF) events were observed in the marginal ice zone (MIZ) twice. Fig. 3.16 shows the nucleation event observed on June 18 when *Polarstern* transitioned from the ice-covered area into the open ocean. The particle growth follows the classical banana-shaped curve as described by Kulmala et al., (2001). Bursts of ultrafine particles (i.e. particles with diameters below 20 nm) and of particles with diameters in the range from 20 nm to 40 nm were also frequently observed during the time *Polarstern* spent in the pack ice region. However, no classical nucleation with subsequent growth was recorded within the ice-covered region, indicating transport from the MIZ or from aloft rather than formation at the site.

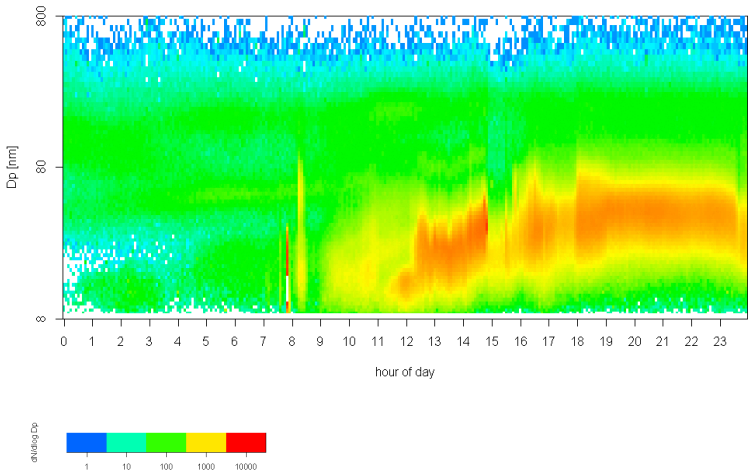

Fig. 3.16: New Particle Formation event on June 18

Cloud Condensation Nuclei (CCN) concentrations were characterized by periods where almost all particles activate at the second lowest supersaturation (0.15%). These periods were often associated with low particle concentrations and hint to a very homogenous, probably local source with low hygroscopicity. In periods where back-trajectories suggest a more continental influence, the supersaturation steps were more distinct, which supports the idea of a more heterogenous continental aerosol. Fig. 3.17 shows the transition from a period with high concentrations at distinct supersaturation steps to to a period with less variation at the different supersaturations.

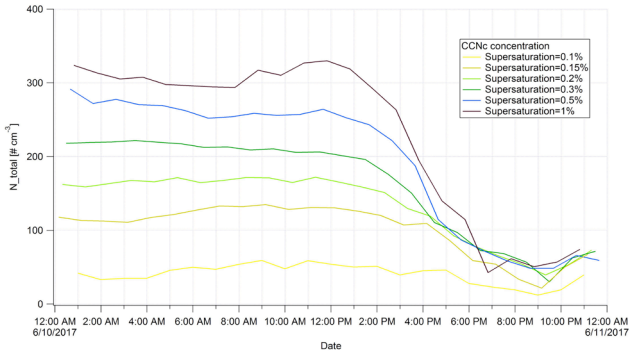

Fig. 3.17: CCN concentrations at different supersaturations on June 10

Black carbon particles have been monitored using an SP2-XR from 25 May (Fig. 3.18). BC mass concentration in open sea below 65 degrees north, were quantified in 160±90 ng m^{-3}, and represent a consistent component of aerosol number concentration with diameter between 80 and 1,000 nm (15 % in number). BC concentration showed severe decrease during the late evening of the 27th, with a daily averaged BC mass concentration for the 28 May of 25 ± 11 ng m^{-3} (2%). This sudden decrease was most probably caused by the change in the air parcel origin from southern to arctic latitudes (Fig. 3.19). Above 80 degrees north, BC mass concentration was observed to vary between 30 ng m^{-3} and less than 1 ng m^{-3}. However most part of the observation are representative of pristine conditions, the influence of ship activity is preponderant under certain meteorological conditions, leading to abrupt increase of BC concentration up to 20-25 µg m^{-3}. Interestingly, measurements influenced by the *Polarstern* exhaust showed a defined increase of the BC diameter compared to background conditions. The aerosol population is then dominated in number by BC particles accounting for 50- 80 % of total number of particles.

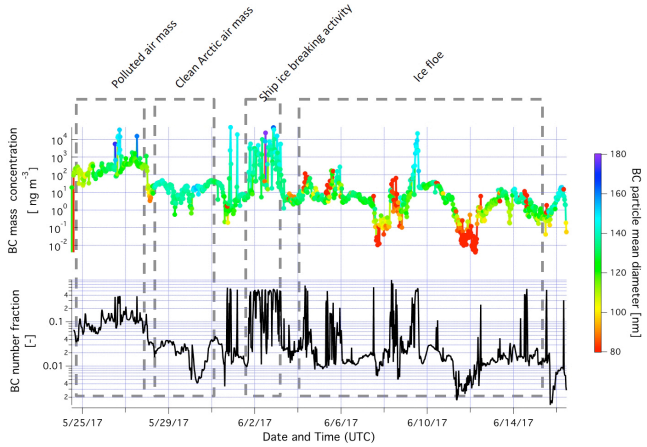

Fig. 3.18: Black Carbon time series

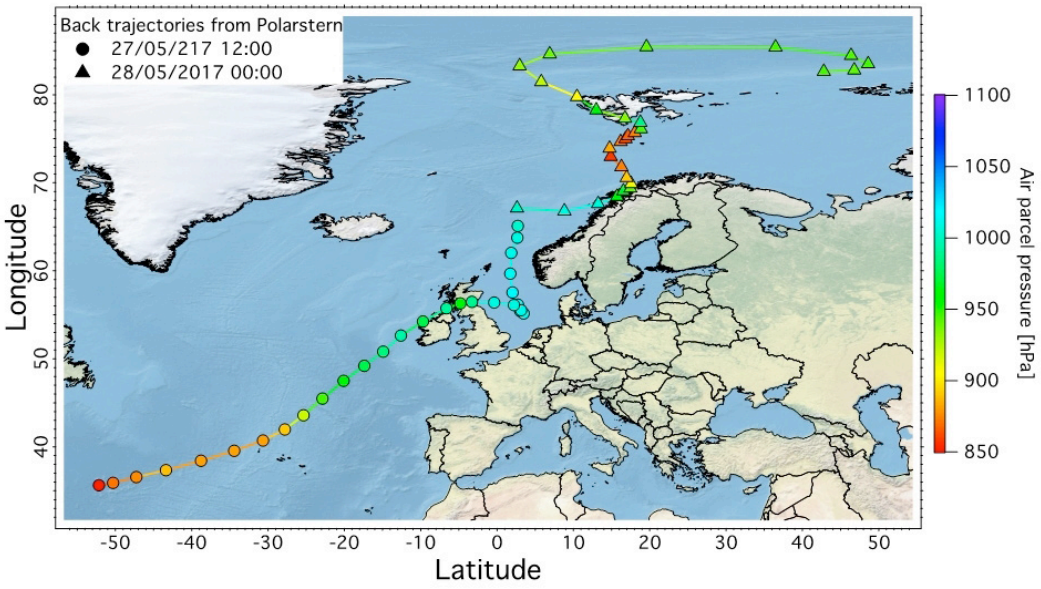

Fig. 3.19: Back trajectories from Polarstern for 27 May 12:00 and 28 May 0:00

c) Tethered balloon-borne measurements of energy budget of the cloudy atmospheric boundary layer in the central Arctic

The data of the balloon platforms needs careful data processing as icing and tilting of the sensors can strongly affect the measurements. Afterwards, the following parameters can be derived from our measurements:

1. Measurements of 20Hz 3D wind speed, humidity and other, lower resolved meteorological parameters (mast)
2. Vertical structure of 50Hz resolved three-dimensional wind speed (Ultrasonic anemometer)
3. Vertical structure of temperature and humidity as well as its variability for validation of satellite products (all packages)
4. Vertical profiles and the time development of solar and terrestrial irradiance to calculate heating rates within the clouds (broadband packages)
5. Measurements of solar spectral radiance to derive cloud optical thickness and cloud effective radius (spectrometer package)

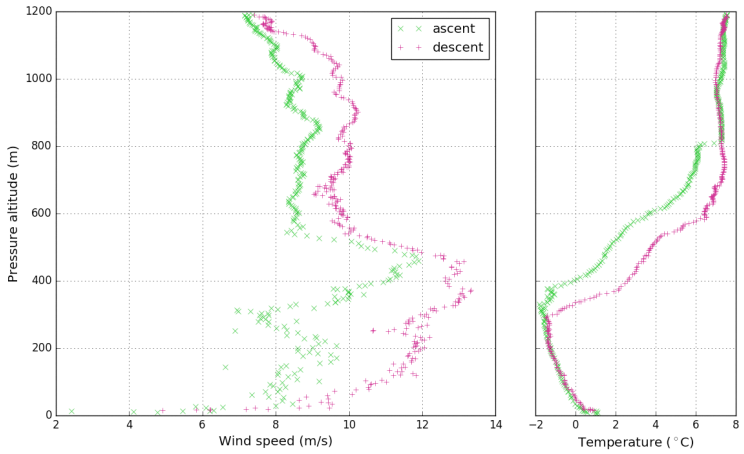

Fig. 3.20: Vertical profile of wind speed and temperature (raw data of hotwire anemometer package) of 28_TBT_1 with strong wind below a temperature inversion

Fig. 3.20 gives an example for the raw data recorded by the hotwire anemometer package on June 11, 2017 (28_TBT_1). The vertical profiles of wind speed and temperature show ascent and descent of the flight up to 1,200 m altitude. Wind speed and wind speed variability is highest below the temperature inversion starting in 400 m and decline above. The time difference between ascent and descent in 600 m altitude is about 30 minutes. At this altitude the measured temperature differs by 2°C, above 800 m and below 300 m no deviation is measured. On that day there was a closed cloud layer between ~270 m and 500 m. Before further interpreting the data careful review of the measured parameters is necessary, e.g. the movement of the instrument is not considered here.

Tab. 3.2: Flight overview of the tethered balloon during the ice floe camp including cloud conditions and instrumentation: Standard Meteorology (SM), Ultrasonic Anemometer (So), Hotwire Anemometer (Hw), Broadband sensors (B1/B2), Spectrometer (Sp), Aerosol sampler (Ae)

.

Station PS106	Time start	Time end	Instruments	Weather
22_TBR_1	05.06.2017T12:35:00	05.06.2017T14:50:00	B1+B2	cloudy, snowfall
22_TBT_1	05.06.2017T12:35:00	05.06.2017T14:50:00	So+SM	
22_TBR_2	05.06.2017T17:24:00	05.06.2017T20:12:00	B1+B2	
22_TBT_2	05.06.2017T17:24:00	05.06.2017T20:12:00	So+SM	
23_TBT_1	06.06.2017T09:30:00	06.06.2017T11:50:00	So+SM	low clouds, later fog
23_TBR_1	06.06.2017T09:30:00	06.06.2017T11:50:00	B2+B1	
24_TBT_1	07.06.2017T09:20:00	07.06.2017T12:00:00	So+SM	cloudy
24_TBR_1	07.06.2017T09:20:00	07.06.2017T10:55:00	B1+B2	
24_TBT_2	07.06.2017T13:15:00	07.06.2017T14:45:00	HW	
24_TBR_2	07.06.2017T13:15:00	07.06.2017T14:45:00	Sp+B1	
25_TBT_1	08.06.2017T09:20:00	08.06.2017T14:00:00	So+SM	First clear, occasionally fog patches/ low clouds
25_TBR_1	08.06.2017T09:20:00	08.06.2017T14:00:00	B1+B2	
25_TBT_2	08.06.2017T14:05:00	08.06.2017T15:45:00	So+SM+Hw	
25_TBR_2	08.06.2017T14:05:00	08.06.2017T15:45:00	B2	
26_TBT_1	09.06.2017T08:50:00	09.06.2017T09:30:00	So+SM	Overcast, could not get balloon over inversion
26_TBR_1	09.06.2017T08:50:00	09.06.2017T09:30:00	B1+B2	
26_TBT_2	09.06.2017T09:30:00	09.06.2017T10:20:00	So+SM	
27_TBT_1	10.06.2017T10:41:00	10.06.2017T11:15:00	SM+Hw	Strong wind speed, clear sky, later overcast
27_TBR_1	10.06.2017T10:41:00	10.06.2017T11:15:00	B1	
27_TBT_2	10.06.2017T14:15:00	10.06.2017T18:00:00	Ae+Hw	
27_TBR_2	10.06.2017T14:15:00	10.06.2017T18:00:00	B1	
28_TBT_1	11.06.2017T13:00:00	11.06.2017T14:12:00	SM+Hw	Low clouds, wind speed a little reduced
28_TBR_1	11.06.2017T13:00:00	11.06.2017T14:12:00	B2	
28_TBT_2	11.06.2017T14:28:00	11.06.2017T16:24:00	SM+Hw	
28_TBR_2	11.06.2017T14:28:00	11.06.2017T16:24:00	B2+B1	
29_TBT_1	12.06.2017T09:20:00	12.06.2017T12:08:00	So+SM	Low level clouds, fog, low wind
29_TBR_1	12.06.2017T09:20:00	12.06.2017T12:08:00	B1+B2	
31_TBT_1	14.06.2017T09:00:00	14.06.2017T11:30:00	So+SM	Thick clouds ~200m – 4km
31_TBR_1	14.06.2017T09:00:00	14.06.2017T11:30:00	B1+B2	

Tab. 3.3: Overview of the 10 m-mast operation (station number represents the time of reading out the data logger)

22_MAST_1	04.06.2017T15:00:00	05.06.2017T12:00:00
24_MAST_1	05.06.2017T12:00:00	07.06.2017T09:00:00
25_MAST_1	07.06.2017T09:25:00	08.06.2017T08:08:00
26_MAST_1	08.06.2017T08:08:00	09.06.2017T07:40:00
27_MAST_1	09.06.2017T08:25:00	10.06.2017T17:57:00
31_MAST_1	10.06.2017T18:05:00	14.06.2017T07:42:00
33_MAST_1	14.06.2017T07:50:00	16.06.2017T07:20:00

d) Sea surface microlayer (SML) measurements

All collected SML, and bulk water samples are stored and frozen. The chemical analysis will be performed after PS106/2 in the laboratories of TROPOS. A first analysis of TEP could be performed on board and showed positive signals in the SML and in the bulk aerosol particles. This is a strong indicator for possible air sea transfer of the TEP. A comprehensive qualitative and quantitative analysis will deliver information about the abundance of organic matter and especially the marine biopolymers in the diverse marine compartments. Enrichment factors will be calculated and their concentration in dependence of different environmental factors (wind speed, chlorophyll-a concentration) will be studied. Such data, together with a simultaneous analysis of the local aerosol particles are very limited to date. Finally, through a combination of the chemical information together with the detection of INPs in marine aerosol particles and sea water we will explore the hypothesis if local marine sources influence the Arctic ice nucleating (and cloud condensation) population.

Data management

All final data will be stored at PANGAEA after post-processing and careful quality checks.

The data processing will be carried out at TROPOS and Leipzig Institute for Meteorology (LIM), respectively. Some of the instruments will be calibrated in the home laboratory to determine the calibration parameters for correct data sets. This will properly take several months. After post processing the complete data sets are available for other cruise participants on request.

References

Brückner M, Pospichal B, Macke A, and Wendisch M (2014) A new multispectral cloud retrieval method for ship-based solar transmissivity measurements. J Geophys Res Atmos, 119, 11,338–11,354, doi:10.1002/2014JD021775.

Bühl J, Seifert P, Myagkov A, and Ansmann A (2016) Measuring ice- and liquid-water properties in mixed-phase cloud layers at the Leipzig Cloudnet station. Atmos Chem Phys, 16, 10609-10620, doi:10.5194/acp-16-10609-2016.

Curry J A (1986) Interactions among turbulence, radiation and microphysics in Arctic stratus clouds. J Atmos Sci, 43, 90–106.

Jeffries MO, Richter-Menge J A, and Overland J E E (2012) Arctic Report Card, http://www.arctiCnoaAgov/reportcard.

Jeffries MO, Overland JE, and Perovich DK (2013) The Arctic shifts to a new normal. Physics Today, 66, 35–40.

Hanschmann T, Deneke H, Roebeling R, and Macke A (2012) Evaluation of the shortwave cloud radiative effect over the ocean by use of ship and satellite observations. Atmos Chem Phys, 12, 12243–12253, doi:10.5194/acp-12-12243-2012.

Kalisch J and Macke A (2012) Radiative budget and cloud radiative effect over the Atlantic from ship-based observations. Atmos Meas Tech, 5, 2391-2401, doi:10.5194/amt-5-2391-2012, 2012.

Macke A, Seifert P, Baars H, Barthlott C, Beekmans C, Behrendt A, Bohn B, Brueck M, Bühl J, Crewell S, Damian T, Deneke H, Düsing S, Foth A, Di Girolamo P, Hammann E, Heinze R, Hirsikko A, Kalisch J, Kalthoff N, Kinne S, Kohler M, Löhnert U, Madhavan BL, Maurer V., Muppa SK, Schween J, Serikov I, Siebert H, Simmer C, Späth F, Steinke S, Träumner K, Trömel S, Wehner B, Wieser A, Wulfmeyer V., and Xie X. (2017) The HD(CP)^2 Observational Prototype Experiment (HOPE) – an overview. Atmos Chem Phys, 17, 4887-4914, doi:10.5194/acp-17-4887-2017.

Madhavan BL, Deneke H, Witthuhn J, and Macke A (2017) Multiresolution analysis of the spatiotemporal variability in global radiation observed by a dense network of 99 pyranometers. Atmos Chem Phys, 17, 3317-3338, doi:10.5194/acp-17-3317-2017.

Overland JE, Wood K R, and Wang M (2011) Warm Arctic–cold continents: Impacts of the newly open Arctic Sea. Polar Res, 30, 15 787, doi:10.3402/polaRv30i0.15 787.

Shupe MD, Persson POG, Brooks IM, Tjernström M, Sedlar J, Mauritsen T, Sjogren S, and Leck C (2013) Cloud and boundary layer interactions over the Arctic sea ice in late summer. Atmos Chem Phys, 13, 9379-9399.

Kanitz T, Ansmann A, Engelmann R, and Althausen D (2013), North-south cross sections of aerosol layering over the Atlantic Ocean from multiwavelength Raman/polarization lidar during Polarstern cruises. J GeophyS ReS, 118, 2642–2655, doi: 100 10.1002/jgrD50273.

Wendisch M, Brückner M, Burrows JP, Crewell S, Dethloff K, Ebell K, Lüpkes CH, Macke A, Notholt J, Quaas J, Rinke A, and Tegen I (2017) Understanding causes and effects of rapid warming in the Arctic. Eos, 98, doi:10.1029/2017EO064803.

Tab. 3.4: SML sampling casts

PS106/1

Date	week day	Station name	Time [MESZ]	Time [UTC]	Latitude	Longitude	Details
25.5.2017	Thursday	PS106_1-1	13:00	11:00	57° 17,28‘N	005° 12,75‘E	Zodiac
26.5.2017	Friday	PS106_2-1	13:00	11:00	61° 06,6‘N	003° 17,97‘E	Zodiac
27.5.2017	Saturday	PS106_3-1	11:00	9:00	64° 41,19‘N	002° 44,55‘E	Zodiac
29.5.2017	Monday	PS106_12-1	10:30	8:30	72° 24,72‘N	005° 35,69‘E	Zodiac
31.5.2017	Wednesday	PS106_16-1	10:20	8:20	79° 19,16‘N	008° 24,6‘E	Zodiac
1.6.2017	Thursday	PS106_17-1	12:30	10:30	80° 25,55‘N	007° 15,88‘E	Zodiac
2.6.2017	Friday	PS106_18_1	14:00	12:00	81° 17,39‘N	009° 17,82‘E	Zodiac
4.6.2017	Sunday	PS106_21-2	9:45	7:45	81° 57,15‘N	010° 30,211‘E	CDT (2,1 m)
4.6.2017	Sunday	PS106_21-2	9:45	7:45	81° 57,15‘N	010° 30,211‘E	CDT (10,1 m)
4.6.2017	Sunday	PS106_21-2	9:45	7:45	81° 57,15‘N	010° 30,211‘E	CDT (34,6 m; Chlorophyll max))
4.6.2017	Sunday	PS106_21-2	19:00	17:00	81° 57‘N	010° 30‘E	SML/Bulk from ice edge
7.6.2017	Wednesday	PS106_24-3	10:00	8:00	81° 56,205‘N	010° 15,057‘E	Zodiac
8.6.2017	Thursday	PS106_25-2	14:00	12:00	81° 53,94‘ N	009° 51,46‘ E	Zodiac
9.6.2017	Friday	PS106_26-2	10:00	8:00	82° 54,50‘N	010° 00,74‘E	Zodiac
10.6.2017	Saturday	PS106_27-1	17:00	15:00	81° 52,32‘N	010° 27,59‘E	Meltpond
11.6.2017	Sunday	PS106_28-2	16:00	14:00	81° 49,69‘N	011° 12,45‘E	SML/Bulk from ice edge
12.6.2017	Monday	PS106_29-2	13:00	11:00	81° 49,42‘N	011° 34, 28‘E	Brine
12.6.2017	Monday	PS106_29-2	13:00	11:00	81° 49,42‘N	011° 34, 28‘E	Brine
12.6.2017	Monday	PS106_29-2	13:00	11:00	81° 49,42‘N	011° 34, 28‘E	ice core
12.6.2017	Monday	PS106_29-2	13:00	11:00	81° 49,42‘N	011° 34, 28‘E	ice core
14.6.2017	Wednesday	PS106_31-2	15:00	13:00	81° 45,87‘N	011° 07,09‘E	Meltpond
15.6.2017	Thursday	PS106_32-2	13:30	11:30	81° 43,33‘N	010° 49,11‘ E	Meltpond

Date	week day	Station name	Time [MESZ]	Time [UTC]	Latitude	Longitude	Details
17.6.2017	Saturday	PS106_34-1	14:30	12:30	80° 59,59‘ N	010° 21,70‘E	Zodiac
18.6.2017	Sunday	PS106_39-1	13:00	11:00	80° 08,82‘N	010° 25,68‘E	Zodiac
19.6.2017	Monday	PS106_41-1	16:00	14:00	78° 39,50‘N	004° 33,23‘ E	Zodiac

PS106/2

Date	week day	Station name	Time (MESZ)	Time (UTC)	Latitude	Longitude	Details
24.6.2017	Saturday	PS106_43-1	12:00	10:00	76° 10,62‘N	019° 58,16‘E	Zodiac
25.6.2017	Sunday	PS106_44-2	12:45	10:45	77° 54,19‘N	030° 05,20‘E	Zodiac
25.6.2017	Sunday	PS106_45-1	21:00	19:00	78° 05,40‘N	030° 27,58‘E	Meltpond
25.6.2017	Sunday	PS106_45-1	23:50	21:50	78° 05,40‘N	030° 27,58‘E	Meltpond
26.6.2017	Monday	PS106_46-1	12:30	10:30	78° 33,33‘ N	033° 57,9‘E	Zodiac
27.6.2017	Tuesday	PS106_48-1	15:00	13:00	79° 50,11‘ N	034° 02,4‘ E	Zodiac
28.6.2017	Wednesday	PS106_50-1	1:30	23:30	80° 32,01‘N	030° 58,15‘E	Meltpond
28.6.2017	Wednesday	PS106_50-2	1:30	23:30	80° 32,01‘N	030° 58,15‘E	Meltpond
29.6.2017	Thursday	PS106_51-1	13:00	11:00	80° 39,93‘N	031° 40,74‘E	Zodiac
30.6.2017	Friday	PS106_56-2	13:45	11:45	81° 41,73‘N	032° 55,28‘E	Zodiac
1.7.2017	Saturday	PS106_64-3	18:10	16:10	81° 25,39‘N	032° 34,6‘E	Zodiac
2.7.2017	Sunday	PS106_66-1	14:45	12:45	81° 39,87‘N	032° 14,67‘E	Zodiac
2.7.2017	Sunday	PS106_66-5	22:00	20:00	81° 38,99‘N	032° 21,97‘E	Snow from ice flow
2.7.2017	Sunday	PS106_66-5	22:00	20:00	81° 38,99‘N	032° 21,97‘E	SML/Bulk from ice edge
2.7.2017	Sunday	PS106_66-5	22:00	20:00	81° 38,99‘N	032° 21,97‘E	SML/Bulk from ice edge
3.7.2017	Monday	PS106_67-2	15:30	13:30	81° 57,92‘N	032° 25,44‘E	Zodiac
5.7.2017	Wednesday	PS106_69-5	12:30	10:30	83° 00,3‘N	033°11,57‘E	Zodiac
6.7.2017	Thursday	PS106_72-2	15:30	13:30	83° 30,02‘N	032° 59,1‘ E	Zodiac

Date	week day	Station name	Time [MESZ]	Time [UTC]	Latitude	Longitude	Details
6.7.2017	Thursday	PS106_73-2	0:45	22:45	83° 39,68‘N	031° 34,83‘E	SML/Bulk from ice edge
6.7.2017	Thursday	PS106_73-2	0:45	22:45	83° 39,68‘N	031° 34,83‘E	Pond
8.7.2017	Saturday	PS106_74-3	12:45	10:45	83° 28,18‘N	027° 54,75‘E	Zodiac
9.7.2017	Sunday	PS106_75-7	14:45	12:45	82° 58,00‘N	025° 08,30‘E	Zodiac
10.7.2017	Monday	PS106_76-5	12:45	10:45	82° 30,27‘N	018° 36, 77‘E	Zodiac
11.7.2017	Tuesday	PS106_78-6	12:00	10:00	82° 02,91‘N	017°55,77‘E	Zodiac
12.7.2017	Wednesday	PS106_80-2	5:00	3:00	81° 18,98‘N	016° 57,32‘E	Meltpond
13.7.2017	Thursday	PS106_83-4	13:10	11:10	81° 13,74‘N	018° 44,63‘E	Zodiac
14.7.2017	Friday	PS106_84-1	13:20	11:20	81° 00,92‘N	026° 52,96‘E	Zodiac
15.7.2017	Saturday	PS106_86-1	12:50	10:50	79° 27,45‘N	028° 07,14‘ E	Zodiac
15.7.2017	Saturday	PS106_86-1	12:50	10:50	79° 27,45‘N	028° 07,14‘ E	Zodiac

Tab. 3.5: Aerosol particle sampling (with Berner impactor and High volume Digitel PM1 sampler)

(A) Berner 93		
Sample name	**Start [UTC +2]**	**End [UTC +2[**
101-105	23.5.17 13:30	24.5.17 18:30
111-115	24.5.17 22:49	26.5.17 18:34
121-125	26.5.17 21:34	29.5.17 13:33
131-135	29.5.17 14:46	1.6.17 10:28
141-145	1.6.17 11:35	4.6.17 10:06
151-155	4.6.17 12:57	7.6.17 10:08
161-165	7.6.17 11:39	10.6.17 10:29
171-175	10.6.17 11:25	13.6.17 13:23
181-185	13.6.17 14:36	16.6.17 10:18
191-195	16.6.17 11:13	19.06.17 11:03
201-205	19.6.17 11:05	25.6.17 12:00
211-215	25.6.17 13:40	28.6.17 11:20
221-225	28.6.17 12:20	4.7.17 10:55
231-235	4.7.17 12:25	7.7.17 10:45
241-245	7.7.17 11:50	13.7.17 11:00
251-255	13.7.17 12:05	16.7.17 12:35

(B) Berner 94		
Sample name	**Start [UTC +2]**	**End [UTC +2]**
106-110	23.5.17 13:30	24.5.17 18:30
116-120	24.5.17 22:50	26.5.17 18:34
126-130	26.5.17 21:35	29.5.17 13:35
136-140	29.5.17 14:47	1.6.17 10:29
146-150	1.6.17 11:29	4.6.17 10:06
156-160	4.6.17 12:58	7.6.17 10:08
166-170	7.6.17 11:37	10.6.17 10:30
176-180	10.6.17 11:22	13.6.17 13:25
186-190	13.6.17 14:33	16.6.17 10:20
196-200	16.6.17 11:13	19.06.17 11:05
206-210	19.6.17 11:05	25.6.17 12:00
216-220	25.6.17 13:40	28.6.17 11:20
226-230	28.6.17 12:20	4.7.17 10:55
236-240	4.7.17 12:25	7.7.17 10:45
246-250	7.7.17 11:50	13.7.17 11:00
256-260	13.7.17 12:05	16.7.17 12:35

(C) Digitel PM1		
Sample name	**Start [UTC +2]**	**End [UTC +2]**
PS_A_1	23.05.2017 18:46	24.05.2017 18:43
PS_A_2	24.05.2017 18:43	25.05.2017 18:43
PS_A_3	25.05.2017 18:43	26.05.2017 18:23
PS_A_4	26.05.2017 18:23	29.05.2017 21:29
PS_A_5	29.05.2017 21:29	01.06.2017 21:29
PS_A_6	01.06.2017 21:29	04.06.2017 21:29
PS_A_7	04.06.2017 21:29	07.06.2017 21:29
PS_A_8	07.06.2017 21:29	10.06.2017 21:29
PS_A_9	10.06.2017 21:29	13.06.2017 21:29
PS_A_11	13.06.2017 21:29	16.06.2017 21:29
PS_A_12	16.06.2017 21:29	19.06.2017 12:38
PS_A_13	19.06.2017 12:38	25.06.2017 10:15
PS_A_14	25.06.2017 10:15	28.06.2017 10:15
PS_A_15	28.06.2017 10:15	04.07.2017 10:57
PS_A_16	04.07.2017 10:57	07.07.2017 10:57
PS_A_17	07.07.2017 10:57	13.07.2017 10:57
PS_A_18	13.07.2017 10:57	16.07.2017 10:57
PS_A_19	16.07.2017 10:57	17.07.2017 12:48
PS_A_20	Field-Blank	Field-Blank

4. WIND MEASUREMENTS USING A WIND LIDAR

Svenja Kohnemann[1] [1]UTR
not on board: Günther Heinemann[1]

Grant-No. AWI_PS106/1_2-00

Objectives

The representation of the atmospheric boundary layer (ABL) in the Arctic is a major challenge for numerical weather forecast models and regional climate models. Reference data sets are rare, particularly over the ocean areas. The group of the University of Trier performed measurements of vertical and horizontal profiles of wind, turbulence and aerosols for the verification of a regional climate model (COSMO-CLM; Kohnemann et al., 2017, Gutjahr et al., 2016) and for process studies.

Work at sea

To measure the wind, turbulence and aerosols of the ABL, a Doppler wind LIDAR (see Fig. 4.1) was used on *Polarstern* during PS106/1 and PS106/2. The operational principle of the wind lidar is an outgoing laser beam that is backscattered at aerosol and cloud particles. Thereby, the resulting frequency change of the light is measured (Doppler effect). The lidar can operate with a maximum range of 10 km and operates at a wavelength of 1.5 µm with a pulse rate of 15 kHz. The instrument is eye-safe (class 1 m).

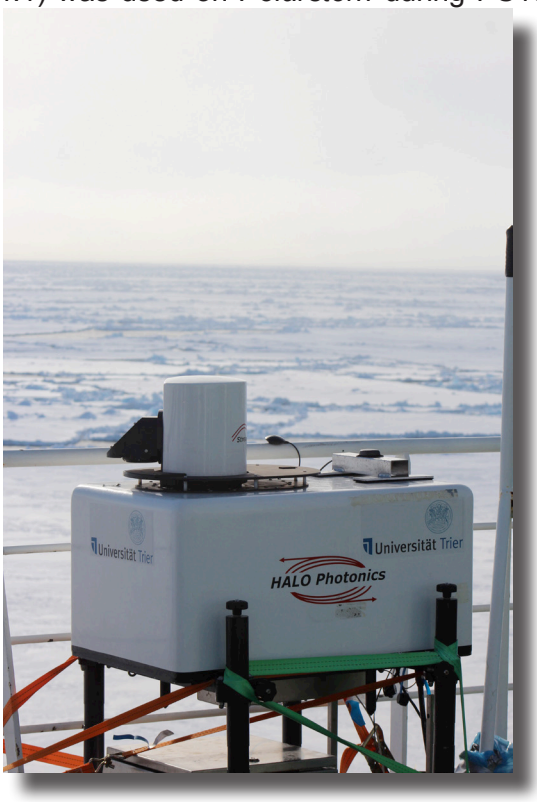

Fig. 4.1: Doppler LIDAR on the backbord side of the upper deck

On board of *Polarstern*, the instrument was installed on the backboard side on the lower part of the upper deck. An Attitude Heading Reference System (AHRS) was used to measure the ship's movement and orientation, which is needed to correct the single laser beams by the inclination angles of the ship's movement. Both instruments could measure continuously for 24 h a day during the cruise. However, weather conditions like fog and conditions with low aerosol concentration restricted the measurements.

The lidar scan pattern was different for measurements taken along the ship route and at a certain station.

The system ran mostly in two programmes. Time sequences consisting of constant elevation, scanning azimuth scans (VAD) at 75° elevation

angle during ship movements and vertical slice scans of fixed azimuth varying elevation (RHI) in addition during ship station times. Both programs included a zenith stare period.

Upper-air soundings by radiosondes are available at 00:00, 6:00, 12:00, 18:00 UTC to verify the measured lidar wind profiles.

Preliminary results

The first use of the wind lidar on *Polarstern* in June 2014 (PS85) already showed that the measured wind data show good results of vertical and horizontal profiles of wind. Also the first use in the Antarctica on cruise PS96 (Dec2015 – Jan2016) gives highly realistic results.

On this cruise we were not allowed to build up the instrument on the starboard side of the upper deck due to antenna effects of the ship. Instead, we built the instrument on the backboard side. The viewing angle is a bit smaller than on the starboard side, but with other measuring angles, it is still possible to cover most wind directions.

With the RHI scans, we could measure the transition of the boundary layer structure (e.g wind speed velocity and turbulence) between the open water and ice covered areas. Using the VAD mode, wind profiles in the atmospheric boundary layer could be measured with high spatial (15 m) and temporal resolution (2 min). Fig. 4.2 shows an overview over three weeks of the cruise.

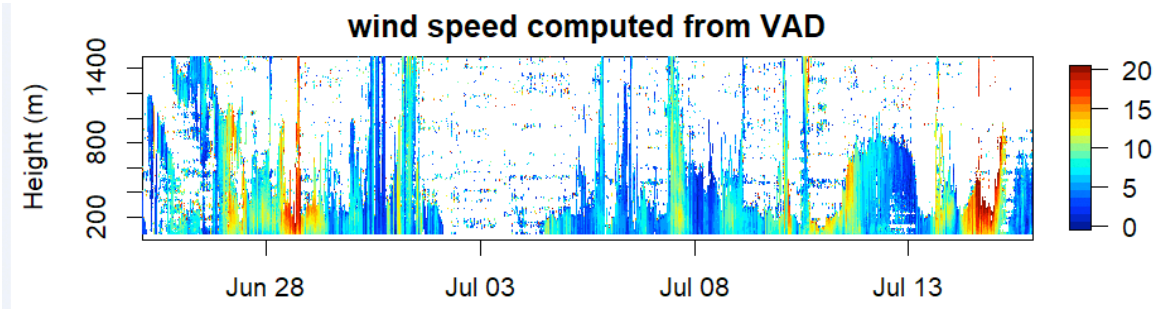

Fig. 4.2: Wind speed measurements for 26 June to 15 July 2017 (PS106/2)

The wind lidar data are highly important to verify the COSMO-CLM simulations. Especially as the region around Svalbard is a big challenge for climate models due to small-scale topographic effects. The continuous measurements of the wind profiles for that long time period will be used for the verification of simulations and for process studies.

Data management

The data are saved at the servers of the Environmental Meteorology Department of the University of Trier. The validated wind of profiles of the lidar will be made available via the online data base PANGAEA (www.pangaea.de).

References

Gutjahr O, Heinemann G, Preußer A, Willmes S, and Drüe C (2016) Quantification of ice production in Laptev Sea polynyas and its sensitivity to thin-ice parameterizations in a regional climate model. The Cryosphere ,10, 2999-3019, https://doi.org/10.5194/tc-10-2999-2016.

Kohnemann SH, Heinemann G, Bromwich DH, and Gutjahr O (2017) Extreme Warming in the Kara Sea and Barents Sea during the Winter Period 2000–16. J. Climate, 30, 8913–8927, https://doi.org/10.1175/JCLI-D-16-0693.1.

5. OCEAN COLOUR REMOTE SENSING: MEASUREMENTS OF WATER-LEAVING REFLECTANCE AND WATER CONSTITUENTS

Martin Hieronymi[1], Peter Gege[2], Marcel König[3], Andreas Macke[4], Natascha Oppelt[3], Thomas Ruhtz[5]

[1]HZG
[2]DLR
[3]CAU
[4]TROPOS
[5]FUB

Grant-No. AWI_PS106/1_2-00

Objectives

a) Determination of reflectance properties of the atmosphere-ocean interface

Satellite remote sensing of ocean colour provides large-scale and global monitoring of the marine biomass and other water constituents. It is particularly suited for observations of remote and difficult accessible areas such as the North Atlantic and the Arctic Ocean. But, the higher the latitudes the more difficult is the atmospheric correction of the ocean colour signal, especially with the low sun elevation angle, the consequently longer path of radiance through the atmosphere, and increased reflectance at the sea surface. Reflectance (and transmittance) properties of the sea surface depend on the incidence angle of radiance and wind-dependent roughness of the surface, where the latter is even more important in the high-wind regions of the high latitudes. Objectives of the campaign were to measure the radiance distribution of sun and sky light in combination with the underwater light field. One focus was to study the degree of polarization of the downwelling light field. The final aim is to compare different instrumentations and their measurements with theoretically determined polarized reflectance properties of the sea surface (Hieronymi, 2016), as well as vector radiative transfer models as MOMO (Hollstein and Fischer, 2012) and the water colour simulator WASI (Gege, 2004). One additional aim of this study is to provide a better sea surface reflectance factor, which is used to determine the water-leaving radiance and remote sensing reflectance, which in turn is basis for satellite remote sensing of ocean colour.

b) Determination of optically-active water constituents

The water colour is determined by spectral absorption and scattering properties of water constituents: pure sea water, phytoplankton, coloured dissolved organic matter (CDOM), and non-algae particles. Water samples from the upper mixed layer (<5 m) should be collected and directly analysed in the laboratory. The aim is to determine the main quantities of ocean colour: inherent optical properties of the water samples as well as concentration of chlorophyll (biomass).

c) Validation of Ocean Colour algorithms and match-ups with Sentinel-3/OLCI

The remote sensing group at HZG is part of the Sentinel-3 validation team, and therefore aims to achieve match-ups with Sentinel-3 and the sensor OLCI (Ocean and Land Colour Imager)

with contemporaneous *in-situ* sampling. The first of a new satellite series, Sentinel-3A, was launched early 2016. Real match-ups are difficult to accomplish; the scenery must be cloud free and the sampling must occur ±3 h of the satellite imagery. The expedition is interesting for validation purposes because of infrequent sampling in this sea area. Furthermore, chances of match-ups increase in higher latitudes since the polar-orbiting satellite passes the ship position up to six times per day. OLCI provides data with 300 m spatial resolution. Thus, there was a chance to observe areas between ice fields and study adjacency effects as well.

The radiometric measurements serve as validation of the atmospheric correction of OLCI scenery, i.e., the retrieved remote sensing reflectance (at the sea surface). The associated water sampling serves the validation of ocean colour retrievals, in particular the new neural network based algorithm ONNS by Hieronymi et al. (2017). The final aim is to extend the exploitability of satellite imagery in high latitudes.

Work at sea

As a supplement to PASCAL, the radiative budget at the sea surface of light in the visible range had been investigated during stations of RV *Polarstern*. By means of different spectrometers, the incoming irradiance and sky radiance had been measured above and in water as well as the backscattered upwelling-directed and water-leaving radiance. Thus, the water colour-containing and remote sensing-relevant information – remote sensing reflectance – had been determined based on these measurements. In addition, the polarization properties of the sky radiance and from the sea upwardly directed radiance had been characterized. The following instruments had been deployed; the corresponding data are summarized in Table 5.1:

- different hyperspectral (UV, VIS, and NIR) radiometers (TriOS Ramses, Ocean Optics, Ibsen FREEDOM VIS) to measure irradiance and radiance,
- a polarimeter (URMS/AMSSP) for water, ice, and atmosphere to measure multi-angle polarized reflectance and radiance,
- a Pandora-2s system to derive atmospheric parameters (AOD, trace gases), and
- a Microtops II sun photometer (AOD)
-

Water samples from the upper mixed layer of the sea (and of melt ponds) have been collected. The spectral (UV, VIS, NIR) absorption of particles and coloured dissolved organic matter (CDOM) have been directly analysed in the wet lab by means of a Psicam and LWCC. GF/F filters with marine particles have been stored for later laboratory analysis of the total biomass (chlorophyll) concentration.

Tab. 5.1: Overview of accomplished measurements (mostly during ship stations). Measured quantities: upwelling radiance below water (L_u^-), downwelling irradiance below and above water (E_d^-, E_d^+), upwelling radiance above water (L_{surf}), sky radiance (L_{sky}), estimated chlorophyll concentration (Chl), CDOM absorption (a_{CDOM}), total absorption (a_{tot}), filtration (GFF). Test, Single, and Auto measurements of URMS are with 10° increment azimuth and elevation.

Nr.	Station	Date (2017)	Start [CET]	End [CET]	Latitude	Longitude	Pangaea Device: RAMSES-1 (Zodiak)	Pangaea Device: FLU (Zodiak)	Pangaea Device: RAMSES-2 (2nd Float)	Pangaea Device: RMASES-3 (Railing)	Pangaea Device: URMS (Railing)	Pangaea Device: Pandora (Railing)	Pangaea Device: WS (Laboratory)
1	PS106_2-2	26.05.	13:10	13:45	61° 6.35`N	3° 17.82`E	L_u^-, E_d^-, E_d^+	Chl	L_u^-, E_d^-	E_d^+, L_{surf}, L_{sky}			
2	PS106_2-2	26.05.	13:10	13:45	61° 6.35`N	3° 17.82`E						11:37–12:52	
3	PS106_3-1	27.05.	11:00	11:30	64° 42.4`N	2° 44.0`E	L_u^-, E_d^-, E_d^+	Chl	L_u^-, E_d^-	E_d^+, L_{surf}, L_{sky}		06:39-09:06	
4	PS106_4	28.05.	08:45	18:46	64° 42.4`N	2° 44.0`E						08:45-18:46	
3	PS106_12-3	29.05.	09:50	11:25	72° 34.56`N	5° 35.41`E	L_u^-, E_d^-, E_d^+	Chl	L_u^-, E_d^-	E_d^+, L_{surf}, L_{sky}			a_{CDOM}, a_{tot}, GFF
4	PS106_12-3	29.05.	06:42	06:45	72° 34`N	05° 35`E					Tests	08:45-18:37	
5	PS106_15-2	30.05.	20:20	20:50	77° 15.71`N	9° 31.57`E				E_d^+, L_{surf}, L_{sky}			a_{CDOM}, a_{tot}, GFF
6	PS106_15-2	30.05.	06:42	18:50	77° 15`N	09° 31`E					Tests		
7	PS106_16-2	31.05.	10:00	10:30	79° 20.3`N	8° 25.9`E	L_u^-, E_d^-, E_d^+	Chl		E_d^+, L_{surf}, L_{sky}	Single		a_{CDOM}, a_{tot}, GFF
8	PS106_17-1	01.06.	12:00	12:40	80° 26.54`N	7° 15.86`E	L_u^-, E_d^-, E_d^+	Chl		E_d^+, L_{surf}, L_{sky}	Single	03:11-16:49	a_{CDOM}, a_{tot}, GFF
9	PS106_18-1	02.06.	14:00	14:30	81° 17.41`N	9° 18.18`E				E_d^+, L_{surf}, L_{sky}			a_{CDOM}, a_{tot}, GFF
10	PS106_24-3	07.06.	09:00	10:20	81° 56.16`N	10° 14.59`E	L_u^-, E_d^-, E_d^+	Chl		E_d^+, L_{surf}, L_{sky}	Single	03:11-16:49	a_{CDOM}, a_{tot}, GFF
9	PS106_25-2	08.06.	09:00	12:15	81° 54.501'N	9° 52.05`E				E_d^+, L_{surf}, L_{sky}		10:38-19:08	a_{CDOM}, a_{tot}, GFF
10	PS106_26-3	09.06.	09:30	10:30	81° 54.51`N	10° 0.679`E	L_u^-, E_d^-, E_d^+	Chl		E_d^+, L_{surf}, L_{sky}		03:10-14:44	a_{CDOM}, a_{tot}, GFF
11	PS106_27-2	10.06.	08:50	10:50	81°54.23`N	10° 0.14`E				E_d^+, L_{surf}, L_{sky}	Auto	06:10-16:25	a_{CDOM}, a_{tot}, GFF
12	PS106_28	11.06.	15:42	15:52	81° 49`N	11° 14`E					Auto	07:05-18:58	
13	PS106_29	12.06.	07:26	12:55	81° 49`N	11° 33`E					Auto	03:10-18:57	

Nr.	Station	Date (2017)	Start [CET]	End [CET]	Latitude	Longitude	Pangaea Device: RAMSES-1 (Zodiak)	Pangaea Device: FLU (Zodiak)	Pangaea Device: RAMSES-2 (2nd Float)	Pangaea Device: RMASES-3 (Railing)	Pangaea Device: URMS (Railing)	Pangaea Device: Pandora (Railing)	Pangaea Device: WS (Laboratory)
14	PS106_30	13.06.	06:38	18:52	81° 49`N	11° 34`E					Auto	03:09-18:53	
15	PS106_31	14.06.	05:27	05:27	81° 47`N	11° 17`E					Tests	12:05-16:41	
16	PS106_32	15.06.	07:49	13:22	81° 43`N	10° 51`E					Auto	12:01-12:29	
17	PS106_33	16.06.	06:38	18:52	80° 41‘ N	10° 28‘ E					Auto	11:32-11:43	
18	PS106_34-1	17.06.	14:00	15:00	80° 59.75‘ N	10° 21.94‘ E	L_u^-, E_d^-, E_d^+	Chl		E_d^+, L_{surf}, L_{sky}	Auto		a_{CDOM}, a_{tot}, GFF
19	PS106_39-1	18.06.	12:30	14:00	80°09.38’N	10°38.54‘ E	L_u^-, E_d^-, E_d^+	Chl		E_d^+, L_{surf}, L_{sky}	Auto		a_{CDOM}, a_{tot}, GFF
20	PS106_41-1	19.06.	07:51	14:07	78°32’N	03°52‘ E	L_u^-, E_d^-, E_d^+	Chl		E_d^+, L_{surf}, L_{sky}	Auto		a_{CDOM}, a_{tot}, GFF

Preliminary results

1. Hyperspectral radiance and irradiance have been measured above and in-water to characterize the available light and its polarized angular distribution. From these measurements, the following light field and apparent optical properties can be deduced:

   a) Vertical profile of the underwater light field and reflectance ratio just below the sea surface,

   b) Hyperspectral water-leaving radiance and remote sensing reflectance,

   c) and, due to different sun positions and wind speeds during the measurements, the actual sea surface reflectance factor as function of wind, waves, sun altitude, and atmospheric conditions.

   d) Furthermore, we collected valuable data for the comparison of different sensors.

2. Inherent optical water properties of water samples have been characterized, i.e., total absorption of all marine particles and absorption of CDOM. In addition, GF/F filters have been stored for later lab analysis of the chlorophyll concentrations. First assessment of the data show expected orders of magnitude for the absorptions in the open sea (measurements during stations on the transect) and comparable low concentrations of CDOM and floating biomass in the polynya, the area of open water surrounded by sea ice (measured during the ice station).

3. During clear sky conditions, several match-ups (of *in-situ* radiometric measurements and water sampling) with Sentinel-3/OLCI and Sentinel-2/MSI imagery could be acquired. A high resolution Sentinel-2/MSI image of the floe is shown in Fig. 5.1. The image illustrates the sea ice cover around RV *Polarstern* during ice station at June 10th 2017 and allows estimating the extent of the floe. The image shows the heterogeneity of the ice and water structure. With respect to ocean colour, such imagery will help analysing adjacency effects of the bright ice over dark water and melt ponds.

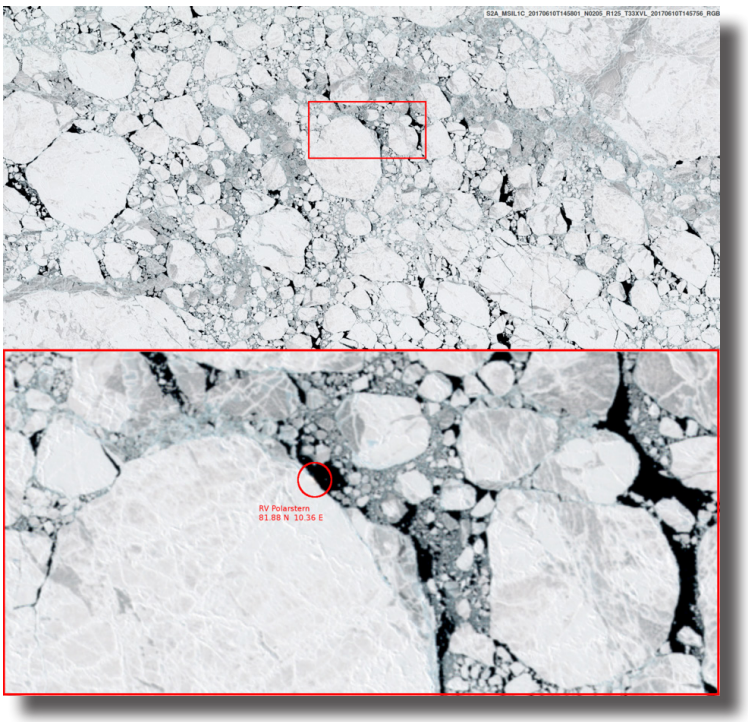

Fig. 5.1: Sentinel-2A MSI image of the ice floe with test site acquired June 10, 2017 at 15:00 UTC with roughly 10 m pixel resolution (contains modified Copernicus Sentinel data [2017] processed by ESA/ HZG). The floe size is approximately 4.1 km in North-South and 3.7 km in East-West directions.

References

Gege P (2004) The water color simulator WASI: an integrating software tool for analysis and simulation of optical in situ spectra. Computers & Geosciences, 30(5), 523-532.

Hieronymi M (2016) Polarized reflectance and transmittance distribution functions of the ocean surface. Optics Express, 24(14), A1045-A1068.

Hieronymi M, Müller D, and Doerffer R (2017) The OLCI Neural Network Swarm (ONNS): A Bio-geo-optical Algorithm for Open Ocean and Coastal Waters. Frontiers in Marine Science, 4, 140.

Hollstein A and Fischer J (2012) Radiative transfer solutions for coupled atmosphere ocean systems using the matrix operator technique. JQSRT, 113(7), 536-548.

6. MEASUREMENTS OF ATMOSPHERIC WATER VAPOR, AEROSOL AND THIN CLOUDS USING FT SPECTROSCOPY IN THE INFRARED

Mathias Palm[1], Philipp Richter[1], Christine Weinzierl[1]
not on board: Justus Notholt[1], Matthias Buschmann[1]

[1]UHB

Grant-No. AWI_PS106/1_2-00

Objectives

This project is embedded in the project AC3 and part of the PASCAL campaign, which aims at understanding the enhanced warming in the Arctic. Clouds and atmospheric feedback are believed to play a major role.

We used mobile FTIR spectrometers onboard the *Polarstern* cruise PS106 (ARK-XXXI/1, ARK-XXXI/2) and PS107 (ARK-XXXII) in the Arctic to study the geographical and temporal distribution of H_2O, HDO, thin clouds and aerosol in the Arctic. Together with the same suite of measurements at the AWIPEV research base in Ny-Ålesund, Spitsbergen the measurements will allow us to assess the representativity of the supersite in Ny-Ålesund for the Arctic.

a) Measurements of columnar H_2O and HDO

Solar absorption spectroscopy in the infrared can be used to determine the distribution of many infrared trace gases in the atmosphere. In particular it is possible to measure H_2O in high quality (Palm, 2008) and the isotopic composition H_2O in the troposphere (Schneider, 2006). The isotopic ratio of H_2O and HDO can be used to study the history of the sampled air parcels (Frankenberg, 2009).

b) Measurements of properties of aerosol layers and thin clouds

Emission spectroscopy in the infrared can be used to study the composition of aerosols and properties of thin clouds (Rathke, 2000a; Rathke, 2000b). Since the self-emission of the the atmosphere is measured, those measurements are independent of an external light source like moon or sun.

Work at sea

Two FTIR instruments are housed in a custom build container for measurements in emission and solar absorption mode. The measurements were performed whenever weather conditions permitted, i.e. clear sky for solar absorption measurements and dry conditions (no precipitation) for emission measurements. The performance of the measurements requires manual operation and oversight, therefore two participants took over to cover most of day and night. *Tables 6.1 and 6.2 list the measurements that had been taken on both legs.*

Tab. 6.1: Measurements taken on PS106/1

Date	Measurement in Mode
26.5.2017	Emission
28.5.2017	Emission
29.5.2017	Emission
30.5.2017	Emission, Absorption
31.5.2017	Emission, Absorption
1.6.2017	Emission, Absorption
2.6.2017	Emission
4.6.2017	Emission
7.6.2017	Emission
8.6.2017	Emission, Absorption
10.6.2017	Emission
11.6.2017	Emission
12.6.2017	Emission
13.6.2017	Emission
14.6.2017	Emission
15.6.2017	Emission
16.6.2017	Emission
17.6.2017	Emission
18.6.2017	Emission, Absorption
19.6.2017	Emission
20.6.2017	Emission

Tab. 6.2: Measurements taken on PS106/2

Date	Measurement in Mode
23.6.2017	Emission
24.6.2017	Emission
25.6.2017	Emission
26.6.2017	Emission
27.6.2017	Emission
28.6.2017	Emission
29.6.2017	Emission
30.6.2017	Emission, Absorption
1.7.2017	Emission
2.7.2017	Emission
3.7.2017	Emission, Absorption
4.7.2017	Emission, Absorption
5.7.2017	Emission
6.7.2017	Emission
8.7.2017	Emission
9.7.2017	Emission
10.7.2017	Emission
11.7.2017	Emission
12.7.2017	Emission
13.7.2017	Emission
14.7.2017	Emission
15.7.2017	Emission, Absorption
17.7.2017	Emission
18.7.2017	Emission

Preliminary (expected) results

1. Low altitude resolution profiles of H_2O and HDO and their ratio will be derived from the solar absorption measurements. A trajectory model will be used to track the path of the airparcels measured.

2. The structure of radiation emitted from the atmosphere is analyzed to derive properties like the optical depth, the mean radius, and chemical composition of particles contained in clouds or aerosol layers.

Fig. 6.1 shows two spectra recorded in emission mode for different conditions: clear sky (16:36, blue colour) and a thin cloud at an altitude of around 100 m (14:52, green colour). The imminent effect of a thin cloud is the attenuation of the radiation coming from above and adding radiation, a baseline, due to its temperature. The shape of the baseline contains information on the liquid water path, the optical depth and the mean radius of the droplets in case of water clouds. The question whether there is an effect due to ice is the subject of a PhD study.

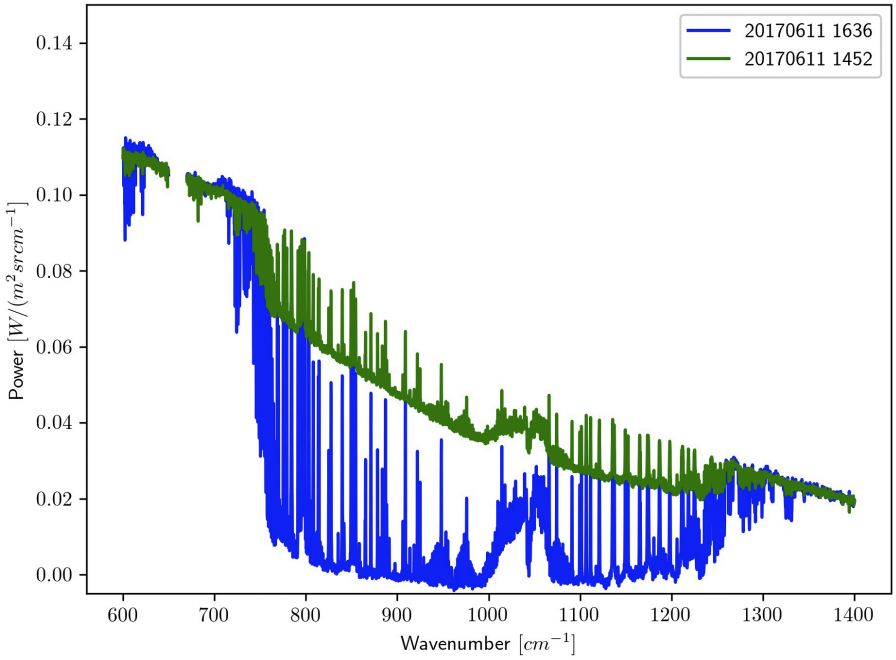

Fig. 6 1: Spectra recorded on 11 June 2017 at two different conditions: clear sky (blue) and cloudy (green)

Data management

The obtained data will be made available to the project partners via the database PANGAEA and made available for the public after publication or 5 years at most.

References

Frankenberg C, Yoshimura K, Warneke T, Aben I, Butz A, Deutscher N, Griffith D, Hase F, Notholt J, Schneider M, Schrijver H & Röckmann T (2009) Dynamic Processes Governing Lower-Tropospheric HDO/H2O Ratios as Observed from Space and Ground. Science, 325, 1374-1377.

Palm M, Melsheimer C, Noël S, Notholt J, Burrows J & Schrems O. (2008) Integrated water vapor above Ny Ålesund, Spitsbergen: a multisensor intercomparison. Atmos Chem Phys Discuss, 8, 21171–21199.

Rathke C & Fischer J (2000a) Retrieval of cloud microphysical properties from thermal infrared observations by a fast iterative radiance fitting method J Atmos Oceanic Technol., 17, 1509-1524.

Rathke C, Armbruster W., Fischer J, Becker E & Notholt J (2000b), Comparison of stratus cloud properties derived from coincident airborne visible and ground-based infrared spectrometer measurements Geophys Res Lett, 27, 2641-2644.

Schneider M, Hase F & Blumenstock T (2006) Ground-based remote sensing of HDO/H2O ratio profiles: introduction and validation of an innovative retrieval approach Atmos Chem Phys, 6, 4705-4722.

7. PHYSICAL CHARACTERISTICS OF MELT PONDS

Natascha Oppelt[1], Gerit Birnbaum[2], Peter Gege[3], Marcel König[1], Nils Fuchs[2]

[1]CAU
[2]AWI
[3]DLR

Grant-No. AWI_PS106/1_2-00

Objectives

Improving the predictive capabilities for the development of Arctic sea ice cover strongly depends on a better understanding of the ice-albedo feedback mechanism. Using a combination of multi- and hyperspectral airborne imagery, field spectroscopy and bio-optical modelling we aim to quantify melt pond fraction, melt pond depth, thickness of underlying ice, pond water constituents (chlorophyll, suspended organic and inorganic matter) and surface albedo in different ice regimes. The main goal is to develop a semi-automated application for melt pond analysis for airborne hyperspectral instruments. A further goal is to employ the collected data to validate and improve parameterizations of melt pond properties used in regional and global climate models. The ground based measurements are essential for the parameterization of bio-optical models as well as for the validation of results derived from airborne measurements, which is crucial for accuracy assessment.

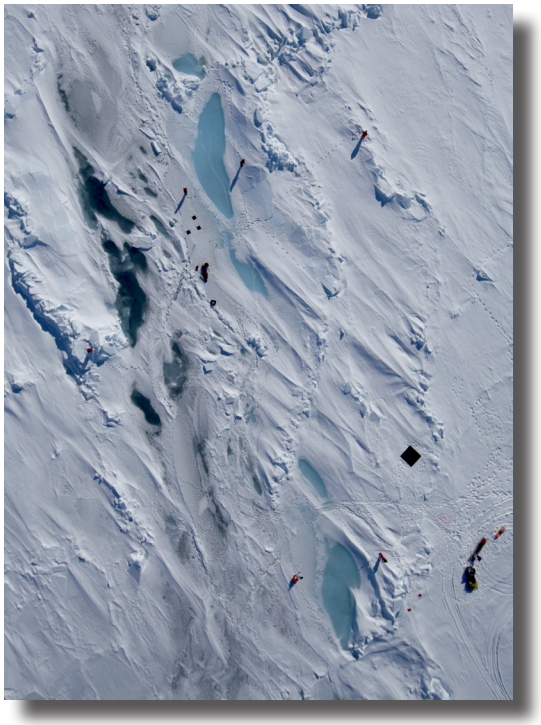

Fig. 7.1: Image taken by the airborne DSLR camera during a sampling area overflight on 10 June, 2017

Work at sea

a) Airborne acquisition of sea ice and melt pond characteristics

Airborne measurements were carried out by use of a helicopter (Tab. 7.1 and 7.2). Two instruments, a Canon DSLR camera and an $AISA_{eagle}$ hyperspectral camera, were mounted at the helicopter. Airborne measurements were conducted mostly under fully overcast conditions, but a few times also under clear sky conditions. To couple ground based and airborne measurements, the flight pattern included several overflights of the sampling areas at different altitudes ranging from 200 ft to 10,000 ft. To correct for ice drift, stable targets (dark targets) were used (see Fig. 7.1). To collect as much airborne data over ponded sea ice as possible, camera flights had also been conducted during steaming.

b) Measurements of melt pond characteristics

Field measurements were carried out stand-alone and simultaneously to helicopter overflights and satellite overpasses (Sentinel 2 and 3) to provide

match ups (Tab. 7.1 and 7.2). During PS106/1 melt ponds started to appear with pond depths of up to 30 cm. Optical properties of ice-free, shallow ponds were therefore determined using hyperspectral radiance and irradiance measurements (Ocean Optics, 350 – 850 nm, ~2 nm spectral resolution) above the water surface. To characterize surface reflectance as a function of bottom depth we measured along horizontal transects in the ponds. At each radiation measurement point along these transects pond depth had been measured using a centimetre stick. To determine ice thickness under the pond, ice drillings accompanied spectral and depth measurements. Measurements of pond length and width were conducted using a laser distance-meter.

To determine the influence of the pond bottom on above-water observations we took Ocean Optics reflectance measurements of very shallow pond areas and bidirectional reflectance spectra of bare ice. To obtain spectral data of pond bottom reflectance, we measured the irradiance reflectance of the area directly neighbouring the pond with a field spectrometer (ASD, 350 – 2,500 nm, spectral resolution 3-8 nm).

c) Determination of optically active water constituents

The water colour is determined by spectral absorption and scattering properties of water constituents: pure pond water, phytoplankton, coloured dissolved organic matter (CDOM), and non-algae particles. During ice stations, water samples of melt ponds have been collected. The spectral (UV, VIS, NIR) absorption of particles and dissolved organic matter (CDOM) was directly analysed in the wet laboratory by means of two absorption spectrometers (Psicam and LWCC). GF/F filters with pond particles have been stored for later analysis of the total suspended matter and pigment biomass (chlorophyll) concentration (HPLC). Chlorophyll concentrations have also been derived via *in-situ* measurements using a fluorometer (algae torch).

d) Determination of reflectance properties of surrounding sea ice surfaces

The Arctic environment shows high contrasts between water surfaces with relatively low reflectance and neighbouring areas of high reflecting ice and snow. To consider adjacency effects in remote sensing observations, ice and snow covered areas neighbouring the melt ponds were measured using different types of field spectrometer covering different wavelength regions, i.e. ASD and Ocean Optics.

To determine near-surface broadband up- and downwelling irradiance a radiation rack with ventilated short- and longwave radiation sensors mounted on a Nansen-sledge and a mobile tripod with a net radiometer were operated during PS106/1 over sea ice surfaces.

The analysis of remote sensing data from melt ponds has to account for the spectral and angular properties of the areas neighbouring the ponds in order to correct for atmospheric stray light from these areas (adjacency effect). For this purpose bi-directional reflectance properties of four snow and ice surfaces were measured during clear sky conditions on an ice floe using the FELGO goniometer. A vertical arm allows to point the fore-optics of a spectrometer in 10° steps from nadir (0°) to a zenith angle of 60°, and using a circular frame attached to the ground with ice screws, the arm can be rotated in a full circle covering all azimuth angles in 10° steps. The collected light is transferred via glass fibre to a spectrometer (Ibsen FREEDOM VIS FSV-305) covering the spectral range from 320 to 850 nm with a resolution better than 2 nm. As an example of the preliminary results, Fig. 7.2 shows the anisotropy factor of ice in the principal plane, i.e. the reflectance spectra relative to nadir for an azimuth angle of 0 relative to the sun.

Snow and ice sampling had been performed in collaboration with the sea ice physics and SIEMO groups.

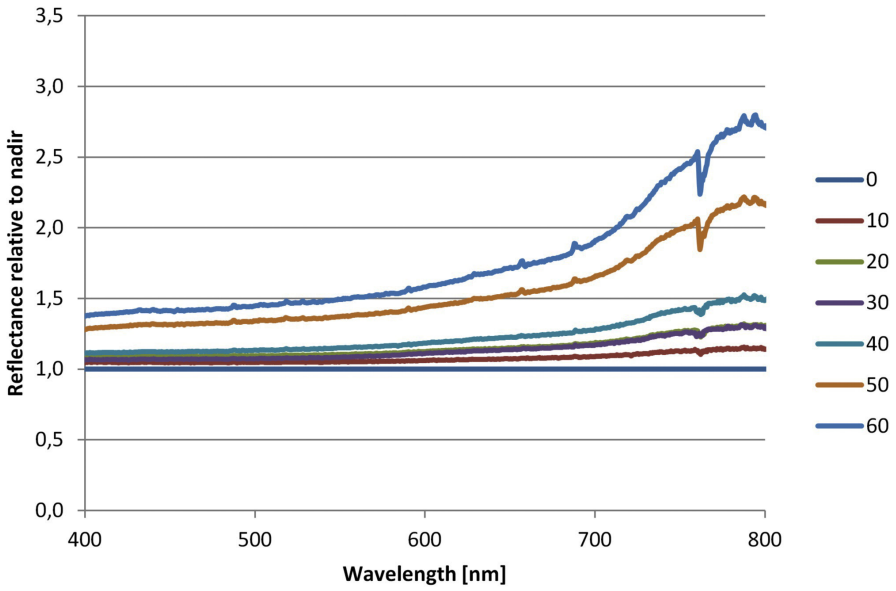

Fig. 7.2: Anisotropy factor of ice in the principal plane for zenith angles from 0 to 60°

e) Model development

A spectral model of a three layer system pond – ice – ocean has been developed and programmed during the cruise. It shall be used for data analysis of the airborne hyperspectral measurements introduced in section (a). The measurements described in (b) and (c) will be used to validate and further improve the model.

Tab. 7.1: List of helicopter flights

Nr.	Helicopter	Date/Time start [UTC]	Date/Time end [UTC]	Flight time
1	SUR	2017-06-05T08:46:00	2017-06-05T09:24:00	0:38
2	AIRRGBCAM	2017-06-05T11:55:00	2017-06-05T12:26:00	0:31
3	AIRRGBCAM, AIRHYPCAM	2017-06-07T11:18:00	2017-06-07T12:18:00	1:00
4	SUR	2017-06-08T08:15:00	2017-06-08T08:19:00	0:04
5	SUR	2017-06-08T09:19:00	2017-06-08T09:35:00	0:16
6	AIRRGBCAM, AIRHYPCAM	2017-06-08T13:25:00	2017-06-08T14:20:00	0:55
7	AIRRGBCAM, AIRHYPCAM	2017-06-10T07:16:00	2017-06-10T09:07:00	1:51
8	AIRRGBCAM, AIRHYPCAM	2017-06-10T11:42:00	2017-06-10T13:12:00	1:30
9	AIRRGBCAM, AIRHYPCAM	2017-06-14T11:38:00	2017-06-14T12:52:00	1:14
10	AIRRGBCAM, AIRHYPCAM	2017-06-15T11:39:00	2017-06-15T13:12:00	1:33

Nr.	Helicopter	Date/Time start [UTC]	Date/Time end [UTC]	Flight time
11	AIRRGBCAM, AIRHYPCAM	2017-06-17T11:41:00	2017-06-17T13:34:00	1:53
12	AIRRGBCAM, AIRHYPCAM	2017-06-18T07:53:00	2017-06-18T09:52:00	1:59
13	AIRRGBCAM, AIRHYPCAM	2017-06-25T19:07:00	2017-06-25T21:01:00	1:54
14	AIRRGBCAM, AIRHYPCAM	2017-06-26T11:25:00	2017-06-26T13:14:00	1:49
15	AIRRGBCAM	2017-06-27T13:58:00	2017-06-27T14:23:00	0:25
16	AIRRGBCAM	2017-06-27T15:07:00	2017-06-27T16:43:00	1:36
17	AIRRGBCAM, AIRHYPCAM	2017-06-30T13:40:00	2017-06-30T14:57:00	1:17
18	AIRRGBCAM, AIRHYPCAM	2017-07-01T13:37:00	2017-07-01T15:23:00	1:46
19	AIRRGBCAM, AIRHYPCAM	2017-07-02T16:41:00	2017-07-02T18:42:00	2:01
20	AIRRGBCAM, AIRHYPCAM	2017-07-03T09:44:00	2017-07-03T11:41:00	1:57
21	AIRRGBCAM, AIRHYPCAM	2017-07-03T16:00:00	2017-07-03T17:26:00	1:26
22	AIRRGBCAM	2017-07-05T10:17:00	2017-07-05T11:52:00	1:35
23	AIRRGBCAM	2017-07-09T13:31:00	2017-07-09T15:14:00	1:43
24	AIRRGBCAM, AIRHYPCAM	2017-07-11T10:38:00	2017-07-11T12:34:00	1:56
25	AIRRGBCAM, AIRHYPCAM	2017-07-12T08:28:00	2017-07-12T10:23:00	1:55
26	AIRRGBCAM	2017-07-14T13:19:00	2017-07-14T14:15:00	0:56
27	AIRRGBCAM, AIRHYPCAM	2017-07-15T12:36:00	2017-07-15T14:36:00	2:00

Table 7.2: List of waypoints and measurements during helicopter flights

Nr.	Waypoint	Lat	Lon	Time start [UTC]	Time end [UTC]
1	21_CAME_1	81.94984	10.44637	2017-06-04T09:19:00	2017-06-04T23:59:00
2	22_CAME_1	81.93833	10.74068	2017-06-05T00:00:00	2017-06-05T12:11:00
3	22_RADSLD_1	81.94095	10.74649	2017-06-05T00:00:00	2017-06-15T23:59:59
4	22_SPRA_ASD_1	81.93348	10.93500	2017-06-05T12:17:12	2017-06-05T12:59:41
5	22_SPRA_ASD_2	81.92759	10.92187	2017-06-05T13:15:10	2017-06-05T13:47:26
6	22_SPRA_ASD_3	81.92777	10.94574	2017-06-05T14:27:24	2017-06-05T15:01:56
7	22_USA_1	81.94095	10.74649	2017-06-05T00:00:00	2017-06-15T23:59:59
8	23_CAME_1	81.94854	10.85298	2017-06-06T12:08:00	2017-06-06T23:59:00
9	23_RADSTA-BB_1	81.93378	10.87807	2017-06-06T00:00:00	2017-06-15T23:59:59
10	24_CAME_1	81.94952	10.50581	2017-06-07T00:00:00	2017-06-07T23:59:00
11	24_SPRA_ASD_1	81.92521	10.10560	2017-06-07T12:13:03	2017-06-07T12:20:52
12	24_SPRA_OO_1	81.92389	10.03052	2017-06-07T13:41:59	2017-06-07T13:48:26
13	24_SPRA_OO_2	81.91746	10.01679	2017-06-07T14:10:19	2017-06-07T14:30:22
14	24_SPRA_OO_3	81.91169	10.00877	2017-06-07T14:42:23	2017-06-07T14:55:01
15	24_SRPA_ASD_2	81.92630	10.06404	2017-06-07T12:51:01	2017-06-07T12:53:43
16	25_CAME_1	81.90958	9.86426	2017-06-08T00:00:00	2017-06-08T23:59:00
17	25_SPRA_OO_1	81.90183	9.81412	2017-06-08T11:54:13	2017-06-08T12:43:38
18	26_CAME_1	81.89744	9.86908	2017-06-09T00:00:00	2017-06-09T23:59:00
19	26_FLU_1	81.89973	9.99384	2017-06-09T14:19:29	2017-06-09T14:23:45
20	26_FLU_2	81.90167	10.00027	2017-06-09T15:26:11	2017-06-09T15:27:54
21	26_SPRA_OO_1	81.89946	9.99513	2017-06-09T14:31:25	2017-06-09T14:48:31
22	26_SPRA_OO_2	81.89944	9.99643	2017-06-09T14:50:21	2017-06-09T14:57:33
23	26_SPRA_OO_3	81.90166	10.00042	2017-06-09T15:27:25	2017-06-09T15:29:20
24	26_WS_1	81.89973	9.99384	2017-06-09T14:19:29	2017-06-09T14:23:45
25	26_WS_2	81.90167	10.00027	2017-06-09T15:26:11	2017-06-09T15:27:54
26	27_CAME_1	81.90114	10.02681	2017-06-10T00:00:00	2017-06-10T13:48:00
27	27_FLU_1	81.88360	10.34526	2017-06-10T12:07:44	2017-06-10T12:09:28
28	27_FLU_2	81.88050	10.35797	2017-06-10T12:50:39	2017-06-10T12:56:57
29	27_FLU_3	81.87933	10.36450	2017-06-10T13:14:56	2017-06-10T13:26:52
30	27_FLU_4	81.87051	10.45177	2017-06-10T17:32:30	2017-06-10T17:39:56
31	27_HID_1	81.88504	10.33912	2017-06-10T11:45:47	2017-06-10T12:01:19
32	27_HID_2	81.88238	10.35116	2017-06-10T12:23:25	2017-06-10T13:05:02
33	27_HID_3	81.87907	10.36469	2017-06-10T13:23:07	2017-06-10T14:05:51
34	27_HID_4	81.87049	10.45185	2017-06-10T17:31:19	2017-06-10T17:41:37

Nr.	Waypoint	Lat	Lon	Time start [UTC]	Time end [UTC]
35	27_MPDS_1	81.88504	10.33912	2017-06-10T11:45:47	2017-06-10T12:01:19
36	27_MPDS_2	81.88238	10.35116	2017-06-10T12:23:25	2017-06-10T13:05:02
37	27_MPDS_3	81.87907	10.36469	2017-06-10T13:23:07	2017-06-10T14:05:51
38	27_MPDS_4	81.87049	10.45185	2017-06-10T17:31:19	2017-06-10T17:41:37
39	27_SPRA_ASD_1	81.87572	10.38375	2017-06-10T14:30:20	2017-06-10T14:48:23
40	27_SPRA_OO_1	81.88504	10.33912	2017-06-10T11:45:47	2017-06-10T12:01:19
41	27_SPRA_OO_2	81.88238	10.35116	2017-06-10T12:23:25	2017-06-10T13:05:02
42	27_SPRA_OO_3	81.87907	10.36469	2017-06-10T13:23:07	2017-06-10T14:05:51
43	27_SPRA_OO_4	81.87049	10.45185	2017-06-10T17:31:19	2017-06-10T17:41:37
44	27_WS_1	81.88360	10.34526	2017-06-10T12:07:44	2017-06-10T12:09:28
45	27_WS_2	81.88050	10.35797	2017-06-10T12:50:39	2017-06-10T12:56:57
46	27_WS_3	81.87933	10.36450	2017-06-10T13:14:56	2017-06-10T13:26:52
47	27_WS_4	81.87051	10.45177	2017-06-10T17:32:30	2017-06-10T17:39:56
48	28_CAME_1	81.84240	11.10107	2017-06-11T12:11:00	2017-06-11T23:59:00
49	29_CAME_1	81.82124	11.29774	2017-06-12T00:00:00	2017-06-12T23:59:00
50	29_FLU_1	81.82296	11.54930	2017-06-12T11:33:31	2017-06-12T11:35:44
51	29_SPRA_OO_1	81.82296	11.54930	2017-06-12T11:33:31	2017-06-12T11:35:44
52	29_WS_1	81.82296	11.54930	2017-06-12T11:33:31	2017-06-12T11:35:44
53	30_CAME_1	81.81453	11.49574	2017-06-13T00:00:00	2017-06-13T23:59:00
54	31_CAME_1	81.80575	11.33666	2017-06-14T00:00:00	2017-06-14T23:59:00
55	31_FLU_1	81.77628	11.24378	2017-06-14T11:18:02	2017-06-14T11:20:42
56	31_FLU_2	81.77378	11.23164	2017-06-14T11:50:03	2017-06-14T11:55:27
57	31_FLU_3	81.77058	11.21463	2017-06-14T12:30:31	2017-06-14T12:36:05
58	31_FLU_4	81.76526	11.16834	2017-06-14T13:54:39	2017-06-14T13:58:03
59	31_HID_1	81.77628	11.24378	2017-06-14T11:18:02	2017-06-14T11:20:42
60	31_HID_2	81.77378	11.23164	2017-06-14T11:50:03	2017-06-14T11:55:27
61	31_HID_3	81.77058	11.21463	2017-06-14T12:30:31	2017-06-14T12:36:05
62	31_MPDS_1	81.77628	11.24378	2017-06-14T11:18:02	2017-06-14T11:20:42
63	31_MPDS_2	81.77378	11.23164	2017-06-14T11:50:03	2017-06-14T11:55:27
64	31_MPDS_3	81.77058	11.21463	2017-06-14T12:30:31	2017-06-14T12:36:05
65	31_SPRA_OO_1	81.77628	11.24378	2017-06-14T11:18:02	2017-06-14T11:20:42
66	31_SPRA_OO_2	81.77378	11.23164	2017-06-14T11:50:03	2017-06-14T11:55:27
67	31_SPRA_OO_3	81.77058	11.21463	2017-06-14T12:30:31	2017-06-14T12:36:05
68	31_SPRA_OO_4	81.76526	11.16834	2017-06-14T13:54:39	2017-06-14T13:58:03
69	31_WS_1	81.77628	11.24378	2017-06-14T11:18:02	2017-06-14T11:20:42

Nr.	Waypoint	Lat	Lon	Time start [UTC]	Time end [UTC]
70	31_WS_2	81.77378	11.23164	2017-06-14T11:50:03	2017-06-14T11:55:27
71	31_WS_3	81.77058	11.21463	2017-06-14T12:30:31	2017-06-14T12:36:05
72	31_WS_4	81.76526	11.16834	2017-06-14T13:54:39	2017-06-14T13:58:03
73	32_CAME_1	81.74059	10.88348	2017-06-15T00:00:00	2017-06-15T23:59:00
74	32_FLU_1	81.72278	10.80896	2017-06-15T11:41:33	2017-06-15T11:43:53
75	32_FLU_2	81.71956	10.75311	2017-06-15T13:54:02	2017-06-15T13:56:04
76	32_FLU_3	81.70929	10.81542	2017-06-15T14:58:45	2017-06-15T15:02:01
77	32_FLU_4	81.70776	10.80700	2017-06-15T15:24:28	2017-06-15T15:27:46
78	32_FLU_5	81.70707	10.79787	2017-06-15T15:45:21	2017-06-15T15:47:34
79	32_SPRA_ASD_1	81.72284	10.81035	2017-06-15T11:50:17	2017-06-15T12:13:00
80	32_SPRA_ASD_2	81.71865	10.80156	2017-06-15T12:20:24	2017-06-15T12:58:31
81	32_SPRA_ASD_3	81.71111	10.78664	2017-06-15T13:15:26	2017-06-15T13:22:34
82	32_SPRA_OO_1	81.72173	10.80308	2017-06-15T12:05:00	2017-06-15T12:04:07
83	32_SPRA_OO_2	81.71682	10.79113	2017-06-15T13:02:13	2017-06-15T13:22:22
84	32_SPRA_OO_3	81.71886	10.75288	2017-06-15T13:58:10	2017-06-15T13:57:31
85	32_SPRA_OO_4	81.70880	10.81181	2017-06-15T15:07:40	2017-06-15T14:10:12
86	32_SPRA_OO_5	81.71799	10.74369	2017-06-15T14:21:54	2017-06-15T14:25:39
87	32_SPRA_OO_6	81.70866	10.81104	2017-06-15T15:09:37	2017-06-15T15:19:25
88	32_SPRA_OO_7	81.70758	10.80384	2017-06-15T15:29:34	2017-06-15T15:38:59
89	32_SPRA_OO_8	81.70681	10.79667	2017-06-15T15:48:15	2017-06-15T16:01:34
90	32_WS_1	81.72278	10.80896	2017-06-15T11:41:33	2017-06-15T11:43:53
91	32_WS_2	81.71956	10.75311	2017-06-15T13:54:02	2017-06-15T13:56:04
92	32_WS_3	81.71766	10.74216	2017-06-15T14:29:07	2017-06-15T14:29:40
93	32_WS_4	81.70929	10.81542	2017-06-15T14:58:45	2017-06-15T15:02:01
94	32_WS_5	81.70776	10.80700	2017-06-15T15:24:28	2017-06-15T15:27:46
95	32_WS_6	81.70707	10.79787	2017-06-15T15:45:21	2017-06-15T15:47:34
96	33_CAME_1	81.70583	10.59459	2017-06-16T00:00:00	2017-06-16T08:49:00
97	35_FLU_1	81.00209	10.34703	2017-06-17T12:22:34	2017-06-17T12:50:26
98	35_MER_1	81.00209	10.34703	2017-06-17T12:22:34	2017-06-17T12:50:26
99	40_FLU_1	80.15243	10.63666	2017-06-18T10:56:34	2017-06-18T11:53:34
100	40_MER_1	80.15243	10.63666	2017-06-18T10:56:34	2017-06-18T11:53:34
101	41_FLU_1	78.66592	4.57039	2017-06-19T13:32:05	2017-06-19T13:59:53
102	41_MER_1	78.66592	4.57039	2017-06-19T13:32:05	2017-06-19T13:59:53
103	45_CAME_1	78.09705	30.48085	2017-06-25T20:55:00	2017-06-25T03:13:00
104	45_FLU_1	78.09180	30.46654	2017-06-25T20:20:04	2017-06-25T20:24:56

Nr.	Waypoint	Lat	Lon	Time start [UTC]	Time end [UTC]
105	45_FLU_2	78.09187	30.44959	2017-06-25T22:27:23	2017-06-25T22:29:26
106	45_FLU_3	78.09273	30.44791	2017-06-25T22:48:13	2017-06-25T22:50:07
107	45_FLU_4	78.09387	30.44411	2017-06-25T23:23:24	2017-06-25T23:25:17
108	45_FLU_5	78.09692	30.45172	2017-06-25T00:22:32	2017-06-25T00:24:56
109	45_SPRA_OO_1	78.09180	30.46654	2017-06-25T19:53:51	2017-06-25T20:03:07
110	45_SPRA_OO_2	78.09187	30.44959	2017-06-25T22:16:21	2017-06-25T22:21:29
111	45_SPRA_OO_3	78.09273	30.44791	2017-06-25T22:39:42	2017-06-25T22:45:36
112	45_SPRA_OO_4	78.09387	30.44411	2017-06-25T23:12:54	2017-06-25T23:20:26
113	45_SPRA_OO_5	78.09692	30.45172	2017-06-25T00:39:19	2017-06-25T00:58:54
114	45_WS_1	78.09180	30.46654	2017-06-25T20:20:04	2017-06-25T20:24:56
115	45_WS_2	78.09187	30.44959	2017-06-25T22:27:23	2017-06-25T22:29:26
116	45_WS_3	78.09273	30.44791	2017-06-25T22:48:13	2017-06-25T22:50:07
117	45_WS_4	78.09387	30.44411	2017-06-25T23:23:24	2017-06-25T23:25:17
118	45_WS_5	78.09692	30.45172	2017-06-25T00:22:32	2017-06-25T00:24:56
119	49_FLU_1	80.52209	30.96378	2017-06-28T23:16:10	2017-06-28T23:19:26
120	49_FLU_2	80.53041	30.95812	2017-06-28T23:49:55	2017-06-28T23:51:29
121	49_FLU_3	80.53841	30.96515	2017-06-29T00:24:09	2017-06-29T00:27:10
122	49_FLU_4	80.55048	30.99424	2017-06-29T01:21:57	2017-06-29T01:22:51
123	49_SPRA_OO_1	80.52209	30.96378	2017-06-28T22:53:08	2017-06-28T23:13:31
124	49_SPRA_OO_2	80.53041	30.95812	2017-06-28T23:46:43	2017-06-28T23:58:13
125	49_SPRA_OO_3	80.53841	30.96515	2017-06-29T00:07:59	2017-06-29T00:21:15
126	49_SPRA_OO_4	80.55048	30.99424	2017-06-29T01:10:03	2017-06-29T01:12:56
127	49_WS_1	80.52209	30.96378	2017-06-28T23:16:10	2017-06-28T23:19:26
128	49_WS_2	80.53041	30.95812	2017-06-28T23:49:55	2017-06-28T23:51:29
129	49_WS_3	80.53841	30.96515	2017-06-29T00:24:09	2017-06-29T00:27:10
130	49_WS_4	80.55048	30.99424	2017-06-29T01:21:57	2017-06-29T01:22:51
131	66_CAME_1	81.65337	32.35975	2017-07-02T20:40:00	2017-07-03T04:58:00
132	66_FLU_1	81.64901	32.43541	2017-07-03T01:05:43	2017-07-03T01:07:35
133	66_FLU_2	81.64951	32.44425	2017-07-03T01:38:03	2017-07-03T01:39:37
134	66_SPRA_ASD_1	81.65149	32.36788	2017-07-02T19:36:44	2017-07-02T21:01:06
135	66_SPRA_ASD_3	81.64887	32.42188	2017-07-03T00:07:27	2017-07-03T00:12:11
136	66_SPRA_IBS_1	81.65000	32.45000	2017-07-03T02:08:13	2017-07-03T02:39:33
137	66_SPRA_IBS_3	81.65000	32.45000	2017-07-02T19:05:33	2017-07-02T20:06:48
138	66_SPRA_IBS_4	81.65000	32.45000	2017-07-02T20:33:34	2017-07-02T21:33:02
139	66_SPRA_OO_1	81.64901	32.43541	2017-07-03T00:54:56	2017-07-03T01:01:19

Nr.	Waypoint	Lat	Lon	Time start [UTC]	Time end [UTC]
140	66_SPRA_OO_2	81.64951	32.44425	2017-07-03T01:29:19	2017-07-03T01:35:08
141	66_SRPA_ASD_2	81.65000	32.45000	2017-07-02T21:53:41	2017-07-03T00:02:34
142	66_SRPA_IBS_2	81.65000	32.45000	2017-07-02T22:28:59	2017-07-02T23:14:30
143	66_WS_1	81.64901	32.43541	2017-07-03T01:05:43	2017-07-03T01:07:35
144	66_WS_2	81.64951	32.44425	2017-07-03T01:38:03	2017-07-03T01:39:37
145	67_FLU_1	81.96740	32.37925	2017-07-03T13:13:43	2017-07-03T13:47:44
146	67_MER_1	81.96740	32.37925	2017-07-03T13:13:43	2017-07-03T13:47:44
147	80_CAME_1	81.30849	16.90150	2017-07-12T04:53:00	2017-07-12T10:39:00
148	80_FLU_1	81.30895	16.90702	2017-07-12T03:07:02	2017-07-12T03:08:16
149	80_FLU_2	81.31256	16.93816	2017-07-12T04:06:56	2017-07-12T04:07:21
150	80_FLU_3	81.31431	16.95381	2017-07-12T04:36:11	2017-07-12T04:38:19
151	80_FLU_4	81.31718	16.97559	2017-07-12T05:30:11	2017-07-12T05:31:22
152	80_FLU_5	81.32155	16.99990	2017-07-12T06:28:59	2017-07-12T06:30:09
153	80_FLU_6	81.32464	17.00817	2017-07-12T07:06:33	2017-07-12T07:12:52
154	80_SPRA_OO_1	81.30895	16.90702	2017-07-12T03:24:00	2017-07-12T03:31:51
155	80_SPRA_OO_2	81.31256	16.93816	2017-07-12T03:55:58	2017-07-12T04:03:31
156	80_SPRA_OO_3	81.31431	16.95381	2017-07-12T04:27:05	2017-07-12T04:33:29
157	80_SPRA_OO_4	81.31718	16.97559	2017-07-12T05:21:55	2017-07-12T05:27:36
158	80_SPRA_OO_5	81.32155	16.99990	2017-07-12T05:42:34	2017-07-12T06:02:42
159	80_SPRA_OO_6	81.32464	17.00817	2017-07-12T06:36:37	2017-07-12T06:49:39
160	80_WS_1	81.30895	16.90702	2017-07-12T03:07:02	2017-07-12T03:08:16
161	80_WS_2	81.31256	16.93816	2017-07-12T04:06:56	2017-07-12T04:07:21
162	80_WS_3	81.31431	16.95381	2017-07-12T04:36:11	2017-07-12T04:38:19
163	80_WS_4	81.31718	16.97559	2017-07-12T05:30:11	2017-07-12T05:31:22
164	80_WS_5	81.32155	16.99990	2017-07-12T06:28:59	2017-07-12T06:30:09
165	80_WS_6	81.32464	17.00817	2017-07-12T07:06:33	2017-07-12T07:12:52

8. UAV MEASUREMENTS DURING PS106/1

Marius O. Jonassen[1], Priit Tisler[2] [1]UNIS
not on board: Christof Lüpkes[3] [2]FMI
[3]AWI

Grant-No. AWI_PS106/1_2-00

Objectives

The main goal of this project was to obtain data of the structure of the Arctic atmospheric boundary layer (ABL) over sea ice during late spring. Airborne observations were carried out with two unmanned air vehicles (UAV) that have already been used successfully during an Antarctic cruise with *Polarstern* (ANT-XXIX/6) (Jonassen et al., 2015). The project (measurement and data analysis) consists of joint work by groups from the Finnish Meteorological Institute in Helsinki (FMI), the University Centre in Svalbard (UNIS) and the Alfred Wegener Institute Helmholtz Centre for Polar and Marine Research in Bremerhaven. It is based on the operation of two fixed-wing SUMO UAVs from UNIS and two quadrocopters owned by FMI. The data from these airborne instruments supplement the other measurements of the atmospheric boundary layer during PASCAL, and especially the balloon-borne measurements of mean meteorological variables by TROPOS. Based on the profiles of mean quantities (wind, humidity temperature), which were obtained by the UAVs, the structure of the ABL during the drift station will be characterized. Subsequently, the obtained data will also be compared against airborne measurements by *Polar 5* and *6* (campaign ACLOUD).

Work at sea

Work at sea was restricted to the operation of the UAVs from the ice during the ice station, as no UAV operations were permitted from *Polarstern*. During the ice station, that was situated roughly at 82°N,10°E in the time period 03.06-17.06.2017, the SUMO aircraft were operated up to 1,000 m height above the ice and quadrocopter flights were done up to altitudes between 50 and 100 m above the ice. With its fast sensor and slow ascent and descent speeds, the quadrocopter is an ideal tool for obtaining accurate and high resolution profiles of the lowest part of the boundary layer. In addition, a weather mast was deployed during the ice station. Temperature was measured at 0.1 m, 0.5 m and at 2 m height and wind speed and wind direction were measured at 2 m height. The UAV operations were limited at times by meteorological conditions and other air traffic. Occasionally, also the wind speed was too high (above 10 m/s) and / or the visibility was too low (less than a few hundred metres) for safe operations. In addition, no UAV operations were allowed when the *Polarstern* helicopter or the *Polar 5* or *Polar 6* were operating in the area.

Preliminary (expected) results

We have obtained a unique and high-quality dataset of the vertical structure of the ABL over the Arctic sea ice in late spring and especially with respect to the temporal development of the ABL. Previous measurements are available mostly from aircraft or soundings which cannot investigate the evolution in high temporal resolution. A total of 26 SUMO (Fig. 8.1) flights and

12 quadrocopter (Fig. 8.2) flights were conducted during the ice station. Together with the other meteorological measurements during PASCAL the new data set will allow increasing our knowledge on the Arctic climate system and especially on the role of clouds for the ABL structure. Data can be used later for e.g. the validation of operational weather prediction models. Key details of the SUMO, quadrocopter and weather mast observations are given in Table 8.1.

Tab. 8.1: Summary of SUMO and quadrocopter (QC) flights. Maximum altitudes of profiles per flight are given along with the measurement period of the weather mast during the ice-station.

ICE-STATION LOCATION	UAV FLIGHTS					WEATHER MAST (measurement period)
	SUMO	QC	DATE	TIME [UTC]	HEIGHT	
N81.93 E010.96		X	05.06.2017	14:16-15:13	Test	13:03 UTC (03.06.2017) -13:25 UTC (15.06.2017)
N81.95 E010.80	X X		06.06.2017	07:56-08:18 08:19-08:24	Test Test	
N81.94 E010.28	X X		07.06.2017	07:22-07:39 07:41-07:56	Test 399 m	
N81.90 E009.85	X X X X X		08.06.2017	07:22-07:41 08:33-08:49 15:09-15:26 15:35-15:53 15:55-16:12	997 m 681 m 999 m 1002 m 709 m	
N81.90 E010.01	X X X		09.06.2017	08:01-08:15 08:19-08:33 08:40-08:54	695 m 996 m 997 m	
N81.90 E010.25	X X X	 X X 	10.06.2017	07:01-07:13 07:21-07:35 07:36-07:51 07:52-08:03 08:05-08:20	522 m 51 m 995 m 51 m 769 m	
N81.82 E011.55	X	 X	12.06.2017	08:52-09:07 09:13-09:20	713 m 50 m	
N81.79 E011.25	X X X X	 X X X 	14.06.2017	07:57-08:13 08:18-08:30 08:29-08:43 08:46-08:55 08:56-09:09 09:10-09:20 09:20-09:32	996 m 50 m 998 m 65 m 995 m 49 m 997 m	
N81.73 E010.85	X X X X X	 X X X X 	15.06.2017	06:52-07:08 07:11-07:22 07:24-07:39 07:41-07:55 07:52-08:06 08:07-08:17 08:18-08:32 08:33-08:44 08:45-08:58 08:59-09:10 09:10-09:24	999 m 52 m 997 m 50 m 996 m 50 m 997 m 50 m 999 m 53 m 1000 m	

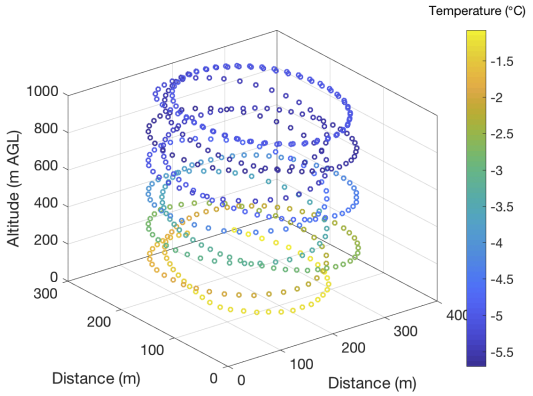

Fig 8.1: Example of SUMO's helical flight track used for profiling the ABL. Air temperature is indicated with colours. The profile was obtained between 09:10 and 09:24 UTC on the 15.06.2017.

Fig. 8.2: Priit Tisler landing the quadrocopter

Data management

All data obtained during this *Polarstern* expedition will be stored by the FMI and UNIS groups for post-processing. Access to data will be possible on request when processing and corrections have been finalized, and results are published in a peer-reviewed journal.

Fig. 8.3: Priit Tisler launching the SUMO

References

Jonassen MO, Tisler P, Altstädter B, Scholtz A, Vihma T, Lampert A, König-Langlo G, Lüpkes C (2015) Application of remotely piloted aircraft systems in observing the atmospheric boundary layer over Antarctic sea ice in winter. Polar Research, 2015, 34, 25651, http://dx.doi.org/10.3402/polar.v34.25651.

9. PHYSICAL OCEANOGRAPHY

Anna Nikolopoulos[1], Céline Heuzé[2], Torsten Linders[2], Elin Andrée[2], Sandra Sahlin[2]

[1]ABWR
[2]UGOT

Grant-No. AWI_PS106/1_2-00

Objectives

The physical oceanography (PO) component of PS106 aimed to map the physical water properties of the study region, with a focus on describing the prevailing hydrographic conditions along the cruise track connected to the objectives of SIPCA. The PS106 data collection includes measurements of temperature, salinity, fluorescence, oxygen and transmissivity from the southwestern Nansen Basin, the continental slope north of Svalbard, and the Svalbard area in the Barents Sea, see Fig. 9.1. During the ice drift of PS106/1 measurements of water velocities and the vertical distribution and composition of particles were additionally carried out under the sea ice. The measurements of particle composition continued through PS106/2, during which also water samples were taken for age analysis of the inflowing Atlantic water. In a more long-term effort to monitor the AW inflow, eight bottom landers were deployed to record the water temperature at eight different locations along the shelf-slope and in the Kvitøya through.

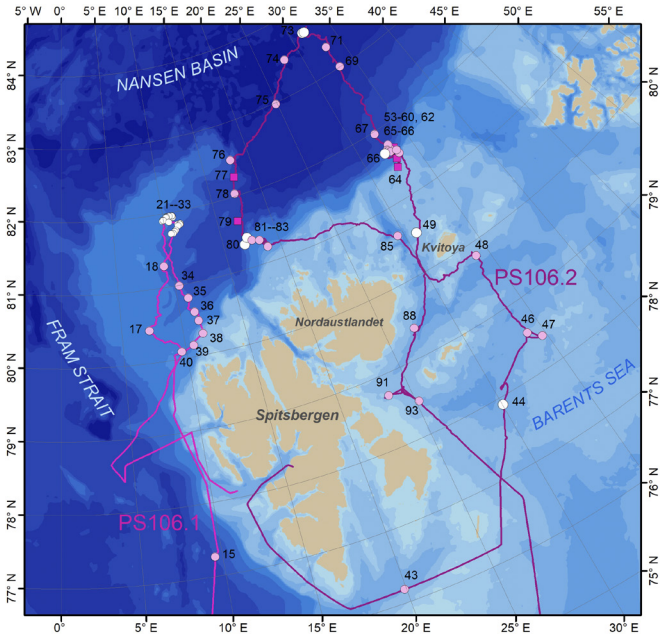

Fig. 9.1: Overview map of the cruise tracks of both legs, and all CTD stations of PS106. Circles show regular CTD/RO casts (white symbols indicate casts at the dedicated ice stations). Casts by XCTD are shown as squares. The hydrographic measurements during PS106/1 were made over the eastern rim of the Yermak Plateau and the shelf slope north of Spitsbergen, while the measurements of PS106/2 were made in the Barents Sea, over the shelf slope north of Nordaustlandet and Kvitøya as well as in the deeper parts of the Nansen Basin.

In this sector of the Arctic Ocean, the dominant hydrographic feature is the Atlantic water (AW) inflow from the Nordic Seas. The ice drift area over the Yermak Plateau and the continental slope are affected by the Fram Strait inflow branch of the AW, while the study area south and east of Svalbard also are characterised by typical shelf water masses. Earlier hydrographic results from the PS106 study area have been provided by e.g. Rudels et al. (1997; 2005; 2013), Våge et al. (2016), Meyer (2017), and Pérez-Hernández (2017). The PS106/1 cruise track, as well as the western-most cross-shelf track of PS106/2 also coincided with the study area of the PS92 TRANSSIZ cruise (Peeken et al., 2015), which was carried out during the corresponding season in 2015. Our observations may, therefore, be brought into both short and long-term perspectives and understanding of e.g. the heat-bringing AW boundary current dynamics, the variability of deep waters, and of how the sea ice is influenced by the subsurface waters.

Work at sea

Hydrographic measurements

Recurrent measurements of the general hydrographic (Conductivity/Temperature/Depth) conditions were carried out from the ship with the onboard standard CTD/Rosette water sampler system (CTD/RO) from Sea-Bird Electronics Inc (Fig. 9.2). The SBE911+ CTD was equipped with duplicate temperature (SBE3; SN2460/2417) and conductivity sensors (SBE4; SN2055/2054), a pressure sensor (SBE9+; SN0485) as well as an altimeter (Benthos; SN1228), and was connected to a SBE32 Carousel Water Sampler with 24 bottles á 12 liters. Additional sensors for fluorescence (WETLabs ECO-AFL/FL; SN1670), dissolved oxygen (SBE43; SN0880) and beam transmission (WETLabs C-Star; SN946) were also mounted on the carousel.

Fig. 9.2: The shipboard CTD/RO deployed from the aft of RV Polarstern

A Laser In-Situ Scattering and Transmissometry (LISST) particle size analyser was mounted on the CTD/RO on some of the shallow casts (to maximum 300 m depth due to limited depth range of this instrument). The LISST complemented the profiles with data on suspended volume and size distribution of particles of 2.5 – 500 µm size. An AQUAlogger 210TY was occasionally used together with the LISST on the CTD/RO to measure turbidity. Both the LISST and the AQUAlogger played their main roles in the under-ice measurements, see further under *Ice Work*.

Due to failure of the ship aft thruster the deployments of the CTD/RO in ice covered waters from June 8 (stn 25-4) and onward had to be shifted from its normal starboard side winch (Einleiterwinde; EL31) to the A-frame winch (Speicherwinde), to which it was brought to and from by a pallet jack (Fig. 9.2). Despite this change, the CTD/RO measurement programme could be undertaken largely as planned (Fig. 9.1 and Tab. 9.1).

During PS106/2 temperature and conductivity profiles were also obtained with expendable CTDs (XCTD-1) intended to increase the spatial resolution of the measurements across the continental slope and the southward transit (Fig. 9.1, Tab. 9.1). Due to faulty probes, however, only six XCTD casts could be successfully performed.

In total, 72 CTD profiles (66 CTD/RO, 6 XCTD) were obtained between 100 and 3,985 meters depth. Twenty-two of these profiles were obtained during the ice floe drift of the first cruise leg. Sixteen profiles were obtained specifically for describing the AW inflow along the continental slope in three transects across the boundary current. The remaining profiles were obtained in connection to other measurement activities along the cruise track. Eight casts were performed with the LISST attached to the CTD/RO (four of these also with the AQUAlogger attached).

Seawater samples were taken regularly from the CTD/RO Niskin bottles for salinity analysis for the post-cruise processing of the CTD data and calibration of the CTD sensors, and on leg2 also as complement to the transient tracer analysis, see below. All salinity samples were analysed underway with the onboard Optimare Precision Salinometer (OPS); 34 samples at 19 stations of PS106/1, and 87 samples at 11 stations od PS106/2 (Tab. 9.1). Seawater samples were also collected for testing appropriate sampling methodologies for environmental DNA analyses. These samples were taken either from the Niskin bottles (22 samples; various water depths), the FerryBox seawater inlet (6 samples; water from the keel at 11 m depth), or with a Kemmerer bottle from under the ice floe in connection to the LISST measurements (6 samples; various depths), see Table 9.1. The samples were filtered onto 0.22 micron Sterivex filters, either manually or with help of a MASTERFLEX® L/S® peristaltic pump system, and stored refrigerated until the analysis on land is undertaken. During PS106/2, seawater samples were additionally collected for transient tracers; chlorofluorocarbon (CFC-12, CFC-13) and sulfur hexafluoride (SF6). These samples were flame sealed and will be analysed by GEOMAR once back ashore.

The CTD/RO sensor data were preliminary processed underway with help of the ManageCTD software routine, to provide preliminary bottle data and data in ODV format, as presented here. The final post-cruise quality check, data processing and sensor calibrations will be undertaken on land before data in their final version are uploaded to the PANGAEA database.

Tab. 9.1: Metadata for all CTD/RO and XCTD casts of PS106. Asterisk by the station number denotes the use of XCTD (leg2), and 'A' denotes casts from the A-frame. CFC, Sal., and eDNA show the numbers of seawater samples taken for analyses of these respective parameters. Last column gives use of the LISST (L) and AQUAlogger (A) on the CTD/RO

Station PS106_	Date [UTC]	Time [UTC]	Lat [dd]	Lon [dd]	Cast depth [m]	Bottom depth [m]	CFC	Sal.	eDNA	LiSST/ AQUA-logger
12-2	29.05.2017	08:57	72.578	5.593	300	2324				L/A
15-1	30.05.2017	17:26	77.264	9.539	300	2041				L
15-2	30.05.2017	18:38	77.263	9.530	1001	2045		1		
17-2	01.06.2017	10:35	80.442	7.287	666	693		2		
18-2	02.06.2017	13:16	81.291	9.320	1289	1337		1		
21-1	04.06.2017	05:27	81.949	10.388	960	1000		2		
21-3	04.06.2017	08:39	81.951	10.481	300	1014				L
22-2	05.06.2017	08:31	81.938	10.943	1037	1078		2		
22-4	05.06.2017	19:29	81.928	10.932	1037	1076		2	2	
23-1	06.06.2017	05:34	81.947	10.902	1031	1071				
23-3	06.06.2017	07:51	81.949	10.886	300	1070				

Station PS106_	Date [UTC]	Time [UTC]	Lat [dd]	Lon [dd]	Cast depth [m]	Bottom depth [m]	CFC	Sal.	eDNA	LiSST/ AQUA-logger
23-4	06.06.2017	18:30	81.953	10.610	981	1020			2	
24-1	07.06.2017	05:34	81.945	10.336	955	992				
24-4	07.06.2017	07:44	81.939	10.276	300	984				L
24-7	07.06.2017	18:25	81.914	9.929	900	938		2	2	
25-4[A]	08.06.2017	18:47	81.896	9.854	895	931			1	
26-1[A]	09.06.2017	05:50	81.909	10.000	911	946		2		
27-6[A]	10.06.2017	19:21	81.871	10.472	1026	1066		2		
28-5[A]	11.06.2017	18:44	81.821	11.261	1343	1381		2		
29-1[A]	12.06.2017	05:39	81.829	11.528	1000	1524				
29-8[A]	12.06.2017	18:55	81.814	11.522	1514	1563		4	2	
30-2[A]	13.06.2017	14:59	81.814	11.497	1511	1556		4	3	
31-1[A]	14.06.2017	05:46	81.799	11.287	1437	1487				
31-3[A]	14.06.2017	18:40	81.748	10.986	1453	1502		2	4	
32-1[A]	15.06.2017	05:41	81.732	10.853	1010	1607				
32-5[A]	15.06.2017	18:38	81.706	10.691	1419	1470		2		
33-1[A]	16.06.2017	05:40	81.707	10.507	1000	1408				
34-2[A]	17.06.2017	13:17	80.993	10.364	1465	1475		2	3	
35-1[A]	17.06.2017	19:07	80.806	10.931	1435	1482				
36-1[A]	18.06.2017	01:15	80.603	11.251	1020	1057		2		
37-1[A]	18.06.2017	04:14	80.474	11.426	682	709			1	
38-1[A]	18.06.2017	07:36	80.290	11.567	175	191				L/A
39-2[A]	18.06.2017	11:19	80.159	10.653	442	458			1	
40-1[A]	18.06.2017	14:44	80.095	9.622	518	533			1	
43-1	24.06.2017	09:47	76.178	19.909	177	194				
44-1	25.06.2017	10:22	77.895	30.043	246	259				L
46-1	26.06.2017	00:19	78.554	33.959	192	204				
47-3	26.06.2017	09:22	78.406	34.702	151	163				L/A
48-2	27.06.2017	02:41	79.816	34.022	270	284				L/A
49-1[A]	28.06.2017	02:52	80.517	30.970	136	148				
53-1[A]	30.06.2017	05:30	81.570	33.425	271	279	6	6		
54-1*	30.06.2017		81.620	33.331						
55-1*	30.06.2017		81.672	33.266						
56-1[A]	30.06.2017	11:17	81.693	32.913	1590	1628	10	10		
57-1[A]	30.06.2017	06:25	81.748	32.940	1979	1996				
58-1[A]	30.06.2017	00:48	81.693	32.632	1601	1631				
59-1[A]	30.06.2017	22:49	81.676	32.687	1336	1356				
60-1[A]	01.07.2017	00:55	81.650	32.802	1023	1057				
62-1*	01.07.2017		81.518	32.977						
64-1*	01.07.2017		81.413	32.615						
65-1[A]	02.07.2017	01:41	81.624	33.361	580	608				
66-2[A]	02.07.2017	13:10	81.665	32.248	200	1787				
67-3[A]	03.07.2017	14:20	81.966	32.411	2752	2811	7	7		
69-4[A]	05.07.2017	11:41	83.005	33.187	3653	3723	8	8		

Station PS106_	Date [UTC]	Time [UTC]	Lat [dd]	Lon [dd]	Cast depth [m]	Bottom depth [m]	CFC	Sal.	eDNA	LiSST/ AQUA-logger
71-1[A]	06.07.2017	01:09	83.331	33.086	1004	3899				
73-1[A]	06.07.2017	20:51	83.666	31.563	101	4029				
73-4[A]	07.07.2017	03:09	83.665	31.781	3961	4025	8	8		
74-1[A]	08.07.2017	08:47	83.471	28.010	3985	4050	8	8		
75-1[A]	09.07.2017	02:53	82.980	24.870	3986	4049	8	8		
76-1[A]	10.07.2017	05:41	82.491	18.016	1000	1904				
77-1*	10.07.2017		82.252	17.855						
78-1[A]	10.07.2017	22:13	82.035	17.408	2681	2721	8	8		
79-1*	11.07.2017		81.663	16.902						
80-1[A]	12.07.2017	00:44	81.326	16.930	101	1098				
80-7[A]	12.07.2017	23:32	81.407	17.283	955	978	6	6		
81-1[A]	13.07.2017	01:39	81.359	17.640	764	801				
82-1[A]	13.07.2017	05:27	81.327	18.299	580	608				
83-1[A]	13.07.2017	09:03	81.206	18.823	419	434	8	8		
85-1[A]	14.07.2017	19:46	80.611	29.489	301	288	9	10		
88-2	15.07.2017	18:22	79.393	27.173	265	275				
91-4	16.07.2017	16:01	78.710	23.450	121	122				
93-4	17.07.2017	10:33	78.470	25.205	176	180				

Ice work

During the drift phase of PS106/1, a top anchored mooring line was deployed through the ice equipped with one 1200 kHz and two 300 kHz upward looking RDI Acoustic Doppler Current Profilers (ADCP) and three SBE microCAT CTDs, see Fig. 9.3. This set of instruments were used to measure the under-ice vertical and horizontal water velocities and the temperature/ salinity characteristics in the uppermost 180 m of the water column. The mooring line was deployed between June 4 and June 16 which added up to twelve days of data recording by all instruments.

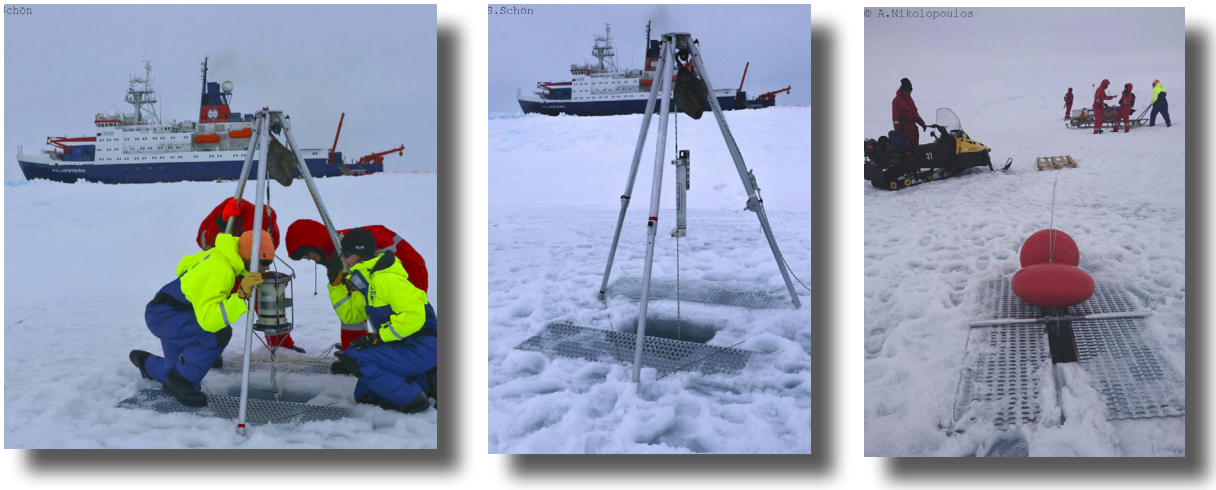

Fig. 9.3: Listening to the pings of one of the ADCPs prior to deployment (left), one of three microCAT CTDs (middle), the top anchor of the mooring line (right)

Under-ice measurements were additionally made with the LISST particle size analyser, the AQUAlogger and one microCAT CTD, both in profiling and constant-depth mode, see Figure 9.4.

The deployments during PS106/1 resulted in vertical profiles down to 200 m as well as time series at fixed depths, for up to 48 hours (Tab. 9.2). During the five ice stations of PS106/2, the LISST was deployed at fixed depths for durations of four to nine hours, mainly around UTC midnight to early morning. The deployments were made close to the ADCP mooring line (PS106/1) as well as the sediment trap and primary production measurements (Chapter 13).

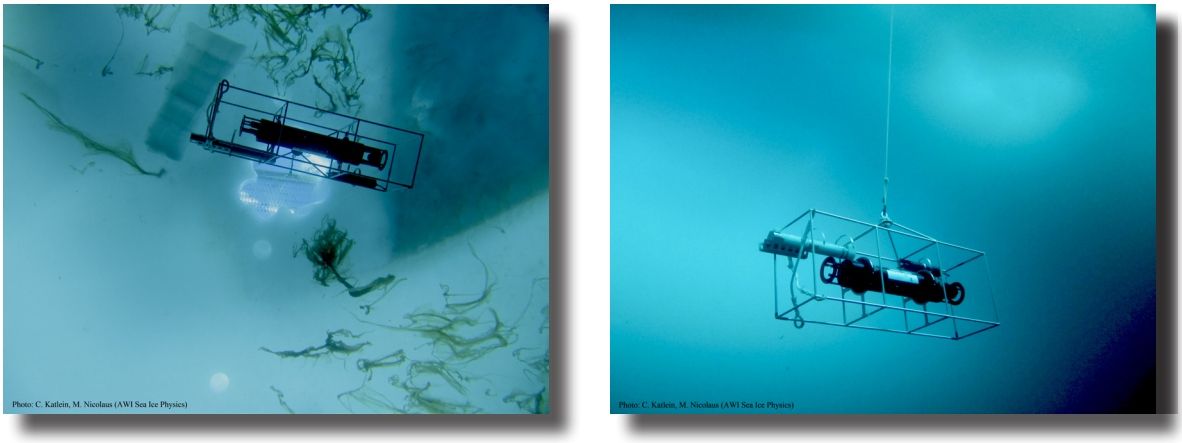

Fig. 9.4: Photos of the LISST taken by the ROV team during the overnight deployment just below the sea ice (3 m depth) (left) and the 48-hr deployment at 25 metres depth (right). The LISST is the larger instrument in the centre of the frame, while the smaller white instrument is a MicroCAT CTD, and the smallest black instrument is an AQUAlogger for turbidity.)

Tab. 9.2: Metadata for the LISST measurements undertaken from the ship or from the ice. The measurements were made at constant depth or as profiles, as indicated by the deployment and profile depths, respectively. The relative location on the ice floe, or ship, is given in the comment. eDNA indicates water sampling for eDNA analysis in connection to the LISST-measurement.

Station/ LISST cast PS106_	Lat	Lon	start [UTC]	end [UTC]	depl. depth [m]	profile depth [m]	comment
22-1/1	81.93968	10.92995	2017-06-05 16:48	2017-06-06 07:20	55	-	AZFP2
24-2/1	81.94226	10.30758	2017-06-07 17:06	2017-06-07 17:18	-	55	AZFP2, eDNA
26-2/1	81.90876	10.00602	2017-06-09 08:05	2017-06-09 09:19	-	200	Sedim. trap hole
26-6	81.90794	10.01342	2017-06-09 15:23		-	85	Ship side, after boxcorer
27-1/1	81.90416	10.23033	2017-06-10 11:27	2017-06-10 12:29	-	200	Garden, eDNA
27-1/2	81.90416	10.23033	2017-06-10 17:26	2017-06-10 17:56	-	200	Garden
27-1/3	81.90416	10.23033	2017-06-10 18:07	2017-06-10 22:26	5	-	Garden
27-1/4	81.90416	10.23033	2017-06-10 22:35	2017-06-10 23:08	-	200	Garden
27-1/5	81.90416	10.23033	2017-06-10 23:16	2017-06-11 06:18	5	-	Garden
28-2/1	81.86524	10.73605	2017-06-11 06:26	2017-06-11 06:57	-	200	Garden
28-2/2	81.86524	10.73605	2017-06-11 07:02	2017-06-11 10:27	5	-	Garden
28-2/3	81.86524	10.73605	2017-06-11 10:33	2017-06-11 11:02	-	200	Garden, eDNA
29-6	81.81687	11.553254	2017-06-12 14:57	2017-06-12 16:11	20	150	Ship aft, after boxcorer
31-2/1	81.79807	11.28479	2017-06-14 10:32	2017-06-16 09:13	25	-	Garden

Station/ LISST cast PS106_	Lat	Lon	start [UTC]	end [UTC]	depl. depth [m]	profile depth [m]	comment
45-1/1	78.11134	30.47859	2017-06-25 18:42	2017-06-26 00:47	19	-	Sedim. trap area
50-1/1	80.50841	30.98369	2017-06-28 23:24	2017-06-29 05:12	20	-	Sedim. trap area
66-5/1	81.65542	32.34167	2017-07-02 18:58	2017-07-03 01:39	20	-	Sedim. trap area
73-2/1	83.66128	31.58055	2017-07-07 00:39	2017-07-07 04:54	10	-	Sedim. trap area
80-2/1	81.30809	16.88646	2017-07-12 04:12	2017-07-12 13:13	10	-	Sedim. trap area

Deployment of bottom landers

Seven bottom landers were deployed during the two slope transects of PS106/2, and one in the Kvitøya trough into which the AW boundary current at times has been found to divert to (Pérez-Hernández et al. 2017), see Fig. 9.5, Table 9.3. These are expendable temperature sensors that sit at the ocean floor and measure the water temperature every 30 minutes. They have been programmed to automatically stop measuring in summer 2019, burn their connection to their anchor, float back to the surface and send their data by satellite.

The LoTUS bottom landers manufactured by the Royal Institute of Technology KTH (Sweden) were pre-programmed upon arrival onboard, whereas the Tpop manufactured by the University of Rhode Island (US) were started manually and programmed on 27 June 2017. The deployment was done by rope, simultaneously lowering the lander and its anchor from the aft deck on the starboard side as the ship was still (Fig. 9.6). When both the anchor and the lander were touching the water, the anchor was released from the rope first, then the lander. All deployments occurred straight after a CTD or XCTD cast for calibration purposes, except for LoTUS#43 whose corresponding XCTD failed.

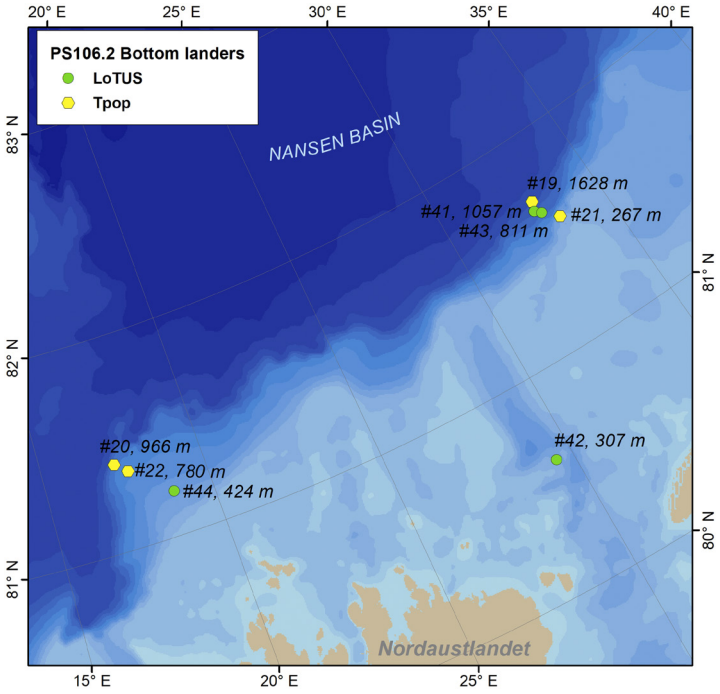

Fig. 9.5: The locations of the four LoTUS and four Tpop bottom landers deployed during PS106/2.

Fig. 9.6: Deployment of LoTUS 41 by lowering with two ropes

Tab. 9.3: Metadata for the eight bottom landers deloyed during PS106/2; Model, Buoy ID, deployment Station, Latitude (dd), Longitude (dd), Depth (m), Date and Time as well as their respective programmed Release date.

Model	Buoy ID	Station PS106_	Latitude	Longitude	Depth [m]	Date	Time [UTC]	Release
Tpop	21	53-2	81.567	33.420	267	30.06.2017	06:00	27.06.2019
Tpop	19	56-2	81.690	32.917	1628	30.06.2017	12:00	01.09.2019
LoTUS	41	60-2	81.650	32.806	1057	01.07.2017	01:35	20.07.2019
LoTUS	43	61-1	81.623	32.984	811	01.07.2017	04:06	20.07.2019
Tpop	20	80-6	81.405	17.284	966	12.07.2017	00:10	01.09.2019
Tpop	22	81-1	81.357	17.643	780	13.07.2017	02:04	27.06.2019
LoTUS	44	83-1	81.204	18.806	424	13.07.2017	09:27	20.07.2019
LoTUS	42	85-1	80.604	29.503	307	14.07.2017	20:13	20.07.2019

Preliminary results – to be confirmed after post-cruise sensor calibration

Hydrographic measurements

The water mass characteristics as monitored along the track of PS106 are summarized in Fig. 9.7, following the definitions mainly by Rudels et al. (2000), except for intermediate and deeper water masses (IW/DW) which were not characterized in detail here. The distribution in TSσ-space is typical for this region of the Arctic ocean and reflects the interactions between the main components Polar Surface Water (PSW), Atlantic Water (AW) and deep water-masses resulting in the mixed products warm Polar Surface Water (wPSW) and Modified Atlantic Water (MAW).

The sea-ice covered conditions encountered during major parts of PS106 are exhibited by the cold Polar Surface Waters (PSW), which are at freezing temperature until salinities of 34.2 (at the typical lower 'knee' of the diagram (e.g. Steele and Boyd, 1998). When out of the ice a warmer version of PSW (wPSW) resides the very surface layers (e.g. at station 37-40 northwest of Svalbard, *cf*. Fig. 9.7).

Atlantic Water (AW) was present at all locations, with the maximum temperatures decreasing with distance from the Fram Strait. The overall maximum temperature of AW observed during PS106 was 4.67°C (station 40, at 35 m depth). Moving away from the continental slope and into the Nansen basin or the Barents Sea, the AW successively loses its heat (as can be seen by the associated 'TS-triangles' being more confined towards colder temperatures), and the maximum temperatures are found deeper in the water column. Over the north-eastern parts

of the Yermak Plateau (PS106/1 drift), the maximum AW temperatures averaged 2.3°C at an average depth of 195 m. Similar AW temperatures were observed further east along the shelf-slope during PS106/2.

Mixing of AW with PSW results in the fresher left 'leg' of MAW, while mixing between AW and deep water masses give rise to the saltier MAW. Further analysis of the CFC samples as well as oxygen measurements will reveal which mixings occurred between each water mass.

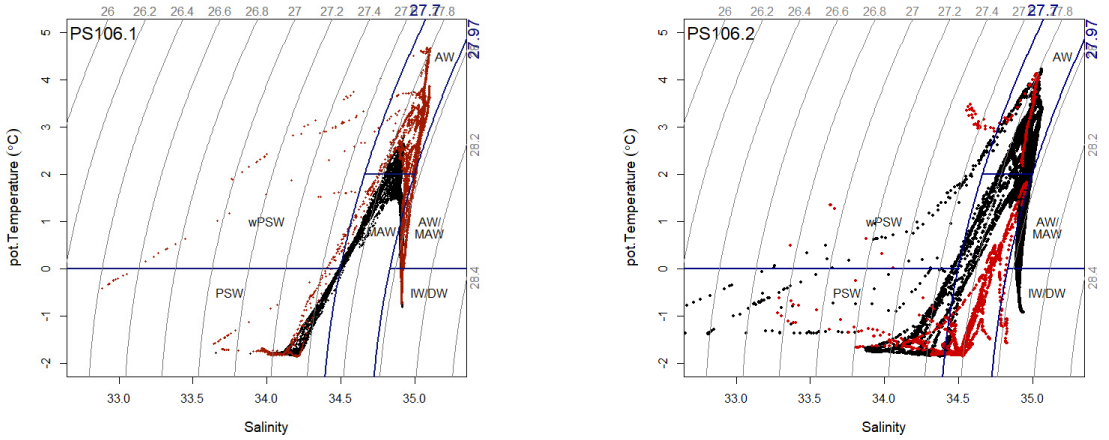

Fig. 9.7: Potential temperature/salinity diagram for all CTD/RO data measured during PS106/1 (left) and PS106/2 (right). Curved isopycnals indicate the potential density anomaly (sigma; sq), and denser water masses from left to right. Classification of the encountered water masses during PS106/1 mainly follow Rudels et al. (2000) as indicated by labels. Blue isolines in both diagrams indicate temperature (q=0 and 2° C) and density (sq=27.7 and 27.97) values crucial for these definitions. For PS106/1 (left) black dots show the casts during ice-floe drift and red dots all other casts. For PS106/2 (right) red dots show Barents Sea measurements and black dots all other casts.

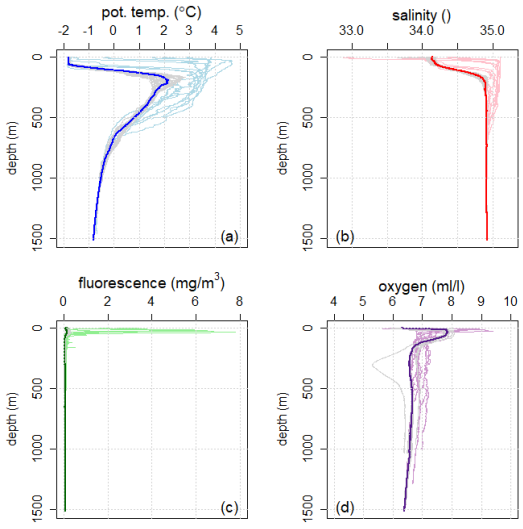

Fig. 9.8: All CTD/RO profiles measured during PS106/1, full depth. Thin grey lines show the recurrent casts during the ice-floe drift, with the median conditions over this period as thick solid lines.

For an overview of the parameter ranges over depth, all CTD/RO profiles of temperature, salinity, fluorescence and oxygen are shown in Fig. 9.8 (PS106/1) and Fig. 9.9 (PS106/2). The deepest casts of PS106 were made to almost 4,000 m at the northernmost position of PS106/2 (3,986 m at stations 74 and 75). The deepest cast of PS106/1 was made down to 1,514 m (station 29, during the drift).

The 30 km by 30 km (16 nm x 16 nm) region over which the ice-floe drift took place was subject to relatively small variability (cast depths 930-1,600 m), as indicated by the narrowly composed data "cloud" around the overall-drift median values (thick solid lines in Fig. 9.8). The largest variability in temperature is seen over the depths associated with AW and MAW (about 1.5°C difference between the coldest and warmest waters at ~175 m depth).

For both cruise legs, there was a clear difference in hydrographic properties between the ice-free and ice-covered regions. During

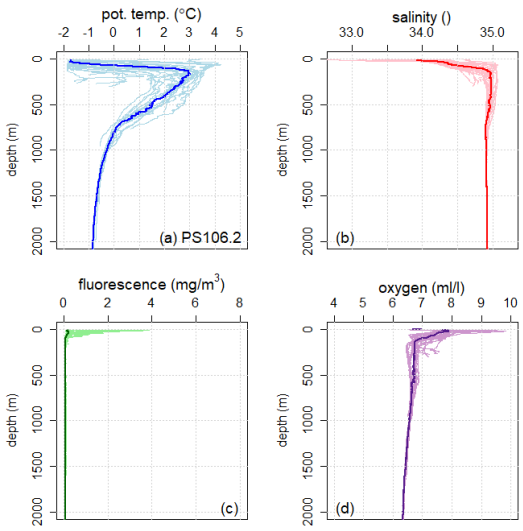

Fig. 9.9: All CTD/RO profiles measured during PS106/2, down to 2000 m (note that several casts were made deeper than this, see Table 9.1). Thick solid lines show the median.

PS106/1, casts performed during the ice-floe drift had a deep halocline (Fig. 9.8, grey lines), whereas the halocline and thermocline were as shallow as 20 m in the ice-free areas (thin coloured lines).

Although the AW core is located rather shallow (100-200 m), the whole Atlantic layer (AW or MAW) extends down to ~750 m depth (*cf.* Fig. 9.12 and 9.13). The top 700 metres of most casts are turbulent and at times unstable, exhibiting some double diffusion, probably caused by the mixing of colder and warmer water masses. The 700 – 1,500 m depth interval also exhibits some mixing, with sudden temperature, salinity and oxygen changes happening over 50 m vertical range, suggesting the intrusion of another water mass or mixing with deep waters.

In correspondence with the thick sea ice cover along major parts of our cruise track, only very low fluorescence values (Chl *a*) were measured. In ice-free regions, however, chlorophyll maxima around 6-7 mg/m^3 were observed. For example, when steaming southward towards the north-western Svalbard, through the marginal ice zone and eventually in mostly open waters, the largest fluorescence values were found at station 37 (7.8 mg/m^3, 34 m depth. Note: preliminary values), followed by station 40 (6.6 mg/m^3, 25 m), and 38 (6.5 mg/m^3, 19 m), see Fig. 9.10. These maxima were 'sitting' on the pycnocline in the relatively warm wPSW and AW, see Fig. 9.11. At station 39 the chlorophyll maximum was found just below the surface (3.8 mg/m^3, 4 m) in cooler (shelf?) waters. Similar results were found during the shallower casts of PS106/2.

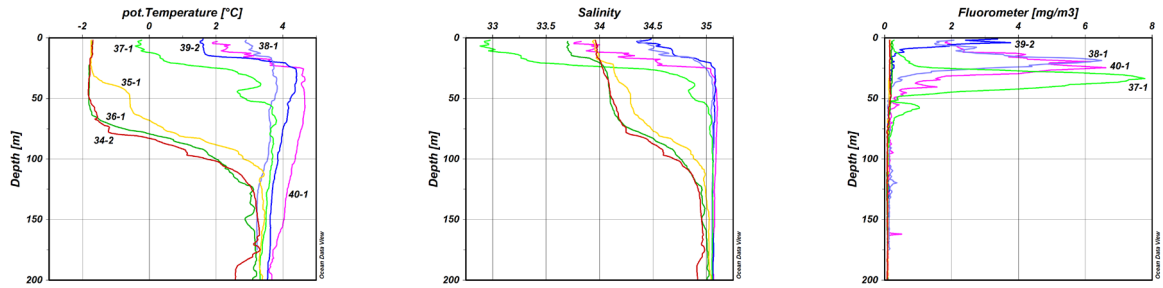

Fig. 9.10: The upper 200 m of the CTD/RO profiles at stations 34-40 of PS106/1. Elevated fluorescence values were encountered over the shelf-slope stations along this transect, concurrently with the decreasing ice cover.

From the transient tracer samples collected during PS106/2, we will be able to determine the age of the AW (that is, its formation year in the North Atlantic). The results will be compared to measurements taken further upstream (Fram Strait) for investigating where the AW is advected from, and how fast it propagates around the Arctic Ocean. The analyses will also give information about age and mixing properties of other water masses of interest encountered during the deep casts of leg 2. A practical aim with these measurements is also to assess the feasibility of the sampling, which traditionally are not performed by the PO team.

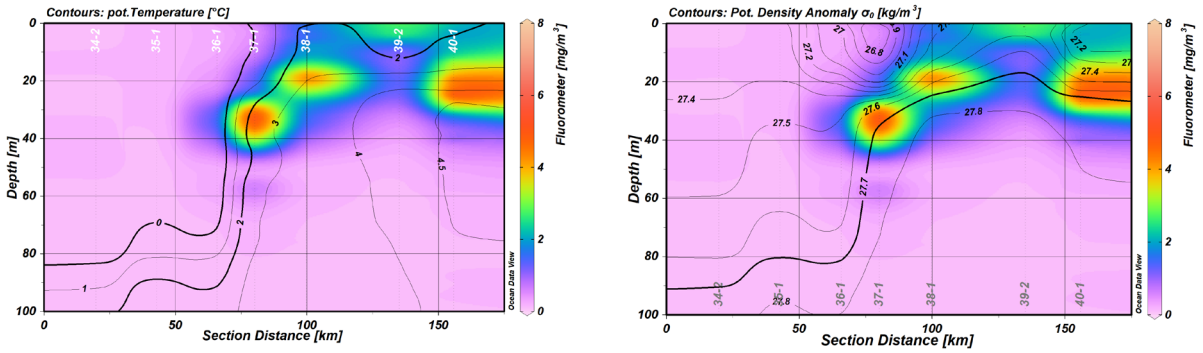

Fig. 9.11: Contoured sections of fluorescence overlaid by potential temperature (left) and density anomaly s_q (right), for the upper 100 m of stations 34-40. The maximum fluorescence values are found in the pycnocline within the relatively warm AW/wPSW, cf. the TS-diagram in Fig. 9.7. The full-depth temperature and salinity distributions are shown as sections in Fig. 9.12.

Hydrographic cross-slope transects

Three transects were performed across the shelf-slope during PS106, although the opportunistic stations 34-40 of PS106/1 were made at much coarser horizontal resolution than the two scheduled high-resolution transects of PS106/2, cf. Fig.s 9.2, 9.12 and 9.13. The detailed analysis of these transects requires calibration of the CTD sensors and the results from the sampled sea water analyses.

At the north-western corner of Svalbard the Atlantic Water is, as expected, found very close to the surface at the shelf-slope stations 38-40, while it is submerged underneath the considerably colder and fresher PSW at the stations further north, cf. Fig. 9.7. At this location the bulk of the AW/MAW layer (27.7 < s_q < 27.97) is found between 100-500 m. At the first transect of leg 2 at 33°E (Fig. 9.10), the Atlantic Water is found to reside below 50 metres depth over the Barents Sea shelf as well as in the deep basin, where it extents to 400 m (core at 200 m). Due to faulty XCTDs and the presence of an ice floe over our initially targeted positions it is unclear if the cold and salty layer around 150 m at 10 km is unique to this location or a common feature of the shelf slope (possible mixing product of AW and PW influenced by the topography). Double diffusion is observed between 400 and 600 m (visible in individual profiles).

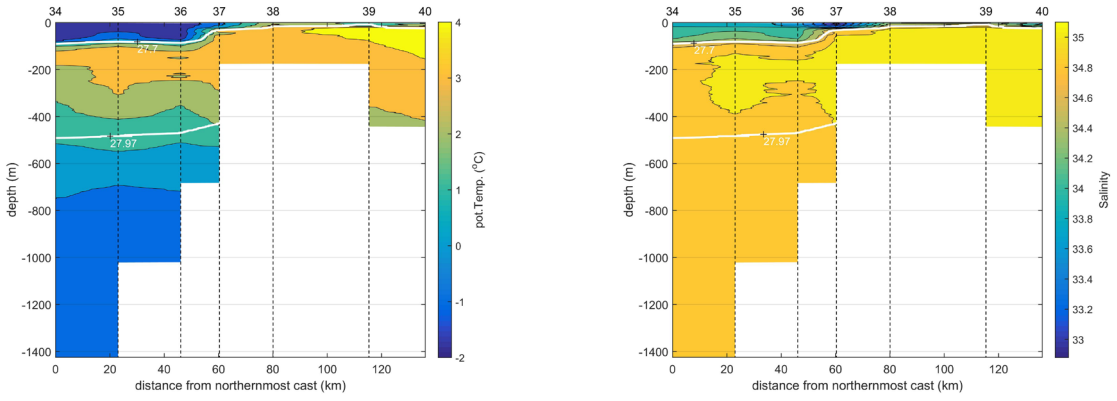

Fig. 9.12: Potential temperature (left) and salinity (right) across the shelf as measured during the transect of PS106/1. White lines show the sigma 27.7 and 27.97 isopycnals, respectively, cf. the TS-diagram in Fig. 9.4. Dashed vertical lines indicate the location of the casts (top labels), travelling from the north towards the shelf slope in a knee-shaped path as shown by Fig. 9.2.

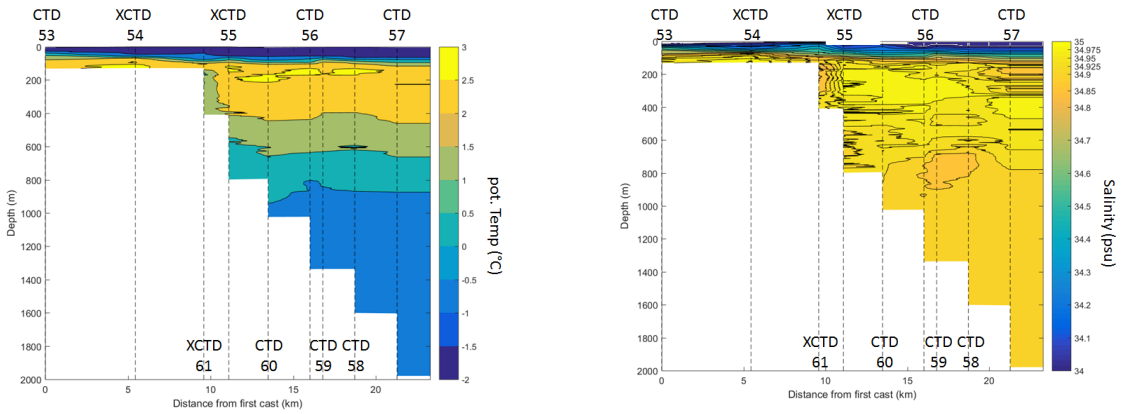

Fig. 9.13: Potential temperature (left) and salinity (right) across the shelf as measured during the first transect of PS106/2. Dashed vertical lines indicate the location of the casts, travelling northward from the shelf to the deep ocean (top labels) and back to the shelf (lower labels).

Ice work

The top-most ADCP (1200 kHz) of the mooring line was deployed in upward looking mode on 10 m depth to measure turbulent velocities in the uppermost layer of the water column. These data will be used particularly to study the vertical exchange processes right underneath the sea ice. The two deeper ADCPs (300 kHz) were deployed at 100 m and 180 m depth, respectively, also in upward looking mode. These measurements will be used to analyse both vertical and horizontal water current velocities between the approx. 10-180 m depth covered by the instruments.

Except for water velocities, which is the most "direct" product of this type of instrument, the ADCP data will be further processed for the acoustic mean echo strength and absolute backscatter to outline potential sound scattering layers. The aim of this analysis is to identify the characteristics of present scatterers (for the 300 kHz instruments, typically small mesozooplankton a few millimetres in size), their possible vertical migration patterns, and if these patterns are linked to specific properties of the water. A qualitative analysis of such sound scattering layers will subsequently require complementary data from e.g. the under-ice LISST measurements and eDNA sampling, as well as the results from the sediment traps and the various net sampling. From both a technical and scientific aspect, a comparison between the results gained from these moored ADCPs and the concurrently deployed Acoustic Zooplankton Fish Profiler (AZFP) (Chapter 13), would be valuable and add further insights about the applicability of both respective technologies in this under-ice environment.

The first preliminary results of the LISST measurements of PS106/1 indicate that:

- particles larger than 100 µm dominate the total suspended volume at all depths,
- a secondary mode with sizes around 10 µm are typically present below 100 m, and these sizes correspond largely to what is found in the sediments by box coring,
- at least one overnight deployment showed a temporal variation pattern for 5 µm particles at a depth of around three metres, with the maximum volume coinciding with the solar minimum, see Fig. 9.14 (left).
- during the last 48-hour deployment, coinciding with increased sea ice melting, one event lasting 4 h occurred with major changes in suspended volume (order of magnitude) in most size classes, see Fig. 9.14 (right).

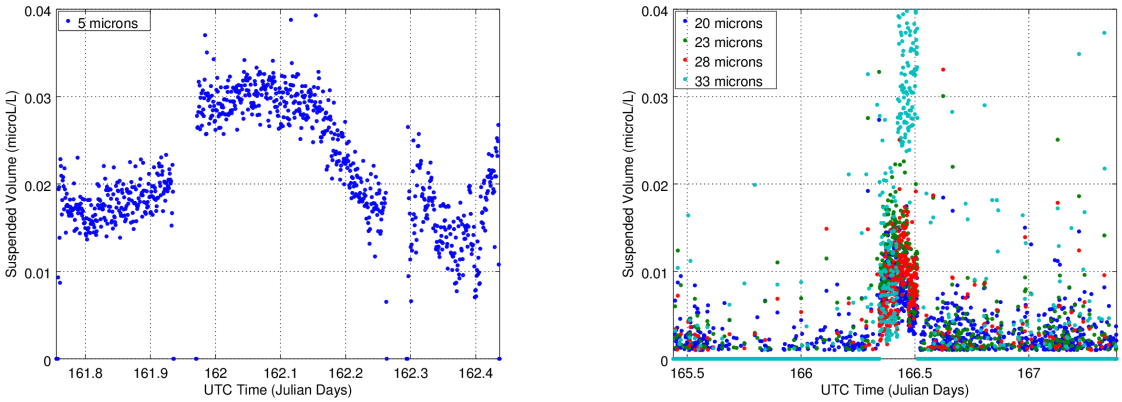

Fig. 9.14: LISST data (selected size class) from overnight deployment under the ice at 3 m depth (left) and from a 48 h deployment at 25 m (right). Gaps in data in the left panel are due to vertical profiling with LISST. Note that solar minimum at longitude 10 °E is after UTC midnight.

Data management

The oceanographic data collected during PS106 will be delivered to the PANGEA database and to the appropriate national data centres after post-cruise sensor calibration and data processing.

References

Meyer A, Sundfjord A, Fer I, Provost C, Villacieros Robineau N, Koenig Z, Onarheim IH, Smedsrud LH, Duarte P, Dodd PA, Graham RM, Schmidtko S, and Kauko HM (2017) Winter to summer oceanographic observations in the Arctic Ocean north of Svalbard. J. Geophys. Res. Oceans, doi: 10.1002/2016JC012391.

Pérez-Hernández MD, Pickart RS, Pavlov V, Våge K, Ingvaldsen R, Sundfjord A, Renner AHH, Torres DJ, and Erofeeva SY (2017) The Atlantic Water boundary current north of Svalbard in late summer. J. Geophys. Res. Oceans, 122, 2269–2290, doi:10.1002/2016JC012486.

Peeken I (editor) (2015) The Expedition PS92 of the Research Vessl POLARSTERN to the Arctic Ocean in 2015. http://hdl.handle.net/10013/epic.46750, doi:10.2312/BzPM_0694_2016, ISSN 1866-3192.

Rudels B, Meyer R, Fahrbach E, Ivanov V, Østerhus S, Quadfasel D, Schauer U, Tverberg V, Woodgate R A (2000) Water mass distribution in Fram Strait and over the Yermak Plateau in summer 1997. Annales Geophysicae 18, 687-705.

Rudels B, Björk G, Nilsson J, Winsor P, Lake I, Nohr C (2005) The interactions between waters from the Arctic Ocean and the Nordic Seas north of Fram Strait and along the East Greenland Current: results from the Arctic Ocean-02 Oden expedition. Journal of Marine Systems 55, 1–30, doi:10.1016/j. jmarsys.2004.06.00.

Rudels B, Schauer U, Björk G, Korhonen M, Pisarev S, Rabe B, Wisotzki A (2013) Observations of water masses and circulation with focus on the Eurasian Basin of the Arctic Ocean from the 1990s to the late 2000s. Ocean Science, 9, 147–169, doi:10.5194/os-9-147-2013.

Steele M and Boyd T (1998) Retreat of the cold halocline layer in the Arctic Ocean. J. Geophys. Res. Oceans, 103, 10419–10435, doi:10.1029/98JC00580.

Våge K, Pickart RS, Pavlov V, Lin P, Torres DJ, Ingvaldsen R, Sundfjord A, and Proshutinsky A (2016) The Atlantic Water boundary current in the Nansen Basin: Transport and mechanisms of lateral exchange. J. Geophys. Res. Oceans, 121, 6946–6960, doi:10.1002/2016JC011715.

10. SEA ICE PHYSICS

Christian Katlein[1], Marcel Nicolaus[1], Anja Sommerfeld[1], Veronica Copalorado[1], Louisa Tiemann[1], Marco Zanatta[1], Hannes Schulz[1], Benjamin Lange[1]

[1]AWI

Grant-No. AWI_PS106/1_2-00

Objectives

The observed shift from thicker multi-year to thinner first-year sea ice in the Arctic has consequences for various physical and biological processes within the sea ice and the upper ocean layer. For example, thin ponded sea ice transmits a significantly higher portion of the incoming solar radiation than snow covered thick ice. Hence, the optical properties of sea ice determine the amount of light (energy) that is transmitted into the ice and further into the upper ocean, contributing to warming and melting of sea ice. In addition, the amount of solar radiation dominates primary production and other biological processes in and below the ice layer. Following up observations during earlier cruises, we quantified the amount of light transmitted through sea ice during the melting season as a function of snow, sea ice, and upper ocean properties. This time of year coincides with the highest radiative fluxes and the onset of in- and under-ice biological productivity. However, a significant lack of data exists in this transition season, so that this expedition provided a great opportunity to measure the changing physical properties of the ice and the evolution of its surface geometry as snow and sea ice start melting.

With increasing energy input to the snow, the snow grains will increase in size and change shape. As a result, the reflectance of the snow cover is reduced and even more solar energy gets absorbed. This amplification loop finally induces and increases snowmelt. Further enhancement is caused by deposition of light absorbing particulate from the atmosphere into the snow. Another main objective was thus the observation of snow optical properties and the quantification of contents of light absorbing particles (black carbon) in the snow over the course of the transition season. The measurements of deposited particles are bridging to the aerosol measurements in the atmospheric boundary layer performed on *Polarstern* during PASCAL and SiPCA (Survival of Polar Cod in a Changing Arctic Ocean) and the vertical profiling of the atmosphere with the research aircraft *Polar 5* and *6* during ACLOUD.

The sea ice mass budget is very sensitive to small changes in the energy budget and dominant processes. Snow melt, melt pond formation, sea ice melt, and ocean surface freshening have strong feedbacks with energy fluxes. These fluxes are directly related to the geometry of sea ice, which exhibits large variation on all scales. The geometric variation can be described in terms of distributions for key variables: ice thickness, snow thickness, floe size, leads, and ice ridges. These are needed especially in sub grid scale, the length scale shorter than the resolution of Arctic ice drift models. Hence the main aim is to quantify these properties and the resulting fluxes as time series representing the floe-scale spatial variation. An additional source of information regarding the state of the Arctic sea ice and its snow cover is visual classification of key sea ice variables by sea ice observers. Though quite subjective, visual

observations have the promise of creating large datasets due to the numbers of vessels in the summer Arctic. Such datasets are of high value to record the ice conditions during various observations during the cruise and for validation of remote sensing products.

One objective of PS106 was to quantify physical-ecological properties of the sea ice environment at multiple spatial scales. This has been accomplished using a helicopter-borne electromagnetic (HEM) sea ice thickness instrument (the EM-bird) and an under-ice profiling platform, the surface and under-ice trawl (SUIT), with a mounted bio-environmental sensor array. In addition, these surveys will be combined with high-resolution, smaller-scale (floe-scale) surveys of the under-ice environment using the remotely operated vehicle (ROV).

Another objective of the long drifting station during the first cruise leg was to test workflows, team coordination, and equipment for setups on long-lasting sea ice stations. This involves experience in avoiding and handling of human influences on measurements and effective logistics needed for the yearlong MOSAiC expedition in 2019/20. Advancing observational capabilities in sea ice studies requires ongoing technical developments of measurement platforms and instruments as well as obtaining expertise in new measurements and inter-calibration of methods. Various advances havTabe been made and further steps are necessary towards MOSAiC. Hence, one aim is to test and quantify new methods and instruments, also in the framework of the FRAM and ACOSS infrastructure programmes.

Work at sea

Most of the sea ice physics work was performed during the ice stations along the cruise track (Fig. 10.1). On leg 106/1, daily work was performed on the two weeks-long drift station from 03 June (Station 020) to 16 June (Station 033). On leg 106/2, the work was performed on each of the 6 ice stations (see Tab. 10.1). All stations and the cruise track are shown in Fig. 10.2. The Fig. also includes the drift track of the main floe after leaving the drift station on 16 June. A suite

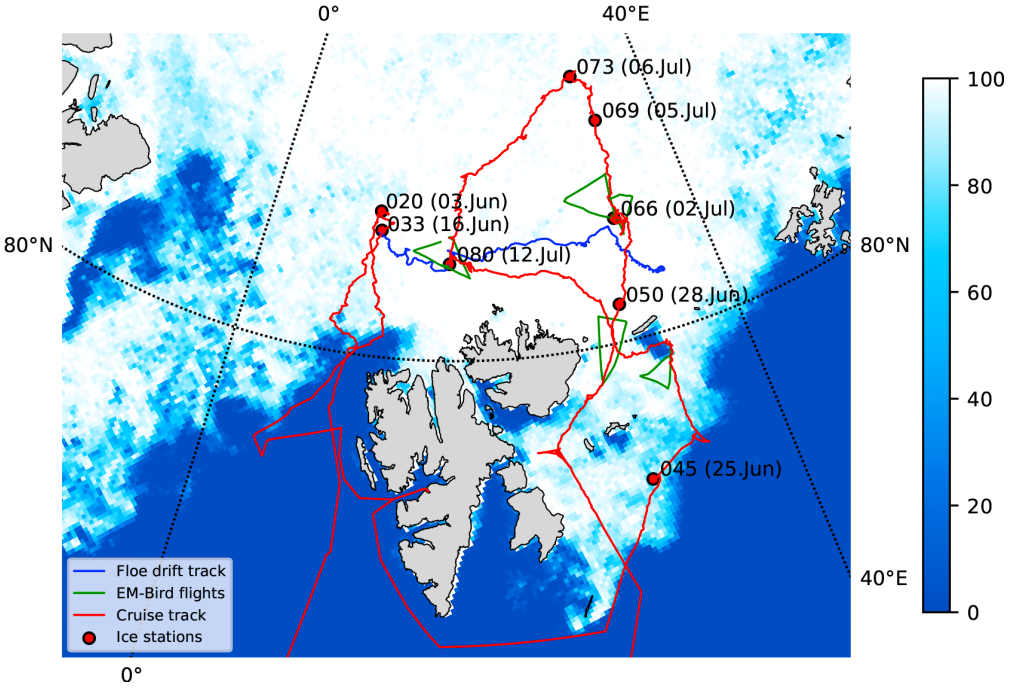

Fig. 10.1: Overview map of all ice stations, the drift of the main floe, and all EM-bird flights during PS106. Labels give station numbers (e.g.020) and date of the station. For the drift from 03 to 16 June, only the first and the last station are listed. A close up of the drift track of the main floe after leaving the floe on 16 June (blue line) given in Fig. 10.2. The background shows the sea ice concentration on 21 June.

of autonomous devices performed additional measurements until re-visit of the ice floe and recovery of most instrumentation (see below) on 11 July. The drift track then continues until 08 August 2017, based on the position data of the Surface Velocity Profiler (SVP, see below), which was left behind to track the floe beyond the expedition PS106.

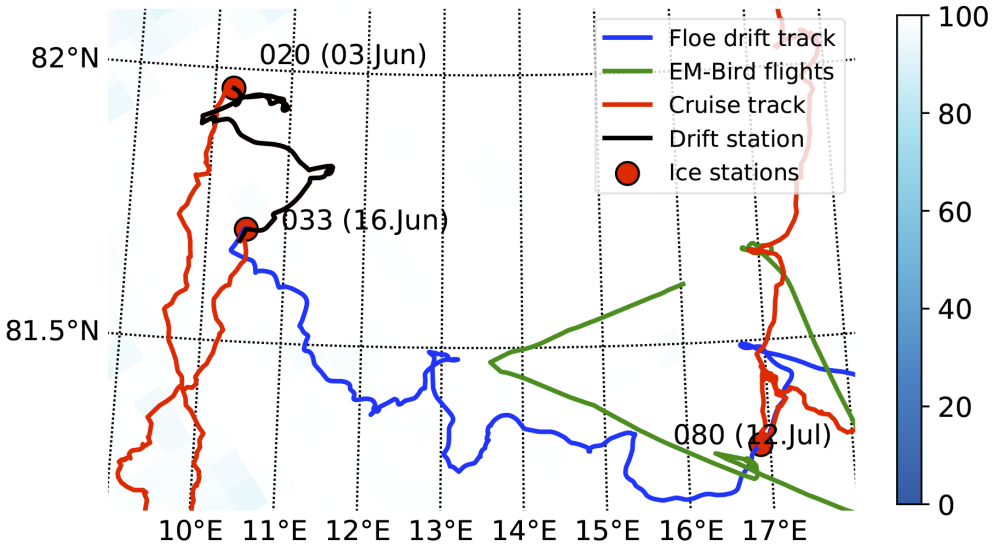

Fig. 10.2: Close up of the drift trajectory of the main ice station after leaving the floe on 16 June. This track shows the position of all autonomous platforms until recovery on 12 July.

Tab. 10.1: Sea ice physics ice station list

IceStationID	Date Time [UTC] Start	Date Time [UTC] End	Comment
021_CAMERA_1	04.06.2017T08:30:00	16.06.2017T18:00:00	Bridge Time Laps
022_GEM2_1	05.06.2017T07:41:00	05.06.2017T09:15:00	Standard transect
024_GEM2_1	07.06.2017T11:10:00	07.06.2017T12:00:00	Calibration
024_GEM2_2	07.06.2017T12:10:00	07.06.2017T13:30:00	Floe zig zag
026_GEM2_1	09.06.2017T06:54:00	09.06.2017T10:30:00	Long transect
031_GEM2_1	14.06.2017T14:09:56	14.06.2017T16:04:15	Standard transect
032_GEM2_1	15.06.2017T13:15:42	15.06.2017T13:41:04	ROV grid
032_GEM2_2	15.06.2017T13:41:22	15.06.2017T14:04:25	ROV grid
045_GEM2_1	25.06.2017T22:18:35	25.06.2017T22:58:30	ROV grid
050_GEM2_1	29.06.2017T01:03:54	29.06.2017T01:29:01	ROV grid
066_GEM2_1	02.07.2017T20:52:45	02.07.2017T21:40:10	ROV grid
066_GEM2_2	02.07.2017T22:18:09	02.07.2017T22:29:33	Ridge Study
069_GEM2_1	05.07.2017T10:23:09	05.07.2017T10:42:15	Calibration
069_GEM2_2	05.07.2017T11:02:46	05.07.2017T11:31:47	Floe transect
073_GEM2_1	07.07.2017T06:40:55	07.07.2017T07:00:24	ROV grid

IceStationID	Date Time [UTC] Start	Date Time [UTC] End	Comment
080_GEM2_1	12.07.2017T02:39:37	12.07.2017T04:06:28	PS106/1 standard transect
080_GEM2_2	12.07.2017T02:31:21	12.07.2017T02:39:17	Way Ship to start of Transect
022_MAGNAP_1	05.06.2017T07:41:00	05.06.2017T09:15:00	Standard transect
026_MAGNAP_1	09.06.2017T08:01:36	09.06.2017T08:15:39	Long transect
026_MAGNAP_2	09.06.2017T08:33:31	09.06.2017T08:41:45	Long transect
026_MAGNAP_3	09.06.2017T09:01:31	09.06.2017T09:10:38	Long transect
026_MAGNAP_4	09.06.2017T09:29:16	09.06.2017T09:42:06	Long transect
026_MAGNAP_5	09.06.2017T09:51:21	09.06.2017T10:01:29	Long transect
031_MAGNAP_1	14.06.2017T14:09:56	14.06.2017T16:04:15	Standard transect
045_MAGNAP_1	25.06.2017T22:11:38	25.06.2017T22:58:34	ROV grid
050_MAGNAP_1	29.06.2017T00:01:28	29.06.2017T00:54:20	ROV grid
050_MAGNAP_2	29.06.2017T01:04:50	29.06.2017T01:29:51	ROV grid
066_MAGNAP_1	02.07.2017T20:51:22	02.07.2017T21:41:12	ROV grid
066_MAGNAP_2	02.07.2017T22:17:54	02.07.2017T22:30:35	Ridge Study
069_MAGNAP_1	05.07.2017T10:57:15	05.07.2017T11:32:38	Floe transect
073_MAGNAP_1	07.07.2017T06:38:11	07.07.2017T07:01:27	ROV grid
080_MAGNAP_1	12.07.2017T02:31:01	12.07.2017T04:32:14	PS106/1 standard transect
022_RADSTA-SPEC_1	05.06.2017T12:10:00	12.07.2017T04:00:00	Spectral radiation station
024_AWS_1	07.06.2017T08:20:00	12.07.2017T04:00:00	Automatic weather station
024_Buoy_1	07.06.2017T08:20:00	12.07.2017T04:00:00	Snow Buoy 2017S53 (300234065725000)
024_CAMERA_1	07.06.2017T08:20:00	12.07.2017T04:00:00	Wildlife cam HIGH
024_CAMERA_2	07.06.2017T08:20:00	12.07.2017T04:00:00	Wildlife cam LOW
033_Buoy_1	08.06.2017T08:00:00	ongoing	SVP 2017P23 (300234062880930)
033_Buoy_2	07.06.2017T08:20:00	21.06.2017T00:00:00	SVP 2017P24 (300234062883920)
033_Buoy_3	16.06.2017T13:15:00	26.06.2017T09:54:03	Drifter 2017P38 (300434061138780)
033_Buoy_4	16.06.2017T13:25:00	12.07.2017T04:00:00	Drifter 2017P39 (300434061138870)
021_ROV_1	04.06.2017T14:00:00	04.06.2017T14:40:00	
023_ROV_1	06.06.2017T08:25:00	06.06.2017T09:30:00	
023_ROV_2	06.06.2017T11:15:00	06.06.2017T11:35:00	
023_ROV_3	06.06.2017T11:35:00	06.06.2017T13:20:00	

IceStationID	Date Time [UTC] Start	Date Time [UTC] End	Comment
025_ROV_1	08.06.2017T08:28:00	08.06.2017T08:39:00	no data
025_ROV_2	08.06.2017T08:45:00	08.06.2017T15:00:00	
027_ROV_1	10.06.2017T11:50:00	10.06.2017T15:20:00	incl. SUIT net
028_ROV_1	10.06.2017T22:50:00	11.06.2017T01:30:00	incl. SUIT net
028_ROV_2	11.06.2017T10:55:00	11.06.2017T14:40:00	incl. SUIT net
031_ROV_1	14.06.2017T07:50:00	14.06.2017T12:00:00	
032_ROV_1	15.06.2017T07:50:00	15.06.2017T13:30:00	incl. SUIT net
045_ROV_1	25.06.2017T20:20:00	25.06.2017T00:20:00	incl. SUIT net
050_ROV_1	29.06.2017T01:50:00	29.06.2017T04:00:00	incl. LOKI
066_ROV_1	02.07.2017T21:30:00	03.07.2017T01:45:00	incl. LOKI+net
073_ROV_1	07.07.2017T00:00:00	07.07.2017T06:20:00	incl. LOKI
080_ROV_1	12.07.2017T09:30:00	12.07.2017T12:50:00	incl. LOKI+net
066_SEAICEC_OPT_1	02.07.2017T23:00:00	03.07.2017T01:00:00	Optical Core
066_RAMSES_1	02.07.2017T23:00:00	03.07.2017T01:00:00	Radiance Profile
069_RAMSES_1	05.07.2017T10:15:00	05.07.2017T12:00:00	Radiance Profile
021_SNOWPIT_1	04.06.2017T09:00:00	04.06.2017T11:30:00	Snow1
022_SNOW_1	05.06.2017T10:00:00	05.06.2017T12:00:00	Snow1
022_SNOWPIT_1	05.06.2017T12:10:00	05.06.2017T13:15:00	Snow4
022_SNOWPIT_2	05.06.2017T13:50:01	05.06.2017T14:15:01	Snow3
022_SNOWPIT_3	05.06.2017T14:45:02	05.06.2017T16:15:02	Snow2
023_SNOW_1	06.06.2017T08:00:00	06.06.2017T08:20:00	Snow1
024_SNOW_1	07.06.2017T11:40:00	07.06.2017T11:50:00	Snow2
024_SNOW_2	07.06.2017T12:10:00	07.06.2017T12:30:00	Snow4
024_SNOW_3	07.06.2017T12:35:00	07.06.2017T13:00:00	Snow3
024_SNOW_4	07.06.2017T13:10:00	07.06.2017T13:40:00	Snow5
024_SNOW_5	07.06.2017T14:10:00	07.06.2017T14:50:00	Snow1
025_SNOW_1	08.06.2017T08:40:00	08.06.2017T10:30:00	Snow1
025_SEAICEC_1	08.06.2017T10:30:00	08.06.2017T11:00:00	Snow4
025_SNOW_2	08.06.2017T11:50:00	08.06.2017T14:00:00	Snow4
026_SNOWPIT_1	09.06.2017T07:30:00	09.06.2017T08:00:00	SnowT1
026_SNOWPIT_2	09.06.2017T08:00:00	09.06.2017T08:30:00	SnowT2
026_SNOWPIT_3	09.06.2017T09:00:00	09.06.2017T09:30:00	SnowT3
026_SNOWPIT_4	09.06.2017T10:00:00	09.06.2017T10:30:00	SnowT4
026_SNOWPIT_5	09.06.2017T11:00:00	09.06.2017T11:30:00	SnowT5
027_SNOW_1	10.06.2017T11:30:00	10.06.2017T12:00:00	SnowPondA
027_SNOW_2	10.06.2017T12:00:00	10.06.2017T12:30:00	SnowPondA
027_SNOW_3	10.06.2017T13:00:00	10.06.2017T13:30:00	SnowPondA

IceStationID	Date Time [UTC] Start	Date Time [UTC] End	Comment
027_SNOWPIT_1	10.06.2017T13:45:00	10.06.2017T14:50:00	SnowPondB
027_SNOW_4	10.06.2017T15:20:00	10.06.2017T16:40:00	Snow1
028_SEAICEC_1	11.06.2017T09:00:00	11.06.2017T09:30:00	Snow2
028_SNOWPIT_1	11.06.2017T09:30:00	11.06.2017T10:30:00	Snow2
028_SEAICEC_2	11.06.2017T13:30:00	11.06.2017T14:30:00	CORAS
028_SNOWPIT_2	11.06.2017T14:30:00	11.06.2017T115:30:00	Snow1
031_SNOW_1	14.06.2017T08:00:00	14.06.2017T08:30:00	Snow1
031_SNOWPIT_1	14.06.2017T08:30:00	14.06.2017T09:30:00	Snow1
031_SNOWPIT_2	14.06.2017T11:00:00	14.06.2017T12:00:00	SnowPondA
031_SNOW_2	14.06.2017T15:00:00	14.06.2017T15:30:00	Snow4
031_SNOW_3	14.06.2017T15:30:00	14.06.2017T16:00:00	Snow3
031_SNOW_4	14.06.2017T16:00:00	14.06.2017T16:30:00	Snow5
032_SNOWPIT_1	15.06.2017T13:00:00	15.06.2017T13:30:00	Snow2
032_SNOWPIT_2	15.06.2017T13:30:00	15.06.2017T13:45:00	Snow5
032_SNOWPIT_3	15.06.2017T13:45:00	15.06.2017T14:15:00	Snow4
033_SNOWPIT_1	16.06.2017T08:00:00	16.06.2017T09:00:00	CORAS
045_SNOWPIT_1	25.06.2017T20:00:00		ROV grid
045_SNOWPIT_2	25.06.2017T23:00:00		Upwind
050_SNOWPIT_1	28.06.2017T01:00:00		ROV grid
050_SNOW1	28.06.2017T02:00:00		Spatial_var
050_SNOW2	28.06.2017T02:30:00		Ridge_melt
050_SNOW3	28.06.2017T03:00:00		Spatial_var
050_SNOW4	28.06.2017T04:00:00		Gangway
066_SNOWPIT_2	02.07.2017T22:00:00		BRDF_2
066_SNOWPIT_1	02.07.2017T20:00:00		BRDF_1
66-5_ SurfaceSnow1	03.07.2017T00:00:00		Spatial_var
66-5_ SurfaceSnow2	03.07.2017T00:30:00		Spatial_var
66-5_ SurfaceSnow3	03.07.2017T00:40:00		Spatial_var
66-5_ SurfaceSnow4	03.07.2017T01:00:00		Spatial_var
069_SNOWPIT_1	05.07.2017T10:40:00		Mid_thickness
069_SNOWPIT_2	05.07.2017T11:30:00		Thicker_snow
069_SNOW_S1	05.07.2017T11:50:00		Spatial_var
069_SNOW_S2	05.07.2017T11:50:00		Spatial_var
069_SNOW_S3	05.07.2017T12:00:00		Spatial_var

IceStationID	Date Time [UTC] Start	Date Time [UTC] End	Comment
069_SNOW_S4	05.07.2017T12:00:00		Spatial_var
069_SNOW_S5	05.07.2017T12:00:00		Spatial_var
069_SNOW_S6	05.07.2017T12:10:00		Spatial_var
069_SNOW_S7	05.07.2017T12:20:00		Spatial_var
073_SNOWPIT_1	06.07.2017T23:00:00		ROV grid
073_SNOW_S1	07.07.2017T00:00:00		SIBio
073_SNOW_S2	07.07.2017T04:30:00		Downwind
073_SNOW_S3	07.07.2017T04:40:00		Downwind
073_SNOW_S4	07.07.2017T04:40:00		Downwind
073_SNOW_S5	07.07.2017T04:40:00		Downwind
073_SNOW_S6	07.07.2017T04:50:00		Downwind
073_SNOW_S7	07.07.2017T04:50:00		Downwind
073_SNOW_S8	07.07.2017T05:00:00		Downwind
073_SNOW_S9	07.07.2017T05:00:00		Downwind
080_Transect_S1	12.07.2017T03:30:00		Transect
080_Transect_S2	12.07.2017T03:35:00		Transect
080_Transect_S3	12.07.2017T03:40:00		Transect
080_Transect_S4	12.07.2017T03:45:00		Transect
080_Transect_S5	12.07.2017T03:50:00		Transect
080_Transect_S6	12.07.2017T03:55:00		Transect
080_Transect_S7	12.07.2017T04:00:00		Transect
080_Transect_S8	12.07.2017T04:05:00		Transect
080_Transect_S9	12.07.2017T04:10:00		Transect
080_Transect_S10	12.07.2017T04:15:00		Transect
080_Transect_S11	12.07.2017T04:20:00		Transect
080_SNOWPIT	12.07.2017T11:00:00		Pond_group
080_SurfaceStudy	12.07.2017T11:00:00		Pond_group

ROV

The most comprehensive data set of the sea ice physics group was collected based on the sensor suite of the new under ice Remotely Operated Vehicle (ROV) system BEAST. This work was performed in close collaboration with other partners of the SIPCA group. The ROV was always operated directly from the sea ice, launched through a hole in the sea ice using a lifting tripod. All operations during leg 106/1 were performed through only one hole, which was prepared at the beginning of the drift, while during leg 106/2, the access to the open water had to be prepared for each single station. Again ice holes were cut into the ice, except for Station 073 (06 July) when the ROV was launched of the floe edge. Control electronics was mounted in a heated cabin. During leg 106/1, the cabin was placed and recovered by helicopter transportation and remained on the ice for the entire drift. On all other stations, the control hut

was lifted by crane onto the ice and pulled with skidoo to the location of the launch hole. Close to the launch hole, transects were marked both at the surface and underside of the ice using marker sticks lowered through the ice. Along these transects ice thickness, freeboard, and snow depth were measured by drill holes with additional distributed measurements using a MagnaProbe (SnowHydro) in conjunction with a GEM2 (Geophex) ice-thickness sensor (see below).

The standard ROV sensor suite consists of

- hyperspectral irradiance and radiance sensors to characterize the variability of the under-ice light field;
- a conductivity, temperature, depth (CTD) sensor combined with a sensor for dissolved concentration, as well as pH and Nitrate sensors to measure bio-physical water properties;
- a Triplet fluorometer (Chlorophyll, CDOM, Backscatter) and an hyperspectral extinction sensor to obtain bio-optical properties of the under-ice water;
- an upward-looking bathymetric multibeam-sonar and a high precision altimeter were used to scan the sea ice bottom topography;
- a manipulator arm was used for simple manipulations.

Situational awareness was provided by a scanning imaging sonar as well as a USBL positioning system. All dives were documented with several video-cameras and an upward looking still camera.

In addition to the standard sensor suite, which was already operated during the first deployments of the ROV BEAST, new developments for net hauls and water sampling were successfully operated (Fig. 10.3):

- a five meter-long net (ROV-NET) similar to the Surface Under Ice Trawl (SUIT) to sample zooplankton along horizontal hauls in different depths, including hauls that collect organisms directly from the sea ice;
- an adapted version of the Lightframe Onsite Keyspecies Investigation (LOKI) system (LOKI-ROV);
- an Acoustic Doppler Current Profiler (ADCP) to measure current velocities relative to the ROV, in particular the speed of the ROV during net sampling;
- a water sampler.

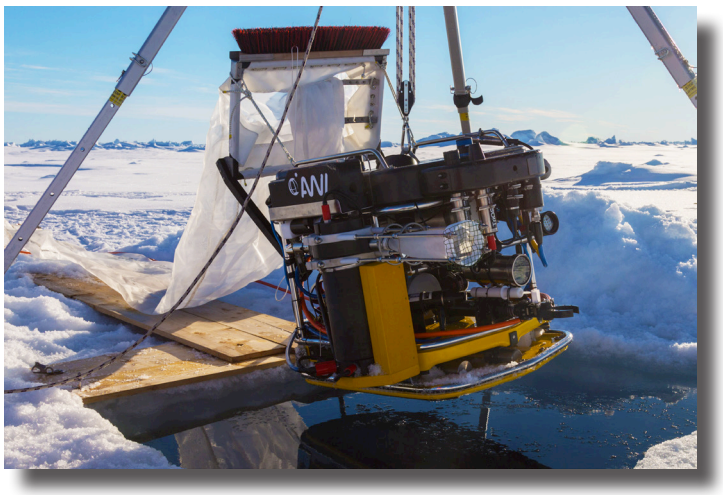

Fig. 10.3: Photograph of the remotely operated vehicle (ROV) BEAST hanging over the access hole. The ROV-NET is mounted in the back and on top of the ROV, the LOKI-ROV in the front on starboard side, and the ADCP on the port side (almost invisible)

Snow and ice thickness surveys

Sea ice thickness and snow depth were measured along transects over the different floes. These measurements did not only complement the ROV observations from under the ice, but also extend beyond these measurements. During PS106/1, these observations were conducted over the ROV grid and along an approx. 3 km long transect over the floe. During PS106/2, the transects focused on the region around the ROV grid. Main instruments were a Magna Probe for snow depth and a GEM-2 electromagnetic induction device for total ice thickness.

Snow properties

To understand and quantify the role of absorbing particulate on the melting rate of the snow pack more then 250 snow samples have been collected. After the cruise, the samples will be analyzed in order to quantify the presence of absorbing aerosols such as metals and black carbon and to quantify their total light absorption. Black carbon in melted snow samples will be analyzed later with a Single Particle Soot Photometer (SP2, DMT) coupled to a nebulizer. The SP2 is the same type of instrument also used for atmospheric measurements of black carbon, thus the same quantity is consistently measured.

Physical parameters as temperature, specific surface area and density were also recorded. Samples and physical measurements were taken at ten different sites over approximately ten days during the long ice station of PS106/1 and at several locations on the six ice floes visited during PS106/2. Surface samples were taken to study spatial variability and the vertical variation was studied with snow pits.

Airborne sea ice thickness measurements

During PS106/2, we conducted 5 helicopter electro magnetic (HEM) surveys, each with an average survey length of 180 km and good overall coverage of the entire study area. For this, the EM-Bird was towed under a *Polarstern* helicopter. All flight tracks are shown in Fig. 10.1 as well as the inset of Fig. 10.4.

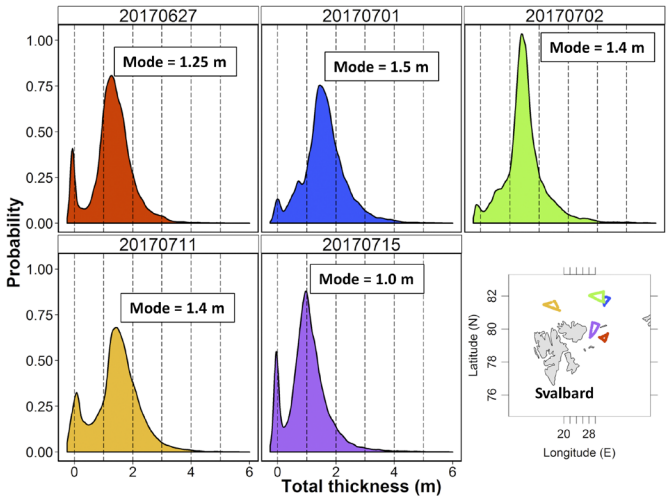

Fig. 10.4: Histograms of total ice thickness as derived from the HEM measurements during PS106/2. The map shows the flight tracks in the color according to the histograms. Dates in the figure captions are given as yyyymmdd.

Autonomous measurements / buoys

Several autonomous measurement devices (buoys) were installed on the main floe of PS106/1 and were recovered during PS106/2. Thus, these measurements cover the period from their deployment in early June and then in particular after leaving the drift station on 16 June until the return to the same ice floe on 11 July (Fig. 10.5 and 10.6), when all units, except the SVP, were recovered. The station consisted of

- a Snow Buoy, measuring snow depth, air temperature and atmospheric pressure. This unit also reported its data and position through the Iridium communication system. In addition, the measurements were forwarded into the Global Telecommunication System (GTS) under WMO ID: 6401650;
- a spectral radiation station, consisting of three Ramses spectral radiometers (Trios GmbH), which measure spectral irradiance (350 to 920 nm) over and under sea ice to obtain spectral albedo and transmittance.
- Two wildlife cameras that took time laps photographs (interval: approx. 15 min) of the buoy station from two opposite sides.
- An Automatic Weather Station (AWS), measuring 2 m air temperature, humidity, wind velocity, wind speed, as well as 1.5 m incoming and outgoing longwave radiation, incoming and reflected shortwave radiation, barometric pressure
- Four additional devices provided geographic positions via the Iridium network: two Surface Velocity Profilers (SVP) and two basic GPS trackers. These units were essential to track the floe and to find it again for recovery. The SVPs also transmitted their position and barometric pressure readings into the GTS.

All position data were received in near real time on *Polarstern* in the IceGIS system. Deployment metadata are summarized in Table 10.2.

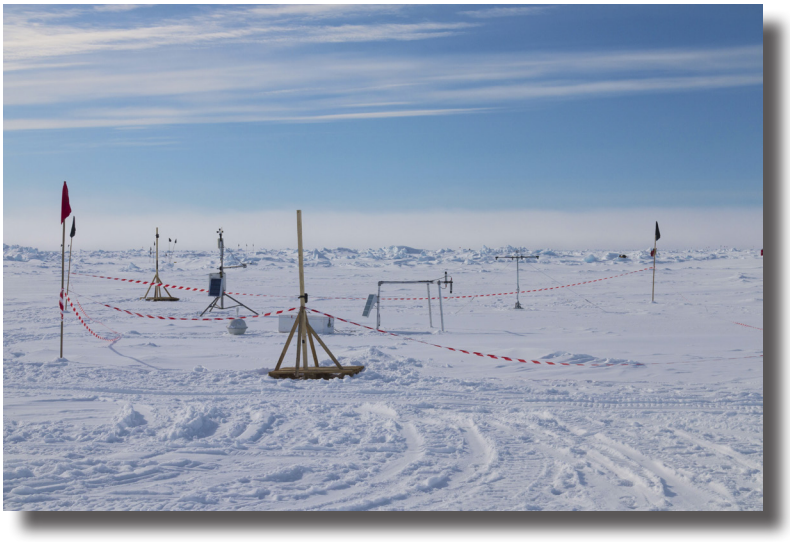

Fig. 10.5: Photograph of the buoy station after deployment of all units on 08 June. (1) The time laps cameras are mounted on the wooden poles in the fore- and the background, (2) the automatic weather station is mounted on the tripod in the back, (3) the surface velocity profiler is the white ball in the center, (4) the radiation station consists of the rack with sensors, the under-ice sensor (not visible), and the data logging and power supply box in white, and (5) the Snow Buoy is installed on the right of the other units.

Tab. 10.2: Overview of autonomous stations (buoys) during PS106. The name refers to the naming convention as used in the data portal of meereisportal.de. Dates and times are UTC.

Type	Name	IMEI	Start	End	Comment
Snow Buoy	2017S53	300234065725000	07 June 08:20	12 July 04:00	recovery
Automatic Weather Station	*none*		07 June 08:20	12 July 04:00	recovery
Radiation Station	*none*		05 June 12:10	12 July 04:00	recovery
Surface Velocity Profiler	2017P23	300234062880930	08 June 8:00	ongoing	
Surface Velocity Profiler	2017P24	300234062883920	07 June 8:20	21 June 00:00	
GPS tracker	2017P38	300434061138780	16 June 13:15	26 June 9:54	
GPS tracker	2017P39	300434061138870	16 June 13:25	12 July 4:00	
Time laps camera	*none*		07 June 8:20	12 July 4:00	recovery
Time laps camera	*none*		07 June 8:20	12 July 4:00	recovery

Fig. 10.6: The buoy station before recovery on 12 July. Only the surface velocity profiler (see Fig. 10.5b) remained on the ice to enable the continued tracking of the floe.

With helicopter flight PS106/1, three systems were partly recovered from the sea ice after approx. 9 months of drift through the Arctic Ocean. During PS101 (Station PS101/0114-1), several buoys were deployed together on one floe on 21 September 2016. Now, we recovered the top part of Snow Buoy 2016S45, the control unit of thermistor chain buoy 2016T21, and the surface parts of the ice tethered bio optical buoy 2016M2. Due to very limited time on the floe, all in- and under-ice parts had to be left behind.

Bridge observations of sea ice conditions

Observations of the sea ice conditions were made occasionally while the ship is moving through the sea ice and in addition for some times during the drift. Over all, 24 observations were made and documented with systematic photos.

IceGIS

To ensure safe and efficient ship operations in remote ice covered areas, new satellite and forecast products and sensors systems are currently being developed and validated by a large *number of projects*. PS106 was, after the first use on PS101, the second expedition that made excessively use of the IceGIS system with systematic tests on board.

Preliminary (expected) results

Over all, the collected data (Tab. 10.3) shall lead to a better understanding of the seasonal evolution of Arctic sea ice, in particular during spring-summer transition, when the icescape melts and starts to be covered by melt-ponds causing a sudden change in the physical properties of the ice pack.

The spectral radiation measurements (together with their meta data and complementary data sets) will help to fill the observational gap of such data for the main melting period when uncertainties are currently highest. These measurements will allow insights into the vertical and horizontal distribution of energy fluxes though summer sea ice in direct relation to habitat properties and ecosystem functions (cooperation in SIPCA).

Tab. 10.3: Sea ice stations and acquired data sets during PS106. For details on buoy deployments see Table 10.2.

Date	Station	Snow	Buoy	ROV	GEM	Optics	MagnaProbe
04.06.17	PS106-021	yes		yes			
05.06.17	PS106-022	yes	yes		yes		yes
06.06.17	PS106-023	yes		yes			
07.06.17	PS106-024	yes	yes		yes		
08.06.17	PS106-025	yes	yes	yes			
09.06.17	PS106-026	yes			yes		yes
10.06.17	PS106-027	yes		yes			
10.06.17	PS106-028	yes		yes			
14.06.17	PS106-031	yes		yes	yes		yes
15.06.17	PS106-032	yes		yes	yes		
16.06.17	PS106-033	yes	yes				
25.06.17	PS106-045	yes		yes	yes		yes
29.06.17	PS106-050	yes		yes	yes		yes
02.07.17	PS106-066	yes		yes	yes	yes	yes
05.07.17	PS106-069	yes			yes	yes	yes
07.07.17	PS106-073	yes		yes	yes		yes
12.07.17	PS106-080	yes		yes	yes		yes

The transect data of snow depth and sea ice thickness will also contribute to similar measurements during earlier campaigns in similar regions and/or times. This will allow comparisons of the 2017 conditions to other years. In addition, these mass- and energy balance data will be directly linked to the other observations. Since the sea ice is an integrator of atmospheric and oceanographic heat fluxes, the data sets will help to interpret these data and lead to a more general understanding of dominant processes at different times or under specific conditions.

The time series from the (mainly) autonomous instruments will help to describe and quantify the progress of the melt season. These data sets are most likely important background data sets for other studies and will help to close observational gaps during this time of the year, which is much less studied than the later summer into freeze up.

ROV

Following up the experiences from PS101, it was possible to demonstrate the additional capabilities of the ROV system BEAST to operate the additional instruments and nets. Data were recorded with the ADCP to quantify the velocity of the vehicle against the water and also the ROV NET and the LOKI ROV were operated successfully on most stations (see Chapter 15). Also the documentation and intervention capabilities of the system were successfully used during PS106. However, the main issues with the reliability and quality of the position data from the Ultra Short Base Line (USBL) systems remained and it was found that this is mostly a principle issue with the interference with the complex under-ice structures and potentially the stratification of the water masses. As a result, it is planned to test an alternative Long Base Line (LBL) system on upcoming expeditions.

Radiation measurements revealed short-wave fluxes and transmittances through snow and sea ice for each individual ice station. Fig. 10.7 shows the broadband (integrated 350 to 920 nm) transmittance ranging up to 0.2 (20 %) with a mode of 0.03. The ROV based radiation measurements during the drift station of PS106/1 reveal the start of snow metamorphism and melt through a reducing albedo and increasing transmittance, as also shown in the data from the radiation buoy (see below, Fig. 10.10). Beyond this, the histogram of transmittance reveals the broad range of transmittances, while the frequency of single bins is also impacted by the sampled ice types (open water is not included here).

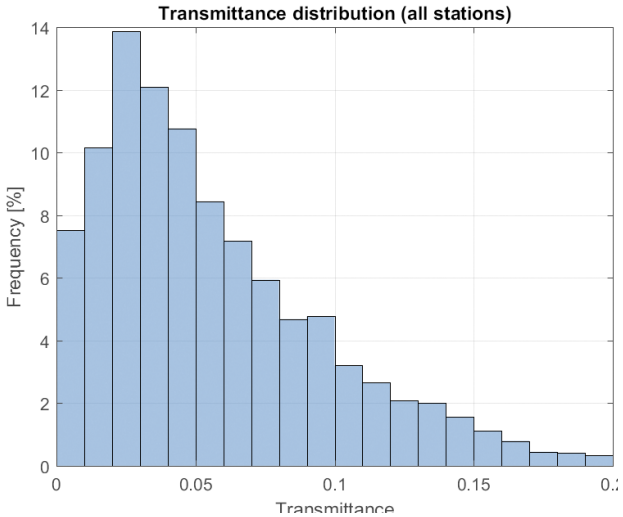

Fig. 10.7: Histogram of light transmittance as measured with the ROV during all sea-ice stations.

All other sensor data are not yet processed, only quick views reveal the generally good data quantity and that the sensors worked in the anticipated way.

Snow properties

An intense melting event was recorded and monitored at the same location between the 9 and 10 June, when the temperature of the surface snow layer increased from roughly -2.5 °C to above zero values (Fig. 10.8a). The change of temperature triggered acceleration in the snow

metamorphism leading to a rapid melting and strong decrease of the specific surface area (Fig. 10.8b). Beside the net decrease of averaged SSA, the melting process homogenized the snow surface reducing the variability of snow morphology (Fig. 10.9).

All ice floes visited between 25 June and 12 July showed strongly altered snow grains, partly freeze-melt crusts or wet snow and an equi-temperate snowpack at 0°C. The snow with decreased albedo was, however, often covered by a thin (0.5 to 1.5 cm) layer of new snow, which exceeded the high SSA observed before melt onset (40 m^2/kg). The new snow event increased the snow albedo, thus altered the shortwave energy balance.

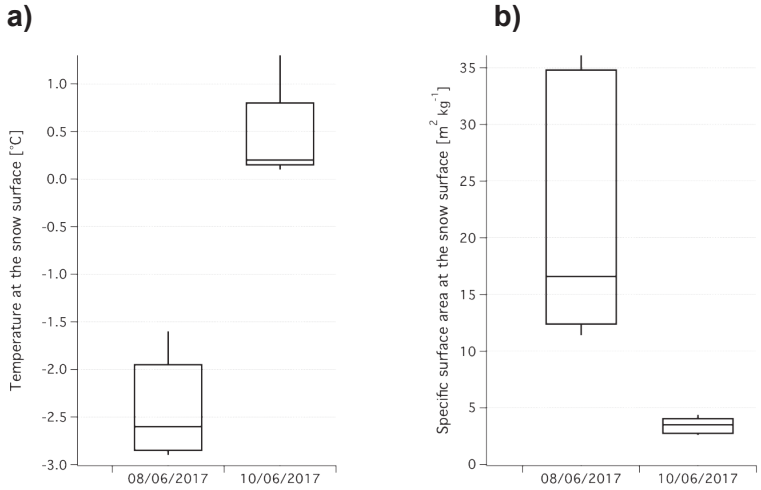

Fig. 10.8: 10, 25, 50, 75, 90 percentiles of temperature (a) and specific surface area (b) before (08/06/2015) and during (10/06/2017) the melting episode.

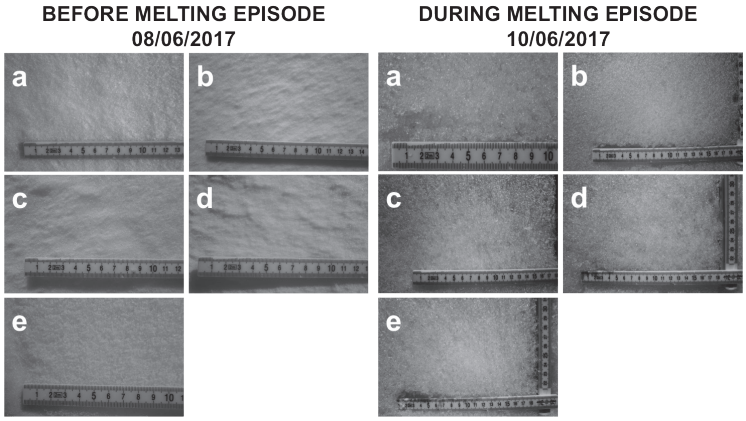

Fig. 10.9: Near infrared pictures of surface snow before and after the melting episode. Pictures were taken at the same location but at five different points within 10 square meters.

Autonomous measurements / buoys

As shown in Figs 10.5 and 10.6, the surface conditions at the buoy site changed significantly between the deployment on 05 June at 12:10 UTC to the recovery on 09 July at 04:40 UTC. Fig. 10.10 shows the broadband integrated (350 to 920 nm) fluxes of the single sensors (plates

a-c) and the albedo and transmittance (plates d+e). Fluxes of individual sensors are dominated by the diurnal cycle with incoming fluxes of 80 to 430 W/m² and transmitted fluxes up to 60 W/m². Highest under ice fluxes were observed on 29 June when a melt pond had formed at the site. The transmittance time series shows the start of strong snow metamorphism after 10 June, while the surface refroze again 5 days later until. Afterwards, snow metamorphism progressed (see also section on snow properties) and resulted in a strong surface melting before the surface refroze again and a snow storm covered all melt features once more. The photos of the time laps cameras (photos not shown here) that observe the buoy site show how ponds and melt structures form on meter-scales and thus strongly impact the point measurements of the radiation station. Melt season progressed with increasing transmittance towards the end of the observation period again. Spectral features of the time series are not yet processed.

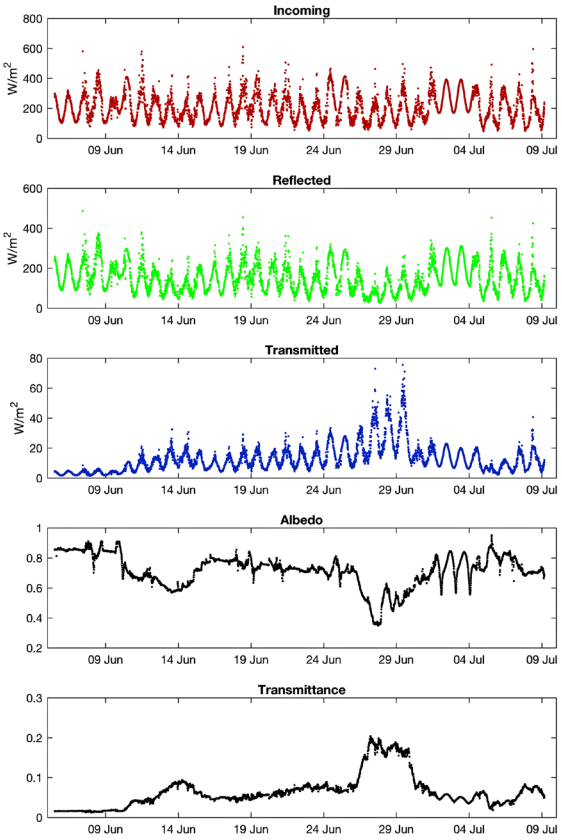

Fig. 10.10: Radiation buoy time series with full temporal resolution of 10 min. (a) incoming, (b) reflected and (c) transmitted fluxes. (d) Surface albedo and (e) transmittance as calculated from the fluxes. Fluxes represent integrated spectra from 350 to 920 nm.

All other buoys (units) recorded the data as expected, but are not shown here. The position data of the SVP are used for the observation of the drift trajectory of the floe (Fig. 10.2).

IceGIS

Further improvements and tests of different settings were performed to optimize data processing for sea ice dynamics, based on PS101 experiences and data sets. For the recovery of buoys (see above) as well as to follow the drift of the PS106/1 floe during PS106/2, the near-real time appearance of the buoy positions in the IceGIS turned out to be most valuable. Additional recoveries were planned, but could not be realized due to ship time limitations.

Data management

All data from the sea ice stations, incl. the ROV based measurements, require post-processing after the cruise. The sensor data will be made publically available in the PANGAEA database within one year. Video recordings are archived in the AWI data archiving system. Visual sea ice observation data will be distributed by a standardized database at the International Arctic Research Center, University of Alaska, Fairbanks, and are already available through the PANGAEA repository. Buoy data and all their meta data are available online in near real time through data.meereisportal.de, after completion of their drift, the final data set will be processed and published through PANGAEA. Data obtained by the IceGIS system during PS101 will be archived at the AWI for later use. Weather data will be made available in the PANGAEA database is currently under discussion.

11. NITROGEN CYCLING AND MICROBIAL ECOLOGY IN THE ARCTIC OCEAN

Allison A. Fong[1] and Eric Raes[1] [1]AWI
not on board: Susanne Spahic[1], Anya M. Waite[1]

Grant-No. AWI_PS106/1_2-00

Objectives

Plankton community composition and primary productivity are controlled by a combination of environmental conditions and biological interactions. In the Arctic Ocean, light availability is considered a major control on primary productivity due in part to variations in sea ice extent and thickness. Nutrient availability is also a critical control on primary productivity and can shape plankton community composition. Nitrogen compounds, such as nitrate and ammonium are readily assimilated by both photosynthetic and heterotrophic microscopic plankton. Therefore, assimilation rates and fluxes of nitrogen compounds, and in turn carbon,are important to quantify with regard to their control on primary productivity and shaping plankton communities.

In more recent years, dinitrogen fixation has been observed as another mechanism by which plankton communities could meet their nitrogen demand. However, this process is limited to specific groups of microbes containing nitrogenase genes. The process of biological dinitrogen fixation is the conversion of dinitrogen gas to ammonia. Dinitrogen fixation is an energetically expensive process and iron is required in nitrogenase enzyme complex. Classically, biological dinitrogen fixation is believed to be limited to subtropical and tropical regions of the worlds' oceans, with waters warmer than 25°C and depleted in inorganic nitrogen, such as nitrate. Recent work has shown a greater geographical extent and more diverse *nifH* phylogeny than previously believed, with low, but measureable rates of dinitrogen fixation (Blais et al., 2012) and recovery of *nifH* genes from polar regions (Blais et al., 2012; Diez et al. 2012, Fernandez-Mendez et al., 2016).

Our aim was to examine the temporal evolution of nitrogen utilization in an ice-covered region of the Arctic Ocean. We utilized a combination of observations and experiments to quantify nitrogen assimilation rates, dinitrogen fixation rates, and identify key microbes in these nitrogen and carbon transformation processes. We characterized the planktonic community through a variety of independent methods, including HPLC pigment biomarkers, light microscopy, and phylogenetic analyses. We will combine biogeochemical, specifically nutrient analyses, and ecological measurements of planktonic biomass and composition, with experimental rate measurements, and molecular analyses of microbial assemblages and their functional diversity. Together, these measurements provide both a mechanistic and more comprehensive understanding of nitrogen and carbon cycling processes in an ice-influenced region oft he Atlantic sector of the Arctic Ocean.

Work at sea

Discrete water column samples from Niskin bottles attached to the shipboard CTD-rosette were collected from 6-10 depth horizons for a suite of ecological and biogeochemical

measurements (fluorometric chl a, macronutrient concentrations, particulate carbon and nitrogen concentrations and isotopic values, cell enumeration, nucleic acids). Nutrient samples (duplicate 12 ml vials) from bottom to surface waters were 0.2 micron filtered, and stored frozen at -20°C until analysis at the AWI. Duplicate 2 ml flow cytometry samples for cell enumerations were also collected from bottom to surface waters. Flow cytometry samples were preserved with paraformaldehyde solution (final conc. 0.02 %), incubated in the dark, and stored at -80°C. Single cell eukaryotes and prokaryotes will be enumerated on an Accuri C6 flow cytometer by auto-fluorescence signatures and in combination with SYBR Green DNA I staining. Also, samples for ^{13}C and ^{15}N natural abundance, and particulate carbon and nitrogen (POC/N) concentration were collected at ice floe stations to determine the isotopic signatures and elemental composition of suspended organic matter. These samples were primarily collected from 3-4 specific depth horizons specific to carbon and nitrogen cycling perturbation experiments. POC/N concentrations and isotopic composition will be analyzed in collaboration with the Biogeochemistry Group at the Max Planck Institute for Marine Microbiology. The suite of parameters collected are summarized in Table 11.1.

Additionally, nucleic acids (DNA and RNA) were collected by positive pressure filtration from 2-4 liters of whole seawater onto 0.2 micron Sterivex filter cartridges. RNA filtration times were limited to 10 minutes L^{-1} to reduce the effect of handling on gene expression patterns. DNA filtration times averaged 12 minutes L^{-1} to ensure sufficient amounts of material for downstream analyses. All nucleic acid samples were flash frozen and will be stored at -80°C until extraction. Samples for gene surveys were collected at 6-8 depth horizons and will be analysed for single cellular eukaryotic (i.e. protists) and prokaryotic (i.e. Bacteria and Archaea) microbial diversity, and functional genes. In cases where there is sufficient material, select samples will also be used for meta- genomic and transcriptomic library generation to elucidate microbial community gene composition and gene expression/regulation. More specifically, we are interested in genes related to nitrogen cycling processes, and organisms that possess these genes. In concert with our perturbation experiments applying light and organic carbon manipulations, we aim to elucidate how these may control gene expression patterns and relate to the rates of nitrogen and carbon utilization we measure by applying stable isotope tracer assays.

Nitrogen and carbon stable isotope tracer incubation experiments were conducted by dual spiking of ^{15}N-Nx-labeled compounds and ^{13}C-bicarbonate into bottles containing natural, whole seawater. Tracer additions allow us to calculate nitrogen assimilation and fixation rates and estimate primary production rates without substantially altering the chemical composition of the microbial environment. Our primary focus on this expedition was to conduct nitrogen fixation rate measurements using the modified gas bubble addition method (Klawonn et al., 2015), and to incubate experimental bottles *in-situ* under-ice when possible. During occupation of the ice floe, we conducted 3 such experiments with these conditions, and the addition of perturbation treatments of light and glucose amendments. Depth horizons sampled for experimental work were surface waters (~2 m), 20 m, 100 m, and 200 m. Experimental samples were either shaded with neutral density screening or attached to a ice-tethered mooring line for *in-situ* deployment under the ice. At our site, the ice thickness was ~ 1.5 m. Snow cover was removed and not replaced, but the 40 cm diameter ice hole was shaded with opaque material. The subset of experimental bottles shaded with neutral density screening were incubated in on-deck incubation chambers plumbed with continuous flow-through surface seawater to mimic and maintain surface water temperatures (11 m depth). On-deck incubations mimic open water conditions and are not intended to directly reproduce ice-covered environmental conditions. Experimental bottles were incubated for 24 hours, and terminated by filtration onto pre-combusted GF/F filter membranes, which were frozen and stored at -20°C. Membrane Inlet Mass Spectrometry (MIMS) subsamples (12 ml) were collected from each experimental bottle at the end of the incubation period. The initial enrichment of ^{15}N-N_2 gas of each bottle will be determined from the MIMS samples and used to calculate nitrogen fixation rates.

Three additional types of experiments were conducted while aboard to test a suite of hypotheses regarding nitrogen transformations, the role of light on controlling microbial gene expression and regulation, and the role of organic carbon and light on microbial processes. The first experiment was to examine the regulation of genes in relation to light perturbations. Natural, whole surface seawater was collected and incubated directly under the ice and at 100 m. Bottles for RNA analyses were sacrificed every 8 hours from both depths, and will be analysed for microbial, specifically Archaeal, and nitrogen-fixing gene expression/regulation patterns due to changes in daily fluctuations of incoming irradiance.

The second type of experiment conducted was to estimate nitrification rates using stable isotope tracers. This set of rate measurements was coordinated with Rolf Gradinger and his measurements of primary productivity and nitrogen compound assimilation rates. The f- ratio concept of Eppley and Peterson (1979) compares primary production based on 'new' nitrogen (NO_3^- and new nitrogen from N_2-fixation), versus productivity driven on 'regenerated' nitrogen (NH_4^+) produced locally via grazing. Work by Yool (2011) suggested that a significant fraction of the nitrate that is taken up by phytoplankton at the surface is in fact generated through recent nitrification near the surface. Global data on nitrification rates at the surface are sparse, but the consequence of surface nitrification pathways might be an overestimation of the classical f-ratio (Yool, 2011, Yool et al., 2007).

Preliminary experiments were conducted along an under ice tethered mooring and in sack holes to measure nitrification rates. Our aim was to test whether nitrification could deliver a new input of NO_3^- to the phytoplankton community. A second aspect of these measurements relate to N_2O production, which occurs during nitrification both during the formation of hydroxylamine from NH_4^+ and during the formation of NO_3^- from NO_2^-. Emissions of nitrous oxide (N_2O) are of an eminent concern as the greenhouse warming power is 300 times stronger than CO_2 (Codispoti, 2010). N_2O is the precursor of nitric oxide (NO) radicals and the single most destructive source of ozone-depletion (Montzka et al., 2011). Marine N_2O production is predicted to increase under global warming scenarios including ocean acidification, sea surface warming and coastal eutrophication (Codispoti, 2010). Yet limited data exists on potential feedback systems in the marine environment.

Lastly, a light perturbation and glucose amendment experiment was conducted with natural, whole seawater to test for light inhibition of nitrogen fixation. In this experiment, seawater from 20 and 200 m depth horizons was collected, spiked with ^{15}N-N_2 and ^{13}C-bicarbonate, with an additional subset spiked with glucose solution (final conc. 1 µmol). Experimental bottles were incubated in the dark in the on-deck incubation chambers for 24 hours and processed according to previous methods outlined above. Additionally, RNA samples were collected at the T_0 and T_{12h} time points to examine gene responses to light and glucose amendments.

Together, the suite of environmental parameters in conjunction with the experimental work conducted at the ice floe will provide important information about the controls on polar marine nitrogen fixation, nitrogen compound utilization and transformations, the microbes which catalyze these transformations, and their potential roles in shaping the chemical and ecological processes.

Tab. 11.1: Biogeochemical and ecological parameters collected on PS106/1

Date	Station cast	Depths [m]	Macro-nutrients	Chl a	POC/N	DNA, RNA, FCM	HPLC	Biogenic Si	Micros-copy	N cycling exp.	Comments
30.05.2017	15-2	[surface], 10, 50, chlmax [65], 100, 200, [1000]	all depths	shallowest 6 depths	10, chlmax, 100, 200	10, 50, chlmax, 100, 200, 1000	nc	nc	nc	yes	on-deck incubation only
01.06.2017	17-2	[surface], 10, chlmax [19], 50, 100, 200, [500]	all depths	shallowest 6 depths	same as chl a	all depths	same as chl a	nc	same as chl a	no	process incubation bottles
02.06.2017	18-2	[surface], 10, chlmax [35], 50, 100, 200, 500, 1000, [btm]	all depths	shallowest 6 depths	nc	nc	nc	nc	same as chl a	no	
04.06.2017	21-1	[surface], 10, chlmax [25] 50, 100, 200, [500], [btm]	all depths	shallowest 6 depths	same as chl a	all depths	same as chl a	same as chl a	same as chl a	no	Diel gene expression experiment, sampling every 8 hours for 24 hours
06.06.2017	23-1	[surface], 10, 20, chlmax [30], 50, 100, 200, [500], [1000]	all depths	shallowest 6 depths	surface, 20, 100, 200	surface, 20, 100, 200	nc	nc	nc	yes	in-situ and on-deck incubations
07.06.2017	24-1	[surface], 10, chlmax [29], 50, 100, 200, [500], [1000]	all depths	shallowest 6 depths	nc	nc	nc	nc	nc	no	process incubation bottles
09.06.2017	26-1	[surface], 10, 20, 50, 100, 200, [500], [1000]	all depths	shallowest 6 depths	surface, 20, 100, 200	surface, 20, 100, 200, 500, 1000	nc	nc	nc	yes	in-situ and on-deck incubations

Date	Station cast	Depths [m]	Macro-nutrients	Chl a	POC/N	DNA, RNA, FCM	HPLC	Biogenic Si	Micros-copy	N cycling exp.	Comments
10.06.2017	27-6	[surface], 10, chlmax [20], 50, 75, 100, [150], 200, [500], [btm]	all depths	shallowest 7 depths	nc	nc	nc	nc	nc	no	process incubation bottles; 150 m warm tongue feature (Atlantic water)
11.06.2017	28-5	[surface], 10, chlmax [30], 50, 75, 100, 200, [500], [1000], [btm]	all depths	shallowest 7 depths	nc	nc	nc	nc	nc	no	
12.06.2017	29-1	[surface], 10, chlmax [35], 50, 75, 100, 200, [500], [1000], [btm]	all depths	shallowest 7 depths	surface, 20, 100, 200	all depths, except [btm]	nc	nc	nc	yes	in-situ and on-deck incubations
13.06.2017	30-2	[surface], 10, chlmax [34], 50, 75, 100, 200, [500], [1000], [1500]	all depths	shallowest 7 depths	nc	nc	nc	nc	nc	no	process incubation bottles
14.06.2017	31-1	[surface], 10, chlmax [25], 50, 75, 100, 200, [500], [1000], [btm]	all depths	shallowest 7 depths	shallowest 7 depths	all depths, except [btm]	same as chl a	same as chl a	nc	yes	on-deck incubation only; light perturbation of nitrogen fixation 20 and 200 m
15.06.2017	32-5	[surface], 10, chlmax [34], 50, 75, 100, 200, [500], [1000]	all depths	shallowest 7 depths	nc	all depths	nc	nc	nc	no	process incubation bottles

Date	Station cast	Depths [m]	Macro-nutrients	Chl a	POC/N	DNA, RNA, FCM	HPLC	Biogenic Si	Micros-copy	N cycling exp.	Comments
16.06.2017	33-1	[surface], 10, chlmax [34], 50, 75, 100, 200, [500], [1000]	all depths	shallowest 7 depths	nc	nc	nc	nc	nc	no	last day at ice floe; no science on ice
17.06.2017	34-2	[surface], 10, chlmax [50], 75, 100, 200, [500], [1000], [btm]	all depths	shallowest 7 depths	nc	nc	nc	nc	nc	no	
18.06.2017	37-1	[surface], 10, chlmax [33], 50, 57, 75, 100, 200, [500], [btm]	all depths, except 57 m	shallowest 8 depths	nc	nc	nc	nc	nc	no	57 m secondary chl max layer
18.06.2017	38-1	[surface], 10, chlmax [17], 50, 75, 100, 150, [btm]	all depths	shallowest 7 depths	nc	nc	nc	nc	nc	no	
18.06.2019	39-2	[surface], chlmax [4], 50	all depths	all depths	nc	nc	nc	nc	nc	no	
18.06.2017	40-1	[surface], 10, chlmax [25], 50, 75, 100, 150, 200, [500]	all depths	shallowest 7 depths	nc	nc	nc	nc	nc	no	

Expected results

We expect to resolve the temporal evolution of nitrogen fixation and nitrogen utilization rates by planktonic microorganisms in ice-covered oceanic waters during the late Arctic spring. Our sampling is expected to provide comprehensive environmental meta data with concurrent measurements of inorganic dissolved nitrogen assimilation rates, coupled to functional gene expression patterns of specific nitrogen transformation processes. Additionally, we intend to characterize the functional diversity of marine microbial assemblages to inform how shifts in community composition affect carbon and nitrogen transformations. A majority of samples will be analysed at the onshore laboratory. Rates, expression patterns, and assemblage composition will be analysed in the context of hydrographic and biogeochemical data.

Data management

Most data will be obtained through laboratory analyses after the cruise. Sample processing times are dependent upon parameter and analysis methods. Chl a and HPLC samples will be processed within the next 6 months. Nutrient analyses will be completed by early 2018. POC/N concentrations and isotopic composition will be completed by the end of 2017, but will be used in primary publications by the lead authors, and therefore will not be widely available until after manuscript submission. DNA and RNA extractions will be continuous and prioritized based on experimental results. DNA and RNA extracts will be shared with other colleagues with whom previous commitments have been made, but future opportunities to utilize these samples will be possible and can be easily coordinated. Gene libraries will be sequenced within the next 12 months. Cruise participants and research partners can obtain data upon request. All biogeochemical and ecological data will be archived on PANGAEA following quality control and assurance. Sequence data will be archived in an open access public database, either ENA or GenBank.

References

Blais M et al. (2012) Nitrogen fixation and identification of potential diazotrophs in the Canadian Arctic. Global Biogeochemical Cycles, 26, GB3022.

Codispoti LA (2010) Interesting times for marine N2O. Science, 327, 1339-1340.

Diez et al. (2012) High cyanobacterial nifH gene diversity in Arctic seawater and sea ice brine. Environmental Microbiology Reports 4(3) 360-366.

Eppley RW, Peterson, BJ (1979) Particulate organic matter flux and planktonic new production in the deep ocean. Nature, 282, 677-680.

Fernandez-Mendez et al. (2016) Diazotroph diversity in the sea ice, melt ponds, and surface waters of the Eurasian basin oft he Arctic Ocean. Frontiers in Microbiology 7: 1884. Doi: 10.3389/fmicb.2016.01884.

Klawonn et al. (2015) Simple approach fort he preparation of 15-15N2-enriched water for nitrogen fixation assessment, evaluation, application and recommendations. Frontiers in Microbiology 6:769. Doi: 10.3389/fmicb.2015.00769.

Montzka S, Reimann S, Engel A, Krüger K, O'doherty S, Sturges W et al. (2011) Ozone depleting substances (ODS's) and related chemicals, Chapter 1 in: scientific assessment of ozone depletion: 2010. Global Ozone Research and Monitoring Project. World Meteorological Organization, Geneva, Switzerland, 516.

Yool A (2011) Modeling the Role of Nitrification in Open Ocean Productivity and the Nitrogen Cycle. Methods in Enzymology, 486, 3.

Yool A, Martin AP, Fernández C, Clark DR (2007) The significance of nitrification for oceanic new production. Nature, 447, 999-1002.

12. PROTISTIAN PLANKTON, BIOGEOCHEMISTRY AND VERTICAL PARTICLE FLUX (FRAM/ PEBCAO GROUP)

Pim Sprong[1], Benjamin Staufenbiel[1], Anique Stecher[1] [1]AWI
not on board: Katja Metfies[1], Eva-Maria Noethig[1]

Grant-No. AWI_PS106/1_2-00

Objectives

The Arctic Ocean is strongly affected by climate change, which in turn will have a large impact on the carbon cycle and sequestering in the pelagic ecosystems. Long-term observations of all plankton size classes, from pico- to large zooplankton, as well as routine measurements of biogeochemical plankton parameters are thus required to understand and predict future ecosystem functioning.

Since the nineties, ecological investigations of unicellular phyto- and protozooplankton biomass, species composition, productivity, sedimentation and biochemical parameters (i.e. chlorophyll *a*, particulate organic carbon (POC) & nitrogen, carbonate and biogenic silica) have been carried out in Arctic waters of the central Arctic Ocean (CAO) during nine cruises between 1993 and 2016 with *Polarstern*. Whereas phytoplankton biomass, chlorophyll *a* (integrated values 0 -100 m), stayed more or less constant in the CAO during late summer cruises, POC distribution patterns for the summertime show slightly different results with a slightly increasing trend other than chlorophyll *a*. Flux rates of POC were at least one order of magnitude lower in CAO than at the LTER HAUSGARTEN site in eastern Fram Strait. Whereas in the CAO ice algae dominate the recognizable flux fraction, fecal material prevailed in eastern Fram Strait traps, pointing towards different systems of organic matter production and modification.

Our work on planktonic protists and biogeochemical fluxes will also focus on monitoring species and biomass distribution, on biogeochemical parameters and on the vertical particle flux of organic matter in relation to season, sea ice cover, nutrient distribution and water circulation patterns. Furthermore, metatranscriptomic analyses will help to give insights into community functioning. Specific hypotheses we intend to test are:

- Shifts in species compositions on different trophic levels will change trophic interactions and change fluxes and export of organic matter.
- Changes in the circulation like the stronger influence of Atlantic water masses may also alter the pelagic system and export fluxes.

Work at sea

Biogeochemical & biological parameters from rosette samples

In total, we sampled 20 CTDs, of which 9 were sampled until the seafloor and 11 were shallow CTDs, with the Atlantic water core being the deepest depth (Fig. 12.1). During every CTD

(except three, that served as calibration points), we filtered seawater from different depths to obtain standard parameters such as pigments (chlorophyll a, HPLC), particulate organic carbon (POC), particulate biogenic silica (PbSi), and nutrients. Additionally to these biogeochemical parameters, different samples to describe the species community and abundance were taken. First of all, samples for microscopic investigation and cell counts of phytoplankton & protozooplankton were taken from the upper water layers (max. depth AW core, around 200 m) and were fixed immediately for later analyses. From the upper 100 m, we additionally took samples for flow cytometry to determine cell sizes of the different communities directly on board. Furthermore, seawater samples from different depths (surface to bottom) were taken to perform molecular analyses to describe the species abundance (16S/18S rDNA biodiversity) and the functioning of the community (metatranscriptomes) in more detail (Tab. 12.1). For this, DNA and RNA samples were immediately frozen at -20°C and -80°C, respectively, for later analyses at the AWI in Bremerhaven.

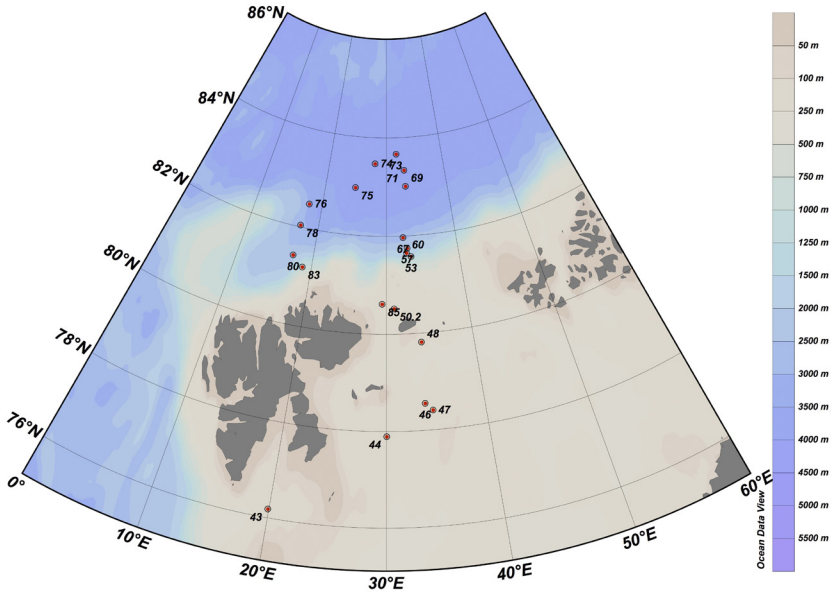

Fig. 12.1: Station map of sampled CTD casts during PS106.2

Tab. 12.1: Sample information of samples taken from CTD casts. x indicates data

Date	Station	Latitude	Longitude	Chloro-phyll	HPLC	POC/ PON	PbSi	RNA	DNA (size fractioned)	Micros-copy	Nu-trients	Flow Cytometry
2017-06-24	PS106_43-2	76°10.699‘ N	19°54.562‘ E	x	x	x	x			x	x	x
2017-06-25	PS106_44-1	77°53.639‘N	30°02.074‘E	x	x	x	x		x	x	x	x
2017-06-26	PS106_46-2	78°33.227‘N	33°57.572‘E	x	x	x	x	x	x	x	x	x
2017-06-26	PS106_47-3	78°24.346‘N	34°24.107‘E	x								
2017-06-27	PS106_48-2	79°49.015‘N	34°01.959‘E	x								
2017-06-28	PS106_50-2	80°30.101‘N	31°00.199‘E								x	x
2017-06-30	PS106_53-1	81°34.123‘N	33°25.430‘E	x	x	x	x	x	x	x	x	x
2017-06-30	PS106_57-1	81°44.957‘N	32°56.328‘E	x	x	x	x	x	x	x	x	x
2017-07-01	PS106_60-1	81°39.012‘N	32°47.961‘E	x	x	x	x	x	x	x	x	x
2017-07-03	PS106_67-3	81°57.979‘N	32°24.672‘E	x	x	x	x	x	x	x	x	x
2017-07-05	PS106_69-4	83°00.288‘N	33°11.234‘E	x	x	x	x	x	x	x	x	x
2017-07-06	PS106_71-1	83°19.664‘N	33°08.708‘E	x	x	x	x	x	x	x	x	x

Date	Station	Latitude	Longitude	Chloro-phyll	HPLC	POC/ PON	PbSi	RNA	DNA (size fractioned)	Micros-copy	Nu-trients	Flow Cytometry
2017-07-07	PS106_73-4	83°39.876'N	31°46.870'E	x	x	x	x	x	x	x	x	x
2017-07-08	PS106_74-1	83°28.256'N	28°00.578'E	x	x	x	x	x	x	x	x	x
2017-07-09	PS106_75-1	82°57.767'N	24°54.966'E	x	x	x	x		x	x	x	x
2017-07-10	PS106_76-1	82°29.455'N	18°00.963'E	x	x	x	x	x	x	x	x	x
2017-07-10	PS106_78-1	17°24.465'E	82°02.128'N	x	x	x	x	x	x	x	x	x
2017-07-12	PS106_80-6	17°16.985'E	81°24.395'N	x	x	x	x	x	x	x	x	x
2017-07-13	PS106_83-1	18°49.400'E	81°12.327'N	x	x	x	x	x	x	x	x	x

Biological parameters from the AutoFIM

The automated filtration unit AutoFIM was used to sample in higher frequencies than the CTD casts (Tab. 12.2). In total, 33 DNA filters were taken by this device. We sampled regularly at each full degree of latitude and additionally to every CTD cast. This device sampled in 10 m depth and is coupled to the ships pump system.

Tab. 12.2: Sample information of AutoFIM sampling events during CTD casts. x indicates data

Date	Station	Latitude	Longitude	AutoFIM filter
2017-06-25	PS106_44-1	77°53	30°02	x
2017-06-25	/	78°01	30°49	x
2017-06-26	PS106_46-2	78°33	33°57	x
2017-06-27	/	79°01	33°43	x
2017-06-28	/	80°00.007	29°53.096	x
2017-06-29	/	81°02.132	32°21.295	x
2017-06-30	PS106_53-1	81°34.123	33°25.430	x
2017-06-30	PS106_57-1	81°44.957	32°56.328	x
2017-07-01	PS106_60-1	81°39	33°47	x
2017-07-03	PS106_67-3	81°57.920	32°25.350	x
2017-06-05	PS106_69-4	83°00	33°13	x
2017-07-06	PS106_71-1	83°19	33°04.880	x
2017-07-07	PS106_73-4	83°39.876	33°13.379	x
2017-07-08	PS106_74-1	83°28.174	27°57.858	x
2017-07-09	PS106_75-1	82°59.345	24°49.203	x
2017-07-10	PS106_76-1	82°29.449	18°00.963	x
2017-07-10	PS106_78-1	82°02.135	17°24.445	x
2017-07-12	PS106_80-1	81°21.363	17°04.785	x
2017-07-13	PS106_80-6	81°24.430	17°16.996	x
2017-07-13	PS106_83-1	81°12.326	18°49.134	x
2017-07-14	PS106_85-1	80°36.820	29°28.818	x
2017-07-15	/	80°01.150	29°57.566	x
2017-07-16	/	79°00.840	25°32.801	x

Date	Station	Latitude	Longitude	AutoFIM filter
2017-07-16	PS106_91-4	78°42.576	23°26.656	x
2017-07-17	PS106_93-5	78°29.580	25°06.985	x
2017-07-17	/	78°01.560	26°04.145	x
2017-07-18	/	77°00.967	27°44.800	x
2017-07-18	/	75°58.43	27°19.415	x
2017-07-18	/	74°55.618	25°52.513	x
2017-07-18	/	74°00.690	24°42.204	x
2017-07-19	/	73°00.950	23°30.02	x
2017-07-19	/	72°00.821	22°21.336	x
2017-07-19	/	72°35.353	21°52.816	x

Preliminary results

We found similar results like we had observed during the other years of our time-series investigations. Results strongly depend on the physical and chemical environmental settings in the field. Since the light is limited under the sea ice in spring for organisms within the water column, only the last CTDs showed a chlorophyll maximum of > 1 mg/m^3.

Data management

During our cruises, we sample a large variety of interconnected parameters. Many of the samples (i.e. pigment analyses, particulate matter in the water column, etc.) will be analysed at AWI within about two years after the cruise. We plan that the full data set will be available about three years after the cruise by the latest. Most of the species samples and samples which will not be analysed immediately will be stored at AWI at least for another ten years and will be available for other colleagues. Data will be made available to the public via PANGAEA after publishing (depending on how many comparisons will be made, long-term study 2 to 5 years after the cruise).

13. SEA ICE BIOLOGY AND BIOGEOCHEMISTRY

Ilka Peeken[1], Giula Castellani[1], Hauke Flores[1,2], Julia Ehrlich[1,2], Benjamin Lange[1], Fokje Schaafsma[3], Rolf Gradinger[4], Brandon Hassett[4], Erin Kunisch[4], Ellen Damm[1], Josefa. Verdugo[1]
not on board: Doreen Kohlbach[1], Martin Graeve[1], Bodil Bluhm[4]

[1]AWI
[2]UHH
[3]WMR
[4]UiT

Grant-No. AWI_PS106/1_2-00

Objectives

Sea ice is of major importance in the polar oceans since it affects the solar radiation fluxes due to its reflective properties, and constitutes a habitat and feeding ground for various organisms of the polar ecosystem. The Arctic Ocean is now in a state of rapid transition that is best exemplified by the marked reduction in age, thickness and extent of the sea ice cover. The European Arctic margin is largely influenced by drift ice formed on the Siberian shelves and carried to the Fram Strait via the Transpolar Drift. Sea ice thickness for the various regions of the Transpolar Drift between 1991 and 2007 showed a reduction in modal ice thickness from 2.5 m towards 0.9 m. A long-term trend towards thinner sea ice has profound implications for the timing and position of the Seasonal Sea Ice Zone, and anticipated ice free summers in the future will have major implications for the entire ecosystem and thus alter current biogeochemical cycles in the Arctic. Due to the generally low solar elevation and extreme seasonality, light is considered to be the key factor for primary production in the ice-covered oceans. Light penetration in the Arctic is generally reduced by the sea ice cover, and additionally snow greatly reduces light transmission through the ice. In the framework of climate warming, the atmospheric moisture budget in the Arctic is forecast to change, resulting in an increasing snow cover and thus reducing the light for primary production. However, the reduction from MYI to seasonal ice and additional increase of melt ponds on FYI will substantially increase light transmission through ice. Additionally, the sea-ice surface topography, i.e. the presence of deformation elements (ridges) and melt ponds, determine the redistribution of snow on the surface. This, together with the above mentioned processes, affects the light transmission and thus affects one of the main limiting factors for algae growth.

Sea-ice physical, chemical and biological properties are highly variable in time and space, thus field sampling and producing representative model output of ice algae are extremely challenging. A big question concerning sea ice sampling is how representative of the surrounding area are the measurements taken at a certain location. Such a problem arises also when trying to upscale these observations, since upscaling always means averaging and simplification. Thus, it is fundamental to determine the temporal and spatial scales of variability of sea-ice algae, and even more to determine any relationship of sea ice algae distribution with the variability of physical and chemical sea ice properties. In addition, special environments for algae growth and survival, such as very young ice and deformed ice have not been fully characterized so far. Particular ridges are an under-sampled component of the sea ice environment in terms of their biogeochemical properties. The presence of ridges may offer an inhomogeneous, albeit favourable, environment for sea-ice algae growth. Thus, particular attention should be given to ridged and deformed ice, which is commonly overlooked as potential algae growth site.

Sea ice harbors a distinct community of prokaryotic and eucaryotic photo- and heterotrophs (Hardge et al., 2017). Sea ice algae contribute substantially (5 to ca 60 %) of total Arctic primary production (Fernández-Méndez et al., 2015), and support not only an ice-based food web, but also provide important food pulses to pelagic and benthic communities. Within the ice, newly formed particulate matter is consumed by various protozoa and metazoa, including Acoela, Crustacea and Rotifera. Sea ice algae are also a source of dissolved organic matter, which is channelled through a microbial network back into the particulate food web. All these ice inhabitants have typically sizes of less than 1 mm, to be able to explore the branched network of brine channels within the ice. In addition, ice algae can be directly consumed by under-ice amphipods and migratory zooplankton. Also specialized curtain-like algal mats have been observed under sea ice, mainly consisting of *Melosira arctica*. Vertical export of sea ice-derived organic matter is mainly driven either by organism release due to ice melt, or by faecal pellet production of grazing amphipods and zooplankton. Changes in sea ice habitat structure and ice algal production will affect the trophic transfer of sea ice-derived carbon through the under-ice community into pelagic food webs. A key role in transferring carbon from ice algae to higher trophic levels is taken by species dwelling at the ice-water interface, such as *Calanus* spp., *Apherusa glacialis* and polar cod *Boreogadus saida* (Kohlbach et al., 2016). The decline of the sea ice can alter the composition and biodiversity of the sea ice flora and fauna. Biodiversity in turn plays a vital role for the stability of ecosystem processes, and is positively coupled with the efficiency of important ecosystem functions, e.g. fluxes of energy, nutrients and organic matter. Thus understanding the relationship of the biodiversity of sea-ice biota with ecosystem functions is important for predicting consequences of climate change in an Arctic ecosystem.

Summer sea ice retreat alters water mass formation and convection, which may have profound effects on natural biogeochemical cycles between sea ice and seawater. Especially feedback effects to pathways of climatically relevant trace gases will loom large in the equation of change. Increasing water stratification during sea ice melting is likely to limit nutrient availability in near-surface water, which in turn hampers the enhancement of primary production. A characteristic feature of the Arctic Ocean is distinct post-bloom nutrient limitation. Nutrient limitation may be also a possible regulator of methane (CH_4) production in surface water. Methanogens form CH_4 via various pathways commonly classified with respect to the type of carbon precursor utilized, e.g. the methylothrophic pathway indicates the intact conversion of a methyl group to CH_4. The contribution of methylated substrates is potentially large in sea ice, and methylothrophic methanogenis may be a principal pathway from which CH_4 is readily formed by microbial activity. However, the direct evidence of this role of methylated substrates in sea ice is still lacking. In this context, the degradation of dimethylsulfoniopropionate (DMSP), an abundant methylated substrate in surface water and sea ice becomes pivotal. DMSP is produced by marine phytoplankton and sea ice algae. Cleavage of DMSP can be carried out by bacteria or by phytoplankton, and leads to formation of DMS (dimethylsulfide) or methanethiol. DMS, an important climate-cooling gas, partly escapes to the atmosphere where it is oxidized to sulphuric acid and methanesulfonic acid. Methanethiol is a key reactive intermediate utilized as sulphur and carbon sources for biosynthesis or energy generation. In anaerobic environments methanethiol act also as precursor for CH_4 production. In the ocean, processes producing N_2O are mainly being controlled by organic matter and dissolved oxygen. This trace gas is mainly produced by nitrification or nitrifier denitrification under oxic and also microaerophilic conditions. Conversely, partial denitrification can produce N_2O under suboxic conditions, whereas the complete reduction is the only reaction able to consume N_2O under suboxic/ anoxic conditions. The assimilative reduction of N_2O to NH_4^+ (N_2O fixation) may be responsible for a certain amount of consumption, but not much is known so far.

The sea ice biogeochemistry and ecology group of PS106 aims for the following objectives:

- Studying the importance of spatial scales for estimating physico-chemical sea ice properties, ice algae biomass and primary production
- Investigating the role of light for the production and biodiversity of sea ice algae
- Studying the importance of physical and biogeochemical properties of sea ice ridges for the growth conditions of ice algae
- Analysing the abundance, biodiversity and community structure of sea ice-associated biota and quantifying ecosystem functions and their relationships with biodiversity
- Using molecular and isotopic biomarkers to trace sea ice-derived carbon in pelagic food webs
- Quantifying the vertical export under sea ice
- Identifying the main triggering processes for climate-relevant compounds (CH_4, N_2O and DMS) in sea-ice and in the underlying water column and quantifying the fluxes across the water-sea ice-air interfaces following the melting cycles in the Arctic Ocean.

Work at sea

General sea ice work

Sea ice cores were taken for biological, chemical and biogeochemical analyses according the experimental set up (see sections below) during the ice camp of PS106/1 and at individual ice stations during PS106/2 (Tab. 13.1). For these stations the coring site table is given in Table 13.2. Occasionally, additional water under the ice and melt pond water were sampled. The depth of the water sampling under the ice was based on vertical profiles of a CTD and fluorescence probe which was launched through a hole in the ice prior to the water sampling. The general sample programme involved the collection of the following environmental parameters: sea ice temperature profiles, snow depth, freeboard and ice thickness. Hyperspectral radiometers were used to measure the spectral composition of the light under the ice for later estimation of ice-algae biomass. Spectral measurements were conducted with sensors mounted on three different platforms: an L-arm for point measurements and calibration (PS106/1 & 106/2), the Surface and Under-Ice Trawl (PS106/2), and the ROV of the sea ice physics group (PS106/1 & 106/2). At L-arm survey sites, ice cores were extracted and processed for chlorophyll a content and marker pigments in order to validate the relationship of ice algal biomass with the under-ice spectral light properties (Lange et al., 2016).

In addition the following parameters were collected: salinity profiles, nutrients, coloured dissolved organic matter (CDOM) and particulate absorption from the salinity cores. Meiofauna samples were collected from the bottom 10 cm of two cores at various sites during PS106/1 and connected to the coring site at PS106/2. Ice cores were melted in filtered sea water and the sample concentrated and preserved for further analysis. Size-fractionated chlorophyll (>10; 3-10 and 0.2-3 µm), marker pigments, Illumina sequencing and cell counts (microscopy and flow cytometer) were collected to determine algae biomass and the taxonomic composition. Also samples for biogenic silicate, particulate organic carbon and nitrogen (POC, PON) and the isotopic composition of POC and PON (δ^{13}CPOC and δ^{15}NPON) were sampled. For detailed records of the sampling see Table 13.3. In addition, flow cytometer and marker pigments (PS106/2) were sampled from the CTD casts in collaboration with the water column biogeochemistry group. Flow cytometer measurements of the pico- and nanoplankton were directly counted on board using a Accuri® C6 Flow Cytometer. All other samples were stored and will be measured at the AWI, UiT, and WMR.

Tab. 13.1: Summary of all collected ice cores during PS106/2 (nm = not measured)

Station	Date	Core Name	Location	Length [m]	Ice Thick-ness [m]	Surface layer [m]	Free-board [m]
PS106_45-1	25.06.2017	CORE-OPT-1	ROV Transects	1.45	1.38	0.29	0.05
PS106_45-1	25.06.2017	CORE-OPT-2	ROV Transects	1.62	1.51	0.07	0.14
PS106_45-1	25.06.2017	CORE-OPT-3	ROV Transects	1.69	1.59	0.07	0.25
PS106_45-1	25.06.2017	CORE-OPT-4	ROV Transects	0.92	0.90	0.00	-0.05
PS106_45-1	25.06.2017	CORE-OPT-5	ROV Transects	0.88	0.81	0.19	0.09
PS106_45-1	25.06.2017	CORE-OPT-6	ROV Transects	0.70	0.73	0.01	0.00
PS106_45-1	25.06.2017	CORE-OPT-7	ROV Transects	0.61	0.64	0.01	0.02
PS106_45-1	25.06.2017	CORE-OPT-8	ROV Transects	0.81	0.81	0.09	0.13
PS106_45-1	25.06.2017	CORE-OPT-9	ROV Transects	0.68	0.79	0.07	0.07
PS106_45-1	25.06.2017	CORE-OPT-10	ROV Transects	0.72	0.79	0.10	0.07
PS106_45-1	25.06.2017	CORE-OPT-11	ROV Transects	0.82	0.84	0.03	0.05
PS106_45-1	25.06.2017	CORE-OPT-12	ROV Transects	0.60	0.64	0.07	0.13
PS106_45-1	25.06.2017	CORE-OPT-13	ROV Transects	0.70	0.70	0.03	0.06
PS106_45-1	25.06.2017	CORE-OPT-14	ROV Transects	0.67	0.69	0.01	0.07
PS106_45-1	25.06.2017	CORE-OPT-15	ROV Transects	0.70	0.70	0.01	0.07
PS106_45-1	25.06.2017	CORE-LSI-4	ROV Transects	1.53	1.56	0.29	0.21
PS106_45-1	25.06.2017	CORE-LSI-5	ROV Transects	0.78	0.75	0.07	0.00
PS106_45-1	25.06.2017	CORE-LSI-6	ROV Transects	0.65	0.79	0.03	0.13
PS106_45-1	25.06.2017	CORE-PP-1	Coring Grid	0.70	0.69	0.07	0.07
PS106_45-1	25.06.2017	CORE-SAL-1	Coring Grid	0.75	0.71	0.06	0.07
PS106_45-1	25.06.2017	CORE-TEMP-1	Coring Grid	0.77	0.75	0.07	0.07
PS106_45-1	25.06.2017	CORE-ARK-1	Coring Grid	0.73	0.71	0.05	0.07
PS106_45-1	25.06.2017	CORE-BIO-1	Coring Grid	0.70	0.70	0.08	0.04
PS106_45-1	25.06.2017	CORE-BIO-2	Coring Grid	0.80	0.71	0.10	0.04
PS106_45-1	25.06.2017	CORE-MEIO-1	Coring Grid	0.80	0.75	0.05	0.06
PS106_45-1	25.06.2017	CORE-MEIO-2	Coring Grid	0.77	0.86	0.05	0.07
PS106_45-1	25.06.2017	CORE-LSI-1	Coring Grid	0.79	0.74	0.05	0.05
PS106_45-1	25.06.2017	CORE-LSI-2	Coring Grid	0.79	0.73	0.03	0.07
PS106_45-1	25.06.2017	CORE-LSI-3	Coring Grid	0.75	0.76	0.06	0.11
PS106_45-1	25.06.2017	CORE-FUNGI-1	Coring Grid	0.05	nm	0.05	nm
PS106_45-1	25.06.2017	CORE-FUNGI-2	Coring Grid	0.05	nm	0.05	nm
PS106_45-1	25.06.2017	CORE-FUNGI-3	Coring Grid	0.05	nm	0.05	nm
PS106_45-1	25.06.2017	CORE-FUNGI-4	Coring Grid	0.08	nm	0.08	nm
PS106_45-1	25.06.2017	CORE-FUNGI-5	Coring Grid	0.06	nm	0.06	nm
PS106_45-1	25.06.2017	CORE-FUNGI-6	Coring Grid	0.06	nm	0.06	nm
PS106_45-1	25.06.2017	CORE-FUNGI-7	Coring Grid	0.06	nm	0.06	nm
PS106_45-1	25.06.2017	CORE-FUNGI-8	Coring Grid	0.07	nm	0.07	nm
PS106_45-1	25.06.2017	CORE-FUNGI-9	Coring Grid	0.06	nm	0.06	nm

Station	Date	Core Name	Location	Length [m]	Ice Thick-ness [m]	Surface layer [m]	Free-board [m]
PS106_50-2	29.06.2017	CORE-OPT-1	ROV Transects	1.11	1.15	0.09	0.06
PS106_50-2	29.06.2017	CORE-OPT-2	ROV Transects	1.11	1.15	0.09	0.11
PS106_50-2	29.06.2017	CORE-OPT-3	ROV Transects	1.00	1.01	0.05	0.06
PS106_50-2	29.06.2017	CORE-OPT-4	ROV Transects	1.00	1.02	0.05	0.06
PS106_50-2	29.06.2017	CORE-OPT-5	ROV Transects	1.11	1.15	0.01	0.08
PS106_50-2	29.06.2017	CORE-OPT-6	ROV Transects	1.03	1.19	0.01	0.09
PS106_50-2	29.06.2017	CORE-OPT-7	ROV Transects	1.19	1.19	0.01	0.10
PS106_50-2	29.06.2017	CORE-OPT-8	ROV Transects	1.23	1.19	0.01	0.10
PS106_50-2	29.06.2017	CORE-OPT-9	ROV Transects	1.27	1.22	0.03	0.06
PS106_50-2	29.06.2017	CORE-OPT-10	ROV Transects	1.23	1.21	0.03	0.06
PS106_50-2	29.06.2017	CORE-OPT-11	ROV Transects	1.13	1.14	0.02	0.03
PS106_50-2	29.06.2017	CORE-OPT-12	ROV Transects	1.21	1.14	0.01	0.01
PS106_50-2	29.06.2017	CORE-OPT-13	ROV Transects	1.13	1.11	0.09	0.06
PS106_50-2	29.06.2017	CORE-OPT-14	ROV Transects	1.11	1.12	0.16	0.09
PS106_50-2	29.06.2017	CORE-OPT-15	ROV Transects	1.09	1.06	0.04	0.08
PS106_50-2	29.06.2017	CORE-LSI-4	ROV Transects	1.03	1.05	0.05	0.06
PS106_50-2	29.06.2017	CORE-LSI-5	ROV Transects	1.04	1.05	0.05	0.06
PS106_50-2	29.06.2017	CORE-LSI-6	ROV Transects	1.04	1.05	0.05	0.06
PS106_50-2	29.06.2017	CORE-PP-1	Coring Grid	1.14	1.15	0.03	0.07
PS106_50-2	29.06.2017	CORE-BIO-1	Coring Grid	1.07	1.14	0.03	0.08
PS106_50-2	29.06.2017	CORE-MEIO-1	Coring Grid	1.05	1.14	0.07	0.09
PS106_50-2	29.06.2017	CORE-BIO-2	Coring Grid	1.04	1.15	0.05	0.07
PS106_50-2	29.06.2017	CORE-MEIO-2	Coring Grid	1.10	1.15	0.08	0.10
PS106_50-2	29.06.2017	CORE-TEMP-1	Coring Grid	1.12	1.13	0.07	0.08
PS106_50-2	29.06.2017	CORE-SAL-1	Coring Grid	1.11	1.15	0.05	0.08
PS106_50-2	29.06.2017	CORE-ARK-1	Coring Grid	1.09	1.14	0.03	0.09
PS106_50-2	29.06.2017	CORE-BIO-3	Coring Grid	1.09	1.11	0.05	0.06
PS106_50-2	29.06.2017	CORE-BIO-4	Coring Grid	1.12	1.15	0.04	0.10
PS106_50-2	29.06.2017	CORE-BIO-5	Coring Grid	1.06	1.18	0.08	0.13
PS106_50-2	29.06.2017	CORE-PP-2	Coring Grid	1.07	1.11	0.06	0.07
PS106_50-2	29.06.2017	CORE-LSI-1	Coring Grid	1.07	1.11	0.08	0.07
PS106_50-2	29.06.2017	CORE-LSI-2	Coring Grid	1.08	1.11	0.04	0.08
PS106_50-2	29.06.2017	CORE-LSI-3	Coring Grid	1.09	1.11	0.07	0.06
PS106_50-2	29.06.2017	CORE-FUNGI-1	Coring Grid	1.12	1.13	0.06	0.08
PS106_50-2	29.06.2017	CORE-FUNGI-2	Coring Grid	1.12	1.13	0.09	0.08
PS106_50-2	29.06.2017	CORE-FUNGI-3	Coring Grid	1.12	1.13	0.09	0.08
PS106_50-2	29.06.2017	CORE-FUNGI-4	Coring Grid	1.12	1.13	0.09	0.08
PS106_50-2	29.06.2017	CORE-FUNGI-5	Coring Grid	1.12	1.13	0.09	0.08
PS106_50-2	29.06.2017	CORE-FUNGI-6	Coring Grid	1.12	1.13	0.06	0.08

Station	Date	Core Name	Location	Length [m]	Ice Thick-ness [m]	Surface layer [m]	Free-board [m]
PS106_50-2	29.06.2017	CORE-FUNGI-7	Coring Grid	1.12	1.13	0.08	0.08
PS106_50-2	29.06.2017	CORE-FUNGI-8	Coring Grid	1.12	1.13	0.08	0.08
PS106_50-2	29.06.2017	CORE-FUNGI-9	Coring Grid	1.12	1.13	0.05	0.08
PS106_66-5	03.07.2017	CORE-OPT-1	ROV Transects	1.62	1.60	0.05	0.12
PS106_66-5	03.07.2017	CORE-OPT-2	ROV Transects	1.58	1.60	0.05	0.18
PS106_66-5	03.07.2017	CORE-OPT-3	ROV Transects	1.54	1.63	0.16	0.18
PS106_66-5	03.07.2017	CORE-OPT-4	ROV Transects	1.57	1.63	0.16	0.18
PS106_66-5	03.07.2017	CORE-OPT-5	ROV Transects	1.68	1.70	0.10	0.16
PS106_66-5	03.07.2017	CORE-OPT-6	ROV Transects	1.74	1.70	0.10	0.16
PS106_66-5	03.07.2017	CORE-OPT-7	ROV Transects	1.68	1.78	0.10	0.15
PS106_66-5	03.07.2017	CORE-OPT-8	ROV Transects	1.68	1.78	0.10	0.15
PS106_66-5	03.07.2017	CORE-OPT-9	ROV Transects	1.63	1.64	0.04	0.14
PS106_66-5	03.07.2017	CORE-OPT-10	ROV Transects	1.55	1.64	0.03	0.18
PS106_66-5	03.07.2017	CORE-OPT-11	ROV Transects	1.64	1.75	0.20	0.25
PS106_66-5	03.07.2017	CORE-OPT-12	ROV Transects	1.66	1.67	0.05	0.17
PS106_66-5	03.07.2017	CORE-RIDGE-2	Ridge	3.29	3.35	0.55	0.40
PS106_66-5	03.07.2017	CORE-RIDGE-3	Ridge	2.89	2.73		0.75
PS106_66-5	03.07.2017	CORE-LSI-4	beside ridge	1.09	1.10	0.09	nm
PS106_66-5	03.07.2017	CORE-LSI-5	beside ridge	1.05	1.05	0.08	nm
PS106_66-5	03.07.2017	CORE-LSI-6	beside ridge	1.07	1.08	0.08	nm
PS106_66-5	03.07.2017	CORE-BIO-1	Coring Grid	1.37	1.43	0.03	0.07
PS106_66-5	03.07.2017	CORE-PP-1	Coring Grid	1.49	1.43	0.02	0.03
PS106_66-5	03.07.2017	CORE-MEIO-1	Coring Grid	1.44	1.52	0.03	0.06
PS106_66-5	03.07.2017	CORE-BIO-2	Coring Grid	1.39	1.47	0.01	0.07
PS106_66-5	03.07.2017	CORE-MEIO-2	Coring Grid	1.41	1.51	0.02	0.06
PS106_66-5	03.07.2017	CORE-TEMP-1	Coring Grid	1.45	1.45	0.02	0.06
PS106_66-5	03.07.2017	CORE-SAL-1	Coring Grid	1.43	1.42	0.02	0.07
PS106_66-5	03.07.2017	CORE-ARK-1	Coring Grid	1.39	1.42	0.03	0.06
PS106_66-5	03.07.2017	CORE-BIO-3	Coring Grid	1.42	1.44	0.02	0.06
PS106_66-5	03.07.2017	CORE-BIO-4	Coring Grid	1.42	1.52	0.02	0.06
PS106_66-5	03.07.2017	CORE-BIO-5	Coring Grid	1.44	1.55	0.02	0.06
PS106_66-5	03.07.2017	CORE-PP-2	Coring Grid	1.42	1.46	0.04	0.06
PS106_66-5	03.07.2017	CORE-LSI-1	Coring Grid	1.42	1.46	0.04	0.06
PS106_66-5	03.07.2017	CORE-LSI-2	Coring Grid	1.42	1.46	0.04	0.06
PS106_66-5	03.07.2017	CORE-LSI-3	Coring Grid	1.42	1.46	0.04	0.06
PS106_66-5	03.07.2017	CORE-FUNGI-1	Coring Grid	1.42	1.46	0.04	0.06
PS106_66-5	03.07.2017	CORE-FUNGI-2	Coring Grid	1.42	1.46	0.04	0.06
PS106_66-5	03.07.2017	CORE-FUNGI-3	Coring Grid	1.42	1.46	0.04	0.06

Station	Date	Core Name	Location	Length [m]	Ice Thick-ness [m]	Surface layer [m]	Free-board [m]
PS106_66-5	03.07.2017	CORE-FUNGI-4	Coring Grid	1.42	1.46	0.04	0.06
PS106_66-5	03.07.2017	CORE-FUNGI-5	Coring Grid	1.42	1.46	0.04	0.06
PS106_66-5	03.07.2017	CORE-FUNGI-6	Coring Grid	1.42	1.46	0.04	0.06
PS106_66-5	03.07.2017	CORE-FUNGI-7	Coring Grid	1.42	1.46	0.03	0.06
PS106_66-5	03.07.2017	CORE-FUNGI-8	Coring Grid	1.42	1.46	0.03	0.06
PS106_66-5	03.07.2017	CORE-FUNGI-9	Coring Grid	1.42	1.46	0.03	0.06
PS106_73-2	07.07.2017	CORE-BIO-1	Coring Grid	1.37	1.42	0.10	0.09
PS106_73-2	07.07.2017	CORE-MEIO-1	Coring Grid	1.32	1.40	0.15	0.17
PS106_73-2	07.07.2017	CORE-BIO-2	Coring Grid	1.32	1.39	0.07	0.15
PS106_73-2	07.07.2017	CORE-MEIO-2	Coring Grid	1.34	1.34	0.10	0.11
PS106_73-2	07.07.2017	CORE-BIO-5	Coring Grid	1.36	1.37	0.08	0.14
PS106_73-2	07.07.2017	CORE-TEMP-1	Coring Grid	1.34	1.51	0.09	0.16
PS106_73-2	07.07.2017	CORE-SAL-1	Coring Grid	1.36	1.38	0.05	0.12
PS106_73-2	07.07.2017	CORE-ARK-1	Coring Grid	1.43	1.42	0.08	0.15
PS106_73-2	07.07.2017	CORE-BIO-3	Coring Grid	1.37	1.42	0.08	0.17
PS106_73-2	07.07.2017	CORE-BIO-4	Coring Grid	1.33	1.40	0.07	0.12
PS106_73-2	07.07.2017	CORE-PP-2	Coring Grid	1.35	1.41	0.04	0.14
PS106_73-2	07.07.2017	CORE-PP-1	Coring Grid	1.35	1.41	0.04	0.14
PS106_73-2	07.07.2017	CORE-LSI-1	10 m from coring grid	1.35	1.41	0.04	0.14
PS106_73-2	07.07.2017	CORE-LSI-2	10 m from coring grid	1.35	1.41	0.04	0.14
PS106_73-2	07.07.2017	CORE-LSI-3	10 m from coring grid	1.35	1.41	0.04	0.14
PS106_73-2	07.07.2017	CORE-LSI-4	near sediment trap	nm	1.38	0.06	nm
PS106_73-2	07.07.2017	CORE-LSI-5	near sediment trap	nm	1.38	0.08	nm
PS106_73-2	07.07.2017	CORE-LSI-6	near sediment trap	nm	1.38	0.07	nm
PS106_73-2	07.07.2017	CORE-FUNGI-1	10 m from coring grid	1.35	1.42	0.04	0.14
PS106_73-2	07.07.2017	CORE-FUNGI-2	10 m from coring grid	1.35	1.42	0.04	0.14
PS106_73-2	07.07.2017	CORE-FUNGI-3	10 m from coring grid	1.35	1.42	0.04	0.14
PS106_73-2	07.07.2017	CORE-FUNGI-4	10 m from coring grid	1.35	1.42	0.04	0.14
PS106_73-2	07.07.2017	CORE-FUNGI-5	10 m from coring grid	1.35	1.42	0.04	0.14
PS106_73-2	07.07.2017	CORE-FUNGI-6	10 m from coring grid)	1.35	1.42	0.04	0.14
PS106_73-2	07.07.2017	CORE-FUNGI-7	10 m from coring grid	1.35	1.42	0.04	0.14
PS106_73-2	07.07.2017	CORE-FUNGI-8	10 m from coring grid	1.35	1.42	0.04	0.14
PS106_73-2	07.07.2017	CORE-FUNGI-9	10 m from coring grid)	1.35	1.42	0.04	0.14
PS106_73-2	07.07.2017	CORE-OPT-L3	L-arm	NA	1.47	0.11	0.17
PS106_73-2	07.07.2017	CORE-OPT-L4	L-arm	NA	1.47	0.05	0.18
PS106_73-2	07.07.2017	CORE-OPT-L5	L-arm	NA	1.47	0.08	0.14
PS106_73-2	07.07.2017	CORE-OPT-L6	L-arm	NA	1.44	0.13	0.14
PS106_73-2	07.07.2017	CORE-OPT-L7	L-arm	NA	1.42	0.06	0.15

Station	Date	Core Name	Location	Length [m]	Ice Thick-ness [m]	Surface layer [m]	Free-board [m]
PS106_73-2	07.07.2017	CORE-OPT-L8	L-arm	NA	1.42	0.11	0.17
PS106_73-2	07.07.2017	CORE-OPT-L9	L-arm	NA	1.36	0.09	0.12
PS106_73-2	07.07.2017	CORE-OPT-L10	L-arm	NA	1.35	0.10	0.10
PS106_73-2	07.07.2017	CORE-OPT-L11	L-arm	NA	1.37	0.08	0.10
PS106_73-2	07.07.2017	CORE-MEIO-1	L-arm	NA	1.18	NA	0.13
PS106_73-2	07.07.2017	CORE-MEIO-2	L-arm	NA	1.20	NA	0.13
PS106_80-2	12.07.2017	CORE-SAL-1	Site B PS106/1	1.50	1.52	NA	0.10
PS106_80-2	12.07.2017	CORE-CHLA-1	Site B PS106/1	1.54	1.51	NA	0.09
PS106_80-2	12.07.2017	CORE-CHLA-2	Site B PS106/1	1.53	1.52	NA	0.11
PS106_80-2	12.07.2017	CORE-TEMP-1	Site B PS106/1	1.53	1.52	NA	0.10
PS106_80-2	12.07.2017	CORE-OPT-L3	L-arm (AZFP2)	1.24	1.31	NA	0.06
PS106_80-2	12.07.2017	CORE-OPT-L4	L-arm (AZFP2)	1.24	1.28	NA	0.04
PS106_80-2	12.07.2017	CORE-OPT-L5	L-arm (AZFP2)	1.25	1.29	NA	0.06
PS106_80-2	12.07.2017	CORE-OPT-L6	L-arm (AZFP2)	1.19	1.29	NA	0.05
PS106_80-2	12.07.2017	CORE-OPT-L7	L-arm (AZFP2)	1.20	1.27	NA	0.03
PS106_80-2	12.07.2017	CORE-OPT-L8	L-arm (AZFP2)	1.16	1.29	NA	0.03
PS106_80-2	12.07.2017	CORE-OPT-L9	L-arm (AZFP2)	1.18	1.25	NA	0.02
PS106_80-2	12.07.2017	CORE-OPT-L10	L-arm (AZFP2)	1.14	1.29	NA	0.04
PS106_80-2	12.07.2017	CORE-OPT-L11	L-arm (AZFP2)	1.17	1.29	NA	0.02
PS106_80-2	12.07.2017	CORE-PP-1	L-arm (AZFP2)	1.05	nm	0.00	nm
PS106_80-2	12.07.2017	CORE-TEMP-1	L-arm (AZFP2)	1.00	nm	0.00	nm
PS106_80-2	12.07.2017	CORE-SAL-1	L-arm (AZFP2)	1.10	nm	0.00	nm
PS106_80-2	12.07.2017	CORE-PP-2	L-arm (AZFP2)	1.05	nm	0.00	nm
PS106_80-2	12.07.2017	CORE-LSI-1	near sed trap (50 m)	nm	nm	0.00	
PS106_80-2	12.07.2017	CORE-LSI-2	near sed trap (50 m)	nm	nm	0.00	
PS106_80-2	12.07.2017	CORE-LSI-3	near sed trap (50 m)	nm	nm	0.00	
PS106_80-2	12.07.2017	CORE-BIO-1	Coring Grid Site A PS106/1	1.22	1.02	0.08	0.02
PS106_80-2	12.07.2017	CORE-MEIO-1	Coring Grid Site A PS106/1	0.64	0.63	0.06	0.03
PS106_80-2	12.07.2017	CORE-KIM-1	Coring Grid Site A PS106/1	0.68	0.74	0.03	0.05
PS106_80-2	12.07.2017	CORE-BIO-2	Coring Grid Site A PS106/1	0.64	0.67	0.04	0.02
PS106_80-2	12.07.2017	CORE-MEIO-2	Coring Grid Site A PS106/1	0.58	0.63	0.05	0.05
PS106_80-2	12.07.2017	CORE-KIM-2	Coring Grid Site A PS106/1	0.63	0.62	0.03	0.03
PS106_80-2	12.07.2017	CORE-TEMP-1	Coring Grid Site A PS106/1	0.61	0.63	0.05	0.03

Station	Date	Core Name	Location	Length [m]	Ice Thick-ness [m]	Surface layer [m]	Free-board [m]
PS106_80-2	12.07.2017	CORE-SAL-1	Coring Grid Site A PS106/1	0.54	0.70	0.04	0.02
PS106_80-2	12.07.2017	CORE-ARK-1	Coring Grid Site A PS106/1	0.65	0.68	0.01	0.03
PS106_80-2	12.07.2017	CORE-BIO-3	Coring Grid Site A PS106/1	0.50	0.55	0.03	0.04
PS106_80-2	12.07.2017	CORE-BIO-4	Coring Grid Site A PS106/1	0.59	0.60	0.02	0.05
PS106_80-2	12.07.2017	CORE-BIO-5	Coring Grid Site A PS106/1	0.59	0.62	0.02	0.02
PS106_80-2	12.07.2017	CORE-KIM-3	Coring Grid Site A PS106/1	0.54	0.55	0.04	0.02
PS106_80-2	12.07.2017	CORE-KIM-4	Coring Grid Site A PS106/1	0.62	0.61	0.01	0.01
PS106_80-2	12.07.2017	CORE-KIM-5	Coring Grid Site A PS106/1	0.55	0.62	0.02	0.02

Tab. 13.2: General setup of each coring grid for the five ice stations during PS106/2. ARC = Archive core, PP = primary production, Temp = temperature core, Sal = salinity core, Bio = biological core, Mei = Meiofauna core, LSI = fatty acid/stable isotope core, Fungi = Fugi DNA core, KIM- amino acid/stable isotope core

Station	Remarks	Coring Grid
PS106_045-1		Fungi-7 Fungi-8 Fungi-9 Fungi-4 Fungi-5 Fungi-6 ARC TEMP SAL Fungi-1 Fungi-2 Fungi-3 PP-2 Bio-2 Meio-2 LSI-3 PP-1 Bio-1 Meio-1 LSI-1 LSI-2
PS106_050-1		PP-2 Bio-4 Fungi-7 Fungi-8 Fungi-9 Bio-3 Fungi-4 Fungi-5 Fungi-6 ARC TEMP SAL Fungi-1 Fungi-2 Fungi-3 Bio-2 Meio-2 LSI-3 Bio-5 PP-1 Bio-1 Meio-1 LSI-1 LSI-2
PS106_066-5		PP-2 Bio-5 Fungi-7 Fungi-8 Fungi-9 Bio-3 Bio-4 Fungi-4 Fungi-5 Fungi-6 TEMP SAL Fungi-1 Fungi-2 Fungi-3 ARC Bio-2 Meio-2 LSI-3 PP-1 Bio-1 Meio-1 LSI-1 LSI-2

Station	Remarks	Coring Grid
PS106_073-2		PP-2 Bio-4 Bio-3 ARC TEMP SAL Bio-2 Meio-2 Bio-5 PP-1 Bio-1 Meio-1
PS106_80-2		Kim-5 Kim-3 Kim-4 Bio-5 Bio-3 Bio-4 ARC TEMP SAL Bio-2 Meio-2 Kim-2 Bio-1 Meio-1 Kim-1

Tab. 13.3: Variables measured from the sea ice core samples from the gardening area during PS106/1 and all biological cores during PS106/2

Station	HPLC	Frac_Chl a (>10µm, 10µm, 0.2-3µm)	DNA (>10µm, 3-10µm, 0.2-3µm)	POC PON Istopes	bPSi	Sal Nuts CDOM PABS
PS106_045-2	X	X	X	X	X	X
PS106_050-2	X	X	X	X	X	X
PS106_066-5	X	X	X	X	X	X
PS106_073-2	X	X	X	X	X	X
PS106_080-2	X	X	X	X	X	X
	MIC	**IP25**	**Flow Cyt.**	**LSI**	**PP**	**TEMP**
PS106_045-2	X		X	X	X	X
PS106_050-2	X		X	X	X	X
PS106_066-5	X		X	X	X	X
PS106_073-2	X	X	X	X	X	X
PS106_080-2	X		X	X	X	X

Primary productivity, nutrient uptake, sediment trap deployments´, lipids and stable isotopes, and Fungi DNA analysis

Water samples were collected from the CTD and using an under-ice Kemmerer bottle water sampler. *Melosira arctica* samples were collected either from broken ice floes, from the ROVnet or from aggregates floating up in ice core holes. For the analysis of sea ice algal photophysiological characteristics, we collected individual ice sections from the bottom 5 cm of the sea ice, and placed those in the dark in a container at near *in-situ* temperature. After ca. 1 hour, small brine volumes were collected within the containers with a syringe and transferred into a cuvette for determination with the PSI instrument. The assessment of the maximum photosynthetic yield and its changes at different light intensities (so called Light Curves, from

10 to 500 umol photons m^{-2} s^{-1}) was conducted using a PSI AquaPen AP-C 100 fluorometer during PS106/1. For sample details see Table 13.4.

Primary productivity and nitrogen uptake rates were determined using ^{13}C and ^{15}N additions to natural sea ice and phytoplankton communities. Incubations were conducted in polycarbonate bottles in water depths of 2 to 90 m through holes in sea ice for 24 hours (During PS106/1 at the trap and the gardening site; during PS106/2 close to the coring site). After filtration the water was sampled onto pre-combusted GF/F filters and stored frozen for further analysis.

Sediment traps (Design KC Denmark) were deployed under sea ice through small holes in the ice in water depths of 5, 20, 40 and 90 m. During PS106/1, traps were recovered after 24 hours, and subsamples were taken for Chlorophyll, POC/N and microscopic analysis of collected material. During PS106/2 deployment times were between 5.15 hours and 6.5 hours. During PS106/1 the traps were located at the trap and the gardening site, during PS106/2 close to the main coring site.

For DNA of fungi, CTD seawater and ice cores were collected at 10 stations along the *Polarstern's* traverse at variable depths (bottom, chlorophyll maximum, and surface layer). Biomass was concentrated on 0.2 µm filters and stored at -80° C (Tab. 13.5). Ice cores (bottom 5 cm) and water samples (via CTD) were also collected for fatty acid/lipid isotopic biomarkers (bulk and compound specific) to track sympagic/pelagic food sources to secondary consumers (Tab. 13.6). The objectives of this sampling effort will be to 1) characterize spatial and temporal variations in trophic maker composition of ice particulate organic matter (iPOM) and pelagic particulate organic matter (pPOM) and 2) quantify how dominant zooplankton species assimilate sea ice and/or pelagic carbon sources. For a list of zooplankton species that were sampled, refer to the nets sampled during PS106/2 (Chapter 15).

Tab. 13.4: Fluorometric determination of photosynthetic parameters (maximum quantum yield, Light Curve) during PS106/1

Station PS106_	Date	Sample
19-1	June 2, 2017	*Melosira arctica*, collected with bucket from the ship while moving through large areas with *Melosira* occurrence
20-1	June 3, 2017	Sea ice brine sample
21-2	June 4, 2017	*Melosira arctica*, collected at site A of spatial variability transect
22-1	June 5, 2017	Sea ice brine samples, from sediment trap location, and gardening experiment
23-2	June 6, 2017	Sea ice brine sample, from sediment trap location
24-2	June7, 2017	Sea ice brine sample, from gardening experiment
25-1	June 8, 2017	*Melosira arctica* sample from ROVnet
26-2	June 9, 2017	Water samples 5 to 30m, sea ice brine from sediment trap location
27-1	June 10, 2017	*Melosira arctica* sample from ROV hole
28-2	June 11, 2017	Sea ice brine sample, from gardening experiment

Station PS106_	Date	Sample
31-2	June 14, 2017	Water samples 5 to 30m, sea ice brine from sediment trap location
32-2	June 15, 2017	*Melosira arctica* sample and sea ice brine sample, from gardening experiment
37-1	June 18, 2017	Water samples, from CTD 5m, chl max, 50m
38-1	June 18, 2017	Water samples, from CTD 5m, chl max, 50m
39-2	June 18, 2017	Water samples, from CTD 5m, chl max, 50m
40-1	June 18, 2017	Water samples, from CTD 5m, chl max, 50m

Tab. 13.5: Stations sampled during PS106/2 with anticipated analyses* for fungi. #collected for culture purposes

Station PS106_	Sample type	Sample depth (m)	DNA*	Cell counts	POC	Chl_A
43-2	Seawater	0.6, 22, 178	x	x		
45-1	PP incubation	2, 5, 20, 40, 90	x	x		
45-1	Sediment traps	5, 20, 40, 90			x	x
45-1	Ice	bottom 0.10	x	x		
48-2	Seawater	1, 20, 269	x	x		
50-1	PP incubation	2, 5, 20, 40, 90			x	x
50-1	Seawater	5, 20, 40, 90	x	x		
50-1	Ice	bottom 0.10	x	x		
57-1	Seawater	1, 36, 1979	x	x		
66-5	PP incubation	2, 5, 20, 40, 90			x	x
66-5	Sediment traps	5, 20, 40, 90	x	x		
66-5	Ice	bottom 0.10	x	x		
69-4	Seawater	2, 25, 3625	x	x		
72-2	PP incubation	2, 5, 20, 40, 90	x	x	x	x
80-1	Seawater	1, 21, 967	x	x		
80-2	PP incubation	2, 5, 20, 40, 90			x	x
80-2	Sediment traps	5, 20	x	x	x	x
91-4#	Seawater	10				

Tab. 13.6: Stations sampled during PS106/1 for anticipated lipid and stable isotope analyses

DATE	STATION PS106_	GEAR/ LOCATION	FILTERED (mL)	SAMPLED
6/1/17	17-2_CTD	CTD	3000	Chlmax
6/1/17	17-2_CTD	CTD	3000	Chlmax
6/1/17	17-2_CTD	CTD	3000	Chlmax
6/2/17	18-2_CTD	CTD	3850	Chlmax

DATE	STATION PS106_	GEAR/ LOCATION	FILTERED (mL)	SAMPLED
6/2/17	18-2_CTD	CTD	7000	Chlmax
6/2/17	19-1_BUCKET	BUCKET	16	surface
6/2/17	19-1_BUCKET	BUCKET	16	surface
6/2/17	19-2_BUCKET	BUCKET	110	surface
6/2/17	19-2_BUCKET	BUCKET	>2	surface
6/4/17	21-1_SEAICEC_1	ICE CORE	860	bottom 5 cm
6/4/17	21-1_SEAICEC_1	ICE CORE	751	bottom 5 cm
6/4/17	21-1_SEAICEC_1	ICE CORE	799	bottom 5 cm
6/4/17	21-1_SEAICEC_1	BY HAND	34	surface
6/6/17	23-1_CTD	CTD	10900	Chlmax
6/7/17	24-2_SEAICEC_4	ICE CORE	300	bottom 5 cm
6/7/17	24-2_SEAICEC_4	ICE CORE	300	bottom 5 cm
6/7/17	24-2_SEAICEC_4	ICE CORE	250	bottom 5 cm
6/9/17	26-2_KEM_2	KEM WATER	8500	30m
6/8/17	025_ROV_1	BY HAND	>2	surface
6/9/17	26-2_SEAICEC_1	ICE CORE	260	bottom 5 cm
6/9/17	26-2_SEAICEC_1	ICE CORE	255	bottom 5 cm
6/9/17	26-2_SEAICEC_1	ICE CORE	300	bottom 5 cm
6/12/17	29-2_KEM_2	KEM WATER	6000	5m
6/12/17	29-2_KEM_2	KEM WATER	3250	5m
6/12/17	29-2_KEM_2	KEM WATER	10000	10m
6/11/17	28-2_SEAICEC_2	ICE CORE	255	bottom 5 cm
6/11/17	28-2_SEAICEC_2	ICE CORE	250	bottom 5 cm
6/11/17	28-2_SEAICEC_2	ICE CORE	300	bottom 5 cm
6/13/17	30-2_CTD	CTD	6000	Chlmax
6/13/17	30-2_CTD	CTD	3900	Chlmax
6/14/17	31-2_SEAICEC_1	ICE CORE	38	bottom 5 cm
6/14/17	31-2_SEAICEC_1	ICE CORE	>2	bottom 5 cm
6/14/17	31-2_SEAICEC_1	ICE CORE	200	bottom 5 cm
6/14/17	31-2_SEAICEC_1	ICE CORE	300	bottom 5 cm
6/14/17	31-2_SEAICEC_1	ICE CORE	305	bottom 5 cm
6/17/17	34-2_CTD	CTD	10500	Chlmax
6/18/17	37-1_CTD	CTD	395.5	Chlmax
6/18/17	37-1_CTD	CTD	445	Chlmax
6/18/17	37-1_CTD	CTD	355	Chlmax
6/18/17	40-1_CTD	CTD	670	Chlmax
6/18/17	40-1_CTD	CTD	650	Chlmax

Experimental approaches carried out during PS106/1

A) The role of scales for biological sea ice sampling

At the beginning of PS106/1 we studied the spatial scales of ice algae biomass. We followed the nested approach by Miller et al., 2015 to extrapolate detailed information to larger scales, based on distinguishing hierarchical layers of detail. We set up a grid along a line of 1,200 m to sample the sea ice at different resolutions. A schematic approach is shown in Fig. 13.1. The black lines in Fig. 13.1 show coring points at a distance of 100 m from each other. Close to the start point A and to the end point B we have been coring at increasing resolution from 50 m step length down to 1 m. step length. Point A was located in the gardening area (see below), while site B was the outermost point of the no go area for the melt pond grid. Fig. 13.2 displays the sampled territory with a few core locations. In total 39 cores were collected and the bottom 5 cm was sampled and transferred to the ship. Filtered sea water (500 ml) was added to each section and after melting samples for POC and HPLC pigments and flow cytometer samples were collected. At site A and site B we collected additional temperature and salinity cores, from the latter we also sampled nutrients. For each core we recorded core length, ice thickness, snow thickness and freeboard. A summary of the cores taken is shown in Table 13.7.

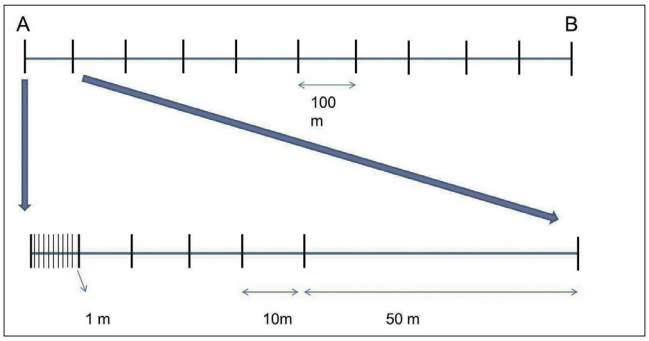

Fig. 13.1: General approach for the spatial variability sampling

B) Gardening

Due to the natural differences in snow accumulation around site A three fields were identified for the sampling of different snow conditions. In one field (Fig. 13.3) the snow was entirely removed (no snow). Adjacent to this field was an area with medium snow (2 cm, medium snow). The third field had a snow cover of 12 cm (high snow). During the cruise these three sites were sampled 4 times (day 0, 2, 6, 10) to monitor the biological evolution under different snow regimes. In particular, biological samples for HPLC, POC; PAB, BPSi, CDOM DNA and fractionated chlorophyll *a* have been collected from the biological cores (for details see Table 13.3). Three additional cores were taken for photophysiological measurements producing rapid light response curves of sea ice algae. During some of the sampling events we conducted under-ice light measurements with RAMSES irradiance and radiance sensors

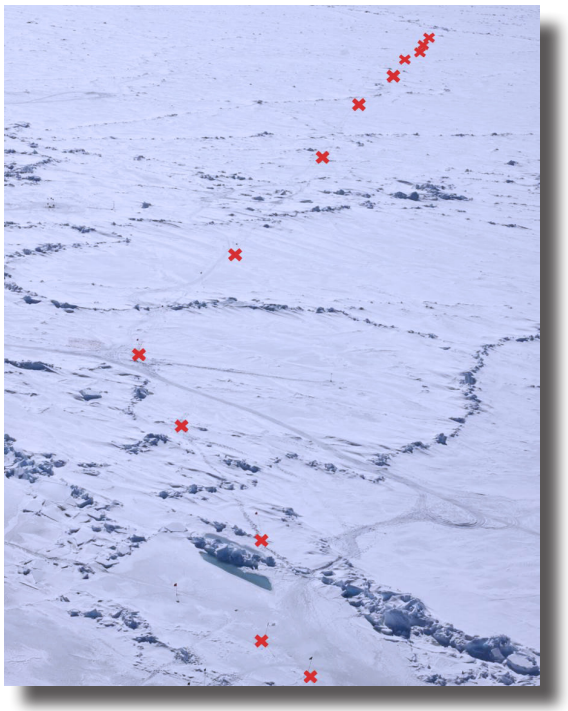

Fig. 13.2: Image of parts of the sampled transect. Red crosses mark sampling points

mounted on an L-shaped arm. At the beginning and at the end of the Gardening experiment bio-optical cores were collected to calibrate spectral measurements for the retrieval of sea-ice chlorophyll *a* content. In Table 13.8 we list the cores taken. In collaboration with the sea ice physic team the light conditions under the ice were monitored several times throughout the experiment.

Tab. 13.7: Sea-ice cores collected during the spatial variability study

Station PS106_	Type of core	# of cores	Day
21-1_SEAICEC_1	Bio	38	04/06/2017
21-1_SEAICEC_1	Salinity	2	04/06/2016
21-1_SEAICEC_1	DMS		04/06/2017

Further sampling during the work on ice

During each ice station we collected daily under-ice profiles with a CTD equipped with a fluorescence probe. After the first few days of the drift station of PS106/1, melting started and the first melt ponds formed on the ice floe. When possible we collected water samples for all biological variables. At uneven frequency we also collected under-ice water samples. Under-ice hyperspectral measurements were collected irregularly at the gardening site. In Table 13.9 we list the CTD (CTDIF), under-ice water (KEM) and hyperspectral measurements (LARM) collected. The location refers to the GPS way point of the different sites.

Fig. 13.3: No snow (left) and medium snow site (right) of the gardening area

Tab. 13.8: Type and numbers of core collected for the gardening experiment (ARC = Archive core, Temp = temperature core, Sal = salinity core, Bio = biological core, Mei = Meiofauna core, LSI = fatty acid/stable isotope core, P/I curve = cores for PHYTO-PAM P/I curve measurements

Station PS106_	Type of core	# of cores	Day
22-1	Bio	3	05/06/2017
22-1	Bio-optical	3	05/06/2017

Station PS106_	Type of core	# of cores	Day
22-1	P/I curve	3	05/06/2017
24-2	Sal/Temp	1	07/06/2017
24-2	Bio	6	07/06/2017
24-2	Mei	2	07/06/2017
24-2	P/I curve	3	07/06/2017
24-2	ARC	1	07/06/2017
28-1	Sal/Temp	1	11/06/2017
28-1	Bio	6	11/06/2017
28-1	Mei	2	11/06/2017
28-1	P/I curve	3	11/06/2017
28-1	ARC	1	11/06/2017
28-1	LSI	3	11/06/2017
32-2	Sal/Temp	1	15/06/2017
32-2	Bio	6	15/06/2017
32-2	Bio-optical	3	15/06/2017
32-2	P/I curve	3	15/06/2017
32-2	Mei	2	15/06/2017
32-2	ARC	2	15/06/2017
33	Mei	2	16/06/2017

Tab. 13.9: Additional sampling during PS106/1

Station PS106_	Location	Day
22-1_LARM_1	68	05/06/2017
22-1_LARM_2	68	05/06/2017
23-2_KEM_1	53	06/06/2017
23-2_KEM_2	53	06/06/2017
23-2_CTDIF_1	53	06/06/2017
24-2_LARM_1	67	07/06/2017
24-2_LARM_2	67	07/06/2017
24-2_LARM_3	68	07/06/2017
24-2_LARM_4	68	07/06/2017
24-2_CTDIF_1	66	07/06/2017
25-1_CTDIF_1	53	08/06/2017
26-2_CTDIF_1	53	09/06/2017
26-2_KEM_1	53	09/06/2017
26-2_KEM_2	53	09/06/2017
27-1_CTDIF_1	53	10/06/2017
28-2_CTDIF_1	68	11/06/2017
29-2_KEM_1	53	12/06/2017
29-2_KEM_2	53	12/06/2017
29-2_CTDIF_1	53	12/06/2017

Station PS106_	Location	Day
31_2_KEM_1	68	14/06/2017
31_2_CTDIF_1	66	13/06/2017
32_2_LARM_1	68	15/06/2017
32_2_LARM_2	68	15/06/2017
32_2_LARM_3	67	15/06/2017
32_2_CTDIF_1	66	15/06/2017
32_2_KEM_1	68	15/06/2017

C) Ridge study

For the ridge study we identified a ridge along the spatial variability transect. We conducted under-ice light measurements with irradiance and radiance sensors mounted on the ROV (sea-ice physics). We conducted a snow transect to study the snow distribution around the ridge. We drilled two sea-ice cores for biological samples (HPLC, POC, DNA, flow cytometer and fractionated chlorophyll *a*) and one core for temperature and salinity measurements, from which also CDOM and nutrient samples have been taken. In addition melt pond samples and water pocket samples were taken for all biological variables. A schematic image of the sampling is shown in Fig. 13.4.

D) Trace gases

Water samples for all gas analysis have been collected at 15 stations. Samples were taken from Niskin bottles mounted on a rosette sampler at discrete depths throughout the water column up to 200 m depth. The number of sampling depths varied as a function of the fluorescence signal and the O_2- sensor signal (Tab. 13.10). Methane concentration samples were immediately measured on board ship, using a gas chromatograph equipped with a flame ionization detector (FID). Methane gas samples were stored for analyses of the $\delta^{13}CCH_4$ values in the home laboratory. Further N_2O samples were stored for concentration and $\delta^{15}N$ values measurements in the home laboratory.

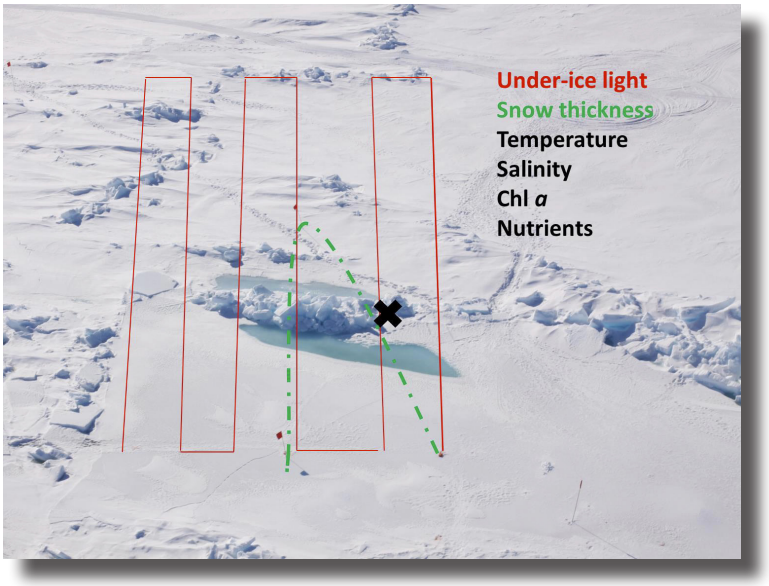

Fig. 13.4: Ridge sampling region. Red transects indicate the ROV transect for under ice light conditions. Green indicate the snow thickness measurements and the black cross indicates the coring site

Ice cores were taken in total from 9 sites. Two were carried out with different groups and were summarised in Table 13.11. For these sites, additional cores for temperature and salinity were taken. The complete ice cores were returned to the vessel into the cold container (-20°C), where they were cut into 10 cm slides. The slides were put in a gas-tight bag (Kynar bags with polypropylene 2-in 1-valve by Keikaventures) and closed. Subsequent the air was removed using a vacuum pump. For methane measurements, the melted water was filled into 120 mL glass vials in which a 5 mL N_2 headspace was created after the vials were crimped. The glass vials were shaken for equilibration at least an hour before retrieving a sample from the headspace with a 1.5 mL syringe. For all other measurements, the melted water was filled in glass vials without air bubbling, poisoned with saturated $HgCl_2$ and immediately crimped. The samples were stored at 4°C in darkness.

Preliminary (expected) results

The aim of this study is to understand the variability and biodiversity of the sea ice-associated biomass with respect to the sea ice conditions and nutrient availability, to assess the role of sea-ice biota for the cryo-pelagic, cryo-benthic coupling under different environmental scenarios from the shelf to the deep sea basin and its temporal development from spring to summer. Linking the various components of the food webs to a joint ice-related ecopath model will improve assessments of the role of climate change on the carbon cycle of the Arctic Ocean.

The chl-*a* data collected will be used to assess the sub-kilometer scales of variability in biological and physical parameters. The development of functions able to represent such variability will improve the parameterization for sea-ice algae modeling that are now used in large-scale global circulation models (e.g., MITgcm, FESOM). The consequences of under-sampling will be assessed with the aim to develop a sampling strategy and protocol that can be used for future field work (e.g., MOSAiC). Investigating the temporal evolution of the biological system will help to identify the timing and length of the spring bloom period, a key process to be represented in numerical simulations. Moreover, a set of conditions and parameters obtained from these field measurements will be used to feed numerical simulations.

Tab. 13.10: Sample list from biogeochemistry CTD cast for Methane, N_2O, nutrients and flow cytometer. (conc. = concentration)

Station PS106_	Depth [m]	Methane conc.	Methane isotopes	N_2O conc.	N_2O-isotopes	Nutrients	Flow-cytometer
15_02	200,100,65,50, 10,2	x					
17_02	200,100,40,19, 15,10,1	x	x	x	x		
18_02	100,75,50,35, 25,10,1.8	x	x	x	x		
21_01	200,100,50,25, 10,1	x	x	x			
22_02	300,200,100,75,525,10,1.5	x	x	x		x	x
23_03	200,100,75,50, 35,10,2	x	x	x	x		x
24_01	200,100,50,30, 10,1.3	x	x	x			x
27_05	100,75,50,21, 10,2	x	x	x			x
28_05	100,75,50,30, 10,2	x	x	x			
29_08	100,75,50,35, 10,1.6	x	x	x	x	x	
30_02	100,75,50,35, 10,2	x	x	x	x		x
31_01	100,75,50,40, 10,2	x	x	x		x	x

Station PS106_	Depth [m]	Methane conc.	Methane isotopes	N_2O conc.	N_2O-isotopes	Nutrients	Flow-cytometer
32_05	100,75,50,35, 10,2	x	x	x			x
34_02	100,75,50,25, 10,2	x	x	x			x
37_01	100,75,58,50,33,10,1	x	x	x			x

Tab. 13.11: Sample list methane ice cores. Location = way point of GPS list

Ice Station ID PS106_	Date	Location
22_1_SEAICEC_3	05.06.2017	68
25_2_SEAICE_1	08.05.2017	72
26_2_SEAICE_2	09.06.2017	53
27_4_SEAICE_1	10.06.2017	40
28_2_SEAICE_3	11.06.2017	80
29_2_SEAICE_1	12.06.2017	68
31_2_SEAICEC_1	13.06.2017	99

In addition, our goal is to achieve high data resolution by continuous measurements of greenhouse gases fluxes across water-sea ice-air interfaces along the late spring; this will also help us to test the sea ice permeability differences through time. We will be able to know the budget of relevant- climate compounds in both compartments, sea ice and sea water, influenced by a melting cycle and to distinguish how the physical and biogeochemical processes trigger concentration/saturation of trace gases.

The role of scales for biological sea ice sampling

During the spatial variability study for each core the core length, ice thickness, snow thickness and freeboard were determined. A plot for these variables is shown in Fig. 13.5. Ice thickness varied from 50 cm to more than 3 m. Snow thickness was also very variable along transect with values from 0 to 70 cm. In some places the snow load was such to depress the sea-ice surface below the sea-water level (negative freeboard).

Primary productivity

All primary productivity samples will be analyzed in a stable isotope facility. Uptake rates of inorganic carbon and nitrogen can be calculated based on changes in the $\delta^{13}C$ and $\delta^{15}N$ ratios before and after the incubation period. Determination of chl a, POC/N and microscopic analysis of the sediment trap material will be determined at the home lab at UiT.

First data exists for the photophysiological measurements during PS106/1. Highest maximum yield values (0.6) were measured for *Melosira arctica* on June 2 and 4, which decreased later substantially to values below 0.3. Sea ice algae had lower maximum yields not exceeding 0.4. The strong chlorophyll a maximum found in the marginal ice zone on the CTD transect on June 18 was characterized by very high maximum yield measurements (over 0.6), while all samples from 50 m depth were below detection limit.

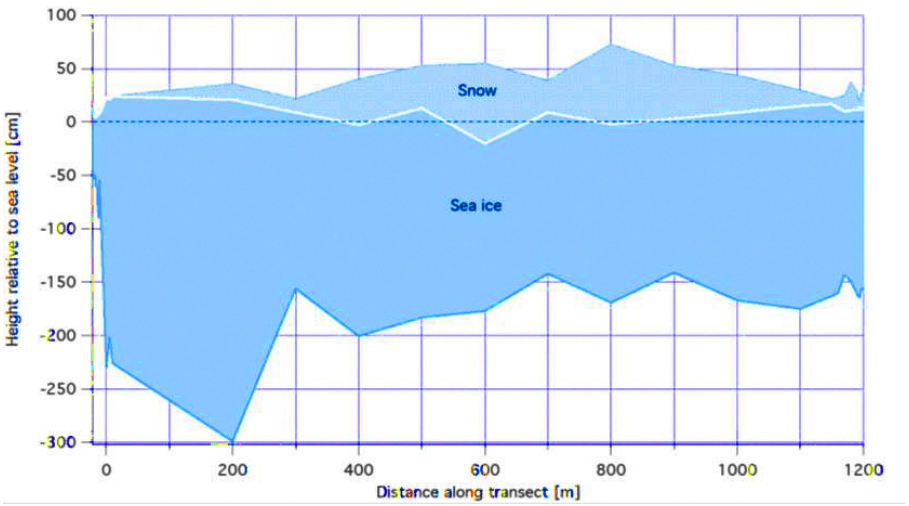

Fig. 13.5: Sea ice and snow thickness along the spatial variability transect. The white line indicates the measured freeboard

A first preliminary evaluation of the Light Curves (example Fig. 13.6) demonstrated a lower light acclimation of sea ice algae versus *Melosria arctica*, which reached its maximum rETR at intensities of 100 to 300 umol photons m^{-2} s^{-1} (data not shown).

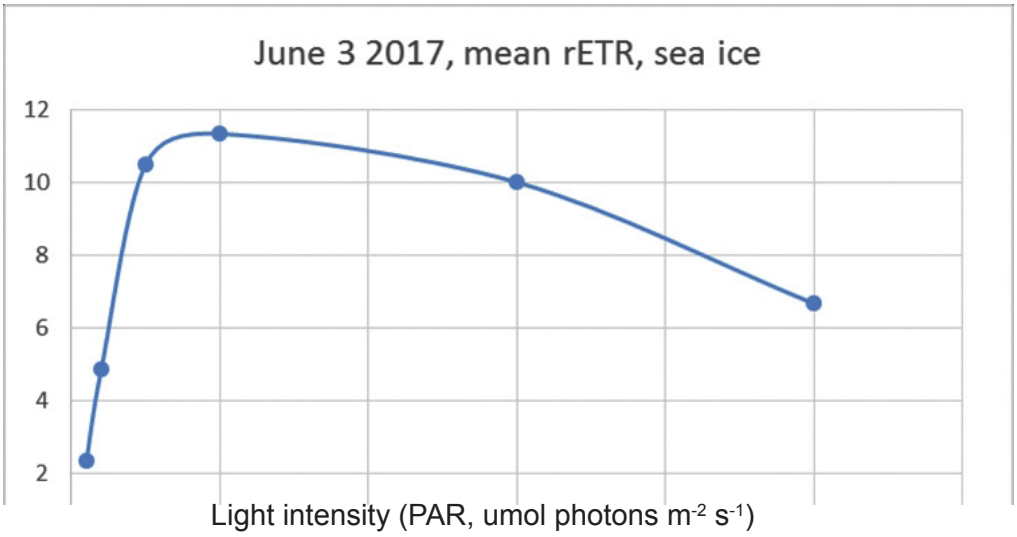

Fig. 13.6: Example of the changes of sea ice algal photophysiological variable relative electron transport rate rETR at different light intensities (sample collected June 2, 2017)

Methane in sea water and sea ice

In the study area, methane concentrations are heterogeneous and correspond to both, a clear under-saturation and a clear super-saturation with respect to the atmospheric equilibrium

concentration. The equilibrium concentration is calculated as a function of the gas solubility on the basis of the measured temperature and salinity properties and varies between 3.2 to 3.9 nM. Methane super-saturation was detected in surface water. Methane under-saturation was revealed in inflowing Atlantic water. In most ice cores methane concentration varied between 3.5 and 5.7 nM.

Data management

Almost all sample processing, such as chemical measurements, species identifications and quantifications, will be carried out in the home laboratories at AWI, WMR and UiT. As soon as the data are available they will be accessible to other cruise participants and research partners on request. Depending on the finalization of PhD theses and publications, data will be submitted to PANGAEA after publication, latest after 5 years. DNA data will be deposited in NCBI's Sequence Read Archive. The unrestricted availability from PANGAEA will depend from the progress of related PhD theses based on the data.

References

Fernández-Méndez M, Katlein C, Rabe B, Nicolaus M, Peeken I, Bakker K, Flores H, Boetius A (2015) Photosynthetic production in the Central Arctic during the record sea-ice minimum in 2012. Biogeosciences 12: 3525–3549.

Hardge K, Peeken I, Neuhaus S, Lange BA, Stock A, Stoeck T, Weinisch L, Metfies K (2017) The importance of sea ice for exchange of habitat-specific protist communities in the Central Arctic Ocean. Journal of Marine Systems 165: 124-138.

Kohlbach D, Graeve M, Lange B, David C, Peeken I, Flores H (2016) The importance of ice algae-produced carbon in the central Arctic Ocean ecosystem: Food web relationships revealed by lipid and stable isotope analyses. Limnology & Oceanography, doi:10.1002/lno.10351.

Lange BL, Katlein C, Nicolaus M, Peeken I, Flores H (2016) Sea ice algae chlorophyll a concentrations derived from under-ice spectral radiation profiling platforms. Journal of Geophysical Research-Oceans, doi:10.1002/2016JC011991.

Miller LA, F Fripiat, BGT Else, JS Bowman, KA Brown, RE Collins, M Ewert, A Fransson, M Gosselin D Lannuzel, KM Meiners, C Michel, J Nishioka, D Nomura, S Papadimitriou, LM Russel, et al. (2015) Methods for biogeochemical studies of sea ice: The state of the art, caveats, and recommendations. Elementa: Science of the Anthropocene, 3, doi: 10.12952/journal.elementa.000038.

14. INVESTIGATIONS ON BENTHIC SEDIMENTS DERIVED FROM AN ICE-FLOE DRIFT STATION OFF SVALBARD

Carolin Uhlir[1], Karen Jeskulke[2]

[1]UHH
[2]DZMB

Grant-No. AWI_PS106/1_2-00

Objectives

There are still large knowledge gaps on the lifecycles and several aspects of biology in the arctic fauna. However, feeding and shelter from predators in the benthic realm might be of considerable importance. To estimate the susceptibility of the benthic ecosystem to future changes induced by Climate Change and their potential impact on Polar cod distribution, it is important to gain more information on the composition of the benthic community in terms of abundance and diversity, and its dependency on sea ice algae.

Gears

Samples were taken by an RP-sledge. The RP-sledge, (Rothlisberg & Percey1977), a type of an epibenthic sledge could be deployed when the ice floe had a good drift in the right direction which allows trawling while staying in contact to the ice floe.

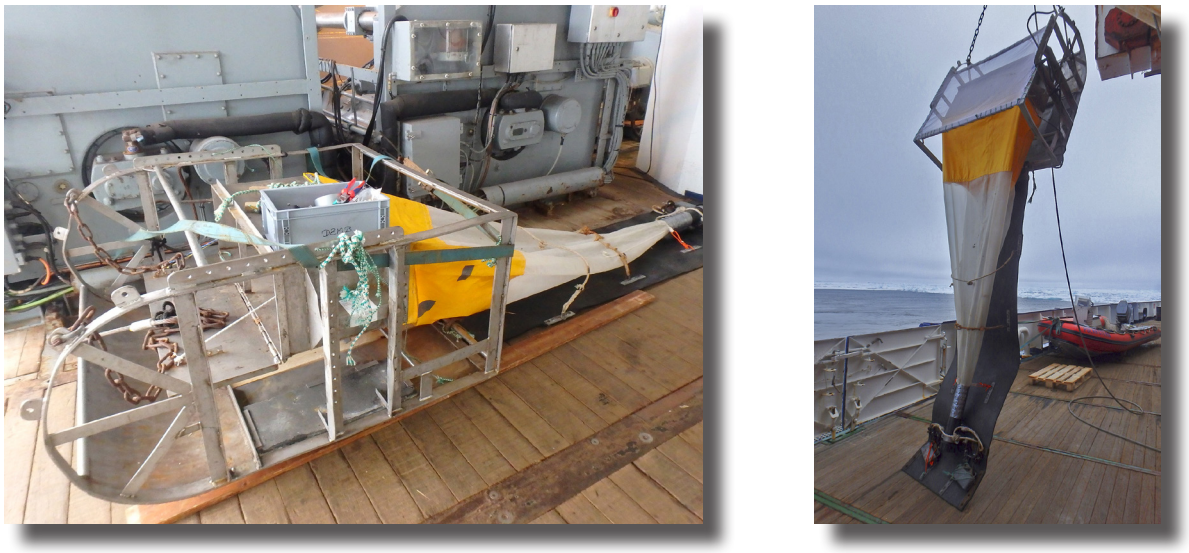

Fig. 14.1: RP-Sledge (Rotlishberg & Percey1977)

Work at sea

In case of the drift velocities below 0.5 kn we sampled with the giant box corer. The Box-Corer (Hessler & Jumars 1974) a modified UNSEL Box Corer is made of galvanized steel (see Fig. 14.2). The dimensions are 2.1x2.3x2.5 m with a weight of 1,000 kg (net). The box is 50x50x60 cm and show subsequently a surface of 0.25 m².

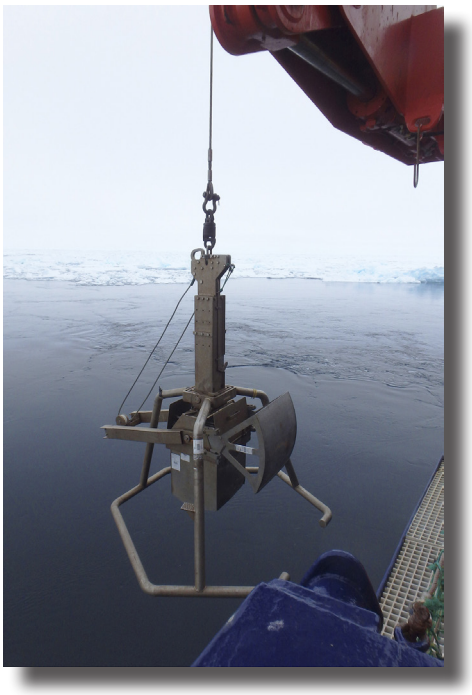

Fig. 14.2: The box corer

Tab. 14.1: List of completed benthic stations during PS106/1

Cruise	Gear	Station	Cast	Station date	Lat_start	Long_start	Depth_ start
PS106/1	BC	22	3	05.06.2017	81° 55.95‘ N	010° 57.57‘ E	1076.5
PS106/1	EBS-RP	24	5	07.06.2017	81° 55.43‘ E	010° 05.09‘ E	947.7
PS106/1	BC	25	5	08.06.2017	81° 53.80‘ N	009° 51.32‘ E	931.4
PS106/1	BC	29	3	12.06.2017	81° 49.46‘ N	011° 34.27‘ E	1551.3
PS106/1	BC	29	4	12.06.2017	81° 49.23‘ N	011° 33.97‘ E	1563.7
PS106/1	BC	29	7	12.06.2017	81° 48.93‘ N	011° 32.61‘ E	1568.7
PS106/1	BC	30	1	13.06.2017	81° 49.32‘ N	011° 32.30‘ E	1546.7
PS106/1	BC	32	3	15.06.2017	81° 43.68‘ N	010° 51.11‘ E	1580.7
PS106/1	BC	32	4	15.06.2017	81° 43.24‘ N	010° 48.68‘ E	1542.9

Preliminary Results

We took samples from different depth on the shelf (Table 14.1). We took 83 Sediment samples fixed in 96 % precooled ethanol in order to allow also future molecular studies. The samples will be sorted at home laboratory of the DZMB in Hamburg for the study of of the benthic community in terms of abundance and diversity. We have seen Ophiuroidea (Echinodermata), Munnopsidae (Malacostraca, Isopoda), Polychaettubes and Porifera on the surface. We could not find fluff from sea ice algae at the surface of the sediment. Fig. 14.3 shows surface from the BC stations 22/3 and 30/1.

Fig. 14.3: Surface from the BC stations 22/3 and 30/1

References

Rothlisberg PC, Pearcy WG (1977) An epibenthic sampler used to study theontogeny ofvertical migration of Pandalus jordani (Decapoda, Caridea). Fish Bull74:994-997.

Hessler RR & Jumars PA (1974) Abyssal community analysis from replicate cores in the central North Pacific. Deep Sea Reasearch and Oceanographic Abstracts. Pp185-209.

Boetius A et al. (2013) Export of Algal Biomass from the Melting Arctic Sea Ice. Science 339, 1430-432. doi: 10.1126/science.1231346

15. UNDER-ICE FAUNA, ZOOPLANKTON AND ENDOTHERMS

Hauke Flores[1,2], Julia Ehrlich[1,2], Benjamin Lange[1], Erik Sulanke[2], Barbara Niehoff[1], Nicole Hildebrandt[1], Martin Doble[3], Fokje Schaafsma[4], André Meijboom[4], Bram Fey[5], Susanne Kühn[4], Elisa Bravo-Rebolledo[4], Michiel van Dorssen[6], Rolf Gradinger[7], Brandon Hasset[7], Erin Kunisch[7] not on board: Doreen Kohlbach[1], Martin Graeve[1], Jan Andries van Franeker[4], Bodil Bluhm[7]

[1]AWI
[2]UHH
[3]Polar Scientific
[4]WMR
[5]NIOZ
[6]v.D. Met.
[7]UiT

Grant-No. AWI_PS106/1_2-00

Objectives

The Arctic Ocean is facing drastic changes, most evidently a significant decline of the extent and duration of sea ice coverage. This process is accompanied by ocean warming in some areas of the Arctic Ocean, and increasing acidification. A reduction and change of sea ice habitats will have consequences on ecosystem functioning since, at high latitudes, ecosystems thrive on carbon produced by ice-associated algae. Grazers in the ice-water interface layer, such as under-ice amphipods and copepods, as well as young polar cod *Boreogadus saida* feeding on them, play a key role in transferring sea ice-derived carbon into pelagic food webs, and ultimately to the birds and mammals inhabiting the Arctic (Kohlbach et al., 2017). Reduction of sea ice habitats may result in insufficient resources for juvenile polar cod and in a potential loss of connectivity between central Arctic sea ice habitats and shelf-based populations (David et al., 2016). Further decline and structural change of Arctic sea ice may thus lead to habitat loss and reduced food availability for this fish. A major decline of polar cod stocks can cause severe ramifications in Arctic ecosystems, and can particularly affect populations of higher predators, such as seals and polar bears. Our group aims to better understand potential impacts of changing sea ice habitats for polar cod, its prey, and its predators.

During PS106, the physical and biogeochemical habitat properties and biodiversity of the sea-ice associated habitat were sampled, with an emphasis on polar cod and its ice-associated and pelagic prey species. The abundance and distribution of under-ice fauna is poorly understood due to the inaccessibility of the under-ice habitat. New sampling methods are therefore warranted to observe and quantify this important functional group of the food web, and its resilience to changing sea ice habitats. To investigate the vertical and horizontal distribution and abundances of abundant zooplankton and under-ice fauna species, meso- and macrofauna were sampled with a Surface and Under-Ice Trawl (SUIT), a Rectangular Midwater Trawl (RMT), a Multinet, an ROV-mounted under-ice net (ROVnet), echosounders (*Polarstern's* EK60 and Acoustic Zooplankton and Fish Profilers, AZFPs). With the zooplankton recorder LOKI (light frame on-sight key species investigator, Fig. 15.3), pictures of the organisms floating in the water column from 1,000 m depth to the surface and during horizontal ROV-transects were taken continuously, which allows to exactly identify horizontal and vertical distribution patterns in relation to environmental conditions.

Polar cod constitutes the staple food of various Arctic and North-Atlantic bird and seal species, thereby indirectly ensuring food sources of polar bears. To assess the relevance

of sea ice-associated resources and polar cod for higher trophic levels, endotherm surveys were conducted to map the association of seabirds, polar bears, seals and whales with the distribution of polar cod and sea-ice habitat properties.

Work at sea

Under-ice fauna sampling

ROVnet

We used a newly designed under-ice net mounted on the ROV of the sea ice physics group to sample zooplankton, under-ice fauna, phytoplankton and under-ice algae at three discrete depth layers. This “ROVnet” consisted of a polycarbonate frame (60 X 40 cm) mounted on top of the ROV, with a zooplankton net (5 m length, 0.5 mm mesh) attached to it. At the end of the net, the catch was collected in a coded bottle (diameter 10 cm). On the top bar of the frame, a street broom was mounted upside-down in order to maintain steady contact of the net with the ice underside during trawling (Fig. 15.1). Optionally, a phytoplankton net (20 x 10 cm opening, 50 µm mesh) could be mounted in the net opening. During ROVnet trawls, current speed and data from the physical environment were recorded, e.g. water temperature, salinity, fluorescence, ice draft, and multi-spectral light transmission. At each sampling event, we aimed to sample 3 depth layers, which were trawled horizontally at a speed of 1.0-1.5 knots: The under-ice surface, 5 m depth, and 10 m depth. Altogether, 24 ROVnet deployments were completed at 9 sampling events. Two hauls were aborted due to technical problems. From 10 to 11 June 2017 (station 27 and 28) we conducted a diurnal vertical distribution study to find out whether the presence of zooplankton and under-ice fauna in the surface layer resembled the diurnal cycle of light. To achieve this, 3 consecutive sampling events were accomplished at noontime, midnight, and the following noontime, respectively. These sampling events were synchronised with corresponding multinet hauls, and compared to the corresponding 24-hour record of the EK60. A 0-50 m double-oblique haul was conducted to assess the comparability of ROVnet catches with multinet hauls of the top 50 m. An overview of the sampling locations is given in Table 15.1 Samples of macrofauna were preserved on 4 % formaldehyde/seawater solution, or frozen (-20°C / -80°C), and will be used for a variety of analyses.

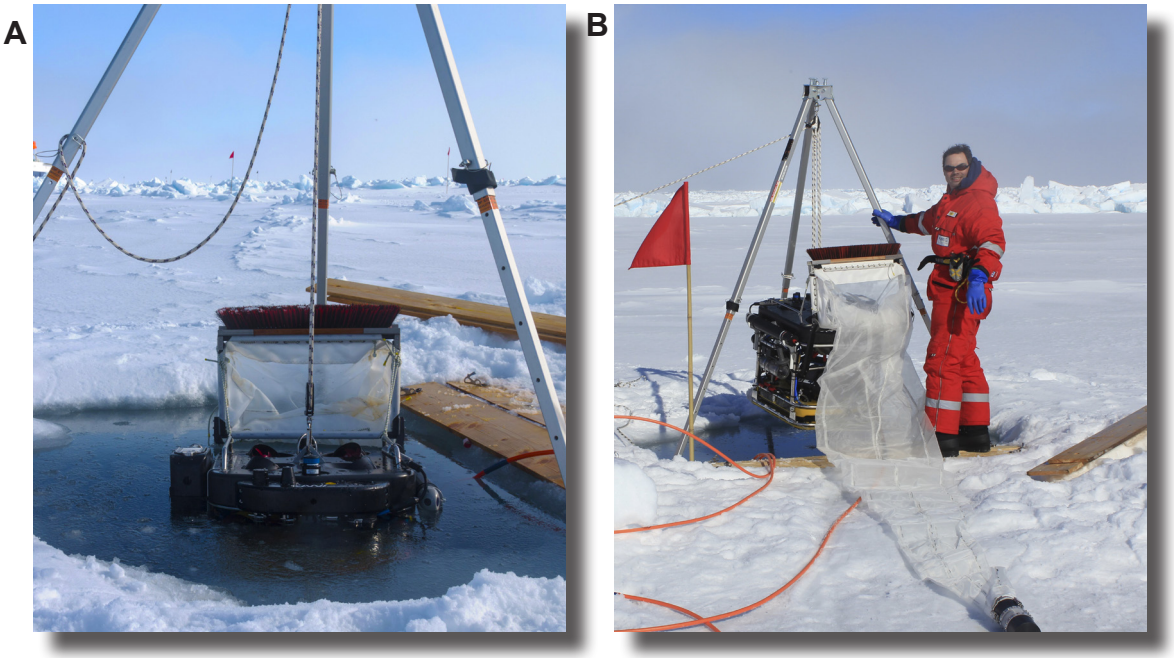

Fig. 15.1: The ROVnet in front view during deployment (A), and in rear view (B)

Tab. 15.1: Summary of ROVnet hauls conducted during PS106/1 and PS106/2. “x” indicates phytoplankton net mounted in ROVnet frame

Station PS106_	Sampling depth [m]	Date	Time start	Duration [min]	Phytopl. net	Remarks
25	0	08-JUN-2017	12:25	16		
25	0	08-JUN-2017	13:10	26		
27	10	10-JUN-2017	11:58	25		
27	5	10-JUN-2017	12:39	24		
27	0	10-JUN-2017	13:12	34		
27	0-50	10-JUN-2017	13:56	9		
27	10	10-JUN-2017	22:57	24		
27	5	10-JUN-2017	23:45	29		
28	0	11-JUN-2017	00:23	9		Haul aborted
28	0	11-JUN-2017	00:46	36		Polar cod seen
28	10	11-JUN-2017	11:01	24		
28	5	11-JUN-2017	11:32	14		
28	0	11-JUN-2017	11:53	34		
32	10	15-JUN-2017	07:57	8	x	
32	5	15-JUN-2017	08:22	16	x	
32	0	15-JUN-2017	08:54	33	x	
45	0	25-JUN-2017	22:42	18	x	Polar cod seen
45	5	25-JUN-2017	23:17	24	x	
45	10	25-JUN-2017	23:58	13	x	
66	0	02-JUL-2017	21:38	24	x	
66	10	02-JUL-2017	22:16	13	x	
66	5	02-JUL-2017	22:50	15	x	
73	0	07-JUL-2017	05:55	16	x	Thruster failure
80	0	12-JUL-2017	11:34	15	x	[1)]
80	10	12-JUL-2017	12:00	10	x	

[1)] Phytopl. net outside main net

SUIT

A Surface and Under-Ice Trawl (SUIT: van Franeker et al., 2009) was used to sample the meso- and macrofauna down to 2 m under the ice. The SUIT had two nets, a 0.15 mm mesh plankton net, and a 7 mm mesh shrimp net. During SUIT trawls, data from the physical environment were recorded, e.g. water temperature, salinity, fluorescence, ice thickness, and multi-spectral light transmission. Twenty-one SUIT deployments were completed in ice-covered waters, of which two were short hauls because the ship got stuck in the ice. An overview of the sampling locations is given in Table 15.2 and Fig. 15.2. Samples of macrofauna were preserved on 4 % formaldehyde/seawater solution, 70 % ethanol, 100 % ethanol or frozen (-20°C / -80°C), and will be used for various analyses. Polar cod caught with SUIT were either kept alive, frozen whole (-20°C) or dissected.

Tab.15.2: Summary of SUIT hauls conducted during PS106/2

Station PS106_	Date	Start time [UTC]	Lat	Lon	Bottom depth [m]	Comments
50-5	29-06-2017	07:23	80.54783	31.249757	104	1 polar cod
63-1	01-07-2017	12:32	81.46119	32.82294	240	1 polar cod
65-4	02-07-2017	06:35	81.58647	33.276123	490.4	
66-3	02-07-2017	14:26	81.66164	32.300751	1661.2	Ship stuck
66-4	02-07-2017	15:52	81.66156	32.29811	1748	1 polar cod
67-5	03-07-2017	18:40	81.96323	32.509246	2789.4	4 polar cod
68-5	04-07-2017	10:44	82.33952	33.031026	3012.7	
69-2	05-07-2017	08:15	82.99238	33.187663	3717.4	
70-1	05-07-2017	17:26	83.11215	32.8157	3810.4	1 polar cod
71-5	06-07-2017	06:47	83.3108	33.21267	3886	
72-5	06-07-2017	15:36	83.493	33.106879	3980.3	
73-7	07-07-2017	08:54	83.68513	32.059667	4022.7	Plankton net lost
74-5	08-07-2017	13:22	83.47481	27.929352	4051	
75-6	09-07-2017	11:12	82.99065	25.268503	4047.4	
76-4	10-07-2017	09:24	82.49111	18.380839	2695.6	
77-2	10-07-2017	15:50	82.25278	17.859558	2009.7	
78-5	11-07-2017	06:55	82.05645	17.806324	3176.6	1 polar cod
79-1	11-07-2017	17:18	81.66496	17.01506	2845.1	
80-3	12-07-2017	17:54	81.44784	16.954695	1996.9	
83-7	13-07-2017	13:28	81.29122	18.60228	520.8	Stuck ship
83-8	13-07-2017	14:49	81.29205	18.558031	528.1	

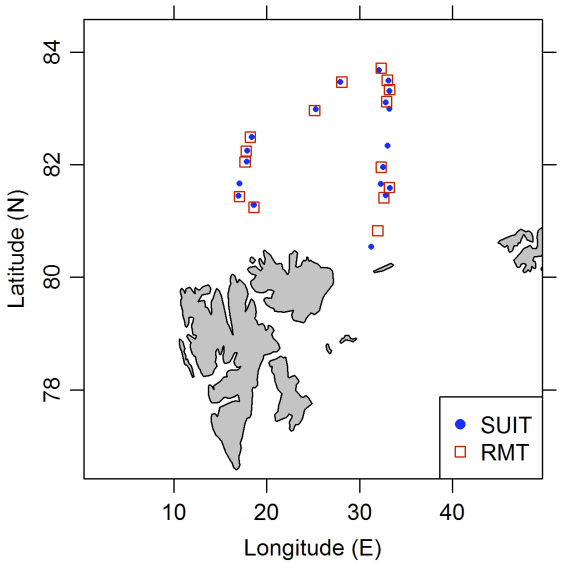

Fig. 15.2: Overview of Surface and Under Ice Trawl (SUIT) and Rectangular Midwater Trawl (RMT) stations

Pelagic sampling

RMT

A Rectangular Midwater Trawl (RMT) was used to sample the pelagic community at 0-100 m depth. During trawling sampling depth was recorded with a depth meter attached to the bridle of the net. We conducted 15 hauls with the RMT. Sample collection and preservation were performed in the analogue procedure described above for SUIT sampling. An overview of the sampling locations is given in Table 15.3.

The catches of the 0.15 mm plankton net of the SUIT and the 0.33 mm plankton net of the RMT were split in two halves, after which one half was size-fractionated. These samples will be used for to assess differences in community structure by comparing the total biomass of the different size fractions.

Tab. 15.3: Summary of RMT hauls conducted during PS106/2

Station PS106_	Date	Time [UTC]	Lat	Lon	Depth [m]
52-1	29-06-2017	14:41	80.82638	31.953966	135
64-2	01-07-2017	14:48	81.41416	32.612201	204.4
65-3	02-07-2017	04:43	81.59516	33.207016	553
67-1	03-07-2017	12:18	81.95435	32.330701	2818.3
70-4	05-07-2017	20:58	83.11927	32.924238	3813.4
71-4	06-07-2017	05:32	83.334	33.237782	3902.6
72-1	06-07-2017	12:39	83.50125	32.981169	3982.7
73-8	07-07-2017	10:38	83.71395	32.337495	4022.3
74-4	08-07-2017	12:26	83.4679	28.085239	4049.1
75-5	09-07-2017	10:08	82.96345	25.135079	4045.9
76-3	10-07-2017	08:25	82.48965	18.224139	2277.8
77-3	10-07-2017	17:15	82.2445	17.782107	2024.9
78-4	11-07-2017	03:32	82.05043	17.643661	3155.8
80-4	12-07-2017	19:25	81.43483	17.034591	1849.4
83-6	13-07-2017	12:15	81.24548	18.605507	472.1

Multinet and LOKI

To investigate the mesozooplankton community composition and depth distribution in the study area, we used a multi net (MN) equipped with 5 nets (mesh size: 150 µm). Vertical net hauls sampling 5 depth intervals were conducted at 9 stations during PS106/1, and at 22 stations during PS106/2 (Tab. 15.4). The depth intervals varied among stations and were dependent on the bottom depths (maximum sampling depth 1,500 m). All samples were immediately preserved in formalin buffered with hexamethylentetramin. At two stations, additional MN casts were taken to sample organisms for later analyses of fatty acid composition and stable isotopes. In addition to the MN hauls, optical (LOKI) and acoustical methods (Aquascat) were used to investigate the small-scale distribution of zooplankton species in the upper 1,000 m of the water column. The LOKI system (Lightframe On-sight Key species Investigation) was equipped with a high-resolution digital camera taking 18 pictures sec-1. At the same time sensors measured temperature, salinity, depth, oxygen and fluorescence, allowing us to relate mesozooplankton distribution patterns to hydrography. The Aquascat system was mounted to the upper part of the LOKI frame facing sideways, and recorded the acoustic backscatter at 0.5, 1, 2 and 4

MHz (Fig. 15.3). During this cruise, we aimed to investigate the mesozooplankton community directly under the ice for the first time, using a LOKI camera mounted on the “Beast! ROV of the Sea Ice Physics Group. At four stations, horizontal transects at 0 to 20 m depth were performed. To optimize the efficiency of the net which is attached to the camera, we tested nets with openings of 5, 10 and 20 cm.

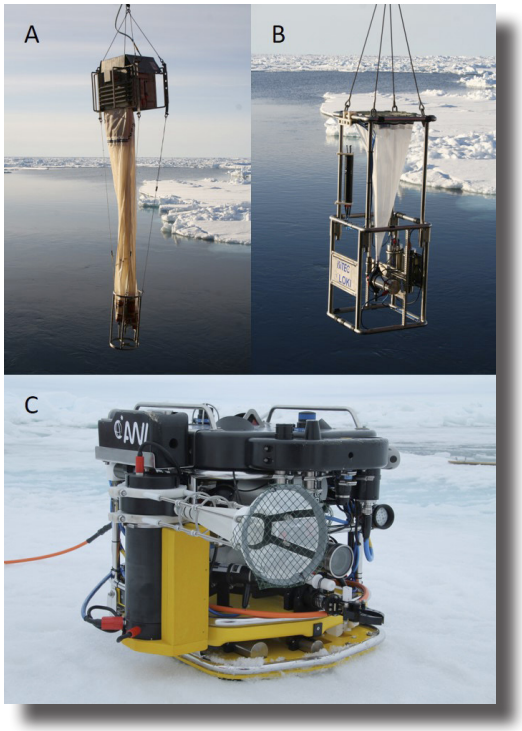

Fig. 15.3: The Multi net (A) and the the LOKI (lightframe on-sight key species investigation; B) during deployment. Attached to the frame of LOKI is the Aquascat system (on the left hand side). (C) The LOKI camera, here with the large net opening, mounted to the ROV “Beast”.

Tab. 15.4: Mesozooplankton sampling during PS106/2. Presented are station identifiers, sampling dates and maximum sampling depths. Empty spaces indicate that no samples were taken with the specific gear due to limited time or opportunity in case the under-ice LOKI / ROV. At two stations, additional Multi net casts were performed for sampling live animals. In that case, two maximum sampling depths are presented. One additional LOKI cast (to 100 m) was performed with the Aquascat transducers turned off, to measure ambient noise levels.

Station	Date	Multi net Midi Max. sampling depth [m]	LOKI / Aquascat Sampling depth [m]	LOKI / ROV Sampling depth [m]
PS106_0025	08.06.17	500	n.a.	n.a.
PS106_0027	10.06.17	800 (3x)	n.a.	n.a.
PS106_0028	10.06.17	500 and 800	n.a.	n.a.
PS106_0030	13.06.17	800	n.a.	n.a.
PS106_0032	15.06.17	800	n.a.	n.a.
PS106_0047	26.06.17	147	155	n.a.

Station	Date	Multi net Midi Max. sampling depth [m]	LOKI / Aquascat Sampling depth [m]	LOKI / ROV Sampling depth [m]
PS106_0049	27.06.17	220	221	n.a.
PS106_0050	29.06.17	135	135	20
PS106_0062	01.07.17	200 and 400	390	n.a.
PS106_0065	02.07.17	500	575	20
PS106_0066	02.07.17	1000	1000	n.a.
PS106_0067	03.07.17	1500	1000	n.a.
PS106_0068	04.07.17	1000	1000	n.a.
PS106_0069	05.07.17	1500	1000	n.a.
PS106_0070	05.07.17	n.a.	1000	n.a.
PS106_0071	06.07.17	1000	1000	n.a.
PS106_0072	06.07.17	n.a.	1000	n.a.
PS106_0073	07.07.17	1500	100 and 1000	20
PS106_0074	08.07.17	n.a.	1000	n.a.
PS106_0075	09.07.17	100 and 1500	1000	n.a.
PS106_0076	10.07.17	n.a.	1000	n.a.
PS106_0077	10.07.17	1000	n.a.	n.a.
PS106_0078	11.07.17	1500	1000	n.a.
PS106_0080	12.07.17	1500	n.a.	20
PS106_0083	13.07.17	400	400	n.a.
PS106_0088	15.07.17	250	261	n.a.
PS106_0091	16.07.17	115	115	n.a.
PS106_0093	17.07.17	160	161	n.a.

Top predator censuses

After leaving the 12 NM zone of Longyearbyen observers started endotherm surveys on a continuous basis. Standard band transect methods, with snapshot methodology for birds in flight (Tasker et al., 1984), and additional line-transect methods for marine mammals (Buckland et al., 2001), were conducted from the peildeck of *Polarstern,* when the ship was steaming between stations. Two observation boxes were installed near the center line of the ship on the peildeck, which gave shelter, comfort and a good view to the observers. Besides the ship- based surveys, 7 helicopter surveys were carried out which normally consist of two pre-determined straight transects of 60 NM over a bandwidth of 250 meters. One helicopter survey was aborted after take- off due to changing weather conditions. Top predator surveys were carried out on an estimated 95 % of the cruise track. Sometimes surveys were cancelled due to bad weather like dense fog or a snowstorm.

Preliminary (expected) results

Under-ice fauna

ROVnet

The catch composition of the ROVnet differed significantly between the under-ice layer and the pelagic (5 m and 10 m) sampling strata. In the under-ice layer, the catch was co-dominated

by copepods and sympagic amphipods. The most abundant sympagic amphipods were *Apherusa glacialis* and *Onisimus* spp., but the larger *Eusirus holmi* and *Gammarus wilkitzkii* were also frequently encountered. In the water column, *Calanus hyperboreus* appeared to dominate the catch composition both in terms of numbers and biomass, according to visual inspection of the catch. In most cases, copepod abundances appeared to be considerably higher at 10 m depth than at 5 m depth (Fig. 15.4A). Abundances of both under-ice fauna and zooplankton were extremely low in the northern part of the research area of P106/2. A preliminary inspection of the catch composition of the diurnal study during PS106/1 (Station 27-28) indicated that the abundance of under-ice fauna was considerably higher at nighttime than at daytime (Fig. 15.4B). However, for a scientifically sound interpretation of these results, they must be compared to other datasets, such as hydroacoustic profiles, and ADCP current patterns under the ice.

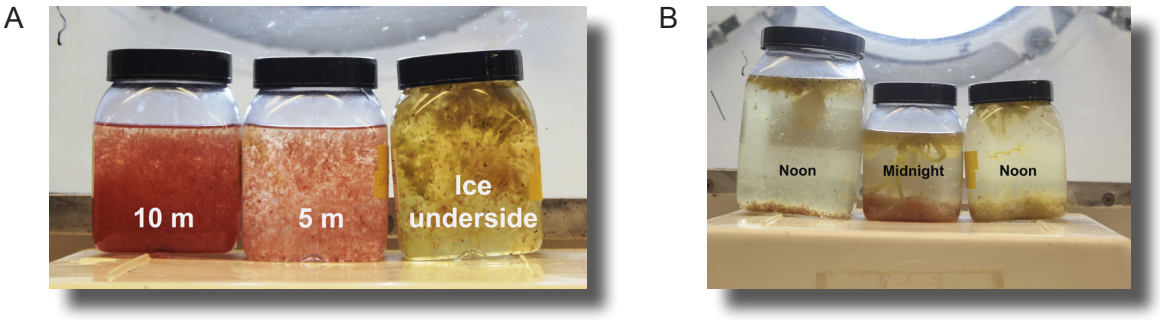

Fig. 15.4: Sampling jars with ROVnet catch. A) Differences in catch abundandance at 10 m depth (left), 5 m depth (center) and the under-ice layer (right); B) differences in catch abundance in the under-ice layer between noontime catches (left and right) and midnight catch (center)

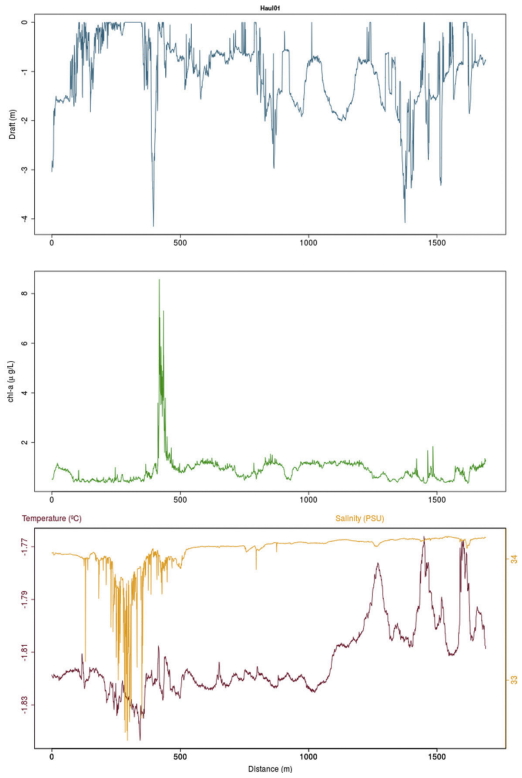

Fig. 15.5: Example of environmental data profiles obtained from the SUIT's sensor array

SUIT

All 21 SUIT hauls were conducted underneath sea ice. Bio-environmental profiles were obtained from each SUIT haul (Fig. 15.5), excluding the two hauls were the ship got stuck soon after starting the trawl. Insight on the biological productivity of the system can be expected as soon as spectral data from the SUIT's RAMSES sensor can be related to the chlorophyll *a* content of sea ice derived from our L-arm measurements and associated ice core sampling (see chapter 13).

The SUIT catch of the 7 mm mesh shrimp net generally included sympagic amphipods such as *Apherusa glacialis*, *Eusirus holmii*, *Gammarus wilkitzkii*, *Onisimus glacialis* and *Onisimus nanseni*. Copepods such as *Calanus hyperboreus*, amphipods such as *Themisto libellula* and *T. abyssorum*, the gastropod *Clione limacina*, chaetognaths, gelatinous species such as *Merstensia spp* and *Beroe cucumis.* At one station on the Barents Sea shelf slope, the SUIT caught high numbers of *Thysanoessa* spp. dwelling in the ice-water interface layer. Total abundances in the northernmost stations were extremely low.

Pelagic fauna

RMT

The catch composition of the RMT was dominated by pelagic zooplankton, whereas sympagic amphipods were practically absent. Particularly on the slope of the Barents Sea shelf, the RMT caught high abundances of krill *Thysanoessa longicaudata* and *T. inermis*. The catch composition of SUIT and RMT not only differed spatially and from each other, but also from the community structure as found in the *Polarstern* expedition PS92, which was conducted on the Svalbard shelf and Yermak plateau in May/June 2015 (Flores et al, 2016). In total nine polar cod were caught with SUIT.

Multinet and LOKI

The mesozooplankton abundances as roughly estimated by eye during preservation were comparably low. Both MN sampling and LOKI casts revealed that the mesozooplankton communities were dominated by calanoid copepods. Females of *Calanus hyperboreus*, the largest of the three Arctic *Calanus* species, were found in high numbers in the upper 50 m of the water column at deep-water stations (>500 m depth). On the shelf east of Svalbard (bottom depth <250 m) sampled towards the end of the cruise (Station 89, 91 and 93), *C. glacialis* prevailed, confirming that this species dominates Arctic zooplankton shelf communities. The guts of female *C. hyperboreus* were almost empty, indicating that their feeding rates were low. In contrast, the guts of *C. glacialis* were full and many faecal pellets were found in the MN samples, indicating that these copepods were feeding at high rates and, thus that their productive season had started. The Atlantic species *C. finmarchicus* was only rarely found. At greater depths (> 200 m) at oceanic stations, chaetognaths (arrow worms) were highly abundant at many locations. Ostracods, hydrozoan medusa and amphipods (Fig. 15.6) occurred regularly, but in lower numbers. Detailed analyses of the multinet samples and LOKI pictures will be conducted at the AWI laboratories in Bremerhaven. The low abundances observed presented a challenge for the acoustic method, with backscatter signal levels being very low except in the surface layers above 50 m. Preliminary results from the acoustic inversion model confirm the presence of larger animals (*Calanus*, krill) in the upper water column, with (acoustically) smaller and less abundant populations below that, often localised into thin layers. An “Aquadopp” acoustic doppler current meter (ADCP) was mounted to the LOKI at Station 88, looking across the net opening. This confirmed our impression that significant horizontal water flow away from the net occurs during the LOKI upcast, causing particles to passively escape detection by the LOKI system. A longer net is suggested as a partial solution to this problem. By combining all approaches (MN, LOKI and Aquascat), we will be able to analyze the zooplankton distribution patterns and thus contribute to our understanding of the feeding regime of Polar cod. The camera mounted on the ROV captured pictures mostly of nauplii (the youngest developmental stages of copepods) and faecal pellets; *Calanus* spp. or other zooplankton species were rarely photographed. Sampling at the first ice station on 29 June revealed that a sampling event in a particular depth should last at least 20 min to account for variations in zooplankton abundance. Sampling at the second ice station revealed that a net opening of at least 10 cm allows for sampling of mesozooplankton. A detailed analysis is, however, mandatory to evaluate whether the camera on the ROV can be used to determine abundances of organisms larger than 1 mm, e.g. late copepodites and adults of the dominating *Calanus* species.

Fig. 15.6: A selection of pictures collected by LOKI: (a) Radiolaria, (b) Appendicularia (Oikopleura sp.), (c) Siphonophora, (d) Copepoda (Calanus hyperboreus), (e) Copepoda (Paraeuchaeta sp.), (f) Euphausiacea (Thysanoessa sp.), (g) Ostracoda, (h) Copepoda (Scaphocalanus magnus), (i) Amphipoda.

Top predator censuses

On the first part of the cruise great amounts of seabirds were counted while flying in and out to the Spitsbergen breeding colonies. The main species were Kittiwake (*Rissa tridactyla*), Northern Fulmar (*Fulmarus glacialis*), Little Auk (*Alle alle*), Black Guillemot (*Cepphus grylle*) and Brunnich's Guillemot (*Uria lomvia*). While rounding the southern tip of Spitsbergen, whales and dolphins were observed including the Blue Whale (*Balaenoptera musculus*), Fin Whale (*Balaenoptera physalus*), Northern Minke Whale (*Balaenoptera acutorostrata*), Humpback Whale (*Megaptera novaeanglia*) and White- beaked Dolphin (*Lagenorhynchus albirostris*). Sailing north along the east coast of Spitsbergen, we entered the pack-ice where Walruses (*Odobenus rosmarus*) were seen. Ringed Seal (*Pusa hispida*), Harp Seal (*Pagophilus groenlandicus*) and Bearded Seal (*Erignathus barbatus*) were found scattered over the pack ice area and sometimes in bigger numbers spread over a great ice floe, near breathing holes. Only Bearded Seals were seen on the ice close to water. Polar Bear (*Ursus maritimus*) were present in a particular part of the expedition. Females with 1-2 cubs were recorded. Only three whales were seen within the pack-ice area, two Northern Minke Whales and one unidentified whale species. Densities of birds within the sea ice were generally low. Ivory Gull (*Pagophila eburnea*), Glaucous Gull (*Larus hyperboreus*), Arctic Tern (*Sterna paradisaea*), Puffin (*Fratercula arctica*), Great Skua (*Stercorarius skua*), Pomarine Skua (*Stercorarius pomarinus*) and Arctic Skua (*Stercorarius parasiticus*) were recorded within the sea-ice area in addition to the earlier mentioned bird species.

Data management

Almost all sample processing, such as chemical measurements and species identifications and quantifications, will be carried out in the home laboratories at AWI and Wageningen Marine Research. As soon as the data are available they will be accessible to other cruise participants and research partners on request. Depending on the finalization of PhD theses and publications, data will be submitted to PANGAEA, and will be open for external use.

References

Buckland ST, Anderson DR, Burnham KP, Laake JL, Borchers DL, Thomas L (2001) Introduction to Distance Sampling: Estimating Abundance of Biological Populations Oxford University Press, Oxford, UK 447pp.

David C, Lange B, Krumpen T, Schaafsma, FL, van Franeker J A, Flores H (2016) Under-ice distribution of polar cod *Boreogadus saida* in the central Arctic Ocean and their association with sea-ice habitat properties Polar Biology 39(6), 981-994, doi:10.1007/s00300-015-1774-0.

Flores H, Castellani G, Schaafsma FL, Vortkamp M, Immerz A, Zwicker S, Van Dorssen M, Tonkes H, Niehoff B, Van Franeker JA (2016) Sea ice ecology, pelagic food web and copepod physiology - iceflux / pebcao (In: The expedition PS92 of the research vessel “Polarstern” to the Arctic Ocean in 2015, Peeken I, ed). Berichte zur Polar- und Meeresforschung, 694, 81 - 90.

van Franeker JA, Van den Brink NW, Bathmann UV, Pollard RT, de Baar HJW, Wolff WJ (2002) Responses of seabirds, in particular prions (*Pachyptila* sp.), to small scale processes in the Antarctic Polar Front Deep-Sea Research II 49, 3931-3950.

van Franeker JA, Flores H, Van Dorsse M (2009) The Surface and Under Ice Trawl (SUIT). In: Flores, H (ED), *F*rozen Desert Alive - The Role of Sea Ice for Pelagic Macrofauna and its Predators. PhD thesis University of Groningen, pp. 181–18.

Kohlbach D, Graeve M, Lange B, David C, Peeken I, Flores H (2016) The importance of ice algae-produced carbon in the central Arctic Ocean ecosystem: Food web relationships revealed by lipid and stable isotope analyses Limnology & Oceanography, doi:10.1002/lno.10351.

Kohlbach D, Schaafsma FL, Graeve M, Lange B, David C, Peeken I, van Franeker JA, Flores H (2017) High trophic dependency of polar cod (*Boreogadus saida*) on sea ice algae-produced carbon: evidence from stomach content, fatty acid and stable isotope analyses Progress in Oceanography, 152, 62-74, doi:10.1016/Jpocean.2017.02.003.

Tasker ML, Hope Jones P, Dixon T, Blake BF (1984) Counting seabirds at sea from ships: a review of methods employed and a suggestion from a standardized approach. Auk, 101,567-577.

16. CLIMATE SENSITIVITY IN ARCTIC FISH: PHYSIOLOGICAL DIFFERENTIATION AND GENETIC BASIS OF DISTINCT POPULATIONS OF THE POLAR COD *BOREOGADUS SAIDA*

Nils Koschnick[1], Jennifer Steffen[1] [1]AWI
not on board: Christian Bock[1], Gisela Lannig-Bock[1], Felix Christopher Mark[1], Magnus Lucassen[1]

Grant-No. AWI_PS106/1_2-00

Objectives

Increasing CO_2 in the atmosphere causes both ocean warming and acidification. Due to its pervasive impact on all biological processes, temperature is a crucial abiotic factor limiting geographical distribution of marine ectothermal animals on large scales. Additional environmental factors like increasing PCO_2, the concomitant drop in water pH and retreating sea ice are thought to narrow the thermal window and the fitness of polar fish, as they are believed to act on the same physiological mechanisms. Nevertheless, thermal windows of individual macromolecules are usually much broader than the temperature window of the whole organism, and the integration of molecules into functional units and systems up to the whole organism level must be taken into account for an understanding of climate-driven evolution.

Previous studies (Kunz et al. 2016) have shown that the Atlantic Cod (*Gadus morhua*) and other boreal fishes migrate into northern geographical regions. Therefore, boreal species become a competitive threat to polar species like the Polar cod (*Boreogadus saida*) as there is no further northward escape possibility.

During its life cycle, *B. saida* populates different habitats from benthos to open water and the underside of sea ice (David et al., 2016). These contrasting environments with their different food supply affect the physiological status of this species (Kunz et al., 2016; Leo et al., 2017). Within the small spatio-temporal scales of SiPCA we will conduct comprehensive comparative physiological and molecular genetic studies of the different populations from all available habitat types. We aim to (i) estimate acclimatory capacities/sensitivity towards combined treatments of warming and hypercapnia, (ii) determine the level of cold adaptation, and (iii) compare samples from laboratory reared animals to *in-situ* samples from the field. The analyses comprise global (RNA-Seq) and targeted (qPCR) gene expression techniques on the background of the population genetic structure, assessment of cellular energy budgets and allocation, as well as metabolic profiling (by means of untargeted nuclear magnetic resonance spectroscopy, NMR).

Work at sea

Bottom trawls between 200 – 800 m were mainly used to explore the fish fauna. For under ice trawling, a custom made surface and under ice trawl (SUIT) was used in collaboration with other groups (H. Flores et al., Chapter 15).

All catches were analysed for species composition, individual size and biomass, sex and maturity stage. Fin-clips from all specimens were taken and preserved in ethanol for population genetics. Additional tissue samples were taken directly after the catch and flash-frozen in liquid nitrogen for later molecular and physiological analyses at the home institute.

200 specimens of alive Polar Cod were kept in an aquarium container to be transported to the AWI's aquarium in Bremerhaven. These animals are highly adapted to the cold temperatures of the Arctic waters and the technical equipment of *Polarstern* allowed their maintenance under these conditions. To guarantee good water quality, the aquarium water was exchanged twice per week with pre-cooled, sterilized sea water and water quality was monitored continuously.

A list of the fish caught is shown in Tab. 16.1 at the end of this chapter.

Data management

Results of respective experiments will be published in scientific literature as well as in the database PANGAE for public access.

References

David C, Lange B, Krumpen T, Schaafsma F, van Franeker JA, Flores H (2016) Under-ice distribution of polar cod *Boreogadus saida* in the central Arctic Ocean and their association with sea-ice habitat properties. Polar Biol, 39(6):981-994.

Kunz K, Frickenhaus S, Hardenberg S, Johansen T, Leo E, Pörtner H O, Schmidt M, Windisch H S, Knust R and Mark FC (2016) New encounters in Arctic waters: a comparison of metabolism and performance of polar cod (*Boreogadus saida*) and Atlantic cod (*Gadus morhua*) under ocean acidification and warming, Polar Biology, 39 (6), pp. 1137-1153.

Leo E, Kunz KL, Schmidt M, Storch D, Pörtner H-O, Mark FC (2017) Mitochondrial acclimation potential to ocean acidification and warming of Polar cod (*Boreogadus saida*) and Atlantic cod (*Gadus morhua*). Frontiers in Zoology, 14(1):21.

Tab. 16.1: Caught fish by station

Species name/Station	46_03	49_01	49_02	63_01	66_04	67_05	70_01	87_01	88_01	89_01	90_01	91_01	92_01	93_01
Gear	BT	BT	BT			SUIT		BT	BT	BT	BT	BT	BT	BT
Agonus decagonus		8	4					7	27	1				
Artediellus europeus		3	7					1	19	12				11
Bathyraja spinicauda	2							5	1	1				
Boreogadus saida				1	1	4	1	1	14	83	89	57	37	40
Careproctus reinhardti		3	1						8	2				3
Clupea harengus													1	
Cuttunculus microps									1					
Eumicrotremus derjugini										1				
Eumicrotremus spinosus										3				
Gadus morhua			1											
Helicolenus dactylopterus	2	6	3											
Hippoglossoides platessoides	5	6	1					7	20	1				
Icelus bicornis										2				
Liparis haefaedis									6					
Liparis kaefoedi								4		9	7	1	1	5
Liparis liparis								10	14	6	4	4	1	9
Lumpenus lampretaefromis		1						1	2	1	1			
Lycodes rossi									12	5		4		3
Mallotus villosus										1	3	1	2	
Pollachius virens		9												
Reinhardtitus hippoglossoides		71	6					2	11					
Sebastes mentella								1	11					
Triclops myrrayi														3
Triclops nybelini	5	61	56					18	92	9				13
Total	**14**	**168**	**79**			**4**		**57**	**238**	**139**	**104**	**67**	**42**	**87**

17. ACKNOWLEDGEMENTS

We kindly acknowledge the logistical support of Captain Thomas Wunderlich and the entire crew of *Polarstern* as well as the logistical and scientific cooperation with AWI, Laeisz and DWD. We gratefully acknowledge the support from the Transregional Collaborative Research Center (TR 172) “ArctiC Amplification: Climate Relevant Atmospheric and SurfaCe Processes, and Feedback Mechanisms (AC)3”, which is funded by the German Research Foundation (DFG, Deutsche Forschungsgemeinschaft). Many thanks to Katja Schmieder from TROPOS for substantial help in type-setting and lay-out of the cruise report.

A.1 TEILNEHMENDEINSTITUTE/PARTICIPATINGINSTITUTIONS

	Address
ABWR	AquaBiota Water Research Löjtnantsgatan 25 SE-11550 Stockholm Sweden
AWI	Alfred-Wegener-Institut Helmholtz-Zentrumfür Polar- und Meeresforschung Postfach 120161 27515 Bremerhaven Germany
CAU	Christian-Albrechts-Universität zu Kiel Christian-Albrechts-Platz 4 D-24098 Kiel Germany
DLR	Deutsches Zentrum für Luft- und Raumfahrt e.V. (DLR) Institut für Methodik der Fernerkundung Experimentelle Verfahren Oberpfaffenhofen 82234 Weßling Germany
DWD	Deutscher Wetterdienst Geschäftsbereich Wettervorhersage Seeschifffahrtsberatung Bernhard Nocht Str. 76 20359 Hamburg Germany
DZMB	German Centre for Marine Biodiversity Research (DZMB) c/o CeNak, Zoological Museum Martin-Luther-King-Platz 3 20146 Hamburg Germany
FMI	Finnish Meteorological Institute P.O. BOX 503 FI-00101 HELSINKI FINLAND
FUB	Freie Universität Berlin Department of Earth Sciences Institute for Space Sciences Carl-Heinrich-Becker-Weg 6-10 12165 Berlin Germany

	Address
HZG	Helmholtz-Zentrum Geesthacht Zentrum für Material- und Küstenforschung Institute of Coastal Research Max-Planck-Straße 1 21502 Geesthacht Germany
LIM	University of Leipzig Faculty of Physics and Earth Sciences Leipzig Institute for Meteorology Stephanstr. 3 04103 Leipzig Germany
NIOZ	Netherlands Institute for Sea Research Landsdiep 4 1797 SZ ‘t Horntje (Texel) The Netherlands
Polar Scientific	Polar Scientific Ltd Dallens, Appin Argyll PA38 4BN Great Britain
SZ	Sächsische Zeitung GmbH Ostra-Allee 20 01067 Dresden Germany
TROPOS	Leibniz Institute for Tropospheric Research Permoserstrasse 15 04318 Leipzig Germany
UGOT	University of Gothenburg, Department of Marine Science P.O. Box 46 405 30 Göteborg Sweden
UHB	University of Bremen Bibliothekstraße 1 28359 Bremen Germany
UHH	University of Hamburg Martin-Luther-King Platz 3 20146 Hamburg Germany

	Address
UiT	University of Tromsø The Arctic University of Norway Hansine Hansens veg 18 N-9019 Tromsø Norway
UNIS	The University Centre in Svalbard Svalbard Science Centre P.O. Box 156 N-9171 Longyearbyen Norway
UTR	Universität Trier Universitätsring 15 54286 Trier Germany
v.D. Met.	Van Dorssen Metaalbewerking bv Schilderend 113 1791 BE Den Burg (Texel) The Netherlands
WMR	Wageningen Marine Research Ankerpark 27 1781 AG Den Helder The Netherlands
ZMT	Leibniz-Zentrum für Marine Tropenforschung (ZMT) GmbH Fahrenheitstr. 6 28359 Bremen Germany

A.2 FAHRTTEILNEHMER / CRUISE PARTICIPANTS

Name/ Last name	Vorname/ First name	Institut/ Institute	Beruf/ Profession	Fachrichtung/ Discipline	Cruise leg
Andrée	Elin	UGOT	Scientist	Physical oceanography	PS106/2
Barrientos	Carola	TROPOS	PhD student	Meteorology	PS106/1
Birnbaum	Gerit	AWI	Scientist	Meteorology	PS106/1&2
Bravo-Rebolledo	Elisa	WMR	Scientist	Biology	PS106/2
Brückner	Marlen	LIM	Scientist	Meteorology	PS106/1
Castellani	Giulia	AWI	Scientist	Bio-physical modelling	PS106/1&2
Conrath	Thomas	TROPOS	Engineer		PS106/1
Coppolaro	Veronica	AWI	PhD student	Sea ice Physics	PS106/2
Damm	Ellen	AWI	Scientist	Biology	PS106/1
Doble	Martin	Polar Scientific	Scientist	Biology	PS106/2
Egerer	Ulrike	TROPOS	PhD student	Meteorology	PS106/1
Ehrlich	Julia	UHH, AWI	PhD student	Biology	PS106/2
Engelmann	Ronny	TROPOS	Scientist	Meteorology	PS106/1
Fey	Bram	NIOZ	Sailor	Biology	PS106/2
Flores	Hauke	AWI, UHH	Chief scientist PS106/2	Biology	PS106/1&2
Fong	Allison	AWI	Scientist	Biology	PS106/1
Fuchs	Niels	AWI	PhD student	Meteorology	PS106/1
Fuchs	Susanne	TROPOS	Technician	Chemistry	PS106/2
Gebhardt	Catalina	AWI	Data manager		PS106/1
Gege	Peter	DLR	Scientist	Physics	PS106/1&2
Gong	Xianda	TROPOS	PhD student	Meteorology	PS106/1&2
Gottschalk	Matthias	LIM	PhD student	Meteorology	PS106/1
Gradinger	Rolf	UiT	Scientist	Biology	PS106/1
Gragalis	Jan	Heli Service	Technician	helicopter	PS106/1&2
Griesche	Hannes	TROPOS	PhD student	Meteorology	PS106/1
Hasset	Brandon	UiT	PhD student	Biology	PS106/2
Heuzé	Céline	UGOT	Scientist	Physical oceanography	PS106/2
Hartmann	Markus	TROPOS	PhD student	Meteorology	PS106/1
Hieronymi	Martin	HZG	Scientist	Remote sensing	PS106/1
Hildebrandt	Nicole	AWI	Scientist	Biology	PS106/2
Jeskulke	Karen	DZMB	Technician	Biology	PS106/1
Jonassen	Marius	UNIS	Scientist	Meteorology	PS106/1

Name/ Last name	Vorname/ First name	Institut/ Institute	Beruf/ Profession	Fachrichtung/ Discipline	Cruise leg
Katlein	Christian	AWI	Scientist	Sea ice Physics	PS106/1&2
Kecorius	Simonas	TROPOS	Scientist	Meteorology	PS106/1&2
Kendzia	Jan	Heli Service	Technician	Helicopter	PS106/1&2
Kleta	Henry	DWD	Engineer	Meteorology	PS106/1
König	Marcel	CAU	PhD student	Remote sensing	PS106/1&2
Kohnemann	Svenja	UTR	PhD student	Meteorology	PS106/1&2
Koschnick	Nils	AWI	Scientist	Biology	PS106/2
Kühn	Susanne	WMR	Scientist	Biology	PS106/2
Küster	Ulrich	FUB	PhD student	Meteorology	PS106/1&2
Kunisch	Erin	UiT	PhD student	Biology	PS106/1&2
Lange	Benjamin	AWI	Scientist	Biology & Sea ice Physics	PS106/2
Lauermann	Felix	LIM	PhD student	Meteorology	PS106/1
Linders	Torsten	UGOT	Scientist	Physical oceanography	PS106/1
Macke	Andreas	TROPOS	Chief scientist PS106/1	Meteorology	PS106/1
Meijboom	André	WMR	Technician	Biology	PS106/2
Miller	Max	DWD	Scientist	Meteorology	PS106/1&2
Nicolaus	Marcel	AWI	Scientist	Sea ice Physics	PS106/1&2
Niessen	Frank	AWI	Scientist	Geo-physics	PS106/1
Niehoff	Barbara	AWI	Scientist	Biology	PS106/2
Nikolopoulos	Anna	ABWR	Scientist	Physical oceanography	PS106/1
Oppelt	Natascha	CAU	Scientist	Remote sensing	PS106/1
Palm	Mathias	Uni-Bremen	Scientist	Physics	PS106/1
Peeken	Ilka	AWI	Scientist	Biology	PS106/1&2
Radenz	Martin	TROPOS	PhD student	Meteorology	PS106/2
Raes	Eric	AWI	PhD student	Biology	PS106/1
Richter	Phillipp	Uni-Bremen	PhD student	Physics	PS106/1&2
Richter	Roland	Heli Service	Pilot		PS106/1&2
Ruhtz	Thomas	FU-Berlin	Scientist	Physics	PS106/1&2
Sahlin	Sara	UGOT	Scientist	Physical oceanography	PS106/2
Schaafsma	Fokje	WMR	PhD student	Biology	PS106/2
Schön	Stephan	SZ	Journalist		PS106/1
Schulz	Hannes	AWI	Scientist	Meteorology	PS106/2
Sommerfeld	Anja	AWI	Scientist	Sea ice Physics	PS106/1

Name/ Last name	Vorname/ First name	Institut/ Institute	Beruf/ Profession	Fachrichtung/ Discipline	Cruise leg
Sonnabend	Hartmut	DWD	Technician	Meteorology	PS106/1&2
Sprong	Pim	AWI	PhD student	Biology	PS106/2
Staufenbiel	Benjamin	AWI	Student	Biology	PS106/2
Stecher	Anique	AWI	Scientist	Biology	PS106/2
Steffen	Jennifer	AWI	Student	Biology	PS106/2
Sulanke	Erik	UHH	Student	Biology	PS106/2
Szodry	Kai	TROPOS	PhD student	Meteorology	PS106/1
Tiemann	Louisa	AWI	PhD student	Sea ice Physics	PS106/2
Tissler	Priit	FMI	Scientist	Meteorology	PS106/1
Uhlir	Carolin	UHH	Student	Biology	PS106/1
van Dorssen	Michiel	v.D. Met.	Technician		PS106/2
Vane	Kim	ZMT	Phd student	Biology	PS106/2
van Pinxteren	Manuela	TROPOS	Scientist	Chemistry	PS106/1
Vaupel	Lars	Heli Service	Pilot		PS106/1&2
Verdugo	Maria Josefa	AWI	PhD student	Biology	PS106/1
Vogl	Teresa	TROPOS	Msc student	Meteorology	PS106/1&2
Weinzierl	Christine	UHB	Engineer	Physics	PS106/2
Welti	André	TROPOS	Scientist	Meteorology	PS106/2
Witthuhn	Jonas	TROPOS	PhD student	Meteorology	PS106/2
Zanatta	Marco	AWI	Scientist	Meteorology	PS106/1
Zeppenfeld	Sebastian	TROPOS	PhD student	Chemistry	PS106/1&2

A.3 SCHIFFSBESATZUNG / SHIP'S CREW PS106/1

No.	Name	Rank
1.	Wunderlich, Thomas Wolf	Master
2.	Lauber, Felix	Chiefmate
3.	Spielke, Steffen	1st Mate
4.	Kentges. Felix	2nd Mate
5.	Peine. Lutz Gerhard	2nd Mate
6.	Westphal. Henning	Chief
7.	Buch, Erik-Torsten	2nd Eng.
8.	Rusch, Torben	2nd Eng.
9.	Schnürch, Helmut	2nd Eng.
10.	Brehme. Andreas	E-Eng.
11.	Hofmann, Walter Jörg	Chief ELO
12.	Feiertag, Thomas	ELO
13.	Ganter, Armin	ELO
14.	Markert, Winfried Gerhard	ELO
15.	Winter, Andreas	ELO
16.	Rudde-Teufel, Claus Frie	Ships doc
17.	Sedlak . Andreas	Bosun
18.	Neisner, Winfried	Carpen.
19.	Clasen , Nils	MP Rat.
20.	Müller, Steffen	MP Rat.
21.	Schröder, Christoph	MP Rat.
22.	Schröder, Norbert	MP Ra t.
23.	Brickmann, Peter	AB
24.	Burzan, Gerd-Ekkeh.	AB
25.	Fölster, Michael	AB
26.	Hartwig-Labahn, Andreas	AB
27.	Beth, Detlef	Storek.
28.	Klein, Gert	MP Rat
29.	Plehn, Markus	MP Rat
30.	Dinse. Horst	MM
31.	Krösche, Eckard	MM
32.	Watzel, Bernhard	MM
33.	Meißner, Jörg	Cook
34.	Möller, Wolfgang Hans He....	Cooksm
35.	Tupy, Maria Gottfried Be.	Cooksm .
36.	Wartenberg, Irina	Chief Stew.
37.	Schwitzky-Schwarz, Carme..	Nurse
38.	Chen, Quan Lun	2nd Stew.
39.	Golla, Gerald	2nd Stew.
40.	Hischke. Peggy	2nd Stew.
41.	Krause, Tomasz	2nd Stew .
42.	Shi, Wubo	2nd Sttw.
43.	Ruan, Hui Guang	Laundrym

SCHIFFSBESATZUNG / SHIP'S CREW PS106/2

No.	Name	Rank
1.	Wunderlich, Thomas Wolf	Master
2.	Lauber, Felix	Chiefmate
3.	Spielke, Steffen	1st Mate
4.	Kentges, Felix	2nd Mate
5.	Peine, Lutz Gerhard	2nd Mate
6.	Westphal, Henning	Chief
7.	Buch, Erik-Torsten	2nd Eng.
8.	Rusch, Torben	2nd Eng.
9.	Schnürch, Helmut	2nd Eng.
10.	Brehme, Andreas	E-Eng.
11.	Christian, Boris	Chief ELO
12.	Feiertag, Thomas	ELO
13.	Frank, Gerhard	ELO
14.	Markert, Winfried	ELO
15.	Winter, Andreas	ELO
16.	Rudde-Teufel, Claus	Ships doc
17.	Sedlak, Andreas	Bosun
18.	Neisner, Winfried	Carpen.
19.	Becker, Holger	MP Rat.
20.	Clasen, Nils	MP Rat.
21.	Müller, Steffen	MP Rat.
22.	Schröder, Christoph	MP Rat.
23.	Schröder, Norbert	MP Rat.
24.	Brickmann, Peter	AB
25.	Burzan, Gerd-Ekkeh.	AB
26.	Fölster. Michael	AB
27.	Hartwig-Labahn, Andreas	AB
28.	Beth, Detlef	Storek.
29.	Klein, Gert	MP Rat
30.	Plehn, Markus	MPRal
31.	Dinse, Horst	MM
32.	Krösche, Eckard	MM
33.	Watzel, Bernhard	MM
34.	Meißner, Jörg	Cook
35.	Möller, Wolfgang .	Cooksm
36.	Tupy, Mario .	Cooksm
37.	Wartenberg, Irina	Chief Stew.
38.	Schwitzky-Schwarz, Carmen	Nurse
39.	Chen, Quan Lun	2nd Stew.
40.	Golla, Gerald	2nd Stew.
41.	Hischke, Peggy	2nd Stew.
42.	Krause, Tomasz	2nd Stew.
43.	Shi, Wubo	2nd Stew.
44.	Ruan, Hui Guang	Laundrym.

A.4 STATIONSLISTE / STATION LIST

Station	Date	Time	Latitude	Longitude	Depth [m]	Gear	Action	Comment
PS106_0_Underway-1	2017-05-24	10:00	53.56683	8.55505	12.9	WST	profile start	
PS106_0_Underway-2	2017-05-24	15:09	54.03406	7.61897	NA	ADCP_150	profile start	
PS106_0_Underway-2	2017-06-22	06:53	78.23437	15.65742	45	ADCP_150	profile end	
PS106_0_Underway-2	2017-06-23	11:32	78.23387	15.65531	46.7	ADCP_150	profile start	
PS106_0_Underway-2	2017-07-19	15:15	71.55055	21.86368	345	ADCP_150	profile end	
PS106_0_Underway-3	2017-05-25	12:00	57.25179	5.24044	55	PCO2_GO	profile start	
PS106_0_Underway-3	2017-06-21	08:00	78.23316	15.65471	46	PCO2_GO	profile end	
PS106_0_Underway-3	2017-06-23	13:30	78.20558	14.55194	190	PCO2_GO	profile start	
PS106_0_Underway-3	2017-07-19	15:00	71.58825	21.88016	351	PCO2_GO	profile end	
PS106_0_Underway-4	2017-05-25	12:00	57.25179	5.24044	55	PCO2_SUB	profile start	
PS106_0_Underway-4	2017-06-21	08:00	78.23316	15.65471	46	PCO2_SUB	profile end	
PS106_0_Underway-4	2017-07-03	14:00	81.96645	32.40074	2815	PCO2_SUB	profile start	
PS106_0_Underway-4	2017-07-19	15:00	71.58825	21.88016	351	PCO2_SUB	profile end	
PS106_0_Underway-5	2017-05-25	12:00	57.25179	5.24044	55	FBOX	profile start	
PS106_0_Underway-5	2017-06-21	08:00	78.23316	15.65471	46	FBOX	profile end	
PS106_0_Underway-5	2017-06-23	13:13	78.22379	14.77615	212	FBOX	profile start	
PS106_0_Underway-5	2017-07-19	15:00	71.58825	21.88016	351	FBOX	profile end	
PS106_0_Underway-6	2017-05-25	12:00	57.25179	5.24044	55	OCEANET	profile start	
PS106_0_Underway-6	2017-06-20	20:30	78.08353	11.18644	238	OCEANET	profile end	
PS106_0_Underway-6	2017-07-19	16:00	71.44511	21.73454	342	OCEANET	profile end	
PS106_0_Underway-7	2017-05-24	18:00	54.48375	7.26146	21.8	UAS	profile start	

Station	Date	Time	Latitude	Longitude	Depth [m]	Gear	Action	Comment
PS106_0_Underway-7	2017-06-20	20:30	78.08353	11.18644	238	UAS	profile end	
PS106_0_Underway-7	2017-06-23	16:15	77.97119	12.57348	161	UAS	profile start	
PS106_0_Underway-7	2017-07-19	16:00	71.44511	21.73454	342	UAS	profile end	
PS106_0_Underway-8	2017-05-27	08:05	64.54076	2.7603	2345	SPR	profile start	
PS106_0_Underway-8	2017-06-20	20:30	78.08353	11.18644	238	SPR	profile end	
PS106_0_Underway-8	2017-06-23	16:15	77.97119	12.57348	161	SPR	profile start	
PS106_0_Underway-8	2017-07-17	09:31	78.47199	25.18652	176	SPR	profile end	
PS106_0_Underway-9	2017-05-24	12:00	53.62295	8.47026	19	RM	profile start	
PS106_0_Underway-9	2017-06-20	20:30	78.08353	11.18644	238	RM	profile end	
PS106_0_Underway-10	2017-05-30	15:04	76.93908	9.22684	NA	TSG_KEEL	profile start	
PS106_0_Underway-10	2017-07-19	15:17	71.54567	21.8579	342	TSG_KEEL	profile end	
PS106_0_Underway-11	2017-05-25	10:00	57.05965	5.40226	46.6	LIDAR	profile start	
PS106_0_Underway-11	2017-06-18	18:00	79.84211	8.56031	512	LIDAR	profile end	
PS106_0_Underway-12	2017-05-25	10:00	57.05965	5.40226	46.6	CRS	profile start	
PS106_0_Underway-12	2017-06-23	16:15	77.97119	12.57348	161	CRS	profile start	
PS106_0_Underway-12	2017-07-19	16:00	71.44511	21.73454	342	CRS	profile end	
PS106_0_Underway-14	2017-05-25	10:00	57.05965	5.40226	46.6	CCNC	profile start	
PS106_0_Underway-14	2017-06-20	20:30	78.08353	11.18644	238	CCNC	profile end	
PS106_0_Underway-14	2017-06-23	16:15	77.97119	12.57348	161	CCNC	profile start	
PS106_0_Underway-14	2017-07-19	16:00	71.44511	21.73454	342	CCNC	profile end	
PS106_0_Underway-15	2017-05-25	10:00	57.05965	5.40226	46.6	DOAS	profile start	
PS106_0_Underway-15	2017-06-20	20:30	78.08353	11.18644	238	DOAS	profile end	

Station	Date	Time	Latitude	Longitude	Depth [m]	Gear	Action	Comment
PS106_0_Underway-15	2017-06-23	16:15	77.97119	12.57348	161	DOAS	profile start	
PS106_0_Underway-15	2017-07-17	09:31	78.47199	25.18652	176	DOAS	profile end	
PS106_0_Underway-17	2017-06-23	16:15	77.97119	12.57348	161	LIDAR	profile start	
PS106_0_Underway-17	2017-07-15	20:00	79.35789	27.11321	286	LIDAR	profile end	
PS106_0_Underway-19	2017-06-21	16:15	78.23403	15.65544	44.9	EK60	profile start	
PS106_0_Underway-19	2017-07-19	14:30	71.66428	21.89666	359	EK60	profile end	
PS106_1-1	2017-05-25	11:16	57.23685	5.24288	51	BOAT	station start	
PS106_1-1	2017-05-25	11:46	57.23097	5.25224	53	BOAT	station end	
PS106_1-2	2017-05-25	11:21	57.2358	5.24374	52	SPR	station start	
PS106_1-2	2017-05-25	11:40	57.2323	5.25152	52	SPR	station end	
PS106_2-1	2017-05-26	11:51	61.10733	3.29765	345	BOAT	station end	
PS106_2-2	2017-05-26	11:25	61.10568	3.29462	350	SPR	station end	
PS106_3-1	2017-05-27	09:00	64.67258	2.72422	2466	BOAT	station start	
PS106_3-1	2017-05-27	09:32	64.68085	2.73056	2453	BOAT	station end	
PS106_3-2	2017-05-27	09:05	64.67287	2.72434	2460	SPR	station start	
PS106_3-2	2017-05-27	09:20	64.67718	2.72785	2458	SPR	station end	
PS106_4-1	2017-05-27	17:35	66.06333	2.46572	NA	SVP	station start	
PS106_5-1	2017-05-27	23:01	66.99175	2.57776	2118	FLOAT	station start	
PS106_6-1	2017-05-28	04:59	68.00005	2.74174	2486	SVP	station start	
PS106_7-1	2017-05-28	11:03	69.00787	3.2083	NA	FLOAT	station start	
PS106_8-1	2017-05-28	16:52	70.00599	3.8304	3272	SVP	station start	
PS106_9-1	2017-05-28	19:58	70.52737	4.16659	3251	HK	station end	
PS106_10-1	2017-05-28	22:58	71.01768	4.49063	3183	FLOAT	station start	
PS106_11-1	2017-05-29	04:34	72.01306	5.1761	2962	SVP	station start	
PS106_12-1	2017-05-29	08:19	72.57938	5.59121	2603	BOAT	station start	
PS106_12-1	2017-05-29	08:58	72.57821	5.59299	NA	BOAT	station end	
PS106_12-2	2017-05-29	08:28	72.57871	5.59471	2324	CTD	station start	
PS106_12-2	2017-05-29	08:57	72.5782	5.59303	NA	CTD	at depth	
PS106_12-2	2017-05-29	09:09	72.57822	5.59294	NA	CTD	station end	
PS106_12-3	2017-05-29	09:15	72.57784	5.59176	NA	SPR	station start	
PS106_12-3	2017-05-29	09:24	72.5764	5.58982	NA	SPR	station end	
PS106_13-1	2017-05-29	15:20	73.00131	5.89197	2580	FLOAT	station start	
PS106_14-1	2017-05-29	20:32	73.89488	6.57931	2745	SVP	station start	
PS106_15-1	2017-05-30	17:11	77.26452	9.54425	2039	CTD	station start	

Station	Date	Time	Latitude	Longitude	Depth [m]	Gear	Action	Comment
PS106_15-1	2017-05-30	17:26	77.26361	9.53903	2041	CTD	at depth	
PS106_15-1	2017-05-30	17:41	77.26256	9.53493	2043	CTD	station end	
PS106_15-2	2017-05-30	18:11	77.2625	9.52909	2045	CTD	station start	
PS106_15-2	2017-05-30	18:38	77.26328	9.53006	2045	CTD	at depth	
PS106_15-2	2017-05-30	19:18	77.26159	9.52748	2046	CTD	station end	
PS106_16-1	2017-05-31	08:03	79.31863	8.4218	190	BOAT	station start	
PS106_16-1	2017-05-31	08:29	79.31581	8.41934	193	BOAT	station end	
PS106_17-1	2017-06-01	11:07	80.44163	7.27141	692	BOAT	station end	
PS106_17-2	2017-06-01	10:10	80.44254	7.30274	696	CTD	station start	
PS106_17-2	2017-06-01	10:35	80.44165	7.28681	693	CTD	at depth	
PS106_17-2	2017-06-01	11:00	80.44212	7.27868	693	CTD	station end	
PS106_18-1	2017-06-02	11:56	81.28851	9.26311	1321	BOAT	station start	
PS106_18-1	2017-06-02	12:30	81.28937	9.28544	1326	BOAT	station end	
PS106_18-2	2017-06-02	12:42	81.28984	9.29716	1329	CTD	station start	
PS106_18-2	2017-06-02	13:16	81.29053	9.31994	1337	CTD	at depth	
PS106_18-2	2017-06-02	13:56	81.29135	9.34656	1349	CTD	station end	
PS106_19-1	2017-06-02	17:02	81.41109	9.78316	1574	BUCKET	station start	
PS106_19-1	2017-06-02	17:04	81.4111	9.7839	1575	BUCKET	station end	
PS106_19-2	2017-06-02	17:06	81.41111	9.78588	1576	BUCKET	station start	
PS106_19-2	2017-06-02	17:08	81.41111	9.78719	1577	BUCKET	station end	
PS106_20-1	2017-06-03	09:30	81.96379	10.24344	979	ICE	station start	
PS106_20-1	2017-06-03	20:03	81.93413	10.29438	985	ICE	station end	
PS106_21-1	2017-06-04	05:00	81.94805	10.37471	998	CTD	station start	
PS106_21-1	2017-06-04	05:27	81.94853	10.38811	1000	CTD	at depth	
PS106_21-1	2017-06-04	05:58	81.94906	10.40385	1001	CTD	station end	
PS106_21-2	2017-06-04	06:07	81.94923	10.40889	1002	ICE	station start	
PS106_21-2	2017-06-04	20:55	81.93915	10.72878	1045	ICE	station end	
PS106_21-3	2017-06-04	08:28	81.95122	10.47567	1013	CTD	station start	
PS106_21-3	2017-06-04	08:39	81.95141	10.48075	1014	CTD	at depth	
PS106_21-3	2017-06-04	09:01	81.95189	10.49027	1015	CTD	station end	
PS106_22-1	2017-06-05	07:25	81.93968	10.92995	1077	ICE	station start	
PS106_22-1	2017-06-05	18:53	81.92851	10.93988	1076	ICE	station end	
PS106_22-2	2017-06-05	07:46	81.93904	10.9349	1077	CTD	station start	
PS106_22-2	2017-06-05	08:31	81.93757	10.94327	1078	CTD	at depth	
PS106_22-2	2017-06-05	09:03	81.9365	10.94742	1078	CTD	station end	
PS106_22-3	2017-06-05	11:11	81.93293	10.95743	1077	GKG	station start	
PS106_22-3	2017-06-05	11:38	81.93248	10.9595	1077	GKG	at depth	
PS106_22-3	2017-06-05	12:05	81.93231	10.96162	1076	GKG	station end	

Station	Date	Time	Latitude	Longitude	Depth [m]	Gear	Action	Comment
PS106_22-4	2017-06-05	19:01	81.92837	10.93805	1076	CTD	station start	
PS106_22-4	2017-06-05	19:29	81.92795	10.93178	1076	CTD	at depth	
PS106_22-4	2017-06-05	19:57	81.92762	10.92507	1077	CTD	station end	
PS106_23-1	2017-06-06	05:03	81.94669	10.90424	1071	CTD	station start	
PS106_23-1	2017-06-06	05:34	81.94737	10.90211	1071	CTD	at depth	
PS106_23-1	2017-06-06	06:07	81.94782	10.89936	1071	CTD	station end	
PS106_23-2	2017-06-06	06:14	81.94782	10.89911	1071	ICE	station start	
PS106_23-2	2017-06-06	15:00	81.95291	10.73329	1034	ICE	station end	
PS106_23-3	2017-06-06	07:37	81.94841	10.88865	1071	CTD	station start	
PS106_23-3	2017-06-06	07:51	81.94847	10.88632	1070	CTD	at depth	
PS106_23-3	2017-06-06	08:13	81.94852	10.88185	1070	CTD	station end	
PS106_23-4	2017-06-06	18:05	81.95278	10.62441	1023	CTD	station start	
PS106_23-4	2017-06-06	18:30	81.95248	10.61002	1020	CTD	at depth	
PS106_23-4	2017-06-06	18:56	81.95212	10.59566	1019	CTD	station end	
PS106_24-1	2017-06-07	05:07	81.94588	10.34617	993	CTD	station start	
PS106_24-1	2017-06-07	05:34	81.94493	10.33557	992	CTD	at depth	
PS106_24-1	2017-06-07	06:05	81.94374	10.32246	990	CTD	station end	
PS106_24-2	2017-06-07	06:40	81.94226	10.30757	988	ICE	station start	
PS106_24-2	2017-06-07	17:59	81.91499	9.94097	938	ICE	station end	
PS106_24-3	2017-06-07	07:20	81.94025	10.28852	985	BOAT	station start	
PS106_24-3	2017-06-07	08:10	81.93771	10.26177	981	BOAT	station end	
PS106_24-4	2017-06-07	07:30	81.93975	10.28334	985	CTD	station start	
PS106_24-4	2017-06-07	07:44	81.93905	10.27616	984	CTD	at depth	
PS106_24-4	2017-06-07	08:05	81.93794	10.2643	982	CTD	station end	
PS106_24-5	2017-06-07	11:06	81.92927	10.1617	959	EBS	station start	
PS106_24-5	2017-06-07	11:58	81.92703	10.13311	955	EBS	at depth	
PS106_24-5	2017-06-07	15:00	81.9202	10.03034	944	EBS	station end	
PS106_24-6	2017-06-07	15:26	81.91942	10.01652	942	LISST	station start	
PS106_24-6	2017-06-07	15:41	81.91888	10.00807	941	LISST	at depth	
PS106_24-6	2017-06-07	15:51	81.91855	10.0032	941	LISST	station end	
PS106_24-7	2017-06-07	18:01	81.91493	9.94011	938	CTD	station start	
PS106_24-7	2017-06-07	18:25	81.91426	9.92885	938	CTD	at depth	
PS106_24-7	2017-06-07	18:48	81.91359	9.91888	937	CTD	station end	
PS106_25-1	2017-06-08	06:10	81.90984	9.87093	931	ICE	station start	
PS106_25-1	2017-06-08	17:45	81.8964	9.85462	931	ICE	station end	
PS106_25-2	2017-06-08	11:35	81.90099	9.85732	931	BOAT	station start	
PS106_25-2	2017-06-08	12:36	81.89945	9.85721	930	BOAT	station end	
PS106_25-3	2017-06-08	16:46	81.89641	9.85482	931	MN_M7	station start	

Station	Date	Time	Latitude	Longitude	Depth [m]	Gear	Action	Comment
PS106_25-3	2017-06-08	17:12	81.89638	9.85461	931	MN_M7	at depth	
PS106_25-3	2017-06-08	17:41	81.89641	9.85464	931	MN_M7	station end	
PS106_25-4	2017-06-08	18:18	81.8964	9.85396	931	CTD	station start	
PS106_25-4	2017-06-08	18:47	81.89638	9.85366	931	CTD	at depth	
PS106_25-4	2017-06-08	19:24	81.89641	9.85382	931	CTD	station end	
PS106_25-5	2017-06-08	19:54	81.89648	9.85413	931	GKG	station start	
PS106_25-5	2017-06-08	20:19	81.89659	9.85533	931	GKG	at depth	
PS106_25-5	2017-06-08	20:42	81.89676	9.8566	932	GKG	station end	
PS106_26-1	2017-06-09	05:20	81.90834	9.99425	946	CTD	station start	
PS106_26-1	2017-06-09	05:50	81.90862	9.99946	946	CTD	at depth	
PS106_26-1	2017-06-09	06:36	81.90878	10.00587	947	CTD	station end	
PS106_26-2	2017-06-09	06:37	81.90876	10.00602	947	ICE	station start	
PS106_26-2	2017-06-09	16:00	81.90114	10.01281	942	ICE	station end	
PS106_26-3	2017-06-09	07:55	81.90847	10.01203	949	BOAT	station start	
PS106_26-3	2017-06-09	08:35	81.90794	10.01342	951	BOAT	station end	
PS106_27-1	2017-06-10	06:45	81.90416	10.23033	983	ICE	station start	
PS106_27-1	2017-06-10	19:21	81.87117	10.472	1066	ICE	station end	
PS106_27-2	2017-06-10	07:49	81.90216	10.25018	986	CTD	station start	
PS106_27-3	2017-06-10	11:09	81.89249	10.2997	990	MN_M7	station start	
PS106_27-3	2017-06-10	11:43	81.89051	10.30707	986	MN_M7	at depth	
PS106_27-3	2017-06-10	12:24	81.88807	10.31678	984	MN_M7	station end	
PS106_27-4	2017-06-10	14:52	81.88015	10.3592	1006	MN_M7	station start	
PS106_27-4	2017-06-10	15:25	81.87876	10.37101	1027	MN_M7	at depth	
PS106_27-4	2017-06-10	16:07	81.87721	10.38923	1039	MN_M7	station end	
PS106_27-5	2017-06-10	17:03	81.87537	10.41409	1060	MN_M7	station start	
PS106_27-5	2017-06-10	17:41	81.87425	10.43024	1058	MN_M7	at depth	
PS106_27-5	2017-06-10	18:26	81.87289	10.44868	1060	MN_M7	station end	
PS106_27-6	2017-06-10	18:42	81.87236	10.45575	1061	CTD	station start	
PS106_27-6	2017-06-10	19:21	81.87118	10.47182	1066	CTD	at depth	
PS106_27-6	2017-06-10	20:18	81.86946	10.49602	1074	CTD	station end	
PS106_28-1	2017-06-10	22:01	81.86683	10.5477	1095	MN_M7	station start	
PS106_28-1	2017-06-10	22:35	81.86624	10.56878	1102	MN_M7	at depth	
PS106_28-1	2017-06-10	23:20	81.86572	10.59995	1110	MN_M7	station end	
PS106_28-2	2017-06-11	17:40	81.82196	11.25228	1371	ICE	station end	
PS106_28-3	2017-06-11	10:30	81.84175	11.10342	1186	MN_M7	station start	
PS106_28-3	2017-06-11	10:50	81.8405	11.10976	1195	MN_M7	at depth	
PS106_28-3	2017-06-11	11:21	81.83871	11.1195	1201	MN_M7	station end	
PS106_28-4	2017-06-11	12:06	81.83617	11.13565	1221	BUCKET	station start	

Station	Date	Time	Latitude	Longitude	Depth [m]	Gear	Action	Comment
PS106_28-4	2017-06-11	13:00	81.83326	11.15712	1252	BUCKET	station end	
PS106_28-5	2017-06-11	18:03	81.82134	11.25605	1376	CTD	station start	
PS106_28-5	2017-06-11	18:44	81.82059	11.26136	1381	CTD	at depth	
PS106_28-5	2017-06-11	19:35	81.82013	11.26789	1389	CTD	station end	
PS106_29-1	2017-06-12	05:11	81.82875	11.51749	1522	CTD	station start	
PS106_29-1	2017-06-12	05:39	81.82894	11.52776	1524	CTD	at depth	
PS106_29-1	2017-06-12	06:21	81.82914	11.54043	1532	CTD	station end	
PS106_29-2	2017-06-12	06:31	81.82914	11.54267	1534	ICE	station start	
PS106_29-2	2017-06-12	17:45	81.81499	11.53684	1568	ICE	station end	
PS106_29-3	2017-06-12	11:12	81.82508	11.57114	1549	GKG	station start	
PS106_29-3	2017-06-12	11:50	81.82409	11.5711	1551	GKG	at depth	
PS106_29-3	2017-06-12	12:29	81.82294	11.57119	1555	GKG	station end	
PS106_29-4	2017-06-12	12:39	81.82261	11.57109	1557	BC	station start	
PS106_29-4	2017-06-12	13:56	81.82049	11.56623	1564	BC	at depth	
PS106_29-4	2017-06-12	14:54	81.8187	11.56193	1565	BC	station end	
PS106_29-5	2017-06-12	14:33	81.81937	11.56376	1565	BC	station end	
PS106_29-6	2017-06-12	15:02	81.81848	11.56108	1566	LISST	station start	
PS106_29-6	2017-06-12	15:16	81.81809	11.55953	1566	LISST	station end	
PS106_29-6	2017-06-12	15:27	81.81776	11.55818	1567	LISST	station start	
PS106_29-6	2017-06-12	16:03	81.81687	11.55325	1568	LISST	at depth	
PS106_29-6	2017-06-12	16:11	81.81668	11.55205	1568	LISST	profile end	
PS106_29-6	2017-06-12	16:15	81.81664	11.55175	1568	LISST	station end	
PS106_29-7	2017-06-12	16:35	81.81618	11.54876	1569	BC	station start	
PS106_29-7	2017-06-12	17:07	81.81554	11.54354	1569	BC	at depth	
PS106_29-7	2017-06-12	17:45	81.81499	11.53686	1568	BC	station end	
PS106_29-8	2017-06-12	18:11	81.81467	11.53137	1566	CTD	station start	
PS106_29-8	2017-06-12	18:55	81.81435	11.52208	1563	CTD	at depth	
PS106_29-8	2017-06-12	19:50	81.81428	11.51112	1561	CTD	station end	
PS106_30-1	2017-06-13	11:03	81.82319	11.54499	1547	GKG	station start	
PS106_30-1	2017-06-13	11:38	81.82202	11.53837	1547	GKG	at depth	
PS106_30-1	2017-06-13	12:14	81.82068	11.53106	1546	GKG	station end	
PS106_30-2	2017-06-13	14:15	81.81556	11.50661	1560	CTD	station start	
PS106_30-2	2017-06-13	14:59	81.81368	11.4969	1556	CTD	at depth	
PS106_30-2	2017-06-13	15:53	81.81152	11.48432	1550	CTD	station end	
PS106_30-3	2017-06-13	16:09	81.81094	11.48007	1548	MN_M7	station start	
PS106_30-3	2017-06-13	16:50	81.80969	11.46782	1543	MN_M7	at depth	
PS106_30-3	2017-06-13	17:38	81.80834	11.45039	1534	MN_M7	station end	
PS106_31-1	2017-06-14	05:06	81.80019	11.28973	1488	CTD	station start	

Station	Date	Time	Latitude	Longitude	Depth [m]	Gear	Action	Comment
PS106_31-1	2017-06-14	05:46	81.799	11.28745	1487	CTD	at depth	
PS106_31-1	2017-06-14	06:43	81.79708	11.28138	1484	CTD	station end	
PS106_31-2	2017-06-14	06:14	81.79807	11.28479	1486	ICE	station start	
PS106_31-2	2017-06-14	17:23	81.75272	11.03079	1480	ICE	station end	
PS106_31-3	2017-06-14	18:06	81.74997	11.00572	1487	CTD	station start	
PS106_31-3	2017-06-14	18:40	81.74803	10.9861	1502	CTD	at depth	
PS106_31-3	2017-06-14	19:28	81.7456	10.9587	1513	CTD	station end	
PS106_32-1	2017-06-15	05:12	81.73194	10.85082	1607	CTD	station start	
PS106_32-1	2017-06-15	05:41	81.73158	10.85339	1607	CTD	at depth	
PS106_32-1	2017-06-15	06:11	81.73127	10.85577	1608	CTD	station end	
PS106_32-2	2017-06-15	06:41	81.731	10.85763	1608	ICE	station start	
PS106_32-2	2017-06-15	18:38	81.70599	10.69068	1470	ICE	station end	
PS106_32-3	2017-06-15	09:10	81.7288	10.85564	1589	GKG	station start	
PS106_32-3	2017-06-15	09:45	81.72804	10.85185	1581	GKG	at depth	
PS106_32-3	2017-06-15	10:21	81.72718	10.84675	1573	GKG	station end	
PS106_32-4	2017-06-15	12:30	81.72226	10.81894	1549	GKG	station start	
PS106_32-4	2017-06-15	13:02	81.72072	10.81125	1543	GKG	at depth	
PS106_32-4	2017-06-15	13:36	81.719	10.80288	1536	GKG	station end	
PS106_32-5	2017-06-15	18:02	81.70668	10.70773	1470	CTD	station start	
PS106_32-5	2017-06-15	18:38	81.706	10.69089	1470	CTD	at depth	
PS106_32-5	2017-06-15	19:24	81.70556	10.66918	1476	CTD	station end	
PS106_32-6	2017-06-15	19:39	81.70548	10.66243	1478	MN_M7	station start	
PS106_32-6	2017-06-15	20:11	81.70538	10.64597	1480	MN_M7	at depth	
PS106_32-6	2017-06-15	20:55	81.7055	10.62367	1476	MN_M7	station end	
PS106_33-1	2017-06-16	05:12	81.70719	10.50888	1409	CTD	station start	
PS106_33-1	2017-06-16	05:40	81.70701	10.50678	1408	CTD	at depth	
PS106_33-1	2017-06-16	06:13	81.70684	10.50369	1407	CTD	station end	
PS106_33-2	2017-06-16	06:37	81.70667	10.50156	1406	ICE	station start	
PS106_33-2	2017-06-16	15:30	81.68505	10.42624	1508	ICE	station end	
PS106_34-1	2017-06-17	12:09	80.99593	10.36577	1475	BOAT	station start	
PS106_34-1	2017-06-17	13:01	80.99351	10.36072	1465	BOAT	station end	
PS106_34-2	2017-06-17	12:29	80.99476	10.36743	1480	CTD	station start	
PS106_34-2	2017-06-17	13:17	80.9931	10.36409	1475	CTD	at depth	
PS106_34-2	2017-06-17	14:04	80.992	10.37238	1509	CTD	station end	
PS106_35-1	2017-06-17	18:36	80.80521	10.92842	1481	CTD	station start	
PS106_35-1	2017-06-17	19:07	80.8057	10.93081	1482	CTD	at depth	
PS106_35-1	2017-06-17	19:45	80.80631	10.93612	1482	CTD	station end	
PS106_36-1	2017-06-18	00:48	80.6027	11.24653	1057	CTD	station start	

Station	Date	Time	Latitude	Longitude	Depth [m]	Gear	Action	Comment
PS106_36-1	2017-06-18	01:15	80.60268	11.25092	1057	CTD	at depth	
PS106_36-1	2017-06-18	01:47	80.60319	11.25825	1059	CTD	station end	
PS106_37-1	2017-06-18	03:55	80.47471	11.41923	714	CTD	station start	
PS106_37-1	2017-06-18	04:14	80.47405	11.42582	709	CTD	at depth	
PS106_37-1	2017-06-18	04:46	80.47248	11.43465	701	CTD	station end	
PS106_38-1	2017-06-18	07:28	80.2908	11.56704	192	CTD	station start	
PS106_38-1	2017-06-18	07:36	80.29035	11.56658	191	CTD	at depth	
PS106_38-1	2017-06-18	07:56	80.28942	11.56264	191	CTD	station end	
PS106_39-1	2017-06-18	10:45	80.15645	10.64237	463	BOAT	station start	
PS106_39-1	2017-06-18	12:02	80.16282	10.65225	454	BOAT	station end	
PS106_39-2	2017-06-18	11:02	80.15773	10.65297	458	CTD	station start	
PS106_39-2	2017-06-18	11:19	80.15937	10.65343	458	CTD	at depth	
PS106_39-2	2017-06-18	11:42	80.16159	10.65037	457	CTD	station end	
PS106_40-1	2017-06-18	14:26	80.09549	9.62324	533	CTD	station start	
PS106_40-1	2017-06-18	14:44	80.09543	9.62174	533	CTD	at depth	
PS106_40-1	2017-06-18	15:12	80.09494	9.62233	533	CTD	station end	
PS106_41-1	2017-06-19	13:18	78.66592	4.59703	2406	BOAT	station start	
PS106_41-1	2017-06-19	14:15	78.6594	4.56161	2408	BOAT	station end	
PS106_42-1	2017-06-20	06:05	78.98985	9.33366	219	OCEANET	station start	
PS106_42-1	2017-06-20	10:00	78.99168	9.33332	219	OCEANET	station end	
PS106_43-1	2017-06-24	09:29	76.17718	19.9105	194	BOAT	station start	
PS106_43-1	2017-06-24	10:20	76.17803	19.90771	194	BOAT	station end	
PS106_43-2	2017-06-24	09:34	76.17758	19.91036	193	CTD	station start	
PS106_43-2	2017-06-24	09:47	76.17824	19.90901	194	CTD	at depth	
PS106_43-2	2017-06-24	09:58	76.17847	19.91022	194	CTD	station end	
PS106_44-1	2017-06-25	10:08	77.89389	30.04517	259	CTD	station start	
PS106_44-1	2017-06-25	10:22	77.89478	30.04322	259	CTD	at depth	
PS106_44-1	2017-06-25	10:35	77.89593	30.04259	259	CTD	station end	
PS106_44-2	2017-06-25	10:26	77.89504	30.04224	259	BOAT	station start	
PS106_44-2	2017-06-25	11:20	77.89956	30.05147	259	BOAT	station end	
PS106_45-1	2017-06-26	01:45	78.10237	30.47172	233	ICE	station start	
PS106_45-1	2017-06-26	01:46	78.1024	30.47184	233	ICE	station end	
PS106_46-1	2017-06-26	10:03	78.55336	33.95977	205	BOAT	station start	
PS106_46-1	2017-06-26	11:00	78.55495	33.96427	203	BOAT	station end	
PS106_46-2	2017-06-26	10:09	78.55359	33.95951	204	CTD	station start	
PS106_46-2	2017-06-26	10:19	78.55378	33.95953	204	CTD	at depth	
PS106_46-2	2017-06-26	10:32	78.55421	33.96214	206	CTD	station end	
PS106_46-3	2017-06-26	13:17	78.55598	33.97991	202	BT	station start	

Station	Date	Time	Latitude	Longitude	Depth [m]	Gear	Action	Comment
PS106_46-3	2017-06-26	13:56	78.52968	33.82532	200	BT	profile start	
PS106_46-3	2017-06-26	14:45	78.50886	33.75634	193	BT	station end	
PS106_47-1	2017-06-26	18:05	78.41096	34.71286	154	MN_M7	station start	
PS106_47-1	2017-06-26	18:13	78.40958	34.71253	156	MN_M7	at depth	
PS106_47-1	2017-06-26	18:28	78.40738	34.70976	162	MN_M7	station end	
PS106_47-2	2017-06-26	18:46	78.40554	34.70663	167	LOKI	station start	
PS106_47-2	2017-06-26	18:53	78.40538	34.70529	167	LOKI	at depth	
PS106_47-2	2017-06-26	19:00	78.4053	34.70422	165	LOKI	station end	
PS106_47-3	2017-06-26	19:10	78.40532	34.70327	165	CTD	station start	
PS106_47-3	2017-06-26	19:22	78.40576	34.70179	163	CTD	at depth	
PS106_47-3	2017-06-26	19:34	78.40584	34.69982	161	CTD	station end	
PS106_47-4	2017-06-26	19:37	78.40581	34.69912	161	XBT	station start	
PS106_47-4	2017-06-26	19:41	78.40572	34.69849	160	XBT	at depth	
PS106_47-4	2017-06-26	19:45	78.40553	34.69828	160	XBT	station end	
PS106_48-1	2017-06-27	12:16	79.81497	34.01404	282	BOAT	station start	
PS106_48-1	2017-06-27	13:10	79.81884	34.04209	276	BOAT	station end	
PS106_48-2	2017-06-27	12:41	79.81547	34.02239	284	CTD	at depth	
PS106_48-2	2017-06-27	12:57	79.81694	34.0326	271	CTD	station end	
PS106_49-1	2017-06-27	13:37	79.84077	34.05081	259	BT	station start	
PS106_49-1	2017-06-27	14:06	79.80871	34.08038	284	BT	profile start	
PS106_49-1	2017-06-27	14:16	79.79844	34.10664	296	BT	profile end	
PS106_49-1	2017-06-27	14:49	79.78402	34.17887	310	BT	station end	
PS106_49-2	2017-06-27	15:56	79.88787	33.86546	236	BT	station start	
PS106_49-2	2017-06-27	16:24	79.85607	33.80668	248	BT	profile start	
PS106_49-2	2017-06-27	16:39	79.84316	33.78531	248	BT	profile end	
PS106_49-2	2017-06-27	17:08	79.82761	33.76637	254	BT	station end	
PS106_49-3	2017-06-27	17:46	79.87988	33.88739	236	MN_M7	station start	
PS106_49-3	2017-06-27	17:56	79.87901	33.88835	236	MN_M7	at depth	
PS106_49-3	2017-06-27	18:12	79.87714	33.88908	234	MN_M7	station end	
PS106_49-4	2017-06-27	18:32	79.88197	33.89738	237	LOKI	at depth	
PS106_49-4	2017-06-27	18:54	79.88	33.89686	238	LOKI	station end	
PS106_49-5	2017-06-27	19:22	79.87511	33.88954	238	BONGO	station start	
PS106_49-5	2017-06-27	19:29	79.86901	33.88062	241	BONGO	at depth	
PS106_49-5	2017-06-27	19:48	79.8582	33.86452	243	BONGO	station end	
PS106_50-1	2017-06-28	22:09	80.50841	30.98369	156	ICE	station start	
PS106_50-1	2017-06-29	05:54	80.55676	31.20774	105	ICE	station end	
PS106_50-2	2017-06-28	22:43	80.51496	30.97224	151	CTD	station start	
PS106_50-2	2017-06-28	22:52	80.51678	30.97018	148	CTD	at depth	

Station	Date	Time	Latitude	Longitude	Depth [m]	Gear	Action	Comment
PS106_50-2	2017-06-28	23:06	80.51977	30.96765	149	CTD	station end	
PS106_50-3	2017-06-29	00:12	80.53501	30.97066	153	LOKI	station start	
PS106_50-3	2017-06-29	00:20	80.53698	30.97305	153	LOKI	at depth	
PS106_50-3	2017-06-29	00:29	80.53894	30.97593	153	LOKI	station end	
PS106_50-4	2017-06-29	00:40	80.54158	30.98072	164	MN_M7	station start	
PS106_50-4	2017-06-29	00:50	80.54368	30.98522	166	MN_M7	at depth	
PS106_50-4	2017-06-29	00:59	80.54569	30.99017	160	MN_M7	station end	
PS106_50-5	2017-06-29	07:12	80.54684	31.2413	102	SUIT	station start	
PS106_50-5	2017-06-29	08:10	80.54814	31.33898	93	SUIT	station end	
PS106_51-1	2017-06-29	10:44	80.65874	31.70176	150	BOAT	station start	
PS106_51-1	2017-06-29	11:15	80.66189	31.68944	148	BOAT	station end	
PS106_52-1	2017-06-29	14:33	80.83113	31.95887	139	RMT	station start	
PS106_52-1	2017-06-29	14:41	80.82638	31.95397	135	RMT	profile start	
PS106_52-1	2017-06-29	14:58	80.81857	31.95466	132	RMT	profile end	
PS106_52-1	2017-06-29	15:01	80.81805	31.95638	132	RMT	station end	
PS106_53-1	2017-06-30	05:16	81.57168	33.42422	286	CTD	station start	
PS106_53-1	2017-06-30	05:30	81.57035	33.42452	279	CTD	at depth	
PS106_53-1	2017-06-30	05:52	81.5682	33.42353	270	CTD	station end	
PS106_54-1	2017-06-30	07:30	81.61977	33.33849	553	XBT	station start	
PS106_54-1	2017-06-30	07:30	81.61977	33.33846	534	XBT	profile start	
PS106_54-1	2017-06-30	07:35	81.61985	33.33513	448	XBT	profile end	
PS106_54-1	2017-06-30	07:35	81.61986	33.33501	473	XBT	station end	
PS106_55-1	2017-06-30	09:17	81.66839	33.24759	846	XBT	station start	
PS106_55-1	2017-06-30	09:17	81.6684	33.24759	846	XBT	profile start	
PS106_55-1	2017-06-30	09:21	81.66861	33.24731	846	XBT	profile end	
PS106_55-1	2017-06-30	09:21	81.66862	33.24731	846	XBT	station end	
PS106_56-1	2017-06-30	10:43	81.69336	32.9153	1623	CTD	station start	
PS106_56-1	2017-06-30	11:17	81.69329	32.91279	1628	CTD	at depth	
PS106_56-1	2017-06-30	12:00	81.69454	32.91707	1652	CTD	station end	
PS106_56-2	2017-06-30	11:20	81.69329	32.91298	1633	BOAT	station start	
PS106_56-2	2017-06-30	12:06	81.69469	32.91768	1651	BOAT	station end	
PS106_56-3	2017-06-30	12:13	81.69495	32.91869	1654	TPOP	station start	
PS106_57-1	2017-06-30	15:42	81.74981	32.93792	1986	CTD	station start	
PS106_57-1	2017-06-30	16:25	81.74802	32.93992	1996	CTD	at depth	
PS106_57-1	2017-06-30	17:12	81.74515	32.941	2041	CTD	station end	
PS106_58-1	2017-06-30	20:12	81.69534	32.63097	1662	CTD	station start	
PS106_58-1	2017-06-30	20:48	81.6926	32.63154	1631	CTD	at depth	
PS106_58-1	2017-06-30	21:23	81.69048	32.63105	1606	CTD	station end	

Station	Date	Time	Latitude	Longitude	Depth [m]	Gear	Action	Comment
PS106_59-1	2017-06-30	22:18	81.67636	32.68413	1357	CTD	station start	
PS106_59-1	2017-06-30	22:49	81.67614	32.68706	1356	CTD	at depth	
PS106_59-1	2017-06-30	23:18	81.67652	32.69033	1365	CTD	station end	
PS106_60-1	2017-07-01	00:28	81.65003	32.79749	1064	CTD	station start	
PS106_60-1	2017-07-01	00:55	81.65041	32.80231	1057	CTD	at depth	
PS106_60-1	2017-07-01	01:25	81.65059	32.80945	1050	CTD	station end	
PS106_60-2	2017-07-01	01:26	81.65059	32.8095	1049	TPOP	station start	
PS106_61-2	2017-07-01	04:10	81.62815	32.98609	813	XBT	station start	
PS106_61-3	2017-07-01	04:15	81.62874	32.98776	813	XBT	station start	
PS106_62-1	2017-07-01	07:12	81.51846	32.97615	436	XBT	station start	
PS106_62-1	2017-07-01	07:12	81.51843	32.97612	436	XBT	profile start	
PS106_62-1	2017-07-01	07:16	81.51821	32.97577	433	XBT	profile end	
PS106_62-1	2017-07-01	07:16	81.51817	32.9757	433	XBT	station end	
PS106_62-2	2017-07-01	07:41	81.51667	32.97476	421	MN_M7	station start	
PS106_62-2	2017-07-01	07:56	81.51575	32.9746	414	MN_M7	at depth	
PS106_62-2	2017-07-01	08:17	81.51449	32.97299	409	MN_M7	station end	
PS106_62-3	2017-07-01	08:25	81.51411	32.97158	408	MN_M7	station start	
PS106_62-3	2017-07-01	08:38	81.51338	32.96915	407	MN_M7	at depth	
PS106_62-3	2017-07-01	08:59	81.51189	32.97022	404	MN_M7	station end	
PS106_62-4	2017-07-01	09:19	81.51156	32.96156	409	LOKI	station start	
PS106_62-4	2017-07-01	09:36	81.51065	32.96206	408	LOKI	at depth	
PS106_62-4	2017-07-01	09:54	81.51007	32.95842	406	LOKI	station end	
PS106_63-1	2017-07-01	12:23	81.45766	32.8147	223	SUIT	station start	
PS106_63-1	2017-07-01	12:32	81.46119	32.82294	NA	SUIT	profile start	
PS106_63-1	2017-07-01	12:52	81.46638	32.88299	240	SUIT	profile end	
PS106_63-1	2017-07-01	13:05	81.46562	32.90044	233	SUIT	station end	
PS106_64-1	2017-07-01	14:45	81.4117	32.61955	197	XBT	station start	
PS106_64-1	2017-07-01	14:46	81.41173	32.61917	198	XBT	at depth	
PS106_64-2	2017-07-01	14:53	81.41144	32.6221	197	RMT	station start	
PS106_64-2	2017-07-01	14:58	81.41416	32.6122	204	RMT	profile start	
PS106_64-2	2017-07-01	15:15	81.41876	32.58386	207	RMT	station end	
PS106_64-3	2017-07-01	15:53	81.4154	32.61456	199	BOAT	station start	
PS106_64-3	2017-07-01	16:32	81.41353	32.62058	201	BOAT	station end	
PS106_65-1	2017-07-02	01:19	81.62421	33.35176	612	CTD	station start	
PS106_65-1	2017-07-02	01:41	81.62379	33.36084	608	CTD	at depth	
PS106_65-1	2017-07-02	01:59	81.62343	33.36848	605	CTD	station end	
PS106_65-2	2017-07-02	02:20	81.62295	33.3779	601	LOKI	station start	
PS106_65-2	2017-07-02	02:42	81.62236	33.38778	596	LOKI	at depth	

Station	Date	Time	Latitude	Longitude	Depth [m]	Gear	Action	Comment
PS106_65-2	2017-07-02	03:07	81.62157	33.39896	589	LOKI	station end	
PS106_65-3	2017-07-02	04:33	81.59458	33.24857	532	RMT	station start	
PS106_65-3	2017-07-02	04:42	81.59516	33.20828	552	RMT	at depth	
PS106_65-3	2017-07-02	04:43	81.59516	33.20702	553	RMT	profile start	
PS106_65-3	2017-07-02	04:58	81.59509	33.13851	609	RMT	profile end	
PS106_65-3	2017-07-02	05:04	81.59501	33.12638	618	RMT	station end	
PS106_65-4	2017-07-02	06:25	81.58989	33.23903	519	SUIT	station start	
PS106_65-4	2017-07-02	06:35	81.58647	33.27612	490	SUIT	profile start	
PS106_65-4	2017-07-02	06:58	81.5723	33.35324	338	SUIT	profile end	
PS106_65-4	2017-07-02	07:12	81.56574	33.35135	306	SUIT	station end	
PS106_66-1	2017-07-02	12:21	81.66414	32.22943	1779	BOAT	station start	
PS106_66-1	2017-07-02	13:07	81.66455	32.24451	1792	BOAT	station end	
PS106_66-2	2017-07-02	12:59	81.66431	32.23697	1785	CTD	station start	
PS106_66-2	2017-07-02	13:10	81.66459	32.2475	1787	CTD	at depth	
PS106_66-2	2017-07-02	13:21	81.66472	32.25699	1765	CTD	station end	
PS106_66-3	2017-07-02	14:15	81.6659	32.28122	1727	SUIT	station start	
PS106_66-3	2017-07-02	14:48	81.66127	32.3096	1633	SUIT	station end	
PS106_66-4	2017-07-02	15:44	81.66362	32.32066	1591	SUIT	station start	
PS106_66-4	2017-07-02	15:52	81.66156	32.29811	NA	SUIT	profile start	
PS106_66-4	2017-07-02	15:58	81.65955	32.2763	1712	SUIT	at depth	
PS106_66-4	2017-07-02	16:05	81.65964	32.24422	1748	SUIT	profile end	
PS106_66-4	2017-07-02	16:32	81.65914	32.2419	1746	SUIT	station end	
PS106_66-5	2017-07-02	18:00	81.65542	32.34167	1506	ICE	station start	
PS106_66-5	2017-07-03	03:29	81.65046	32.4558	1484	ICE	station end	
PS106_66-6	2017-07-02	21:11	81.6489	32.37207	1334	LOKI	station start	
PS106_66-6	2017-07-02	21:49	81.64829	32.37699	1346	LOKI	at depth	
PS106_66-6	2017-07-02	22:28	81.64797	32.38246	1358	LOKI	station end	
PS106_66-7	2017-07-02	22:49	81.64792	32.38546	1377	MN_M7	station start	
PS106_66-7	2017-07-02	23:26	81.64801	32.39251	1400	MN_M7	at depth	
PS106_66-7	2017-07-03	00:11	81.64838	32.40245	1428	MN_M7	station end	
PS106_67-1	2017-07-03	12:08	81.94919	32.31414	2815	RMT	station start	
PS106_67-1	2017-07-03	12:18	81.95435	32.3307	2818	RMT	profile start	
PS106_67-1	2017-07-03	12:34	81.96078	32.36037	2822	RMT	station end	
PS106_67-2	2017-07-03	13:03	81.96128	32.37322	2820	BOAT	station start	
PS106_67-2	2017-07-03	14:16	81.96662	32.40942	2812	BOAT	station end	
PS106_67-3	2017-07-03	13:23	81.96293	32.38208	2817	CTD	station start	
PS106_67-3	2017-07-03	14:20	81.96632	32.4112	2811	CTD	at depth	
PS106_67-3	2017-07-03	15:26	81.96408	32.43023	2805	CTD	station end	

Station	Date	Time	Latitude	Longitude	Depth [m]	Gear	Action	Comment
PS106_67-4	2017-07-03	15:40	81.96368	32.43512	2803	MN_M7	station start	
PS106_67-4	2017-07-03	16:35	81.96061	32.43711	2800	MN_M7	at depth	
PS106_67-4	2017-07-03	17:35	81.95948	32.45358	2795	MN_M7	station end	
PS106_67-5	2017-07-03	18:25	81.95776	32.48194	2786	SUIT	station start	
PS106_67-5	2017-07-03	18:35	81.9602	32.49538	2786	SUIT	at depth	
PS106_67-5	2017-07-03	18:40	81.96323	32.50925	2789	SUIT	profile start	
PS106_67-5	2017-07-03	18:58	81.97299	32.57542	2770	SUIT	profile end	
PS106_67-5	2017-07-03	19:12	81.97722	32.60195	2767	SUIT	station end	
PS106_67-6	2017-07-03	19:55	81.98209	32.64049	2765	LOKI	station start	
PS106_67-6	2017-07-03	20:32	81.98193	32.63551	2765	LOKI	at depth	
PS106_67-6	2017-07-03	21:12	81.98276	32.6368	2767	LOKI	station end	
PS106_68-1	2017-07-04	06:31	82.32897	32.92437	3018	XBT	station start	
PS106_68-1	2017-07-04	06:31	82.329	32.92433	3018	XBT	profile start	
PS106_68-1	2017-07-04	06:34	82.32901	32.92416	3018	XBT	profile end	
PS106_68-2	2017-07-04	06:49	82.33093	32.93191	3018	MN_M7	station start	
PS106_68-2	2017-07-04	07:28	82.33308	32.94863	3016	MN_M7	at depth	
PS106_68-2	2017-07-04	08:12	82.33616	32.96837	3014	MN_M7	station end	
PS106_68-3	2017-07-04	08:15	82.33627	32.96891	3014	HCTD	station start	
PS106_68-3	2017-07-04	08:18	82.33634	32.9692	3014	HCTD	at depth	
PS106_68-3	2017-07-04	08:19	82.33634	32.96921	3014	HCTD	station end	
PS106_68-4	2017-07-04	08:44	82.33756	32.97554	3017	LOKI	station start	
PS106_68-4	2017-07-04	09:23	82.3396	32.98595	3020	LOKI	at depth	
PS106_68-4	2017-07-04	10:03	82.34215	33.00031	3022	LOKI	station end	
PS106_68-5	2017-07-04	10:36	82.3369	33.02589	3009	SUIT	station start	
PS106_68-5	2017-07-04	10:44	82.33952	33.03103	3013	SUIT	profile start	
PS106_68-5	2017-07-04	10:56	82.35123	33.05211	3022	SUIT	profile end	
PS106_68-5	2017-07-04	11:21	82.35485	33.06915	3021	SUIT	station end	
PS106_69-1	2017-07-05	05:11	82.98743	33.17741	3716	MN_M7	station start	
PS106_69-1	2017-07-05	06:10	82.98935	33.17937	3717	MN_M7	at depth	
PS106_69-1	2017-07-05	07:15	82.99058	33.18016	3718	MN_M7	station end	
PS106_69-2	2017-07-05	08:09	82.99359	33.17986	3718	SUIT	station start	
PS106_69-2	2017-07-05	08:30	82.98275	33.22007	3710	SUIT	profile end	
PS106_69-2	2017-07-05	08:55	82.98391	33.22273	3710	SUIT	station end	
PS106_69-3	2017-07-05	09:41	82.99949	33.12643	3728	ICE	station start	
PS106_69-3	2017-07-05	12:10	83.00494	33.20806	3721	ICE	station end	
PS106_69-4	2017-07-05	10:30	83.00029	33.16161	3724	CTD	station start	
PS106_69-4	2017-07-05	11:41	83.0048	33.18723	3723	CTD	at depth	
PS106_69-4	2017-07-05	13:10	83.00744	33.24114	3722	CTD	station end	

Station	Date	Time	Latitude	Longitude	Depth [m]	Gear	Action	Comment
PS106_69-5	2017-07-05	11:35	83.00425	33.18515	3723	BOAT	station start	
PS106_69-5	2017-07-05	11:40	83.00466	33.18645	3723	BOAT	station end	
PS106_69-6	2017-07-05	13:23	83.00788	33.2489	3721	LOKI	station start	
PS106_69-6	2017-07-05	14:02	83.00892	33.26964	3722	LOKI	at depth	
PS106_69-6	2017-07-05	14:42	83.00996	33.28845	3721	LOKI	station end	
PS106_70-1	2017-07-05	17:18	83.1104	32.80092	3808	SUIT	station start	
PS106_70-1	2017-07-05	17:26	83.11215	32.8157	3810	SUIT	profile start	
PS106_70-1	2017-07-05	17:53	83.12253	32.97266	3805	SUIT	profile end	
PS106_70-1	2017-07-05	18:12	83.1227	32.99039	3802	SUIT	station end	
PS106_70-2	2017-07-05	18:45	83.11966	32.90084	3816	LOKI	station start	
PS106_70-2	2017-07-05	19:24	83.1206	32.89173	3816	LOKI	at depth	
PS106_70-2	2017-07-05	20:05	83.11991	32.89839	3816	LOKI	station end	
PS106_70-3	2017-07-05	19:40	83.12063	32.89037	3816	HCTD	station end	
PS106_70-4	2017-07-05	20:49	83.12072	32.96476	3806	RMT	station start	
PS106_70-4	2017-07-05	20:57	83.11943	32.92617	3813	RMT	at depth	
PS106_70-4	2017-07-05	20:58	83.11927	32.92424	3813	RMT	profile start	
PS106_70-4	2017-07-05	21:06	83.11595	32.89319	3810	RMT	profile end	
PS106_70-4	2017-07-05	21:14	83.11386	32.87319	3809	RMT	station end	
PS106_71-1	2017-07-06	00:43	83.33115	33.07889	3899	CTD	station start	
PS106_71-1	2017-07-06	01:09	83.33109	33.08643	3899	CTD	at depth	
PS106_71-1	2017-07-06	01:39	83.33028	33.10022	3898	CTD	station end	
PS106_71-2	2017-07-06	01:50	83.32881	33.11692	3897	MN_M7	station start	
PS106_71-2	2017-07-06	02:29	83.32774	33.14514	3896	MN_M7	at depth	
PS106_71-2	2017-07-06	03:17	83.3266	33.17793	3895	MN_M7	station end	
PS106_71-3	2017-07-06	03:43	83.32838	33.1781	3896	LOKI	station start	
PS106_71-3	2017-07-06	04:22	83.32833	33.19204	3896	LOKI	at depth	
PS106_71-3	2017-07-06	05:02	83.32812	33.20936	3897	LOKI	station end	
PS106_71-4	2017-07-06	05:23	83.33891	33.25254	3907	RMT	station start	
PS106_71-4	2017-07-06	05:32	83.334	33.23778	3903	RMT	at depth	
PS106_71-4	2017-07-06	05:51	83.32473	33.21685	3895	RMT	station end	
PS106_71-5	2017-07-06	06:41	83.30934	33.20761	3885	SUIT	station start	
PS106_71-5	2017-07-06	06:47	83.31079	33.21267	3886	SUIT	profile start	
PS106_71-5	2017-07-06	07:33	83.33994	33.36063	3910	SUIT	station end	
PS106_72-1	2017-07-06	12:31	83.50209	33.02191	3984	RMT	station start	
PS106_72-1	2017-07-06	12:39	83.50125	32.98117	3983	RMT	at depth	
PS106_72-1	2017-07-06	12:52	83.50325	32.94242	3983	RMT	station end	
PS106_72-2	2017-07-06	13:19	83.50221	32.96177	3983	BOAT	station start	
PS106_72-2	2017-07-06	14:02	83.50107	32.97398	3983	BOAT	station end	

Station	Date	Time	Latitude	Longitude	Depth [m]	Gear	Action	Comment
PS106_72-3	2017-07-06	13:37	83.50174	32.95804	3983	LOKI	station start	
PS106_72-3	2017-07-06	14:16	83.50047	32.98344	3982	LOKI	at depth	
PS106_72-3	2017-07-06	14:55	83.49877	33.00483	3982	LOKI	station end	
PS106_72-4	2017-07-06	14:19	83.50033	32.98519	3982	HCTD	station start	
PS106_72-4	2017-07-06	14:22	83.50021	32.98698	3982	HCTD	at depth	
PS106_72-4	2017-07-06	14:24	83.50015	32.98801	3982	HCTD	station end	
PS106_72-5	2017-07-06	15:27	83.49164	33.11674	3980	SUIT	station start	
PS106_72-5	2017-07-06	15:36	83.493	33.10688	3980	SUIT	profile start	
PS106_72-5	2017-07-06	16:04	83.50834	33.19111	3985	SUIT	profile end	
PS106_72-5	2017-07-06	16:20	83.50762	33.20608	3984	SUIT	station end	
PS106_73-1	2017-07-06	20:46	83.66608	31.55722	4029	CTD	station start	
PS106_73-1	2017-07-06	20:51	83.66634	31.56326	4029	CTD	at depth	
PS106_73-1	2017-07-06	21:01	83.66645	31.56961	4029	CTD	station end	
PS106_73-2	2017-07-06	22:00	83.66128	31.58055	4029	ICE	station start	
PS106_73-2	2017-07-07	07:33	83.66537	31.90567	4023	ICE	station end	
PS106_73-3	2017-07-06	23:15	83.66237	31.61696	4028	MN_M7	station start	
PS106_73-3	2017-07-07	00:10	83.66325	31.65202	4028	MN_M7	at depth	
PS106_73-3	2017-07-07	01:14	83.66401	31.69716	4027	MN_M7	station end	
PS106_73-4	2017-07-07	01:48	83.6643	31.72142	4027	CTD	station start	
PS106_73-4	2017-07-07	03:09	83.6646	31.78117	4025	CTD	at depth	
PS106_73-4	2017-07-07	04:41	83.66446	31.83716	4024	CTD	station end	
PS106_73-5	2017-07-07	05:06	83.66426	31.84992	4024	LOKI	station start	
PS106_73-5	2017-07-07	05:44	83.66418	31.86684	4024	LOKI	at depth	
PS106_73-5	2017-07-07	06:24	83.66449	31.8828	4024	LOKI	station end	
PS106_73-6	2017-07-07	06:31	83.66457	31.88535	4024	LOKI	station start	
PS106_73-6	2017-07-07	06:36	83.66461	31.88719	4023	LOKI	at depth	
PS106_73-6	2017-07-07	06:50	83.66477	31.89177	4023	LOKI	station end	
PS106_73-7	2017-07-07	08:47	83.68356	32.05169	4023	SUIT	station start	
PS106_73-7	2017-07-07	08:54	83.68513	32.05967	4023	SUIT	profile start	
PS106_73-7	2017-07-07	09:30	83.70282	32.2408	4022	SUIT	profile end	
PS106_73-7	2017-07-07	09:48	83.70928	32.29622	4023	SUIT	station end	
PS106_73-8	2017-07-07	10:29	83.71652	32.38325	4022	RMT	station start	
PS106_73-8	2017-07-07	10:38	83.71398	32.33814	4022	RMT	at depth	
PS106_73-8	2017-07-07	10:38	83.71395	32.33749	4022	RMT	profile start	
PS106_73-8	2017-07-07	10:52	83.70998	32.2698	4023	RMT	profile end	
PS106_73-8	2017-07-07	10:58	83.70913	32.25173	4023	RMT	station end	
PS106_74-1	2017-07-08	07:22	83.47335	28.0554	4050	CTD	station start	
PS106_74-1	2017-07-08	08:47	83.47094	28.00963	4050	CTD	at depth	

Station	Date	Time	Latitude	Longitude	Depth [m]	Gear	Action	Comment
PS106_74-1	2017-07-08	10:13	83.46944	27.95631	4050	CTD	station end	
PS106_74-2	2017-07-08	10:27	83.46935	27.94807	4050	LOKI	station start	
PS106_74-2	2017-07-08	11:03	83.46937	27.92799	4050	LOKI	at depth	
PS106_74-2	2017-07-08	11:42	83.46987	27.90966	4050	LOKI	station end	
PS106_74-3	2017-07-08	10:41	83.46931	27.93996	4050	BOAT	station start	
PS106_74-3	2017-07-08	11:20	83.46952	27.9199	4051	BOAT	station end	
PS106_74-4	2017-07-08	12:18	83.46498	28.11783	4049	RMT	station start	
PS106_74-4	2017-07-08	12:26	83.4679	28.08524	4049	RMT	at depth	
PS106_74-4	2017-07-08	12:41	83.47344	28.01732	4050	RMT	station end	
PS106_74-5	2017-07-08	13:14	83.47596	27.90758	4051	SUIT	station start	
PS106_74-5	2017-07-08	13:22	83.47481	27.92935	4051	SUIT	profile start	
PS106_74-5	2017-07-08	13:54	83.4615	28.07559	4049	SUIT	profile end	
PS106_74-5	2017-07-08	14:25	83.45735	28.09616	4048	SUIT	station end	
PS106_75-1	2017-07-09	01:33	82.98909	24.82004	4050	CTD	station start	
PS106_75-1	2017-07-09	02:53	82.98019	24.86994	4049	CTD	at depth	
PS106_75-1	2017-07-09	05:00	82.96278	24.91609	4047	CTD	station end	
PS106_75-2	2017-07-09	05:18	82.96038	24.91673	4046	LOKI	station start	
PS106_75-2	2017-07-09	05:55	82.95577	24.9152	4046	LOKI	at depth	
PS106_75-2	2017-07-09	06:36	82.9514	24.91083	4046	LOKI	station end	
PS106_75-3	2017-07-09	06:46	82.95048	24.90951	4045	MN_M7	station start	
PS106_75-3	2017-07-09	07:42	82.94661	24.90043	4044	MN_M7	at depth	
PS106_75-3	2017-07-09	08:51	82.94443	24.89525	4045	MN_M7	station end	
PS106_75-4	2017-07-09	08:58	82.9443	24.8948	4044	MN_M7	station start	
PS106_75-4	2017-07-09	09:02	82.94423	24.89437	4044	MN_M7	at depth	
PS106_75-4	2017-07-09	09:13	82.94405	24.89413	4044	MN_M7	station end	
PS106_75-5	2017-07-09	09:58	82.96027	25.17511	4045	RMT	station start	
PS106_75-5	2017-07-09	10:07	82.96335	25.13645	4046	RMT	at depth	
PS106_75-5	2017-07-09	10:08	82.96345	25.13508	4046	RMT	profile start	
PS106_75-5	2017-07-09	10:22	82.96711	25.083	4046	RMT	profile end	
PS106_75-5	2017-07-09	10:30	82.9684	25.06625	4047	RMT	station end	
PS106_75-6	2017-07-09	11:05	82.99111	25.27466	4048	SUIT	station start	
PS106_75-6	2017-07-09	11:12	82.99065	25.2685	4047	SUIT	profile start	
PS106_75-6	2017-07-09	11:39	82.97856	25.14304	4047	SUIT	profile end	
PS106_75-6	2017-07-09	12:05	82.9768	25.13298	4047	SUIT	station end	
PS106_75-7	2017-07-09	12:28	82.97645	25.15875	4047	BOAT	station start	
PS106_75-7	2017-07-09	13:01	82.97516	25.20668	4047	BOAT	station end	
PS106_76-1	2017-07-10	05:02	82.49081	18.01732	1905	CTD	station start	
PS106_76-1	2017-07-10	05:41	82.49091	18.01606	1904	CTD	at depth	

Station	Date	Time	Latitude	Longitude	Depth [m]	Gear	Action	Comment
PS106_76-1	2017-07-10	06:12	82.49136	18.02064	1911	CTD	station end	
PS106_76-2	2017-07-10	06:26	82.49042	18.05861	1949	LOKI	station start	
PS106_76-2	2017-07-10	07:03	82.4908	18.05108	1940	LOKI	at depth	
PS106_76-2	2017-07-10	07:44	82.49198	18.0551	1952	LOKI	station end	
PS106_76-3	2017-07-10	08:14	82.48855	18.27031	2460	RMT	station start	
PS106_76-3	2017-07-10	08:24	82.48958	18.22681	2288	RMT	at depth	
PS106_76-3	2017-07-10	08:25	82.48965	18.22414	2278	RMT	profile start	
PS106_76-3	2017-07-10	08:38	82.49179	18.16409	2119	RMT	profile end	
PS106_76-3	2017-07-10	08:42	82.49208	18.15212	2095	RMT	station end	
PS106_76-4	2017-07-10	09:16	82.49033	18.3637	2661	SUIT	station start	
PS106_76-4	2017-07-10	09:23	82.49102	18.37934	2692	SUIT	at depth	
PS106_76-4	2017-07-10	09:24	82.49111	18.38084	2696	SUIT	profile start	
PS106_76-4	2017-07-10	09:52	82.50099	18.53477	3086	SUIT	profile end	
PS106_76-4	2017-07-10	10:07	82.50524	18.58424	3139	SUIT	station end	
PS106_76-5	2017-07-10	10:36	82.50674	18.59732	3136	BOAT	station start	
PS106_76-5	2017-07-10	11:10	82.50489	18.6101	3143	BOAT	station end	
PS106_77-1	2017-07-10	15:18	82.25222	17.84665	2007	XBT	station start	
PS106_77-1	2017-07-10	15:27	82.25209	17.85846	2012	XBT	at depth	
PS106_77-2	2017-07-10	15:46	82.25277	17.85313	2008	SUIT	station start	
PS106_77-2	2017-07-10	15:50	82.25278	17.85956	2010	SUIT	profile start	
PS106_77-2	2017-07-10	16:10	82.24686	17.95284	2074	SUIT	profile end	
PS106_77-2	2017-07-10	16:26	82.24655	17.97086	2086	SUIT	station end	
PS106_77-3	2017-07-10	17:05	82.25152	17.79139	2003	RMT	station start	
PS106_77-3	2017-07-10	17:15	82.2445	17.78211	2025	RMT	at depth	
PS106_77-3	2017-07-10	17:37	82.23311	17.75316	2054	RMT	station end	
PS106_77-4	2017-07-10	17:54	82.23169	17.75364	2056	MN_M7	station start	
PS106_77-4	2017-07-10	17:59	82.23115	17.75052	2058	MN_M7	at depth	
PS106_77-4	2017-07-10	18:10	82.22991	17.74275	2063	MN_M7	station end	
PS106_78-1	2017-07-10	21:17	82.03529	17.39284	2693	CTD	station start	
PS106_78-1	2017-07-10	22:13	82.03547	17.40775	2721	CTD	at depth	
PS106_78-1	2017-07-10	23:17	82.03356	17.40986	2722	CTD	station end	
PS106_78-2	2017-07-10	23:37	82.03357	17.41142	2725	MN_M7	station start	
PS106_78-2	2017-07-11	00:32	82.03398	17.40824	2721	MN_M7	at depth	
PS106_78-2	2017-07-11	01:33	82.03752	17.42861	2742	MN_M7	station end	
PS106_78-3	2017-07-11	01:48	82.03902	17.44064	2759	LOKI	station start	
PS106_78-3	2017-07-11	02:27	82.04269	17.47456	2837	LOKI	at depth	
PS106_78-3	2017-07-11	03:06	82.04751	17.51801	2926	LOKI	station end	
PS106_78-4	2017-07-11	03:24	82.05086	17.67925	3176	RMT	station start	

Station	Date	Time	Latitude	Longitude	Depth [m]	Gear	Action	Comment
PS106_78-4	2017-07-11	03:32	82.05043	17.64366	3156	RMT	at depth	
PS106_78-4	2017-07-11	03:50	82.05338	17.59921	3106	RMT	station end	
PS106_78-5	2017-07-11	06:49	82.05883	17.79218	3169	SUIT	station start	
PS106_78-5	2017-07-11	06:55	82.05645	17.80632	3177	SUIT	profile start	
PS106_78-5	2017-07-11	07:10	82.04577	17.85333	NA	SUIT	profile end	
PS106_78-5	2017-07-11	08:21	82.04428	17.90594	3222	SUIT	station start	
PS106_78-5	2017-07-11	09:07	82.04533	17.91644	3222	SUIT	station end	
PS106_78-6	2017-07-11	09:34	82.0518	17.94035	3216	BOAT	station start	
PS106_78-6	2017-07-11	10:24	82.05145	17.94521	3218	BOAT	station end	
PS106_79-1	2017-07-11	17:11	81.66446	17.02542	2849	SUIT	station start	
PS106_79-1	2017-07-11	17:18	81.66496	17.01506	2845	SUIT	profile start	
PS106_79-1	2017-07-11	17:38	81.66572	16.92066	4283	SUIT	profile end	
PS106_79-1	2017-07-11	17:54	81.66648	16.88684	NA	SUIT	station end	
PS106_79-2	2017-07-11	18:09	81.66618	16.88065	NA	XBT	station start	
PS106_79-2	2017-07-11	18:15	81.66495	16.8845	NA	XBT	at depth	
PS106_79-3	2017-07-11	18:17	81.66462	16.88561	NA	HCTD	station start	
PS106_79-3	2017-07-11	18:19	81.66393	16.88782	NA	HCTD	at depth	
PS106_79-3	2017-07-11	18:22	81.66372	16.88906	NA	HCTD	station end	
PS106_80-1	2017-07-12	00:35	81.32624	16.92755	1102	CTD	station start	
PS106_80-1	2017-07-12	00:44	81.32648	16.93044	1098	CTD	at depth	
PS106_80-1	2017-07-12	00:57	81.32698	16.93405	1094	CTD	station end	
PS106_80-2	2017-07-12	15:16	81.37106	17.12646	1010	ICE	station end	
PS106_80-3	2017-07-12	17:46	81.45011	16.94573	2026	SUIT	station start	
PS106_80-3	2017-07-12	17:54	81.44784	16.9547	1997	SUIT	profile start	
PS106_80-3	2017-07-12	18:16	81.43203	16.97258	2016	SUIT	profile end	
PS106_80-3	2017-07-12	18:33	81.42804	16.97253	2123	SUIT	station end	
PS106_80-4	2017-07-12	19:16	81.43975	17.02899	1818	RMT	station start	
PS106_80-4	2017-07-12	19:25	81.43483	17.03459	1849	RMT	at depth	
PS106_80-4	2017-07-12	19:44	81.42529	17.03984	1873	RMT	station end	
PS106_80-5	2017-07-12	20:02	81.4286	17.03461	1947	MN_M7	station start	
PS106_80-5	2017-07-12	20:56	81.43054	17.03815	1939	MN_M7	at depth	
PS106_80-5	2017-07-12	21:57	81.43566	17.0351	1838	MN_M7	station end	
PS106_80-6	2017-07-12	23:07	81.40524	17.28242	969	CTD	station start	
PS106_80-6	2017-07-12	23:32	81.40659	17.28308	978	CTD	at depth	
PS106_80-6	2017-07-13	00:05	81.40902	17.28537	981	CTD	station end	
PS106_80-7	2017-07-13	00:10	81.40909	17.28942	975	TPOP	station start	
PS106_81-1	2017-07-13	01:19	81.35838	17.6321	799	CTD	station start	
PS106_81-1	2017-07-13	01:39	81.35944	17.64032	801	CTD	at depth	

Station	Date	Time	Latitude	Longitude	Depth [m]	Gear	Action	Comment
PS106_81-1	2017-07-13	01:58	81.36072	17.64764	806	CTD	station end	
PS106_81-2	2017-07-13	02:04	81.36109	17.64914	807	TPOP	station start	
PS106_82-1	2017-07-13	03:40	81.31031	18.23771	583	CTD	station start	
PS106_82-1	2017-07-13	05:27	81.32676	18.29891	608	CTD	at depth	
PS106_82-1	2017-07-13	05:47	81.32769	18.29724	610	CTD	station end	
PS106_83-1	2017-07-13	08:48	81.20542	18.83516	436	CTD	station start	
PS106_83-1	2017-07-13	09:03	81.20546	18.82334	434	CTD	at depth	
PS106_83-1	2017-07-13	09:26	81.20596	18.81065	446	CTD	station end	
PS106_83-3	2017-07-13	09:44	81.21022	18.79034	432	LOKI	station start	
PS106_83-3	2017-07-13	10:00	81.21035	18.78123	432	LOKI	at depth	
PS106_83-3	2017-07-13	10:22	81.21067	18.7653	442	LOKI	station end	
PS106_83-4	2017-07-13	10:47	81.21358	18.74689	438	BOAT	station start	
PS106_83-4	2017-07-13	11:44	81.22092	18.69176	445	BOAT	station end	
PS106_83-5	2017-07-13	10:52	81.2136	18.7438	437	MN_M7	station start	
PS106_83-5	2017-07-13	11:07	81.21417	18.73211	437	MN_M7	at depth	
PS106_83-5	2017-07-13	11:30	81.2166	18.7143	440	MN_M7	station end	
PS106_83-6	2017-07-13	12:15	81.24548	18.60551	472	RMT	at depth	
PS106_83-6	2017-07-13	12:33	81.25513	18.56506	494	RMT	station end	
PS106_83-7	2017-07-13	13:19	81.29326	18.61781	521	SUIT	station start	
PS106_83-7	2017-07-13	13:26	81.29258	18.60932	522	SUIT	at depth	
PS106_83-7	2017-07-13	13:28	81.29122	18.60228	521	SUIT	profile start	
PS106_83-7	2017-07-13	13:43	81.29052	18.57352	526	SUIT	profile end	
PS106_83-7	2017-07-13	13:52	81.29134	18.56922	525	SUIT	station end	
PS106_83-8	2017-07-13	14:29	81.29455	18.57407	530	SUIT	station start	
PS106_83-8	2017-07-13	14:39	81.29205	18.55803	528	SUIT	profile start	
PS106_83-8	2017-07-13	15:00	81.27655	18.50933	541	SUIT	profile end	
PS106_83-8	2017-07-13	15:19	81.27614	18.49233	533	SUIT	station end	
PS106_83-9	2017-07-13	15:56	81.27849	18.49885	518	BONGO	station start	
PS106_83-9	2017-07-13	16:03	81.28176	18.50906	518	BONGO	at depth	
PS106_83-9	2017-07-13	16:17	81.29068	18.50457	527	BONGO	station end	
PS106_84-1	2017-07-14	11:03	81.00845	26.82405	117	BOAT	station start	
PS106_84-1	2017-07-14	11:42	81.01354	26.86652	107	BOAT	station end	
PS106_85-1	2017-07-14	19:31	80.61381	29.47937	285	CTD	station start	
PS106_85-1	2017-07-14	19:46	80.61118	29.48943	288	CTD	at depth	
PS106_85-1	2017-07-14	20:07	80.60779	29.50192	299	CTD	station end	
PS106_86-1	2017-07-15	10:20	79.46081	28.1232	327	BOAT	station start	
PS106_86-1	2017-07-15	11:10	79.45768	28.12065	326	BOAT	station end	
PS106_87-1	2017-07-15	13:20	79.38793	27.19913	280	BT	station start	

Station	Date	Time	Latitude	Longitude	Depth [m]	Gear	Action	Comment
PS106_87-1	2017-07-15	13:52	79.3793	27.42178	289	BT	at depth	
PS106_87-1	2017-07-15	13:52	79.37928	27.4224	289	BT	profile start	
PS106_87-1	2017-07-15	14:07	79.37768	27.49908	300	BT	profile end	
PS106_87-1	2017-07-15	14:39	79.37908	27.57654	313	BT	station end	
PS106_88-1	2017-07-15	16:38	79.32451	27.02413	292	BT	station start	
PS106_88-1	2017-07-15	17:10	79.35513	27.14391	290	BT	profile start	
PS106_88-1	2017-07-15	17:24	79.36984	27.15367	284	BT	profile end	
PS106_88-1	2017-07-15	17:54	79.38581	27.16654	273	BT	station end	
PS106_88-2	2017-07-15	18:10	79.39281	27.1749	275	CTD	station start	
PS106_88-2	2017-07-15	18:22	79.39309	27.17265	275	CTD	at depth	
PS106_88-2	2017-07-15	18:31	79.39333	27.17112	275	CTD	station end	
PS106_88-3	2017-07-15	18:43	79.39353	27.16998	274	MN_M7	station start	
PS106_88-3	2017-07-15	18:53	79.39361	27.16923	273	MN_M7	at depth	
PS106_88-3	2017-07-15	19:13	79.3936	27.16923	274	MN_M7	station end	
PS106_88-4	2017-07-15	19:17	79.39343	27.16936	274	LOKI	station start	
PS106_88-4	2017-07-15	19:27	79.39294	27.16953	274	LOKI	at depth	
PS106_88-4	2017-07-15	19:38	79.39151	27.17237	274	LOKI	station end	
PS106_89-1	2017-07-16	06:47	78.51878	25.02726	150	BT	station start	
PS106_89-1	2017-07-16	07:09	78.49583	25.11009	165	BT	profile start	
PS106_89-1	2017-07-16	07:24	78.48383	25.14802	169	BT	profile end	
PS106_89-1	2017-07-16	07:51	78.46942	25.17426	180	BT	station end	
PS106_90-1	2017-07-16	09:35	78.66434	24.47134	126	BT	station start	
PS106_90-1	2017-07-16	09:56	78.68842	24.4926	132	BT	at depth	
PS106_90-1	2017-07-16	09:57	78.68904	24.4932	132	BT	profile start	
PS106_90-1	2017-07-16	10:35	78.71881	24.52345	135	BT	station end	
PS106_91-1	2017-07-16	13:17	78.70402	23.15905	101	BT	station start	
PS106_91-1	2017-07-16	13:37	78.70486	23.28223	121	BT	profile start	
PS106_91-1	2017-07-16	13:52	78.70566	23.36098	122	BT	profile end	
PS106_91-1	2017-07-16	14:13	78.7077	23.42324	124	BT	station end	
PS106_91-2	2017-07-16	15:07	78.70942	23.43402	123	MN_M7	at depth	
PS106_91-2	2017-07-16	15:19	78.70948	23.43642	123	MN_M7	station end	
PS106_91-3	2017-07-16	15:29	78.70945	23.43901	121	LOKI	station start	
PS106_91-3	2017-07-16	15:34	78.70948	23.44066	120	LOKI	at depth	
PS106_91-3	2017-07-16	15:40	78.70955	23.44245	120	LOKI	station end	
PS106_91-4	2017-07-16	15:53	78.70964	23.44709	121	CTD	station start	
PS106_91-4	2017-07-16	16:01	78.70966	23.44958	122	CTD	at depth	
PS106_91-4	2017-07-16	16:06	78.70965	23.45123	122	CTD	station end	
PS106_92-1	2017-07-17	06:03	78.66633	24.47793	126	BT	station start	

Station	Date	Time	Latitude	Longitude	Depth [m]	Gear	Action	Comment
PS106_92-1	2017-07-17	06:24	78.69151	24.498	132	BT	profile start	
PS106_92-1	2017-07-17	06:39	78.70734	24.5113	135	BT	profile end	
PS106_92-1	2017-07-17	07:04	78.72176	24.51746	138	BT	station end	
PS106_93-1	2017-07-17	08:20	78.51854	25.03869	152	BT	station start	
PS106_93-1	2017-07-17	08:42	78.49555	25.10794	164	BT	at depth	
PS106_93-1	2017-07-17	08:43	78.49519	25.10915	165	BT	profile start	
PS106_93-1	2017-07-17	08:56	78.48338	25.14743	169	BT	profile end	
PS106_93-1	2017-07-17	09:20	78.47255	25.18563	174	BT	station end	
PS106_93-2	2017-07-17	09:35	78.47171	25.18819	178	LOKI	station start	
PS106_93-2	2017-07-17	09:41	78.47146	25.1897	179	LOKI	at depth	
PS106_93-2	2017-07-17	09:48	78.47101	25.19231	179	LOKI	station end	
PS106_93-3	2017-07-17	09:54	78.47067	25.19483	179	MN_M7	station start	
PS106_93-3	2017-07-17	10:01	78.47037	25.19713	180	MN_M7	at depth	
PS106_93-3	2017-07-17	10:13	78.47008	25.20096	178	MN_M7	station end	
PS106_93-4	2017-07-17	10:24	78.46987	25.20365	179	CTD	station start	
PS106_93-4	2017-07-17	10:33	78.46983	25.20531	180	CTD	at depth	
PS106_93-4	2017-07-17	10:39	78.46979	25.20616	179	CTD	station end	
PS106_93-5	2017-07-17	11:01	78.46972	25.21161	174	CTD	station start	
PS106_93-5	2017-07-17	11:03	78.46972	25.21183	174	CTD	at depth	
PS106_93-5	2017-07-17	11:10	78.46984	25.21358	178	CTD	station end	

Gear abbreviations	Gear
ADCP_150	Vessel mounted Acoustic Doppler Current Profiler 150 kHz
BC	Box Corer
BOAT	Boat
BONGO	Bongo Net
BT	Bottom Trawl
BUCKET	Bucket Water Sampling
CCNC	Cloud Condensation Nuclei Counter
CRS	Cloud Radar
CTD	CTD aboard RV *Polarstern*
DOAS	Pandora
EBS	Epibenthossledge
EK60	Fish Finder Echosounder EK60
FBOX	FerryBox

Gear abbreviations	Gear
FLOAT	Float
FTIR	Fourier Transform Infrared Radiometer
GKG	Box Grab
HCTD	Hand CTD
HK	Heli-Kite
ICE	Ice Station
ICEOBS	Ice Observation
LIDAR	Doppler-Wind LIDAR
LISST	Laser In-Situ Scattering and Tranmissometry
LOKI	Light Frame On-sight Keyspecies Investigation Messsystem
MN_M7	Multinet Medium 7 Nets
OCEANET	Atmosphere Observatory
Obs	Observer
PCO2_GO	pCO2 GO
PCO2_SUB	pCO2 Subctech
RM	Radiation Measurements
RMT	Rectangular Midwater Trawl
SPR	RAMSES
SUIT	Surface and Under Ice Trawl
SVP	Sound Velocity Profiler
TPOP	Bottom Temperature Recorder
TSG_KEEL	Thermosalinograph Keel
UAS	Underway Air Sampling
WST	Weatherstation
XBT	Expendable Bathythermograph

Die **Berichte zur Polar- und Meeresforschung** (ISSN 1866-3192) werden beginnend mit dem Band 569 (2008) als Open-Access-Publikation herausgegeben. Ein Verzeichnis aller Bände einschließlich der Druckausgaben (ISSN 1618-3193, Band 377-568, von 2000 bis 2008) sowie der früheren **Berichte zur Polarforschung** (ISSN 0176-5027, Band 1-376, von 1981 bis 2000) befindet sich im electronic Publication Information Center **(ePIC)** des Alfred-Wegener-Instituts, Helmholtz-Zentrum für Polar- und Meeresforschung (AWI); see http://epic.awi.de. Durch Auswahl “Reports on Polar- and Marine Research“ (via “browse”/”type”) wird eine Liste der Publikationen, sortiert nach Bandnummer, innerhalb der absteigenden chronologischen Reihenfolge der Jahrgänge mit Verweis auf das jeweilige pdf-Symbol zum Herunterladen angezeigt.

The **Reports on Polar and Marine Research** (ISSN 1866-3192) are available as open access publications since 2008. A table of all volumes including the printed issues (ISSN 1618-3193, Vol. 377-568, from 2000 until 2008), as well as the earlier **Reports on Polar Research** (ISSN 0176-5027, Vol. 1-376, from 1981 until 2000) is provided by the electronic Publication Information Center **(ePIC)** of the Alfred Wegener Institute, Helmholtz Centre for Polar and Marine Research (AWI); see URL http://epic.awi.de. To generate a list of all Reports, use the URL http://epic.awi.de and select “browse”/ ”type” to browse ”Reports on Polar and Marine Research”. A chronological list in declining order will be presented, and pdf-icons displayed for downloading.

Zuletzt erschienene Ausgaben:

Recently published issues:

719 (2018) The Expeditions PS106/1 and 2 of the Research Vessel POLARSTERN to the Arctic Ocean in 2017, edited by Andreas Macke and Hauke Flores

718 (2018) The Expedition PS111 of the Research Vessel POLARSTERN to the southern Weddell Sea in 2018, edited by Michael Schröder

717 (2018) The Expedition PS107 of the Research Vessel POLARSTERN to the Fram Strait and the AWI-HAUSGARTEN in 2017, edited by Ingo Schewe

716 (2018) Polar Systems under Pressure, 27th International Polar Conference, Rostock, 25 - 29 March 2018, German Society for Polar Research, edited by H. Kassens, D. Damaske, B. Diekmann, D. Fütterer, G. Heinemann, U. Karsten, E.M. Pfeiffer, J. Regnery, M. Scheinert, J. Thiede, R. Tiedemann & D. Wagner

715 (2018) The Expedition PS109 of the Research Vessel POLARSTERN to the Nordic Seas in 2017, edited by Torsten Kanzow

714 (2017) The Expedition SO258/2 of the Research Vessel SONNE to the central Indian Ocean in 2017, edited by Wolfram Geissler

713 (2017) The Expedition PS102 of the Research Vessel POLARSTERN to the Atlantic Ocean in 2016, edited by Karen Wiltshire, Eva-Maria Brodte, Annette Wilson and Peter Lemke

712 (2017) The Expedition PS104 of the Research Vessel POLARSTERN to the Amundsen Sea in 2017, edited by Karsten Gohl

711 (2017) Mid-Range forecasting of the German Waterways streamflow based on hydrologic, atmospheric and oceanic data by Monica Ionita

710 (2017) The Expedition PS103 of the Research Vessel POLARSTERN to the Weddell Sea in 2016/2017, edited by Olaf Boebel

709 (2017) Russian-German Cooperation: Expeditions to Siberia in 2016, edited by Pier Paul Overduin, Franziska Blender, Dmitry Y. Bolshiyanov, Mikhail N. Grigoriev, Anne Morgenstern, Hanno Meyer

ALFRED-WEGENER-INSTITUT
HELMHOLTZ-ZENTRUM FÜR POLAR-
UND MEERESFORSCHUNG

BREMERHAVEN

Am Handelshafen 12
27570 Bremerhaven
Telefon 0471 4831-0
Telefax 0471 4831-1149
www.awi.de

HELMHOLTZ
GEMEINSCHAFT